Surface Modification Strategies for Antimicrobial Titanium Implant Materials with Enhanced Osseointegration

Thesis submitted to De Montfort University in partial fulfilment of the requirements for the degree of Doctor of Philosophy

By

Kennedy F. Omoniala, BPharm, MRes
Faculty of Health and Life Sciences

Leicester School of Pharmacy
Pharmaceutical Technologies Group

De Montfort University

May 2016

Acknowledgements

There are many people I owe thanks! First and foremost, my utmost gratitude goes to the ALMIGHTY GOD, for the grace, resolve, patience, knowledge and understanding to undertake this work. It would however have remained just an aspiration without Dr David Armitage (my first supervisor, who offered me the privilege), and Dr Susannah Walsh (my second supervisor) for the opportunity to carry out this research project in their laboratories, and providing me with encouragement and guidance throughout my studies. Thank you to my colleagues in Hawthorn Lab 235 and fellow postgraduate students, both past and present, for the constant support and inspiration. Thank you to Rachel Armitage and Liz O'Brien for the assistance with all the SEM micrographs, Unmesh Desai and Nazmin Juma for the assistance with AAS, and the folks in the microbiology lab for their patience and kind words

As part of my studies, I spent three months at Lab 202, Hodgkin Building, Toxicology Unit, University of Leicester, an experience which was in equal measure very productive and enjoyable. So, special thanks to Prof Andrew Tobin of the Toxicology Unit of University of Leicester, for the experience, the gift of U2OS cells and reagents, the use of his cell culture facilities and technical assistance in osteosarcoma cell handling.

I am also very grateful for the studentship provided by De Montfort University, Leicester

Last but not the least, a very special thank you to my wife Yvonne, and to my family and friends, especially Rev Samuel Commey, who have been supportive throughout my studies!

I would like to dedicate this thesis to my son, Shadrach and his ‘big’ sisters Ebi and Kuku, for the great company, especially during the late night write ups, and the numerous promises that I’m yet to fulfil!!!

Table of Contents

Notation

Aap	Accumulation associated proteins
AAS	Atomic Absorption Spectroscopy
AMPs	Antimicrobial Peptides
Al	Aluminium
ASTM	American Society for Testing and Materials
Ag	Silver
$AgNO_3$	Silver Nitrate
Ag_2O	Silver Oxide
bMSC	bone Marrow Stem Cells
CaO	Calcium Oxide
CaP	Calcium Phosphate
CDC	Centre for Disease Control
cfu	Colony Forming Units
cDNA	Complementary Deoxyribonucleic Acid
cpTi	Commercially pure titanium
CuO	Copper Oxide
Co-Cr-Mo	Cobalt-Chromium-Molybdenum alloy
R2	Correlation Coefficient
DNA	Deoxyribonucleic acid
DNase	Deoxyribonuclease DNase
e-beam	Electron-beam
ECM	Extracellular Matrix
E. coli	*Escherichia coli*
eDNA	Extracellular Deoxyribonucleic Acid
EDX	Energy Dispersive X-ray
EPS	Extracellular Polymeric Substances
ESB	European Society for Biomaterials
FBS	Foetal Bovine Serum
fnbA	Fibronectin Binding Protein A gene
fnbB	Fibronectin Binding Protein B gene
FnbP	Fibronectin Binding Proteins
Au	Gold
HA	Hydroxyapatite
HAP	Hydroxyl apatite
HCAI	Healthcare Associated Infections
H2O2	Hydrogen peroxide
HI	Hydrophobicity Index
icaC	Interceullular Adhesin C gene
ICP-MS	Inductively Coupled Plasma Mass Spectroscopy
ICU	Intensive Care Unit
IGF-1 and 2	Insulin-like Growth Factors 1 and 2
Fe_2O_3	Iron Oxide
LN_2	Liquid Nitrogen
MEMS	Micro-Electro-Mechanical Systems
$MgCl_2$	Magnesium Chloride
MgO	Magnesium Oxide
mRNA	Messenger Ribonucleic Acid

MRSA	Methicillin Resistant *Staphylococcus aureus*
MRSE	Methicillin Resistant *Staphylococcus epidermidis*
MSSA	Methicillin susceptible *S. aureus*
MTP	Microtitre Plate
MBC	Minimum Bacterial Concentrations
MIC	Minimum Inhibitory Concentration
NaOH	Sodium Hydroxide
NEMS	Nano-Electro-Mechanical Systems
NPs	Nanoparticles
NHS	National Health Service
NiO	Nickel Oxide
NA	Nutrient Agar
NB	Nutrient Broth
PBS	Phosphate Buffered Saline
PC	Polycarbonate
PDGF	Platelet-derived Growth Factor
PIA	Polysaccharide Intercellular Adhesin
PIII	Plasma Immersion Ion Implantation
PJI	Periprosthetic Joint Infection
PTTE	Polymer-poly tetra fluorethylene
PMMA	polymethylmethacralyte
PNAG	Poly-N-acetyl-β-(1-6)-glucosamine
PLA	polylactic acid
PGA	polyglycolic acid
polAg	Polished silver-treated titanium (surface)
polCa	Polished calcium-treated titanium (surface)
polTi	Polished (mirror-finished) titanium (surface)
polZn	Polished zinc-treated titanium (surface)
PTFE	Polytetrafluoroethylene
PVC	Polyvinyl Chloride
PVP	Poly-(N-vinyl-pyrrolidone)
QAC	Quaternary Ammonium Compounds
QS	Quorum Sensing
ROS	Reactive Oxygen Species
RO	Reverse-osmosis
RNA	Ribonucleic Acid
RTVs	Removal Toque Values
S. aureus	*Staphylococcus aureus*
S. epidermidis	Staphylococcus *epidermidis*
SEM	Scanning Electron Microscopy
SiO_2	Silicon Dioxide
SS	Stainless Steel
SSI	Surgical Site Infections
SE/SEM	Standard Error of the Mean
S. aureus	*Staphylococcus aureus*
S. epidermidis	*Staphylococcus epidermidis*
TGF-β	Transforming Growth Factor
Ti	Titanium
Ti6Al4V	A grade 5 Titanium-Aluminium-Vanadium alloy
TiO_2	Titanium Dioxide

TSB	Tryptone Soya Broth
unpolTi	Unpolished commercially pure titanium (surface)
U2OS Cells	Human Bone Osteosarcoma Epithelial Cells
UV	Ultraviolet
WHO	World Health Organisation
Zn	Zinc
ZnO	Zinc Oxide
ZnTi	Zinc treated titanium (surface)
ZOI	Zone of Inhibition

ABSTRACT.

The use of exogenous materials to replace or repair dysfunctional tissues and organs has seen dramatic improvements since the time of the 'physician-hero'. The past three decades have heralded the advancement of various materials and technologies for medical implant devices to repair, replace or regenerate irreversibly damaged tissues. Improvement in health outcomes, evident in life expectancy increase, has brought in its wake the increased need to replace or repair tissues, particularly weight-bearing bone tissues. Titanium (Ti), a non-magnetic, corrosion resistant, osseo-integrating metal, with a higher strength-to-weight ratio than the traditional stainless steel, has emerged as the material of choice for replacing bone and other support tissues. However, the quest for improved performance (osseointegration) and reduction in implant related infection resulting in the need for resection surgeries, has necessitated the need to improve the titanium-tissue interface mediated osseointegration process, and confer antimicrobial properties to the implant material surface.

In this work, a simple cost effective physical and chemical modification strategies have been developed, to alter the surface chemistry, increase the surface water wettability and confer a nano topographic characteristic to the Ti surface. These surface parameters have been demonstrated to enhance the osseointegration process. The chemical treatments resulted in oxides containing the following ions: Calcium (Ca), for improvement of osteogenic cell adhesion to Ti surface, Silver (Ag), and Zinc (Zn) for conferring antimicrobial properties to the novel surface, and their composites (CaAg, CaZn and CaZnAg), Scanning electron microscope (SEM) profiles of the modified surface suggest that, ions are chemically bound and not physically deposited onto the Ti surface. Further evidence of this is provided by the release profile of these elements from the modified surface over a 28-day period. We have also demonstrated that, the physically modified Ti surface is better at incorporating our elements of interest than the commercially pure titanium (cpTi) surface.

The results from a *Staphylococcus aureus* biofilm formation assay, and U2OS bone cell adhesion and proliferation studies, suggest that, the physical modifications enhanced both the antimicrobial performance and the osteoblast-like cell adhesion and proliferation. The suggestion also is that, the incorporated Ca further enhances the adhesion and proliferation of bone-like cells, whereas Zn and markedly Ag improve the modified Ti surface's antimicrobial properties. However, Ag alone has been shown to have a toxic effect on the bone cells; a promising combination treatment involving Ca, Zn and Ag appears to have beneficial response in all tests.

Author's declaration

The author declares that the work presented in this thesis was conducted by the author (except where otherwise acknowledged) and has not previously been submitted for a degree or diploma at this University or any other institution. U2OS osteosarcoma cells used here and related growth media and reagents were kind gifts from Prof Andrew Tobin of the MRC Toxicology Unit at the University of Leicester. This PhD studies was sponsored by the Graduate School, De Montfort University.

Chapter 1 : General Introduction

1.1. Historical Background and Applications of Biomaterials

The introduction of non-biological materials into the human body dates almost as far back as archaeological remains have been able to provide insight into, and records have been kept, the Kennewick man, standing up as a case in point (Ratner et al., 2004) (Rajput et al., 2016). However, it can also be confidently assumed that, any prehistoric implantation has been accidental, as opposed to a deliberate act, which is the common practice today.

The early Egyptians used linen sutures, and Europeans used catgut sutures in the Middle Ages. Galen of Pergamon (circa 130-200AD) first described ligatures of metallic gold wire in Greek literature (Hendriks and Cahalan, 2016, Ring, 1995). Philip Physick, a University of Pennsylvania professor of surgery suggested the use of lead wire as sutures in 1818. Then in 1847, J Marion Sims carried out many successful operations with sutures of silver wire he had had fabricated by a jeweller (Ratner et al., 2004)

The first description of an artificial heart device was made by Etienne-Jules Marey in 1881, but the first such device was patented by Dr Paul Winchell, the ventriloquist, in the mid-1950s. Dr Willen Kolff and his team first tested the artificial heart in animals in 1957. It took till 1891 for the first hip replacement to be attempted by the German surgeon Theodore Gluck, using a cemented ivory ball (Larry L. Hench, 2013, Pennsylvania and Institute, 1992, Ratner et al., 2012, Rajput et al., 2016).

As with other areas of scientific advancements, it appears sustained progress in the use of non-biological materials to replace or improve defective physiological/anatomical functions took off post the world wars. This era saw the advent of the surgeon-heroes, who as a result of their near absolute control on the determination of the life or death of their patient, coupled with

minimal government regulatory activity and minimal human subject protection, had more freedom to take heroic action, usually as the last resort to preserving human life and functionality (Hendriks and Cahalan, 2016). Thus, materials primarily designed for the airplane and automobile industries were taken 'off the shelf' by surgeons and applied to medical problems. These included silicones, polyurethanes, Teflon, nylon, methacrylates, titanium and stainless steel. Prior to this period, materials used in implantation had a low probability of success because of lack of insight into biocompatibility and sterility influencing factors such as chemistry of the implant, leaching, shape, mechanics and design (Scotchford et al., 2016). In 1924, a publication by A. Zierold on tissue reaction to various materials indicated that iron and steel eroded rapidly leading to resorption of adjacent bone, copper, magnesium, aluminium alloy, zinc and nickel discoloured surrounding tissue, while though inadequate mechanically, gold, silver, lead and aluminium were tolerated by living tissue. He reported that Stellite, a Co-Cr-Mo alloy, was well tolerated and mechanically strong. J. Cotton in 1947 first muted the idea of titanium and its alloys for use in medical implant fabrication (Turzo, 2012) .

The knowledge that partial occlusion of coronary arteries leads to angina, diminished heart function and myocardial infarction (when the artery occludes) eventually, led to the advent of the percutaneous transluminal coronary angioplasty (PTCA) procedure, as an option to the major surgery and expensive coronary bypass procedure. Attendant to this procedure however, was the observation that a third of angioplasty re-opened arteries spasmed and closed from the trauma of the procedure. A solution to this problem came in the form of the coronary stent, devised by Dr Julio Palmaz in 1978 from stainless steel wire soldered with silver. Today, well over 2milion coronary artery stenting procedures are performed each year (Ratner et al., 2012, Larry L. Hench, 2013, Yao and Eskandari, 2012).

With all these advancement, has come the shift from the use of 'off the shelf' material by 'hero-surgeons/physicians' to fabricate medical devices, to the development of materials specifically

engineered for biomedical applications. These materials have come to be collectively known as biomaterials.

Biomaterial science evolved around a few pioneering surgeons taking commercially available polymers and metals, fabricating implants and components of medical devices from them, and applying them clinically (Chen and Liu, 2016). With little or no regulation, successes were remarkable. Likewise, the failures were dramatic. This led these pioneering surgeons to recruit the expertise of physical, biological and material scientists and engineers into what has evolved into probably the biggest interdisciplinary collaboration that biomedical engineering is today (Ratner, 1996a, Mooney, 2016).

Biomaterial science, as a study discipline came into recognition post the Clemson University in South Carolina's meeting in 1969 (Geetha et al., 2009b). This was the first of the series of annual symposia that was to be known later as the Annual International Biomaterials Symposium, which led to the formation of the Society for Biomaterials (SFB) in 1974.

Biomaterials are primarily non-viable natural or synthetic materials that are used in contact with biological systems to improve or restore form and function, or to replace lost or damaged biological structure, in an attempt at improving the quality and longevity of the particular imparted biological system or the human life as a whole, in a safe, reliable, economic, and physiologically acceptable manner (Ratner, 1996a, Park and Bronzino, 2003), according to the Consensus Conference of the European Society for Biomaterials in 1986.

The Clemson University Advisory Board for Biomaterials defined a biomaterial as "a systemically and pharmacologically inert substance designed for implantation within or incorporation with living systems. Others defined biomaterials as "a nonviable material used

in a medical device, intended to interact with biological systems" (Latour and Black, 1992, Pilliar et al., 1987).

It has also been defined as "materials of synthetic as well as of natural origin in contact with tissue, blood, and biological fluids, and intended for use for prosthetic, diagnostic, therapeutic, and storage applications without adversely affecting the living organism and its components" (Bruck, 1980). By contrast, a biological material is a material such as skin or artery, produced by a biological system. Artificial materials that simply are in contact with the skin, such as hearing aids and wearable artificial limbs are not included in our definition of biomaterials since the skin acts as a barrier with the external world.

Earlier classification, based on the extent of contact of these materials with the living tissue, grouped materials used in medicine into; Class I which do not make direct contact with bodily tissues, Class II which makes intermittent contact with body tissues, and Class III which are in constant contact with living tissues (Suh, 1998). It is the Class IIIs that are currently commonly referred to as biomaterials. According to the effect evoked on or their biological interaction with the living tissue they are in contact with, these Class III materials are categorised as Bio-inert/Bio-tolerant, Bioactive and Bio-reabsorbable materials (Holzapfel et al., 2013). Contrary to the image the classification name suggests, generally, living tissues tend to reject bio-tolerant or bio-inert materials, to a significant extent, leading to failure of the implant. Materials in this category include Polymer-poly tetra fluorethylene (PTFE), polymethylmethacralyte (PMMA), Ti, and Co–Cr. Bioactive materials, examples Bioglass, and synthetic calcium phosphate including hydroxyl apatite (HAP), tend to be successfully implanted as a result of the formation of bony tissue around the implant material, mimicking the natural bone tissue, leading to integration with the material surface. Bioabsorbable materials however on implantation, eventually dissolve or are absorbed into the body, becoming replaced by the autologous tissue. Examples include polylactic acid (PLA) and polyglycolic acid (PGA), co-polymers and

processed bone grafts, composites of all tissue extracts or proteins and structural support systems (Geetha et al., 2009b, Suh, 1998, Dohan Ehrenfest et al., 2010).

Currently, biomaterials are divided into four major classes, namely polymers, metals, ceramics (including carbons, glass-ceramics, and ceramics) and natural materials (including those from both plant and animal sources). A fifth class, the composites, consists of two different classes of materials put together to form a composite material, example, silica-reinforced silicon rubber, and carbon fibre- or hydroxyapatite particle-reinforces poly (lactic acid) (Ratner and Bryant, 2004). The increasing variety and complexity of materials in medical and biotechnological application today is a testament to the significant strides that have taken place in the biomaterial science world over the past 50 years (Hendriks and Cahalan, 2016).

1.2. Organization of the Thesis

The entire thesis was structured into 5 phases; a general review of the background and advances in implant technologies, surface modification strategies, characterization of the modified surfaces, investigation of the antimicrobial performance of the modified surfaces, and cell culture (*in vitro*) experiments to examine the adhesion, growth and biocompatibility of bone-like cells on the surfaces with the most promise.

In Chapter 1, the historical background is introduced, together with key periods and pioneers in the evolution of biomaterial science and application of natural and synthetic materials' in medical practices, as well as the early definitions and classifications of these materials. **Chapter 2** previews implant materials and devices advances, and their attendant problems, that present the research questions, answers for which this thesis seeks to provide and contribute knowledge to. Titanium surface physical and chemical attributes, and their significance, together with current surface classification and modification strategies were examined. Also,

reviewed in this chapter was the interaction of implant devices surfaces with biological environment of the implant site, including microbial agents. Furthermore, the incidence and causes of implant failures were critically reviewed.

In chapter 3, the techniques developed in this work were presented. This include the physical modification of the commercially pure titanium surface, and the subsequent thermochemical bath treatments. These constituted the reproducible fabrication of surfaces with identical topographies and chemistries. The methods of characterizing the resulting surfaces and testing their performance against biological agents were all outlined in this chapter. A more detailed information about instrumentations used are found here.

The outcome of the initial physical surface modification strategies developed in this thesis, and a comparison of the novel surfaces with the commercially pure Ti surface, the topographic characterization of the novel surface, and surface wetting properties are presented in **Chapter 4**.

Chapter 5 looked at the ion incorporation onto the Ti surface and a detailed presentation of the mechanism underpinning the process. Also, presented in this chapter are proposed characterisation/classification of the novel surfaces.

Chapter 6 examined the effect of (autoclave) sterilization, an important step in the microbiological and osteogenic testing of the novel surface, on the ion-incorporated surface. The profiles of the suspected release of the incorporated ions from the ion-incorporated Ti surfaces are investigated in **Chapter 7.**

The effect of the novel surfaces on biofilm forming bacteria, and the responses of human osteoblast-like cells to the new surfaces are presented in **Chapters 8 & 9**, as cell numbers, cell footprint area or cell sizes, and cell shapes.

The observations made, and inferences drawn, from the results of the various experiments, and the underlying rationale, are all discussed in **Chapter 10.**

A critical evaluation and significance of all the findings of this study and conclusions drawn, as well as the future directions this work may take are presented in **Chapter 11**.

Chapter 2 : Review of Literature

2.1. Advances in biomaterial and Surface Technologies

The past decades have seen the advancement of various materials and technologies for use as medical implant devices. In the process, the essential nature and definition of biomaterials have and are still undergoing tremendous changes. Compared to just a decade ago, the state of affairs today is vastly different (Hench and Polak, 2002, Chen and Liu, 2016).

For the past half century since its inception, an appraisal of trends indicates that, the clinical and non-clinical application of biomaterials has seen steady growth, with increasingly diverse applications and fields of study (Ratner and Bryant, 2004). The 60s and 70s saw the development of the first-generation biomaterials for use routinely as medical implant devices. This improved the quality of life of millions of people. The successes during this period were however based largely on trial and error, and not on material science and biological interaction knowledge. Moving on, the goal of early biomaterial research was to derive a suitable physical and chemical properties combination that closely approaches those of the tissues to be replaced, with the least antagonistic host-foreign body response. It was in this regard that metallic implants systems of plain carbon and vanadium with overt corrosion attributes gave way to the more corrosion resistant stainless steel, then the far more superior, strongly passive cobalt-chromium alloys. The 80s saw the introduction of over 100 devices and implants in clinical use, fabricated from about 30 different materials (Gaharwar et al., 2016, Chen and Thouas, 2015b, Chen and Thouas, 2015a).

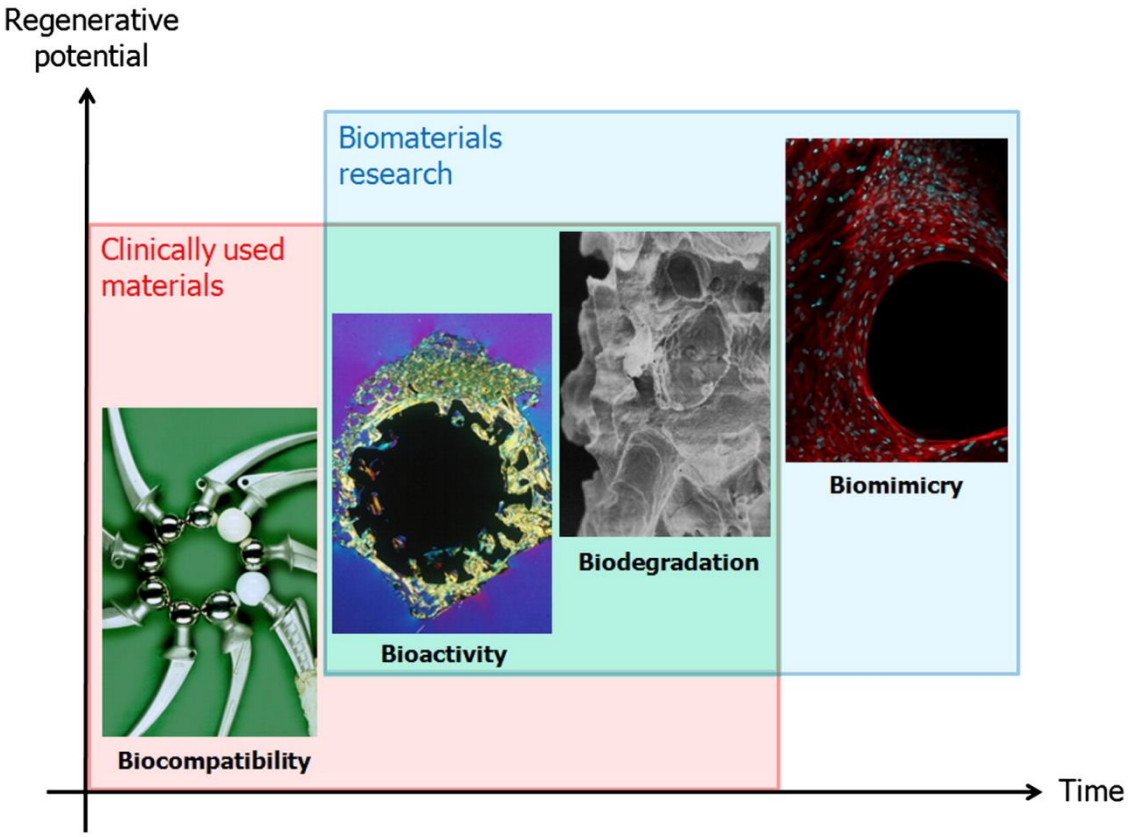

Figure 2.1. Evolution of biomaterials (Jandt, 2007) To adequately substitute for damaged tissues and provide structural support, classic metallic implants must be biocompatible. Research to this end continues to aim at the developing bioactive components capable of improving implant longevity by optimizing the interfaces between the implant and the host tissue. Approaches vary, from biological approaches that focus on repairing by stimulating specific cellular responses at the molecular level, to approaches that focus on developing smart biomaterials that meet the macro-, micro- and nano-structural specifications of tissues they are to replace.

However, by this time, the emphasis had shifted from simple corrosion resistance to reduction in biological activity to a minimum, known as 'inertness', and prevention of biological rejection (Hench, 1980, Huebsch and Mooney, 2009). This shift in paradigm is still valid for some implants still in use today (Bhaskar et al., 2016).

By the 90's as a result of better understanding to the body's response to foreign materials, the emphasis moved on away from the use of inert materials to the evolution of the second generation bioactive materials, which seek to elicit specific biological response at the tissue-implant material physiological interface (Hench and Thompson, 2010, Hench, 1998). The applications (in a variety of orthopaedic, dental and cardiovascular situations) of these generation of materials (including various composition of metal and ceramics) has led to the argument that the field of biomaterials have developed alongside novel strategies in surgeries,

leading to less invasive treatment options with more effective outcomes (Huebsch and Mooney, 2009, Jandt, 2007).

Table 2.1. Summary of uses for Biomaterials in medical and non-settings

Medical uses	**Non-medical Uses**
Artery graft	Arrays for DNA and diagnostics
Breast implant	Bioremediation materials
Cochlear implant	Biosensors
Ear drainage tube	Bioseparations, chromatography
Dental implant	Biofouling-resistant materials
Feeding tube	Biomimetics for new materials
Glaucoma drainage tube	Cell culture
Hydrocephalous shunt	Controlled release for agriculture
Intraocular lens	Electrophoresis materials
Joints (hip, knee, shoulder)	Fuel cells (biomass)
Keratoprosthesis	MEMS
Left ventricular assist device (LVAD)	Muscles (artificial) and actuators
Mechanical heart valve	Nanofabrication
Nerve guidance tube	NEMS
Ophthalmic drug delivery device	Neural computing/biocomputer
Pacemaker	Smart clothing for biowarfare
Renal dialyzer	Yeast array chip
Stent	
Tissue adhesive	
Urinary catheter	
Valve, heart	
Wound dressing	
X-ray guide	
Zirconium knee joint	

The development of bioactive materials has also led to increased implant lifetimes (Hench, 1998, Hench and Wilson, 1984, Burns, 2009). For permanent implants, however, issues related to stability, abrasion or wear, and fatigue strength are critical to implant success. For these, bacterial infection causing peri-implantitis, toxic or immunological response resulting in local or systemic reactions and mechanical failure, *inter alia*, present persistent challenging problems (Figure 2.1).

Advances in proteomics, cellular and molecular biology knowledge over the last decade, have provided the foundation for the development of a third-generation biomaterials. These advances have led to a better understanding of biocompatibility, and these understanding have impacted the design, synthesis and use of biomaterials, as well as the clinical demand and patient expectations (Holzapfel et al., 2013, Anderson et al., 2008b). This generation's biomaterials are a convergence of the concepts of bioactive materials and resorbable materials. That is, bioactive materials are being made resorbable, and resorbable materials being made bioactive. The aim being molecular modifications to make the systems initiate specific interactions with integrins and in so doing direct cell proliferation, differentiation and extracellular matrix (ECM) production and organisation. This seek to ultimately activate genes and stimulate the regeneration of living tissues, thereby eliminating or at least delaying the need for permanent implants (Sun and Xi, 2006, Hench and Polak, 2002). Consequently, a fourth generation of biomaterial has followed on, on the hypothesis that it is possible to construct matrices which mimic nature's structural hierarchy and mechanism, that underpin morphology and function, depicted in many natural occurring species and genera. This is the biomimetic or smart biomaterials. These attempts to capture and recreate the cellular, molecular and organ degree of complexity of natural tissue. This is a significant shift in paradigm from the classical idea of the 'biomaterialogists' attempt to replace tissues with permanent implants, to a more biological approach which emphasise repair and reconstitution

of tissue structure and function (Holzapfel et al., 2013, Hutmacher, 2006). In the light of current physical and chemical material understanding, and advances in biology, considerable advancement has taken place in this generation of biomaterials. However, only a relatively few smart biomaterials are in clinical application to date. Nevertheless, it has been estimated by the EU-Report on Nanotechnology that the global market for smart biomaterials alone, which reached $47 billion in 2009, will rise to $113 billion by 2025 (Commission, 2009, Hafner et al., 2014). After declining in 2009, medical device research and development spending in the US rebounded to $2.9 billion in 2010 and $7.3 billion in 2011. The expectation is that, from 2013 to 2020, research and development will rise by up to 5%. Although in some instances, devices such as stents, screws, and artificial joints have not worked better than or as well as cheaper procedures, all medical devices place a large cost-burden on medical spending, whether they are entirely effective or not (Allen, 2011, Sorenson et al., 2011, Nanomedicine–NANOMED, 2013).

Implantable medical devices remain very important in modern medical practice. However, the medical device technology now ranges from drug and gene delivery systems, tissue engineering and cell therapies, organ printing and cell patterning, nanotechnology mediated imaging and diagnostic systems, and microelectronic devices (Table 2.1). Although these technologies still employ the classical metals, ceramics and synthetic polymers, they are increasing putting to use biopolymers, self-assembled systems, nanoparticles, carbon nanotubes and quantum dots (Williams, 2009). Quantum dots are semiconducting material particles or nanocrystals with diameters of 2-10 nanometres. Applications include functionalization with peptide and tumour-specific binding sites for selective binding to peptide and tumour cells, for imaging, diagnostic and targeting purposes (Chen et al., 2015).

2.2. Implant Materials

The need for medical use of implantable devices has increased significantly over a relatively short period. Increase in life expectancy in most advanced nations, primarily as a result of advances in and better healthcare service and practices (Bunker, 2001), together with lifestyle choices has resulted in people living increasingly longer, and having better survival outcomes in accidental situations, than during the pre-war periods(Langer and Peppas, 2003). This has led to a corresponding increase in the aging populace (Geetha et al., 2009b). Attendant to this is a considerable increase in the number of people in need of hip and knee replacements. This increase in life expectancy, together with advances in cardiovascular, orthopaedic, dental and maxillofacial surgery, and other medical procedures have led to the increased application of biomaterials, in preference to simple mechanical devices, for the replacement of worn, damaged and defective biological systems (2003, Ratner, 1996a).

Implantable devices have therefore found use in almost all facets of medical practice, ranging from short term use as in catheters and drug release systems, including some intra-uterine devices to longer term use as in coronary stents, intra-ocular lenses and load-bearing dental and skeletal tissue support systems(Ratner and Bryant, 2004). The long-term success of implants depends primarily on rapid healing with safe integration into the surrounding tissue. However, geometry and surface characteristics are crucial for the short- and long-term success of implantable devices (Le Guehennec et al., 2008).

The market for these implants is therefore expanding, and this is as a result of a combination of the afore mentioned increase in life expectancy, and increased body mass of the general population (Fordham et al., 2012). Figures obtained in 2010, indicated that the cost to the NHS of primary hip implants was 238 million pounds (Mirza et al., 2010). In the United State for example, the number of implanted internal fixation devices and total joint arthroplasties has

seen an increasing trend. It is currently estimated that more than 4.4 million people have an internal fixation device and over 1.3 million people possess an artificial joint (Chen et al., 2006). Earlier projections indicated that nearly 600,000 total hip replacements and 1.4 million knee replacements surgeries will be completed in the year 2015 (Kim, 2008, Bongartz et al., 2008, Kurtz et al., 2012). However, more recent estimates suggest that the relative incidence of prosthetic joint infection (PJI) is between 2.0% and 2.4% of the total hip arthroplasties and total knee arthroplasties. This is an appreciable increased over time. Critically, and typical of US hospitals, the annual cost of infected revisions increased from $320 million in 2001 to $566 million in 2009, and is projected to exceed $1.62 billion by 2020 (Kurtz et al., 2012, Fordham et al., 2012). The significance of this is that, as the demand for joint arthroplasty is expected to increase substantially over the coming decade, so too will the economic burden of prosthetic infections. The true economic burden of PJI here in the UK, in the US and on health care systems around the world, is currently unknown, as there are scantily few relevant published studies on the subject (Kurtz et al., 2007, Kurtz et al., 2008, Parvizi et al., 2010b, Bozic and Ries, 2005, Sculco, 1993). However, the relatively few sources also indicate a high demand of orthopaedic surgeries for both new patients every year, and for patients who must receive revision surgeries. This is in spite of the fact that most implants will last up to 20 years in more than 80% of the patient population (Losina et al., 2004).

Common problems associated with patients who require revision surgeries are instability, aseptic loosening, infection, wear, osteolysis, ingrowth failure, and periprosthetic fracture (Jafari et al., 2010). Application of novel surface modification techniques to reduce the failure rates and increase the longevity of implants offers considerable potential for cost savings while also providing obvious benefit to patients (Smith et al., 2012, Fordham et al., 2012).

Due soaring demand, particularly of knee and hip replacement implants, recent research in this area has been directed at finding ways of increasing the lifespan of these implanted devices.

This if successful, will have both patient related benefits, as the need for repeated replacement surgery will be reduced, as well as economic and resource related benefit (Jones, 2001).

Longevity of implanted devices is therefore an important issue. Failures with implants may be due to mechanical loosening, integration of debris and wear because of repeated loading, particularly for joints, leading to inflammation. Even micron-scale displacement at the interface may lead to cellular damage and induce inflammation (Yang et al., 2010, O'Connor et al., 2004). Corrosion and degradation are generally harmful, especially if toxic species result (Hallab et al., 2001). Failures may also be caused by biological processes (Puleo and Nanci, 1999b).

Biomaterial device interaction with the body is dependent on the component material of the device and the place in the body where the device is situated or placed, e.g. within the circulatory system, inside the oropharyngeal cavity, inside the urinary tract, within a bone tissue, etc (Trindade et al., 2014, Hanson, 2016, Williams, 2016). After insertion, a so-called conditioning film from the organic matter of the surrounding tissue/fluid deposits on the biomaterial surface. This may be saliva, tissue fluid, tear fluid, urine, blood or serum, and may be made up of adsorbed proteins. For serum, these are mainly albumin, immunoglobulin, fibrinogen and fibronectin. In the ideal situation, the implanted biomaterial surface will be colonised by host derived cells that form a thin capsule around the implant (Gilbert et al., 1997, Piattelli and Iezzi, 2016, Miron et al., 2016, Miron and Bosshardt, 2016). Physico-chemical properties, including chemical composition, hydrophilicity/hydrophobicity and surface charge, of the biomaterial surface influence the composition of the conditioning fluid. Albumin may be adsorbed to the more hydrophilic end and fibrinogen to the hydrophobic end of a polyethylene hydrophobicity gradient exposed to blood serum (Merritt et al., 1999, Ning et al., 2016). Blood cells may also adhere to the biomaterial surface of blood contacting biomaterial, and depending on the location, e.g. in artificial vascular graft, may initiate the blood

coagulation cascade leading to thrombosis. Calcification of the biomaterial is another phenomenon that can reduce the necessary flexibility of implants, particularly in prosthetic heart valves (Schoen and Levy, 2005).

The host tissue will also normally interact actively with the invasively implanted biomaterial surface as a foreign body. This interaction may activate the complimentary system leading to fibrin network formation and opsonisation of the biomaterial. The innate immune system may then be activated leading to an inflammation response (Franz et al., Trindade et al., 2014, Velard et al., 2013). This initial response may disappear after conditioning and encapsulation of the biomaterial. In many cases, however, the tissue-biomaterial interface remains in a chronic state of inflammation, as only a few of the commonly used biomaterials, e.g. stainless steel, cobalt-chromium alloy, polyethylene, silicone-acrylate, Teflon, dacronpolyurethane, silicon-collagen composite, titanium etc, can remain physico-chemically inert in the warm, wet, oxygenated proximity of living tissue. The immune response and chronic inflammation may impair tissue growth on the implant (osteointegration, in the case of bone), cause chronic pain and may ultimately lead to implant rejection of failure (Dondossola et al., 2016, Oliveira et al., 2015, Chen et al., 2014).

Bacterial colonization at the implant-biological interface (biofilm formation) is another pertinent problem associated with the long-term use of the so-called permanent implants (Gao et al., 2011, Seddiki et al., 2014, Lindeque et al., 2014, Campoccia et al., 2013, Busscher et al., 2012b). This is particularly worrisome as biofilm formation has the potential to lead to bacterial resistance to the common antibiotic used for their treatment (Gilbert et al., 1997, Lindeque et al., 2014, Fitzgerald, 2014, Parvizi et al., 2010a). This is especially so in areas where blood supply, hence drug distribution is poor, such as the synovial region of the knee and ball-socket joint of the hip (Lyden and Dellinger, 2016, Namba et al., 2013). The incidence of this kind infection varies with the site and type of implant, ranging from 10-20% for urinary implant

(catheters), 0.5-12% for percutaneous implants such as short in-dwelling catheters, temporary pacemaker, peritoneal dialysis catheters and CV catheters, and 2.6-4% for bone (prosthetic hip and total knee) implants, over a three months' period (Smith et al., 2012, Kurtz et al., 2012, Bongartz et al., 2008). The most common cause of orthopaedic implants failure resulting from bacterial infections comes from the Gram-positive *Staphylococcus epidermidis* (*SE*) and *Staphylococcus aureus (SA)*, and the Gram-negative *Pseudomonas aeruginosa* (*PA*) pathogens. SA and *SE* is known to be associated with approximately 66% of all bacterial colonies that form on orthopaedic implants (Campoccia et al., 2006, Aggarwal et al., 2014, Zmistowski et al., 2013). As a result of this, methods to reduce the incidence of infection in patients, post implant placement, are of great interest to the medical community.

To achieve this reduction, the implantable surface must have a number or combinations of ideal properties (Williams, 2016, Alatorre- Meda and Mano, 2016, Chen and Thouas, 2015b, Mirza et al., 2010). Prominent amongst them are the properties listed in Table 2.2.

Table 2.2. Ideal Properties of Implantable Materials. These play key roles in their selection and specific application as implant device materials.

Ideal Properties of Implantable Materials

Manufacturing

- Quality of available raw material
- Ease of fabrication
- Consistency of product
- Conformity to requirement
- Ease and efficiency of sterilization

Compatibility

- Tissue reactions
- Compromise in
  - Physical
  - Chemical and
  - Mechanical properties
- Degradations leading to
  - Local harmful effects
  - Systemic harmful effects

Mechanical Properties

- Strength to weight ratio
- Ultimate strength
- Fatigues strength
- Wear resistance
- Corrosion resistance
- Hardness
- Wear resistance
- Elasticity
- Yield stress
- Toughness
- Ductility
- Time dependent deformation
- creep

2.2.1. Properties of Metallic Implants

Analysis of the component of structural human tissue suggests that it is made up of bones materials (ceramics), proteins (self-assembled polymers) and trace elements of metals with molecular function (Chen and Thouas, 2015b). Metals have therefore always been part of the human structure, albeit mostly in a form not readily identified as such. The 'Sherman Vanadium Steel' was the first metal to be developed specifically for application in human, for the manufacture of bone fracture plates and screws (Park and Lakes, 2007b). Particularly with orthopaedics however, metals and their alloys have found routinely successful clinical applications, albeit with issues relating to the maintenance of long-term implant integrity (Chen and Thouas, 2015b).

Historically, the clinical application for metallic implants started with the Industrial Revolution when the metal industry began to expand, and this was driven primarily by the need for new approaches to bone repair and fracture fixation of long bones. However, most of these early attempts were unsuccessful until Lister put forward his aseptic surgical technique in the 1860s (Park and Lakes, 2007a). Metallic implants have since dominated the orthopaedic practice. They have also found extensive application in the dental and orthodontic practices concurrently. However, in spite of the large numbers of metals/alloys the industry has made available, only a few are compatible and durable enough for successful long-term use as implant materials. These few are grouped into four, based on the major alloying metal: stainless steels, cobalt-based alloys, titanium-based alloys and miscellaneous others (e.g. NiTi and alloys of Mg and Ta) (Chen and Thouas, 2015a). A variety of medical implant devices made of these materials are in routine orthopaedic use. However, the miscellaneous group materials, which are the most recently developed group, for their unique material properties such as shape memory for NiTi and degradability for Mg alloys, which could potentially meet specialised tissue needs, are yet to be approved and find their place in routine application, as a result of

significant problems related to biocompatibility (Okazaki and Gotoh, 2008). Table 2.3 shows a summary of the clinical applications and status of the four classes of metallic biomaterial in current use.

Table 2.3 Summary of the categories of metallic biomaterials and their primary applications as implants.

Type	**Primary Application**
Stainless steels	Temporary devices (fracture plates, screws, hip nails, *etc.*) (Class II)
	Total hip replacements (Class II)
Co-based alloys	Total joint replacements (wrought alloys) (Class II)
	Dentistry castings (Class II)
Ti-based alloys	Stem and cup of total hip replacements with CoCrMo or ceramic femoral heads (Class II)
	Other permanent devices (nails, pacemakers) (Class III)
NiTi	Orthodontic dental archwires (Class I)
	Vascular stents (Class III)
	Vena cava filter (Class II)
	Intracranial aneurysm clips (Class II)
	Contractile artificial muscles for an artificial heart (Class III)
	Catheter guide wires (Class II)
	Orthopaedic staples (Class I)
Mg	Biodegradable orthopaedic implants (Class III)
Ta	Wire sutures for plastic surgery and neurosurgery (Class III)
	A radiographic marker (Class II)

2.3. Titanium as an Implant Material

The emergence of Titanium-based materials for implantation is due to a combination of a number of favourable characteristics that it demonstrates, in both physicochemical and biomechanical environments (Kuroda et al., 1998), (Geetha et al., 2009a), compared to other materials. These include its outstandingly high strength, low density (high specific strength), high immunity to corrosion, complete inertness to body environment, enhanced

biocompatibility (it is non-toxic and is not rejected by the body) (Ratner, 2001), low modulus and high capacity to join with bone and other tissues (Chua et al., 2008). It thus meets the key requirements of resistance, adaptability and biocompatibility. It is nearly as resistant to corrosion as platinum, and resists most solutions, except highly concentrated acids. Most applications of titanium are as a result of its excellent combination of high-strength and light-weight. It may be 60% heavier than aluminium, but it is 100% stronger. It is also as strong but 45% lighter than steel. It is therefore ideal for applications where weight-bearing strength is required, light weight an advantage, and where metal fatigue an issue (Asaoka et al., 1985). On exposure to room temperature and oxygen saturation conditions, the Ti surface spontaneously forms a highly tenacious and stable, permanently thin, passive titanium oxide film that renders the metal surface resistant to corrosion and tarnishing. This oxide film acts as a barrier to the oxidative stress, keeping it inert and passive in physiological and biological environment (Jiang et al., 2011).

Over time, titanium has found applications and become the metal of choice for biomedical application from head to toe in the human body (Chen and Thouas, 2015a, Chen and Thouas, 2015b, Steinemann, 1998). This is because of its near-absolute inertness in the human body (Anderson et al., 2008a), immunity to attack from bodily fluids, compatibility with bone growth, and its comparative strength and flexibility. In cranioplasty and neurosurgery, titanium plates and meshes have been used in repair and to speed up recovery, as well as reduce the chances of infection. Bone conduction hearing aids anchors have been fashioned out of titanium, as well as attachment pegs for false eyes and ears. In dentistry and maxillofacial surgery, artificial root implants and maxillofacial implants respectively have been made from titanium, to provide a secure base for full arch teeth, and as stabilizers for soft tissue prostheses. In orthodontics, titanium braces have been found stronger, lighter and more compatible than steel. Shoulder and elbow joint implants are commonly fashioned from titanium, and more

recently, expandable rib cages of titanium has made it possible for a child's rib cage to 'grow' with the patient. Heart valves, pacemaker cases and vascular access ports of titanium, have found use in coronary angioplasty. Medication mini-pumps that flex and change shape in response to an electric current have been fabricated from nickel-titanium shape memory alloys. It has also found use in urethral stents to treat urethral strictures. One of the most common use of titanium is in spinal fusion cages, implants, and correction and fixation parts. The most common biomedical application is in hip replacements, as well as nearly half of all knee replacements are of titanium. Tibial nails for lower leg fracture repair reinforcement have been made from titanium, as well as toe and finger implants. Reconstructive titanium bone plates and mesh to support broken bones, and fixation devices such as bone screws, rods, hooks, cables and staples are all in common use today (Figure 2.2). Other titanium instruments also in common use include surgical devices, dental drills, marker bands, optical procedure devices, vena cava clips, needles, blades and forceps (Hench, 1998, Ratner, 1996b)

At present, no definitive allergic reactions associated with the use of titanium has been reported. However, failure rates because of tissue responses and bacterial colonization of the tissue-implant interface remain a major source of concern.

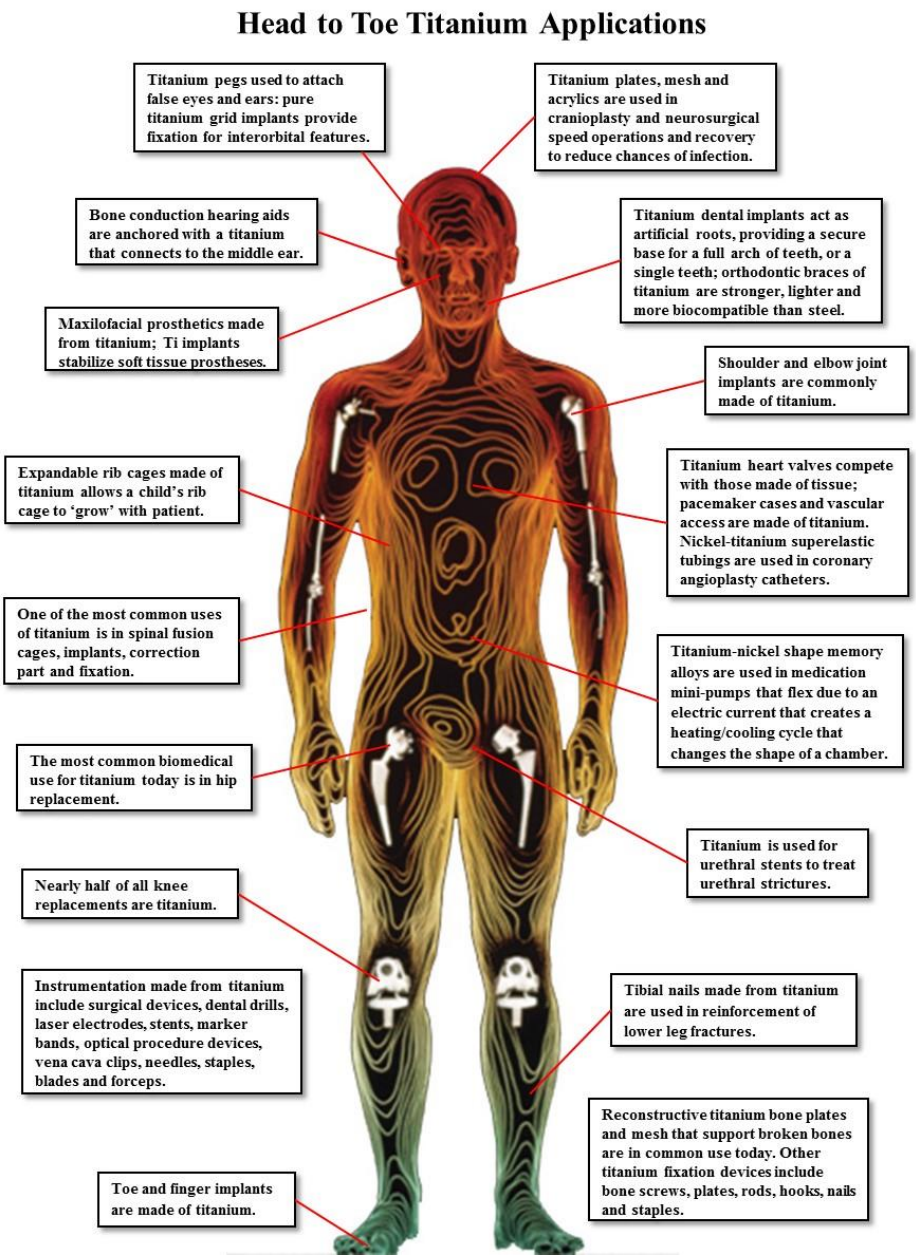

Figure 2.2. Head to Toe Applications of Titanium (Watari et al., 2004).

Titanium and its alloys have found extensive application in dental practice, so much so that commercially pure Ti (cpTi) is currently the dominant material for dental implants, as an alternative to Ag-Pd-Au-Cu alloy. This is not only because of its excellent properties but also due to the increasing cost of Pd (Kulkarni et al., 2014). In spite of titanium's extensive and successful applications as biomaterials in artificial joints and dental implants because of their good mechanical properties or fractural toughness and good biocompatibility (Watari et al., 2004), titanium implants do not actively bond to bone tissue as well as other materials such as

bioglass and bioglass-ceramics (Larsson et al., 1996). To address this, various modification techniques have been developed to improve its interaction with bone tissue (He et al., 2006, Rautray et al., 2010, Liu et al., 2004, Pohler, 2000). The various techniques have their advantages and limitations, influenced by the device physical features and shape, the device application, the modification conditions and cost.

2.4. Titanium Surface Modification for Improved Biological Response

Depending on the intended implant location and/or the desired application of the biomedical device, several different factors may be considered. For example, devices designed as a blood-contacting device (catheter, graft and stent), blood compatibility (haemo-compatibility) of the biomaterials is critical. However, for bone applications osseointegration is the paramount criterion. For both types of applications, the host tissue-device interaction and the severity of the response are strictly influenced by the surface properties of the biomaterial (Kulkarni et al., 2014, Bakir, 2012).

The surface character of implant devices is therefore one important design factor that affects the extent and rate of implant incorporation into the living tissue (Mendonça et al., 2008, Cooper, 1998, Nanci et al., 1998). Application of novel surface modification techniques to reduce the failure rates and increase the longevity of implants offers considerable potential for cost savings while also providing obvious benefit to patients. Many titanium based implants are now offered with coatings aimed at improving the strength of the bone – biomaterial interface. However, these tend to result in increased rates of infection, can have stability issues related to the coating – titanium interface and are expensive to produce (Montali, 2006a, Wang et al., 2011). It has been demonstrated that modifying, in this case roughening of titanium alloy surfaces, to a certain degree, improves integration with tissues in contact with titanium, particularly bone tissue (Khan et al., 2011). This however is a generally accepted position, with

the argument still on-going as to whether the nano or micro topography is best for osteointegration (Puckett et al., 2007, Quirynen et al., 1996, Bollen et al., 1996, Gutwein and Webster, 2004, Ward and Webster, 2007, Gittens et al., 2011, Zhu et al., 2004).

Traditionally, control of surface topography has been the approach to surface modification.

With respect to simplicity and flexibility, a passive surface chemical and physical properties modulation strategy would be preferred in the design of titanium-based implants. Methods used in current research aimed at modifying titanium surfaces so as to improve osteointegration include sandblasting, acid-etching, resorbable media application, and high speed machining (Table 2.4). Ceramic coating, and physicochemical or inorganic approaches have also been employed recently. Currently significant research effort is directed at Biochemical Modification of Titanium Surfaces (BMTiS), which comprises of surface modification by peptides; surface modification by Extracellular Matrix (ECM) proteins; surface modification by Bone Morphogenetic Proteins (BMPs) and growth factors; approaches based on pharmacologically active biomolecules (Morra, 2006, Morra et al., 2010).

Table 2.4 Summary of current strategies for creating nano-features on commercially pure Ti implants. The choice of method is dependent on the desired outcome or device application.

Methods	**Characteristics**
Self-assembly of monolayers	The exposed functional end group could be a molecule with different functions (an osteoinductive or cell adhesive molecule).
Compaction of nanoparticles	Conserves the chemistry of the surface among different topographies. Not readily applied over implant surfaces.
Ion beam deposition	Can impart nanofeatures to the surface based on the material used.
Acid etching	Combined with other methods (sandblasting and/or peroxidation) can impart nanofeatures to the surface and remove contaminants.
Peroxidation	Produces a titania gel layer. Both chemical and topography changes are imparted.
Alkali treatment (NaOH)	Produces a sodium titanate gel layer allowing hydroxyapatite deposition. Both chemical and topographic changes are imparted.

Methods	Characteristics
Anodization	Can impart nanofeatures to the surface creating a new oxide layer (based on the material used).
Sol–gel (colloidal particle adsorption)	Creates a thin-film of controlled chemical characteristics. Atomic-scale interactions display strong physical interactions
Discrete crystalline deposition	Superimposes a nanoscale surface topographical complexity on the surface
Lithography and contact printing technique	Many different shapes and materials can be applied over the surface. Approaches are labour intensive and require considerable development prior to clinical translation and application on implant surface.

This approach seeks to utilise current understanding of the biology and biochemistry of cellular function and differentiation, and the roles of biomolecules, in the remodelling of cells and tissues through the mobilization of proteins and enzymes. The binding of bone-stimulating agent to implant surfaces is another area of current research interest (Morra et al., 2009, Zhang et al., 2008a).

In spite of best efforts, implant failures are still relatively common. In addition to implant failures due to loosening and wear (Losina et al., 2004) as a result of repeated loading, bacterial infection mediated failures are also common (Jafari et al., 2010, Zmistowski et al., 2013). Therefore, methods to reduce the infection rates for patients following implant placement are of great relevance to implantologists, and of benefit to patients.

For devices meant to replace or augment weight bearing tissues, the interaction between the material surface of the device and the calciferous or bone tissue it is in close contact with is particularly crucial for the success or otherwise of the device. The integration process is initiated by the formation of a calcium phosphate layer, similar to bone hydroxyapatite at the interface (Lu et al., 2005, Valagão Amadeu do Serro et al., 2000). Biomineralization, as this

process is known, has been extensively studied to demonstrate the ability of different materials to induce calcium phosphate nucleation, the influence on the surrounding media and the kinetics at play in the precipitation of calcium phosphate from surrounding solutions (Iskandar et al., 2012, Valagão Amadeu do Serro et al., 2000).

Defined as the direct structural and functional connection between the living bone tissue and the surface of the load-bearing implant, osseointegration or osteointegration, a concept described by Branemark (Mavrogenis et al., 2009), is critical for both implant stability and functionality (Zhang et al.). This structural and functional union of the implant with living bone is strongly influenced by the surface properties of the implant material (Schwartz et al., 2005). This process, considered a prerequisite for any material's consideration for use as a load-bearing implant material and its long term clinical and functional success (Palmquist et al.), is dependent on the physical and chemical properties of the material (Albrektsson and Wennerberg, 2004a, Dohan Ehrenfest et al., 2010).

Over the last decade, several surface modification methods have been developed and in current use aimed at promoting faster and improved osteointegration, and enhancing clinical performance. This is because the surface properties of the implant material are prominent, amongst several other parameters, in influencing the success of implants measured in terms of improvement in clinical function and longevity. Surface energy, charge, wettability, topography, chemistry and crystal structure are some of the surface characteristics that influence the speed and strength of osteointegration. Surface roughness of the implant material at the nano-scale level, together with the surface chemistry, plays an important role in the biomaterial's interaction with cells and tissues at the molecular level (MendonÃ§a et al., 2008, Schwartz et al., 2005, Shalabi et al., 2006b). It is this interaction that ultimately determines the successful outcomes such as tissue integration (Kawahara et al., 2004, Lincks et al., 1998).

Surface modification methods in current use can be generally classified into three, namely mechanical, physical and (bio)chemical. These are employed to alter the biomaterial surface structure, morphology and chemistry; to remove surface contaminants, improve wear and corrosion resistance and to stimulate bone formation and osteointegration, leading to improved bio-mechanical properties of the implant. Surface roughness can be divided into three levels depending on the scale of the features: macro-, micro- and nano-sized topologies (Le Guehennec et al., 2007).

2.4.1. Titanium Surface Chemistry

Titanium, Ti, is a transition metal with a white-silvery-metallic colour. It has an atomic number of 22 and atomic weight 47.9 (Table 2.5). It is a strong, lustrous, corrosion-resistant light metal, with many chemical similarities to silica and zirconium, a first transition group element. In aqueous solution, titanium has some similarities with chromium and vanadium, especially in the lower oxidation state. In its pure state, titanium is not soluble in water but is soluble in concentrated acids, and forms a passive but protective oxide coating (leading to corrosion-resistance) upon exposure to air. At room temperatures or ambient conditions, it resists tarnishing, by forming an oxide layer, with an average thickness of 2-7nm (Brunette et al., 2012, Mohammed et al., 2014), resulting in different stochiometries (Fraker et al., 1983). The Ti oxide layer consists mainly of TiO_2 (rutile), with oxidation state of 4^+ (Aniołek et al., 2015, Bessho et al., 1995), and some less stable Ti2O3 and TiO with oxidation states of 3^+ and 2^+ respectively (Jeong et al., 2000). It is this stable, repassivating, chemically inert, corrosion-resistant, and thermodynamically stable oxide layer of highly negative Gibbs' free energy of oxide formation (ΔG_0^{298} per mol of oxide formed = -888.8 kJ/mole) that accounts for the prominent bioinertness of titanium (Brunette et al., 2012). When heated in air, it forms the dioxide, TiO_2. It also combines with the halogens, and reduces the water vapour to hydrogen

and the dioxide. It reacts similarly with hot concentrated acids, forming a trichloride with hydrochloric acid. Salts of all the three oxidation states are common (Diebold, 2003).

In spite of the critical importance of the oxide layer, the existing knowledge and understanding of its properties and formation during Ti implant manufacture is however not at pace with its applications.

The surface chemistry by way of surface composition or charges on titanium implants also vary greatly. These variations depend on their bulk composition and the surface treatments they are subjected to. These variations are also critical to protein adsorption and cell interaction (Le Guéhennec et al., 2007). Osseous and dental implants are usually made from commercially pure titanium (cpTi), of varying degree of purity (graded 1-4) or titanium alloys. The purity is characterised by the content of iron, carbon and oxygen.

Support structure implants are mostly made from grade 4 commercially pure titanium, the strongest of the different grades. However, Ti6Al4V (a grade 5 titanium-aluminium-vanadium alloy), with greater yield strength and fatigue properties than the pure titanium, is the alloy of choice (Steinemann, 1998). The surface chemistry also affects the hydrophilicity of titanium implants surface, in the biological environments where hydrophilic surfaces are more preferable to hydrophobic surfaces (Bagno and Di Bello, 2004, Le Guéhennec et al., 2007, Giavaresi et al., 2003).

Table 2.5 Summary of the physical properties of Titanium.

Atomic number	22
Group	4
Period	4
Block	D
Relative Atomic mass	47.90 $g.mol^{-1}$
Electronegativity according to Pauling	1.5
Density	4.51 $g.cm^{-3}$ at 20°C
Melting point	1660 °C

Boiling point	3287 °C
Vanderwaals radius	0.147 nm
Ionic radius	0.09 nm (+2); 0.068 nm (+4)
Isotopes; key isotope	8; ^{48}Ti
Electronic shell configuration	[Ar] $3d^1$ $4s^2$
Energy of first ionisation	658 kJ.mol $^{-1}$
Energy of second ionisation	1310 kJ.mol $^{-1}$
Energy of third ionisation	2652 kJ.mol $^{-1}$
Energy of fourth ionisation	4175 kJ.mol $^{-1}$
Discovered by	William Gregor in 1791

2.4.2. Mechanical and Physical Modifications

The remodelling, removal and treatment of material surfaces by the application of physical forces constitute mechanical surface modification (Alla et al., 2011). This is usually achieved by processes involving severance or abrasive action or that lead to the deformation of the surface. The most commonly used mechanical processes are machining, particle blasting, grinding and polishing (Alla et al., 2011, Ellingsen et al., 2006a). These can be used to generate particular characteristic surface topographies and compositions. Machining (lathing, milling and threading) produces surface finishes dependent on the machining parameters such as tool speed, tool pressure and lubricant used. The resulting surfaces are characterised by grooves and ridges generally oriented along the machining direction, with roughness values or mean arithmetic roughness (Ra) range of 0.3-10 µm, measured using an optical or stylus profilometry (Larsson et al., 1996) (Wennerberg et al., 1996). The surfaces are plastically deformed (Ellingsen et al., 2006a, Lausmaa, 2001). Mechanical grinding and polishing are similar processes as they both remove part of the material surface by means of a hard abrasive, pressure and lubricant. Grinding, involving the use of coarse particles however removes the surface at a faster rate, creating relatively rougher surface topographies. For example, a P60 (with mean silicon carbide (SiC) particle size of 250 µm) abrasive grinding results in a mean surface roughness of 5-6 µm (Bowers et al., 1991). Polishing essentially involves using a fine abrasive

material, similarly applied to a revolving platen or belt, and the implant surface brought into direct contact with the moving abrasive surface. Coarse abrasive papers of silicon carbide (SiC) or alumina of grit number P120-800 are employed for the initial grinding process. A finer abrasive of about P1200 grit, of SiC, alumina or diamond follows the coarse grinding to produce extremely fine and smooth surfaces. The desired mirror-finished surface may be achieved by the use of a porous neoprene self-adhesive OP-Chem polishing cloth onto which a silica suspension is applied.

Grit or abrasive blasting is another process used to modify the surface properties of metallic implant devices. In this technique, the surface of the metallic implant is bombarded with particles suspended in suspension or hard dry particles travelling at high velocity. Different particle sizes of alumina, silica and other ceramics are used for grit blasting, mainly to descale and roughen surfaces in a bid to increase the surface area of metallic implants for improved osteointegration. Shot peening is a modified form of grit blasting, used to introduce compressive stresses on the implant material surface and to confer specific surface topographies, depending on the size of the particles used (Lausmaa, 2001, Wieland et al., 2002).

Mechanical or physical surface modification methods, involving the physical treatments such as machining, blasting, grinding and polishing, result in changes to the physical surface properties such as roughness and wettability. This has been demonstrated to enhance cell adhesion, differentiation and proliferation (Iskandar et al.).

Other physical methods include plasma spraying (under atmospheric or vacuum conditions, for creating titanium and CaP coating on titanium surface), sputtering (employed to deposit thin films on implant surfaces to enhance mechanical properties such as wear and corrosion

resistance, and to improve biocompatibility and biological activity), and ion deposition. (Chu et al., 2002, Jones, 2001)

2.4.3. Chemical Modifications

The chemical methods are based on the chemical reactions that take place on the interface between the biomaterial and a solution. These methods include chemical treatment with acids, alkali, sol-gel, hydrogen peroxide, chemical vapour deposition and anodization. These methods are widely used to modify surface roughness and composition, and to enhance wettability or surface energy. Acid treatment removes the surface oxide and contamination leading to a clean and homogenous surface. Hydrochloric acid, sulphuric acid, hydrofluoric acid, and nitric acid are the acids commonly used. Acid treatment of surfaces results in uniform roughness with micro pits in size range of 0.5-2 µm, increasing the surface area, and thus improving bio-adhesion. Acid treatment also promotes the migration and retention of osteogenic cells at the implant surface, enhancing osseointegration (Takeuchi et al., 2003).

Alkali treatment involves immersion of the biomaterial in either sodium or potassium hydroxide (a process referred to here as pre-treatment), followed by heat treatment after rinsing in distilled water. This leads to the formation of a bioactive, nano-structured sodium titanate layer on the implant surface. This surface then acts as a site for the subsequent *in vitro* nucleation of calcium phosphates when immersed in a calcium hydroxide solution or simulated body fluids (SBF) (Lee et al., 2012).

The chemical composition or charges on the ready-to-use titanium implant surface, which differ depending on their bulk composition and surface treatments, are critical for protein adsorption and cell attachment. This also affects the hydrophilicity of the surface. The suggestion is that highly hydrophilic Ti surfaces (with contact angle measurements ranging from 0°) are preferred to hydrophobic ones (contact angle measurements up to 140°) with

regards to interactions with biological fluids, cells and tissues (Giavaresi et al., 2003, Bagno and Di Bello, 2004, Zhao et al., 2005, Buser et al., 2004a). Nevertheless, in vivo studies performed by Albrektsson and co-workers (Wennerberg et al., 1990, Carlsson et al., 1989) did not adequately demonstrate higher osseointegration for hydrophilic surfaced implants.

However, the chemical modification strategy presents the simplest means of introducing consistent, standardisable modifications to the metallic implant surface.

2.4.4 Mechanism of Action for Sodium Titanate Formation

$TiO2 + NaOH \rightarrow HTiO_3^- + Na^+$ *(Liu et al., 2004)* *Equation 2.1*

The mechanism of action for sodium titanate formation in this work is similar to the mechanism proposed by Kim et al., (Kim et al., 1996, Kim et al., 1997a). A critical difference however is that, whereas Kim et al employed the commercially pure Ti surface covered with up to 10 nm of natural oxides of Ti (Davis, 2000), this work primarily examined and compared Kim's approach with the mechanically modified to a mirror-finished Ti surface, and found the later superior with respect to better incorporation of other ions onto the Ti surface.

On immersing the samples in NaOH solutions, the titanium surface oxide layer reacts with the hydroxyl groups, leading to the breakup of the oxide layer (Prusi and Arsov, 1992).

$TiO_2 + OH^- \rightarrow HTiO_3^-$ *Equation 2.2*

This leads to a direct interaction between titanium and alkali solutions. Alternatively, there is a migration of the OH^- ions through the structural defects of the thinner or dissolving parts of the natural oxide film (Prusi and Arsov, 1992), leading to the hydration of the Ti metal.

The reactions (Healy and Ducheyne, 1993) between the Ti surface oxide coatings and the NaOH solution may occur as

$TiO_2 + 2H_2O \leftrightarrow Ti(OH)_4$ *Equation 2.3*

The $Ti(OH)_4$ is in equilibrium with $Ti(OH)_3$ and OH^- as described by

$Ti(OH)_4 \leftrightarrow Ti(OH)_3 + OH^-$ *Equation 2.4*

This is followed by the transformation of $Ti(OH)_3$ into hydrated TiO_2 layer:

$Ti\ (OH)_3 \leftrightarrow TiO_2.\ H_20 + 0.5\ H_2$ *Equation 2.5*

The hydrated TiO_2 produces negatively charged hydrates under a further hydroxyl attack:

$TiO_2.nH_2O + OH^- \leftrightarrow HTiO_3^-.\ nH_2O$ *Equation 2.6*

The negatively charged $HTiO_3^-.nH_2O$ then incorporates the positively charged Na^+ ions, resulting in the formation of the sodium titanate layer is formed on the surface of the Ti metal, by the NaOH pre-treatment.

$HTiO_3^-.nH_2O + Na^+ \rightarrow Na^+HTiO_3^-.nH_2O$ *Equation 2.7*

The hydrated sodium titanate has been shown to form spontaneously on the surface of the Ti sample in concentrated sodium hydroxide solution (Chen et al., 2007, Kokubo et al., 1996). This spontaneously formed sodium titanate gel is however been found to be unstable (Kim et al., 1997a, Tsai and Teng, 2006), and has been dehydrated and transformed into an amorphous form, and then densified at temperatures ranging from 400 to 600^{o}C, or the crystalline rutile form at temperatures above 700°C (Kim et al., 1997a, Pattanayak et al., 2011, Tsai and Teng, 2006).

The instability of the sodium titanate sol-gel (Kim et al., 1996) however forms the basis of its ion-exchange (Sun and Li, 2003) ability, a property that was harnessed in this study to introduce other ions onto the titanium surface, and forms the novelty in the introduction of bone-apatite enhancing calcium, and anti-microbial properties conferring silver and zinc onto the titanium surface, in a hydrothermal process.

It has also been suggested that this also stimulate the formation of natural HA when a treated implant is placed in the body. In contact with (S)BF, calcium ions exchange with sodium ions from the sodium titanate to form calcium titanate. The calcium on the surfaces then bonds with

phosphate, eventually forming the apatite which provides a favourable environment for attracting osteogenic cells and the initiation of the osseointegration process (Chosa et al., 2004).

Chemical dissolution and oxidation results from the chemical treatment of implant surfaces with hydrogen peroxide. When titanium surfaces react with hydrogen peroxide, Ti-peroxy gels are formed. The thickness of the gel layer formed can be regulated by adjusting the treatment time. It's been demonstrated that, the thicker layer of the titania gel layer formed on peroxy or alkali treatment, the more apatite deposition occurs when immersed in SBF (Tavares et al., 2007).

The process by which oxide films are deposited on the surface of the implants by means of an electrochemical reaction is known as anodization. In the process, the surface to be oxidized serves as the anode in an electrochemical cell. A dilute acid solution serves as the electrolyte. The thickness of the oxide layer can be modified by varying the parameters of the electrochemical process. These anodized surfaces demonstrate improved cell adhesion and tissue bonding (Landolt et al., 2003, Kim and Ramaswamy, 2009).

The sol-gel process (Schwarz et al., 2009, Le Guéhennec et al., 2007) used in ceramic coatings deposition has been employed to deposit hydroxyapatite (HA) coatings on other implant surfaces. This results in a less than 10 µm thin layer formation, a process that improves the biological activity of the titanium implants and enhances bone formation and osteointegration. Materials such as titanium oxide (TiO_2), calcium phosphate (CaP), TiO_2-CaP composite and silica-based coatings can be coated on the biomaterial surface by this technique.

Chemical vapour deposition involves chemical reactions between chemicals in the gas phase and the surface of the substrate. This leads to the deposition of a non-volatile compound on the substrate surface (Jones, 2001).

The novelty of this study lies in the attempt to harness the ion-exchange capacity of the sodium-titanate formed on treatment of the Ti surface with sodium hydroxide aqueous solution, to introduce calcium ion onto the Ti surface. This technique, compared to the exposure to SBF method, has the advantage of exposing the surface to higher amounts of calcium, as opposed to the quantities limited to the dictates of the SBF composition formula. The expectation is that, this will result in a higher calcium incorporation onto the Ti surface.

Similarly, this method could also readily facilitate the incorporation of antimicrobial silver and zinc ions onto the Ti surface in a controlled, concentration and/or surface area dependent manner. Furthermore, the sodium hydroxide pre-treatment of the Ti surface also presents the possibility of incorporating various combinations of calcium, silver and zinc ions onto the Ti surface, in a concentration, ionic size and/or competition driven manner. This means of introducing multi-ions on the Ti surface eliminates the possibility of overlays and it attendant propensity for delamination, common with methods such as sputtering and spraying.

2.4.5. Biological Modification

B. Ratner had postulated in 2001 that the next evolution in titanium implants would be via biologically inspired specific surface modification (Ratner, 2001), as the science of biocompatibility and osteointegration gathers pace, and biomaterial science becomes an increasingly collaborative field of study. In furtherance of this, Le Gu´ehennec and co-workers in 2005 suggested the incorporation of biologically active drugs into titanium dental implants as a future trend in surface treatment of titanium implants for rapid osseointegration (Le Guéhennec et al., 2007). A review of the objectives behind this approach to surface modification suggests that, this approach is motivated, amongst others, by the quest for a more controlled interaction between the implant surface and the surrounding tissue. This could be specifically distilled down to initiating cell-selective response such as osteogenic cell adhesion and differentiation into specific osteoblast phenotype; disruption of bacterial attachment

capacity, thus reducing infection rate; reduction of inflammation risk; and enhancement of the long-term performance and reliability of implant devices (Schuler et al., 2006b).

A review of current literature suggests that, surface (bio-)chemistry modification of implants in direct contact with biological tissue is achievable through, but not limited to, the use of biological species such as peptides and proteins; organic nano-scale thin monomolecular adlayers interlinked with biomolecules or drugs; biomolecules entrapped in micro-scale thin layer of calcium phosphate/hydroxyapatite; and biomolecules incorporated into micro/millimetre-scale thin layer of hydrogels (Schuler et al., 2006b). Simply dipping the implant into a solution of biological molecules is the easiest way of mobilizing biological molecules onto the implant surface, as is the case in adsorbing fragments of fibronectin and vitronectin onto titanium surfaces (Ku et al., 2005). However, a more controlled means of biological surface modification essentially involves coating the implant surfaces with bone-stimulating agents such as growth factors. Candidates for this include members of the transforming growth factor (TGF-β) superfamily, and in particular bone morphogenetic proteins (BMPs), TGF-β1, platelet-derived growth factor (PDGF) and insulin-like growth factors (IGF-1 and 2) (Le Guéhennec et al., 2007, Boyne and Jones, 2004, Liu et al., 2005b).

The amount of proteins particularly, and the amount and type of other biological species in general, that become adsorbed onto the implanted titanium surface in contact with blood and other body fluid is considered a non-specific response of the body to the implant material (Tengvall, 2001). Ultimately, biological surface modifications seek to eliminate or reduce the non-specific responses, augment bio-responsiveness to the implant material, and in the case of osseous tissue replacement, facilitate and speed up integration and the healing process locally. However, the high specificity of biological modifications, which correlate to gene expression and immune response at the implant-tissue interface, may limit its application in the general

population. Reproducibility and standardization of the biologically modified implant surface may also present additional challenges.

2.5. Surface Roughness and Topography

The success or failure of devices used as implants depends on creating and maintaining an interface between the device and the surrounding (osseous) tissue. This underlines the osseointegration phenomenon, which is a formation of body tissues around the implant device, leading to a direct and stable anchorage between the device and surrounding tissue (Alla et al., 2011).

Thomas and Cook in 1984 (Thomas and Cook, 1985) investigated the influence of 12 parameters on bone response to implant material in close proximity with bone tissue. Of the parameters considered, only the surface parameters, particularly surface texture or roughness, was found to be of most significance. This was however so only for variables influencing implant fixation by direct bone apposition, evaluated by *in vivo* means, and mechanical push-out tested. Subsequently, two main criteria have been employed in examining the effect of surface roughness on osteointegration; histometrical measurement of the amount of bone-implant contact (BIC) as a percentage of the surface area (Trisi et al., 1999), and biomechanical measurement of interface shear strength or removal toque values (RTVs) (Koh et al., 2009). It is now been firmly established from both clinical and *in vivo* studies, that the topography of an implant surface plays an important role in the osteointegration process (Zhu et al., 2004, Wennerberg and Albrektsson, 2009, Wennerberg and Albrektsson, 2000, Tambasco de Oliveira and Nanci, 2004, Shalabi et al., 2006a, Mendonça et al., 2008, Gittens et al., 2011). Implant surface topography is generally characterized by a succession of peaks and valleys, quantified by means of either 2D profiles or 3D parameters (Table 2.6) (Albrektsson and Wennerberg, 2004a).

Alongside other factors, tissue response to implant is predominantly controlled by the texture or roughness of the implant surface. Contrasted with smooth surfaces, textured surfaces provide more surface area for tissue integration, and allows for ingrowth and anchorage of tissues (Lacefield, 1999, Albrektsson T, 2003). A 1999 meta-analysis study comparing endosseous dental implant surfaces suggested that, rough titanium surfaces encourages cellular response better than polished smooth surfaces (Cochran, 1999).

However, a systematic review study in 2009 pointed out that, a supposedly 'rough' surface in one study was frequently 'smooth' in another study, depending on the method of profilometry used. It has also been erroneously assumed in many instances that the method of surface preparation identified the surface roughness (Wennerberg and Albrektsson, 2009, Cooper, 2000).

Table 2.6 Summary of 2D/3D surface profile evaluation parameters

2D Profile evaluation	
Ra	Roughness average of profile (amplitude parameter), defined as the integral of the absolute height values of peaks and valleys along the evaluated profile.
Rz	Vertical parameter: mean height from peak to valley along the roughness profile
Rsm	Horizontal parameter: average inter-peak distance along the roughness profile
3D Profile evaluation	
Sa	Amplitude parameter: average surface height deviation amplitude, calculated on 2D standards extended to 3D standards
Sds	Spatial parameter defined as the density of summits, i.e. the number of peaks per area. This parameter is sensitive to noisy peaks and should be interpreted carefully. Sdr%. Hybrid parameter integrating both the number and height of peaks on a determined surface, and expressing the spatial density
Sdr	Defined as the developed interfacial area ratio and expresses the increment of the interfacial surface area relative to a flat plane baseline. For a totally flat surface, Sdr = 0%. When Sdr = 100%, it means that the roughness of a surface doubled its developed area

Based on the scale of surface features, particularly the amplitude of the mean height deviation (Sa), A. Wennerberg and co-workers subsequently classified implant surfaces as: minimally rough (0.5-1 μm), intermediately rough (1-2 μm) and rough (2-3 μm) (Wennerberg and Albrektsson, 2000, Wennerberg and Albrektsson, 2009, Stanford, 2008). Surfaces with mean roughness measure of 1-100 nm have been classified as nano-rough surfaces (Mendonça et al., 2008). Macro surfaces have roughness range of millimetres to tens of microns. Macro scale roughness increases the mechanical interlocking between the implant and bone surface, helping in initial implant stability. This however introduces a risk of peri-implantitis (Deeksha Arya, 2012). In addition to providing a greater bone-to-implant contact compared to the macro surface, micro scale roughness profiles have been shown to enhance osteoconduction (in-migration of new bone) and osteoinduction (differentiation of new bone) along the implant surface, by using the implant as a localised delivery channel for bioactive agents (adhesion matrix or growth factor such as BMP (Stanford, 2008, Alla et al., 2011). Nano scale topography of implants resulting in a more textured surface, leads to an increase in surface energy. This increases its blood wettability and therefore the spreading, and binding fibrin and other matrix proteins (Wennerberg and Albrektsson, 2009, Sul, 2003). Nano surfaces are therefore critical in the adsorption of proteins, the adhesion, proliferation and differentiation of osteoblasts, and speed up bone ingrowth and osseointegration (Mendonça et al., 2008, Sittig et al., 1999).

Topographic variations, isotopic (without any dominating directional plane) or anisotropic (with distinctive and regular patterns) are achieved by either an additive or ablative methods. The additive methods confer controlled roughness onto the surface by introducing new materials of controlled sizes onto the surface (Popper, 2002). Plasma spraying, hydroxyapatite coating, deposition of bioactive materials, sputtering and antibacterial coating are prime examples. The ablative methods are subtractive procedures, and include machining, polishing, acid etching, and grit blasting (DM, 2001, Ellingsen et al., 2006b, Kohles et al., 2004). These

methods fall into the broad classes of physical, mechanical, chemical, thermal and laser methods, and in addition to modulating the surface topography, some also confer sterility to the implant surface, as well as play a role in disrupting bacterial biofilm formation on the implant surface.

Poor bone quality or volume, characterised by poor fracture resistance and microarchitecture, accumulated microscopic damage, poor quality of collagen, the size of mineral crystals, and the rate of bone turnover (Weng et al., 2003, Sievänen et al., 2007), is the main clinical indication for using an implant with a rough surface. In this instance, high levels of loading would benefit from early and high bone-to-implant contact. In these cases, Ti implants with a rough surface have been shown to facilitate greater bone-to-implant contact, higher resistance to torque removal (Wennerberg and Albrektsson, 2010, Wennerberg et al., 1998), superior clinical outcomes than smooth surfaces (Conner et al., 2003, Zetterqvist et al., 2010). However, the evidence from the Cochrane collaboration is not conclusive on the superiority of any particular implant surface (Conner et al., 2003, Zetterqvist et al., 2010).

The nanometer range surface profile plays a critical role in proteins adsorption, and osteoblastic cells adhesion, and therefore the rate of osseointegration (Schneider et al., 2003, Brett et al., 2004). However, reproducible nanometer range surface roughness is difficult to achieve with the chemical treatments techniques. Furthermore, the optimal surface nano topography for selective adsorption of proteins leading to the adhesion of osteoblastic cells and rapid bone apposition is poorly researched, poorly understood and unknown (Bhat and Balaji, 2014, Surender et al., 2011, Le Guéhennec et al., 2007).

2.6. Implant Device Infections and Biofilm Formation

The incidence of patients, particularly the elderly and trauma sufferers requiring resection surgeries on internal fixation devices or implants has been on a steady increase. This is in spite of the steady advances made in the prevention and treatment of implant associated infections. A primary contributing factor to this is the lifelong risk for bacteria seeding on implanted devices (Zimmerli et al., 2004). Medical device insertion has become a conventional life-saving and lifestyle improving procedure. As at 2001, estimates put total hip replacement around the world at approximately one million a year, and a quarter of a million knee replacements procedures. Indications are that, approximately 30% of all hospital patients have in place one or more vascular catheters, and 10% of hospitalised patients have an indwelling urinary catheter (Schierholz and Beuth, 2001). It's been reported that, exposure to infection arising from invasive procedures requiring the insertion of medical devices is one of the most significant factors accounting for the $11 billion annual bill for the approximately 2 million or 45% of all nosocomial infections. Though the occurrence of infections associated with prosthetic joints are less common than aseptic failures, they present far more devastating complications, with attendant substantial cost and morbidity (Steckelberg and Osmon, 2000, Trampuz and Widmer, 2006). While frantic efforts are underway globally to minimise infection risks, orthopaedic surgical site infections (SSI) remain staggeringly high (Cats-Baril et al., 2013). Current (2013) figures suggest close to 2.5% of primary hip and knee arthroplasties, and up to 20% of revision arthroplasties become complicated by periprosthetic joint infection (PJI) (Gallo et al., 2014). Some authors believe these figures are not only underestimates, but also on the rise, with associated increased morbidity, mortality and enormous cost to healthcare systems globally (Dale et al., 2009, Aggarwal et al., 2014, Zmistowski et al., 2013, Kurtz et al., 2012). For primary hip replacement patients, the infection rate is approximately 1% during the first two years. This is approximately 2% for knee replacement patients. The infection rate

rises considerably to between 5% and 40% after revision surgery. In all, approximately 5% of all implant devices become infected (Darouiche, 2004). Though they are less common than catheter-related infections, surgical implant related infections are on the whole more difficult to manage and require a more prolonged antibiotic therapy, and in some cases, repeated surgical procedures (Darouiche, 2004). Reviews also indicate that, orthopaedic surgical site infections (SSIs) prolong a patient's total hospital stays by an average of two weeks, doubles rehospitalisation rate, and increase healthcare cost by more than 300%. These patients are also shown to have significantly greater physical limitations and reduction in the health –related quality of life (Whitehouse et al., 2002). The risk factors influencing susceptibility to infection are mainly related to the implant and the implantation technique. However, some studies have demonstrated that age of patients, body mass index, surgical site, lifestyle and co-morbidities as concomitant factors significantly increase susceptibility (Lindeque et al., 2014, Peel et al., 2011, Berbari et al., 2010, Lamagni, 2014). The implant factors include material of the implant, the design and the surface properties of the implant (Arens et al., 1996b).

Implant devices disrupt epithelial or mucosal integrity, damaging the barrier and thus predisposing to infection, and supporting microbial organisms by acting as reservoirs. They therefore impair host defence mechanism, and in contaminated state, act as a source of persistent chronic infection or tissue necrosis. Infections resulting from this are highly resistant to host defence mechanisms and to antibiotics, and may persist until their removal.

The adhesion mechanism between tissues cells or microorganisms and the implant surface have been found to be based on both the receptor or membrane molecules and physical factors such as Van der Waals forces and hydrophobic interaction at the micron scale of the material surface. It has been demonstrated by electron microscopy studies that bacteria have a preference for micron-scale rough surfaces, which also improve tissue adherence and bio-integration (Gristina, 2004a, Cordero et al., 1994).

Staphylococcus aureus , *Staphylococcus epidermidis, Pseudomonas* or other Gram-negative rods are mainly responsible for implant-associated infections (Belt et al., 2001). In clinical setting, the infection may be polymicrobial. A retrospective study of 132 consecutive patients with an internal-fixation-device-associated infection indicated this in 27% of the cases. Of this, the most common pathogens were *S. aureus* (30%), coagulase-negative *staphylococci* (22%), and Gram-negative bacilli (10%) (Trampuz et al., 2006). *Staphylococcus aureus* remains the leading cause of both the SSIs and PJIs, and the prevalence of methicillin-resistant *S. aureus* (MRSA) SSI and PJI is an added factor to the increasing financial burden (Parvizi et al., 2010a, Jafari et al., 2010, Aggarwal et al., 2014, Wagner et al., 2011, Hu et al., 2011, Juan et al., 2010, Lamagni, 2014).

The pathogenesis of implant-related infections can be categorised per the route of infection into three; perioperative, contiguous and haematogenous. Perioperative infection results from inoculation of microorganisms into the surgical wound during surgery or immediately after. Symptoms of infections usually show within two weeks, especially if of highly virulent nature, such as caused by *S. aureus* and Gram-negative bacilli. Generally, these infections occur exogenously (pre-operatively) by the penetrating trauma itself, or (intra-operatively) during insertion of the device, or (post-operatively) during disturbed wound healing (Arens et al., 1996a). Wound contamination due to open fractures or from an adjacent focus such as skin and soft tissue lesions may lead to contiguous infection of the implant device. Haematogenous infection of surgically implanted devices result from bacteraemia or microbial spread through the blood or lymph from a distant focus if infection such as the skin, lung or urinary tract. Symptoms show between 2 to 10 weeks especially if caused by low virulence organisms such as coagulase-negative *staphylococci* (Trampuz and Zimmerli, 2006).

Clinical signs of early infections include persisting local pain, erythema and oedema, wound healing disturbance, large hematoma, and fever, common with highly virulent organisms such

as *S. aureus*. In wound healing disturbance cases, necrosis of the wound edges or postoperative hematoma are commonly observed. Delayed or late infection usually presents as persisting or increasing pain, pseudo-arthritis, implant loosening, and occasionally, the development of a sinus tract. In some cases, however, clinical signs and symptoms of infection may be entirely lacking. Also, the classic presentation of infection due to any microorganism may be delayed or absent due to initial antimicrobial treatment, which may have been insufficient for complete microbial eradication (Table 2.7). Low inoculum or virulence of microorganisms introduced during penetrating trauma or peri-operatively may also account for delayed infection with an insidious onset of systemic or local symptoms (Murdoch et al., 2001).

Table 2.7 Summary of classification of infections associated with fracture fixation devices.

Classification	**Characteristic**
Per the route of Infection	
• Perioperative	Inoculation of microorganisms into the surgical wound during surgery or immediately thereafter
• Contiguous	Wound contamination due to penetrating trauma (open fractures) or from an adjacent focus of infection (skin and soft-tissue lesions)
• Haematogenous	Microbial spread through blood or lymph from a distant focus of infection (eg, skin, lung, urinary tract)
Per the onset of symptoms after implantation	
• Early infection (< 2 weeks)	Predominantly acquired during trauma or implant surgery, caused by highly virulent organisms (eg, *S. aureus*, Gram-negative bacilli)
• Delayed infection (2−10 weeks) and late infection (> 10 weeks)	Predominantly acquired during trauma or implant surgery and caused by low virulence organisms (eg, coagulase-negative *staphylococci*); occasionally caused by hematogenous seeding from remote infections

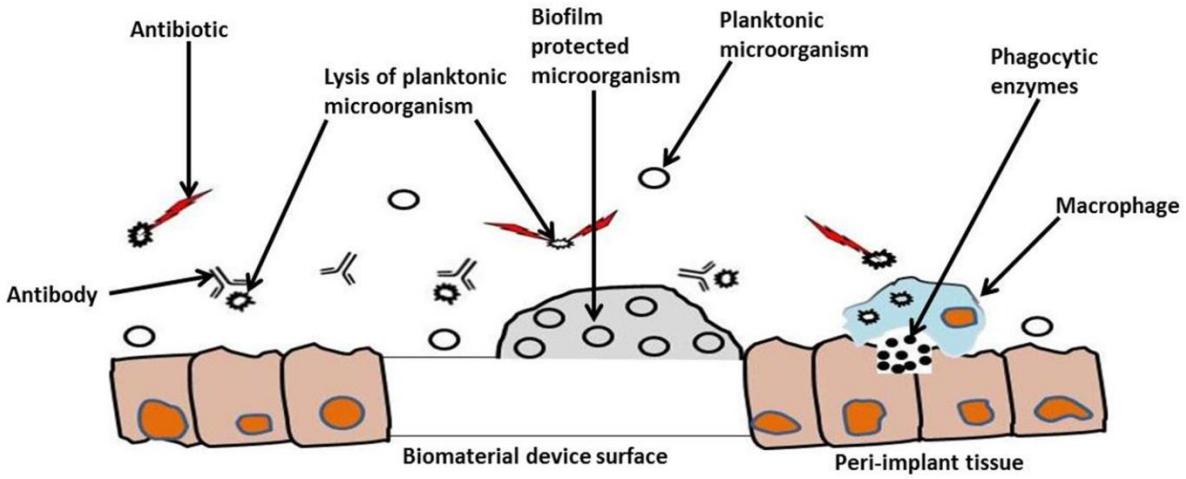

Figure 2.3. Representation of planktonic microorganisms, killed by antibiotics and the immune system, and biofilm microorganisms, attached to a surface and protected in an extracellular matrix. The altered phenotype of the biofilm enables bacteria colonies to survive adverse condition it is presented, thus remaining a persistent source of re-infection.

The pathogenesis of implant associated infection involves interactions between the implant, the host and the microorganism (Costerton et al., 2005). A critical mechanism that enables bacteria to survive the host immune defences and also systemic antibiotic therapy is their biofilm forming ability. The Centre for Disease Control and Prevention (CDC) described a biofilm as microorganisms living in a self-organized community attached to surfaces, interfaces, or each other, embedded in a matrix of extracellular polymeric substances of microbial origin, while exhibiting altered phenotypes with respect to growth rate and gene transcription. The biofilm is the metabolic or accumulative phase of the bacterial cycle where using their pheromone-based quorum sensing mechanism of inter-bacterial communication, bacteria alter their behaviour (Jefferson, 2004a). This involves diminishing their cell growth and baseline metabolism rates, aggregation and expression of a cementing amorphous highly hydrated extracellular matrix substance in which they become encased. The typical biofilm formation mechanism, common amongst the genus *Staphylococcus* including *S. aureus* and *Staphylococcus epidermidis*, the two frequent bacteria implicated in implant infections, involves the production of the Polysaccharide Intercellular Adhesin (PIA). Other mechanisms involve extra-cellular DNA (eDNA), teichoic acid and accumulation associated proteins (Aap)

(Campoccia et al., 2010, Otto, 2008, Mack et al., 2004). The quorum sensing pheromones maintain the biofilm until maturation and the initiation of the next cell cycle, involving detachment, return to planktonic life and infection spread to other anatomic location. In the case of implanted devices, bacterial biofilm protects inner hidden cells from the host innate immune system by inhibiting phagocytosis of neutrophils in the poorly vascularised surface of the implant (Figure 2.3). It also creates a diffusion barrier or electrostatic repulsion and sequestration of antibacterial substances including cationic and anionic antimicrobial peptides (AMPs) (Otto, 2008, Vuong et al., 2004), and in the low metabolic state become insensitive to antibiotic concentration up to a third order magnitude. This may also account for the higher prevalence of antibiotic resistance associated with certain strains of biofilm forming bacteria (Arciola et al., 2005, Arciola et al., 2002, Anwar et al., 1990, Arciola et al., 2012).

The sequence of events in biofilm formation on a biomaterial surface starts with the formation of the so-called 'conditioning film' that covers the biomaterial surface. This is made up of proteins of macromolecules adsorbed from the biological environment in which the biomaterial is placed. Orthopaedic biomaterials are in direct contact with bone and blood; hence plasma proteins form the conditioning film. Similarly, dental implants adsorb salivary proteins, just as contact lenses adsorb lipid and protein components of tear fluid. This event occurs within seconds of exposure to a biological environment. Bacteria therefore adhere not to the bare biomaterial surface but to an adsorbed conditioning film. The next step consists of various mechanisms of microbial mass transport by which they reach the conditioned surface. These include diffusion, convection and sedimentation, common with oral dental implant infection. Direct contamination during surgery is however common with orthopaedic implants. It has also been demonstrated by Schmalzried et al. (1992) that the incidence of infection of haematogenous origin increases concomitantly with increase in follow-up period of patients (Schmalzried et al., 1992). In many cases, microorganisms are transported via the blood stream

to the conditioning film in a mass convective transport, causing late haematogenous infection post urogenital and dental infection (Pollak and Floman, 1983, Stinchfield et al., 1980, Lindqvist and Slatis, 1985). Initial microbial adhesion by means of exopolymer production is the next step in the biofilm formation sequence of events. This initial adhesion is reversible, the process being dependent on the physico-chemical properties of the biological environment, the microbial cell surface and biomaterial surface, (the properties being exploited in this work to confer antibacterial characteristic to the implant surface). The process is made irreversible through exopolymer formation which firmly anchors the microbial cell to the biomaterial surface, forming the so-called 'glycocalix' (Costerton et al., 1987, Gristina, 2004b), an accumulation of glycoprotein on the outer surface of the biomaterial that confers protection against antibiotic and environmental attacks (Neu and Marshall, 1990, Tang et al., 2013). In most cases of orthopaedic biomaterial associated infections, the biofilm colony is mono-microbial. Poly-microbial biofilms are common in urinary and oral infection however, due to the so-called co-adhesion of other strains and species to an existing biofilm. The final step in the sequence of events leading to biofilm formation is the growth of adhering microorganisms. This is the main mechanism of multiplication of the biofilm leading to an increase in the thickness of the original film, onto which new layers are added and bacteria find room to grow and multiply. Organisms at the periphery of the expanding film may detach and be carried to another locus. This is an important step in the septic process.

Microbial adhesion is essentially an interaction between two surfaces in a biological bathing medium, leading to the attachment of microbial organisms to a surface. The microbial and the substrata surface properties are therefore important in the interaction. A microbial-resistant surface will therefore disrupt adhesion to tissue, provoking an inflammatory response (Gristina, 1987).

A combination of attractive Lifshitz-Van der Waals forces, electrostatic and attractive or repulsive acid-base interactions influence the initial adhesion of microbial organisms to the inert substratum. The Lifshitz-Van der Waals forces are attractive long-ranged forces and comes into effect when the interacting surfaces are about 50-100 nm of each other. The acid-base interactions are either attractive or repulsive depending on the surface chemistry of the microbe and substratum. The Lifshitz-Van der Waals forces on surfaces is observed in the contact angle formed by liquids on surfaces. A surface is said to be 'hydrophobic' when water droplets spread poorly over the surface, forming a high contact angle. The surface is 'hydrophilic' when the spread is even with a low contact angle. The types of proteins that are adsorbed from biological bathing fluids such as plasma, urine, saliva or tear fluid, onto a biomaterial surface depends on the hydrophobicity of the biomaterial's surface and the conformations in which these proteins exist. Hydrophobicity therefore control microbial adhesion to conditioning films. Hydrophobic biomaterials have demonstrated less attraction to biofilms than hydrophilic ones (Everaert et al., 1997, Weerkamp et al., 1990).

Electrostatic interactions are usually repulsive, as most naturally occurring and synthetic surfaces are almost always negatively charged (Fröhlich, 2012). The interactions are usually small in a physiological environment due to the high ionic strength of physiological bathing fluids (Thevenot et al., 2008a). Attempts to create highly negatively charged biomaterial surfaces to repel the negatively charged microbe, thus hampering biofilm formation have had only limited success (Bahar and Ren, 2013). However, the growth of microbes has been demonstrated to be slower on positively charged biomaterial surfaces. The suggestion is that the resulting adhesion from the attraction of the oppositely charged molecules may be too strong to allow for cell division and replication (Hamdan et al., 2006).

Another biomaterial surface feature which is important with regards to biofilm formation is roughness. It is however still being debated as to whether microbial adhesion is more or less

extensive on a smooth surface than on a rough surface (Verran and Maryan, 1997, Taylor et al., 1998, Quirynen and Bollen, 1995).

There are four primary incentives for biofilm formation by bacteria. These are: protection from harmful conditions created by the host and medication, sequestration or colonization of a favourable nutrient-rich area, utilization of cooperative benefits of community as in sharing of metabolic load, and finally as the default growth mode (Jefferson, 2004b).

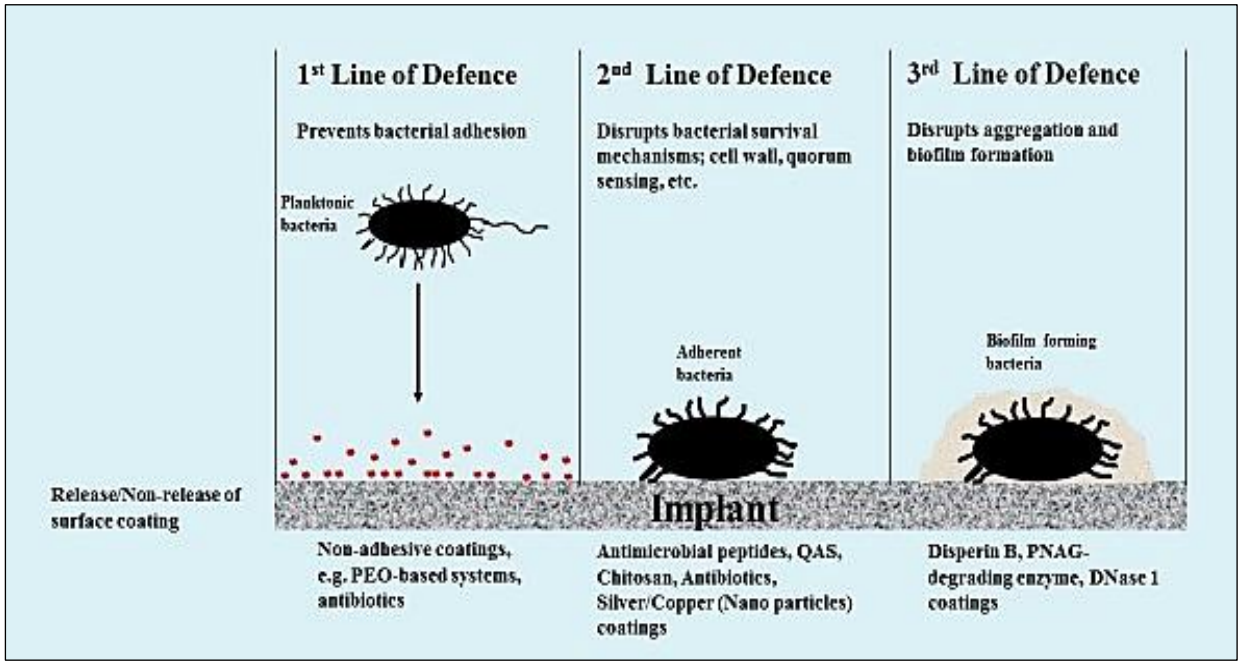

Figure 2.4. Strategies for surface functionalization of implants for three different lines of antimicrobial defence (Arciola et al., 2012). The first defensive line seeks to prevent bacteria attachment to the implant surface using non-adhesive coatings. The second line of defence targets the bacteria post adhesion to the implant surface, whereas the third defensive line agents are designed to disrupt the bacteria's defensive biofilm forming mechanism.

The classical surface functionalization strategies (Figure 2.4) for addressing implant associated infections involves three different lines of defence. Each of these employs a specific additive surface modification procedure to incorporate a microbial activity disrupting agent onto the implant surface. These agents may be leaching or non-leaching, and target specific essential mechanisms in the microbial adaptive pathway in the implant surface colonialization process, a phenomenon loosely described by Grestina as the 'race for the surface' (Busscher et al., 2012b, Arciola et al., 2012). The first line of defence agents including Polyethylene oxide (PEO)-based systems are designed to prevent bacterial adhesion. The second defensive line

agents are selected to immediately disrupt the cellular functions of microbes that have become attached to the implant surface before the microbes have a chance to produce a protective biofilm (Campoccia et al., 2013). Classic agents in this group include antibiotics, chitosan, silver/copper nanoparticles, quaternary ammonium salts and antimicrobial peptides. The third line strategy using agents such as DispersinB, Poly-N-Acetylglucosamine (PNAG)-degrading enzyme and Deoxyribonuclease (DNase) 1, is designed to disrupt the biofilm and the bacteria embedded in the biofilm (Bruellhoff et al., 2010, Shah et al., 2013, Gökçen et al., 2013)

In the quest, therefore, for better and longer-lasting outcomes with regards to tissue replacing biomaterials and devices, titanium has rightly been identified as a comparably effective material, especially in orthopaedic applications such as joint replacements and bone pins, plates and screws for repairing broken bones. However, in its application, several questions and issues have arisen over the years that necessitated a closer look at its fabrication and application, in a bid to improve its (cost) effectiveness, performance and patients' lifestyle related outcomes. Chief amongst these is how to improves its prominent (surface)factors, to enhance its performance with regards to tissue integration, insertion site and heterologous originated bacterial colonization, and *in situ* longevity, in the light of increasing patient indications, resection surgeries and financial burden.

The classical surface functionalization strategy, comprising the additive methods such as coating, plasma spraying, sputtering etc., are expensive, requiring specialist equipment and/or environment, as is ion implantation and anodization. The natural formation of oxides on the Ti surface on exposure to atmospheric conditions, the said oxide rendering the Ti surface oxidatively inactive, suggests that, (surface)chemistry could provide an alternative, simpler and much more cost effective means of modifying the Ti surface to improve its performance as a biomaterial. Can this however be done, is the question for this work.

2.7. Aims

This study aims to develop simple surface modification strategies that confer antimicrobial properties to medical-application grade titanium, and simultaneously enhance titanium osseointegration.

2.8. Objectives of this Study

1. To physically and chemically modify the commercially pure titanium surface, by both ablative and additive methods, in a bid to enhance its osseointegration and confers antimicrobial characteristics to the novel surface.

2. To characterise the surface profile of the novel surfaces developed and the release of agents/elements implanted on the modified titanium surface.

3. To investigate the antimicrobial characteristics of the novel surface, using the biofilm-forming human pathogen *Staphylococcus aureus*.

4. To investigate the effect of the surface modifications on bone cell adhesion, proliferation and/or toxicity using the bone matrix forming osteosarcoma U2OS cell line as an *in vivo* osteogenic model

Chapter 3 : Methods and Equipment

3.1. Introduction

Several techniques were used primarily in the surface modification of the commercially obtained titanium. The thrust in the method employed being a simplification of techniques already in use, to cost effectively achieve similar and/or better results. This essentially involved modifying the titanium material surface by a physical abrasive means, in a bid to reduce the surface topography from a micro-scale to a nano-scale. This is followed by a thermo-chemical surface modification process which seeks to replicably further enhance the surface chemistry in a bid to promote a better interaction between titanium and bone matrix, i.e. promote osteo-integration, and confer antibacterial properties to the implant material. The surface modifications were then characterised by means of scanning electron microscopy, contact angle measurements, and atomic force microscopy. The physico-chemically modified titanium surfaces were then assessed for anti-microbial activity using the CDC biofilm reactor and inhibition zones measurements. The release profiles of the ions introduced onto the titanium surface were then determined by means of atomic absorption spectrometry. Finally, the effect of the various surface modifications on the adhesion and proliferation of bones cells was determined using U2OS osteo-sarcoma cells.

3.2. Sample Preparations

Commercially pure temper annealed titanium (cpTi) foil (300mm×300mm×1mm) of 99.6+% purity, obtained from Goodfellow, Cambridge, were cut into discs of 12mm diameter using a water-jet cutter (FlowWaterjet mach3, Flow, USA), at high pressure.

The flexibility and precision of a Waterjet cutter was employed to design and cut the titanium sheet into precise 12mm discs. The dimensional precision was important for use in the rods of

the biofilm reactor during the microbiological aspect of this work, as well as regarding the size of the 24-well plate used for investigating the respond of human osteogenic cells to the modified surfaces.

The discs were metallographically polished, as the first phase of the surface modification process, to remove the oxide, grease and surface impurities layer on the surface. The polishing was done using a Labol 8-12 Convertible Grinding/Polishing Machine (Extec Corp. Connecticut, USA), water and silica carbide (SiC) emery paper (Struers, UK) of progressively reducing grit sizes.

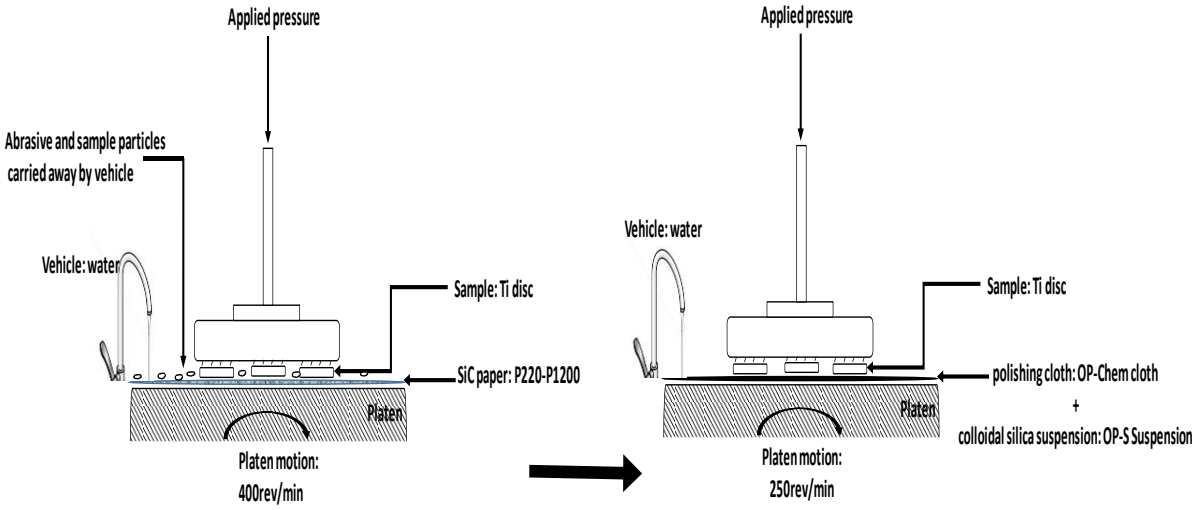

Figure 3.1. Schematic of the physical surface modification process. This essentially involved grinding and polishing the commercially pure Ti surface using a series of grit paper of reducing grit sizes, and finishing with OP-Chem cloth, until a mirror finish is obtained.

Using a padded double sided tape, the titanium discs were firmly attached to a hard-embedding resin (Scandiplast, Agar Scientific, UK). Starting with a grinding paper of grit size P220 affixed to the revolving platen of the grinding/polishing machine (Labol 8-12, Benetec, UK), the speed was set at 400 rev/s. The hard-embedding resin affix with the titanium discs was then held firmly against the revolving grit paper, under a constant overflow of water. The resulting grinding action's effect was periodically examined for homogeneity with the naked eye, and under a bright field (B.F.) illumination light microscope at 100x magnification (Olympus, UK), until a uniform surface of grooves corresponding to the grit size was observed. The grit size

was sequentially reduced from P220 to P320, then P500, P800 and finally P1200. The platen being thoroughly washed between each grit paper change, until the finest grinding result was observed under the light microscope at 100x magnification. In order to ensure that the previous rough grinding debris is removed when grinding by hand, the sample disc was rotated 90 degrees and continually ground until all the scratches from the previous grinding direction were removed. If necessary, the abrasive paper was replaced with a newer paper to increase cutting rates and reduce polishing time.

The platen of the machine was then changed, and the grit paper replaced with a porous neoprene self-adhesive polishing cloth (OP-Chem cloth, Struers, UK). This was initially wetted with the overflow of cold water and the revolving speed set at 250 rev/s, for a more controlled polishing asction. The titanium discs affixed to the resin were then periodically thoroughly washed under running water to remove all traces of grinding debris, and then firmly held against the revolving polishing cloth for the polishing action to take place. The cloth was intermittently wetted with a colloidal silica suspension (OP-S Suspension, Struers, Denmark), and the resulting effect periodically examined under the light microscope. These series of actions were repeated until a mirror finish, with no surface inconsistencies under the light microscope at 100× magnification, was obtained.

The discs were then thoroughly washed under running water and removed from the double-sided tape on the hard resin (Figure 3.1). The whole process was then repeated for the other side of the sample titanium disc, if needed. The mirror-finished polished Ti discs were designated polTi. The unpolished commercially pure group of discs were designated cpTi or unpolTi.

3.3. Chemical and Thermal Surface Treatments

An improved, simple and economical adaptation of the chemical bath deposition method (Pawar et al., 2011, Brémaud et al., 2007, Fernández-Lima et al., 2002) was used to modify and incorporate calcium, silver and zinc ions onto the surface of the physically modified titanium. The process involved a pretreatment with an alkaline solution followed by treatment with the aqueous solution of the ion of interest (Jambure et al., 2014, Kumar et al., 2008).

3.3.1. Pre-Treatment of Physically Modified Ti Surface

Pre-treatment of a titanium surface with alkaline such as sodium hydroxide has been shown to induce apatite formation through the formation of a porous, bioactive, ion-exchangeable sodium titanate complex on the titanium surface (Ravelingien et al., 2009, Clearfield and Lehto, 1988, Kim et al., 1997c, Sauvet et al., 2004, Štengl et al., 2006). The alkaline treatment has been shown to creates roughness on the sub-micrometre scale and negative charges on the surface (OH) that reduce nucleation barriers on the titanium surface (Oh et al., 2005, Akieh et al., 2008). The sub-micro cracks might provide good sites for heterogeneous nucleation (Zhang et al., 2005).

A fresh 10M aqueous solution, prepared by dissolving reagent-grade chemicals (ReAgent, Cheshire, UK) of sodium hydroxide pellets (NaOH), in distilled/de-ionized water was used for the process.

The chemical pre-treatment of titanium involved subjecting the metal surface to the oxidizing action of 10M NaOH, at a temperature of 80 degrees Celsius for 24 hours by soaking in the NaOH solution (Figure 3.2).

The mirror-finished polished, or unpolished titanium discs' surfaces were cleaned by sonication in an Ultrasonic cleaner for 5min in 100ml of de-ionised water. The discs were then washed in acetone, again by sonication for 10min, after which they were washed by sonication

for 5min in de-ionised water, and air-dried at room temperature. Care being taken to prevent the introduction of grease/oils, powders and plastic residues onto the modified Ti surfaces by handling the polished discs with forceps. Again, care was taken with the forceps handling so as not to etch the surface with the sharp tips of the forceps.

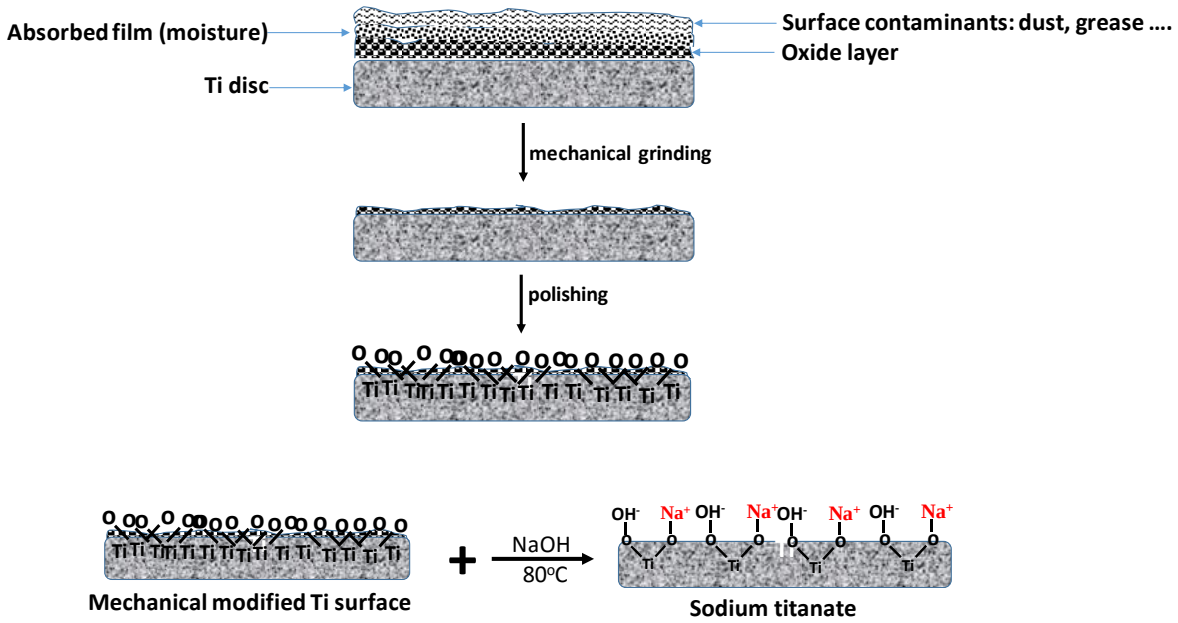

Figure 3.2. Schematic of the physical modification and pre-treatment of the Ti surface. The physical grinding and polishing to a mirror finish led to the removal of foreign matter from the Ti surface. The resulting surface consisted of oxides of Ti mostly. Pre-treatment with NaOH at 80^{0}C resulting in the formation of the ion-exchangeable sodium titanate on the Ti surface.

The cleaned discs were then place in a beaker of sufficient 10M sodium hydroxide solution so that they are completely submerged in the hydroxide solution. This was then placed in an oven (Gallenkamp Hotbox Oven size 2, Sanyo/Weiss), set at 80 degrees Celsius for 24 hours, after which the discs are recovered for treatment with calcium, zinc and silver.

The interaction between the negatively charged species and the alkali ions in the aqueous solution results in the formation of an alkali titanate hydrogel layer. A stable amorphous or crystalline alkali titanate layer is produced when the hydrogel layer is dehydrated and densified during heat treatment (Lee and Yoo, 2015).

3.3.2. Treatment with Calcium, Zinc and Silver

1M fresh aqueous solutions were prepared by dissolving reagent-grade chemicals (ReAgent, Cheshire, UK) calcium chloride ($CaCl_2$), zinc chloride ($ZnCl_2$) anhydrous, calcium hydroxide $Ca(OH)_2$, zinc hydroxide $Zn(OH)_2$ and silver nitrate ($AgNO_3$) in distilled/de-ionized water. These were used for the second phase (chemical bath hydrothermal) process.

The polished and unpolished groups of titanium were then divided into groups corresponding to calcium, silver, zinc, silver-zinc, calcium-silver, calcium-zinc, and calcium-silver-zinc implanted discs, designated Ca or CaTi, Ag or AgTi, Zn or ZnTi and CaAgZn respectively, together with polTi and cpTi discs.

The 12mm titanium discs, pre-treated with 10M NaOH, were briefly rinsed in 100ml de-ionised water and soaked in 5ml of 1M aqueous solution corresponding to their designation (Figure 3.3). They were then incubated in an oven at 80°C for 24 hours, after which they were recovered, briefly rinsed in de-ionised water and air-dried at room temperature.

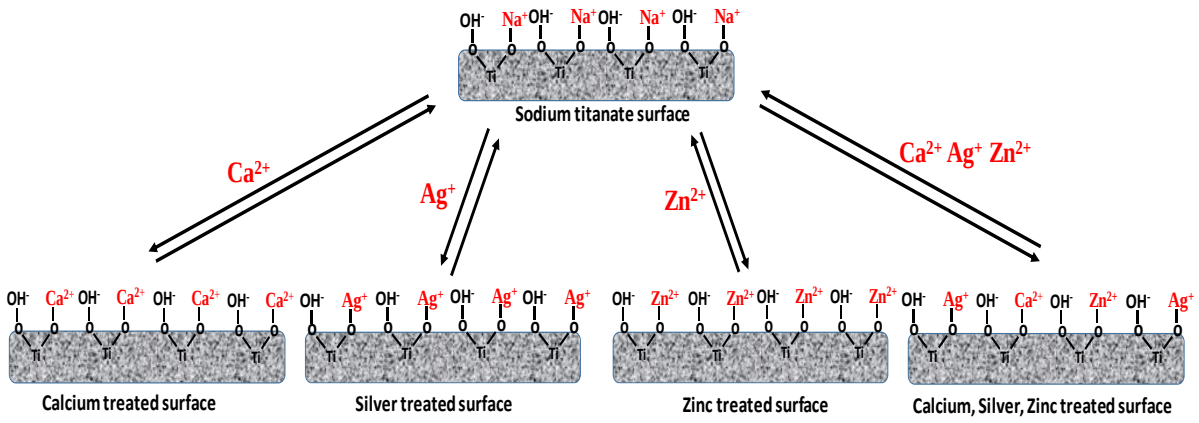

Figure 3.3. The ion-exchanging property of the sodium titanate sol-gel was capitalised on to introduce calcium, silver, and zinc ions onto the Ti surface in separate reaction involving their corresponding aqueous solutions.

The discs' surfaces were subsequently analysed for surface composition by scanning electron microscopy with electron dispersive X-ray spectroscopy (SEM/EDX), characterised for surface roughness or topography by profilometry and atomic force microscopy (AFM), and compared

for effects of the mechanical surface modification on ion implantation. The effects of the surface modifications on bacterial and bone cell adhesion and proliferation were also subsequently examined, using *in vitro* models.

3.4. Surface Characterization

3.4.1. Scanning Electron Microscopy (SEM) with EDS

The scanning electron microscope (Figure 3.4) is typically a microscope that produces magnified images of samples by means of electrons instead of photons as in conventional optical microscopes. It is capable of greater magnification and nanoscale resolution of objects. In operation, a beam of electrons is generated by high voltage heating an element in the electron gun at the top of the microscope. The electron beam is focused using a wehnelt cap through an arrangement of condenser and objective lenses, and scanning coils onto the sample mounted in a holder at the base of the microscope. The scanning coils create a magnetic field which deflect the beam in a controlled raster scan pattern. On hitting the sample surface, the interaction between the electron beam and atoms at or near the surface of the sample leads to the emission of secondary electrons (SE) of weakly bonded conduction-band electrons, together with backscattered electrons (BSE) bouncing off the sample surface, characteristic x-rays from transitioning electrons of the sample, light (cathodoluminescence) (CL), specimen current and transmitted electrons. Detectors for SE collect these electrons, convert them to signals that are displayed as the topography of the sample surface. The BSE signal intensity is related to the atomic number (Z) of the sample, and its detector provides information on elemental distribution of the sample. Detectors for the characteristic x-ray provide information on the elemental composition and abundance in the sample (Ohtaki et al., 2014, Parameswaran and Verma, 2011).

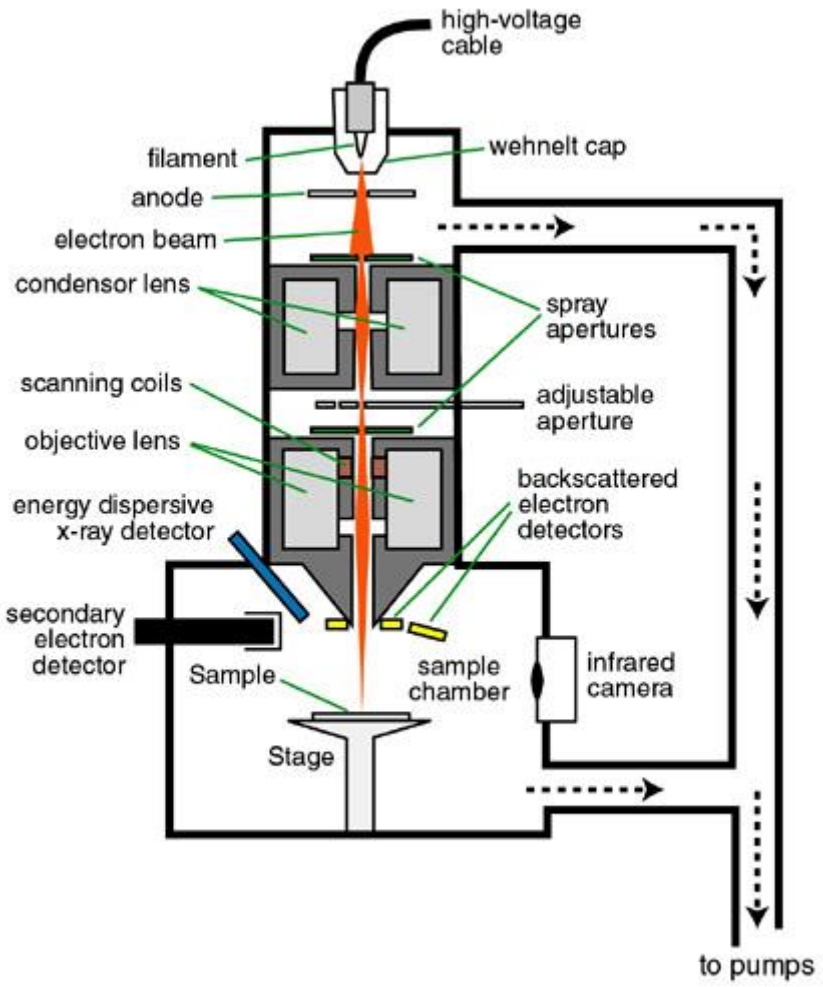

Figure 3.4 A schematic representation of the scanning electron microscope (Springer, USA) (Bhat et al., 2012) showing the travel of the electron beam (in orange), the position of the sample and the various detectors that facilitate the image and data produced by the microscope.

The modified commercially pure titanium (cpTi) and modified titanium (mTi) discs were examined and characterised for bulk surface appearance or morphology and elemental composition by means of a scanning electron microscopy, fitted with an energy-dispersive X-ray detector. The detectors for secondary electrons (SE), back-scattered electrons (BSE) and energy dispersal X-rays (EDX) were used, as described by the manufacturer, to examine and evaluate the surface morphology and composition of the Ti-alkali and Ti-cation treated surfaces. The different techniques, SE, BSE and EDS, offered different contrasts, topography and surface compositional information. The SE are low energy electrons that originate from the ionization process during the electron-solid material interaction. The BSE are high energy

electrons from the electron beam of the microscope (Gaggl et al., 2000). The analyses were carried out in a SIGMA Advanced Analytical Scanning Electron Microscope (EVO HD 15, Carl Zeiss). Sample preparation for SEM involved mounting the treated, washed and dried samples on 0.5" SEM pin stubs (G301F, Agar Scientific, UK), using 12mm Carbon tabs (G3347N, Agar Scientific, UK). Observations were made at 500 times magnification. To quantify the amount of ions incorporated onto the surfaces, an energy dispersal spectroscopic (EDS) analysis was carried out with the same equipment and the EDS data taken for five randomly selected $1mm^2$ surface area on each disc.

Sufficient numbers of each group of discs were treated and analysed for the distribution of data to be statistically normal. Each group was make up of 23 discs, and the experiment conducted three times and data pooled. The statistical normality was determined for the pooled samples, and reported together with the mean and standard error of mean for each group of samples.

3.4.2. Atomic Force Microscopy (AFM)

An atomic force microscopy (5420 SPM, Agilent Technologies) was used to characterise the surface topography of the various surfaces considered. The AFM (Figure 3.5) uses a sharp probe or tip moving over the sample surface in a raster scan. The probe, on the end of a cantilever, bends or deflects in response to forces interacting between the tip and the sample surface. The deflection magnitude is captured by a laser beam incident at the end of the cantilever and is reflected at an oblique angle onto a photodiode, from which the beam is processed into information relating to the surface characteristics of the sample (Salerno et al., 2010, Hilal et al., 2006).

Imaging was carried out in the contact mode, where the force on the cantilever is kept constant, and a sufficiently small distance allowed between the tip and the sample to allow a core repulsion effect. In this mode, changes in topography as the tip move across the sample surface

in a raster scan cause variation in the tip-sample interaction, corresponding to deflections in the cantilever, detected by the photodiode as deflections in light beam. This is then fed back to the piezo controller, which adjust the z-position of the sample to keep the force on the cantilever constant, in a feedback loop. This generates an accurate topography of the sample surface. However, the process is strongly influenced by the physical state of the tip, and the tip geometry (Daniels et al., 2013, Jalili and Laxminarayana, 2004).

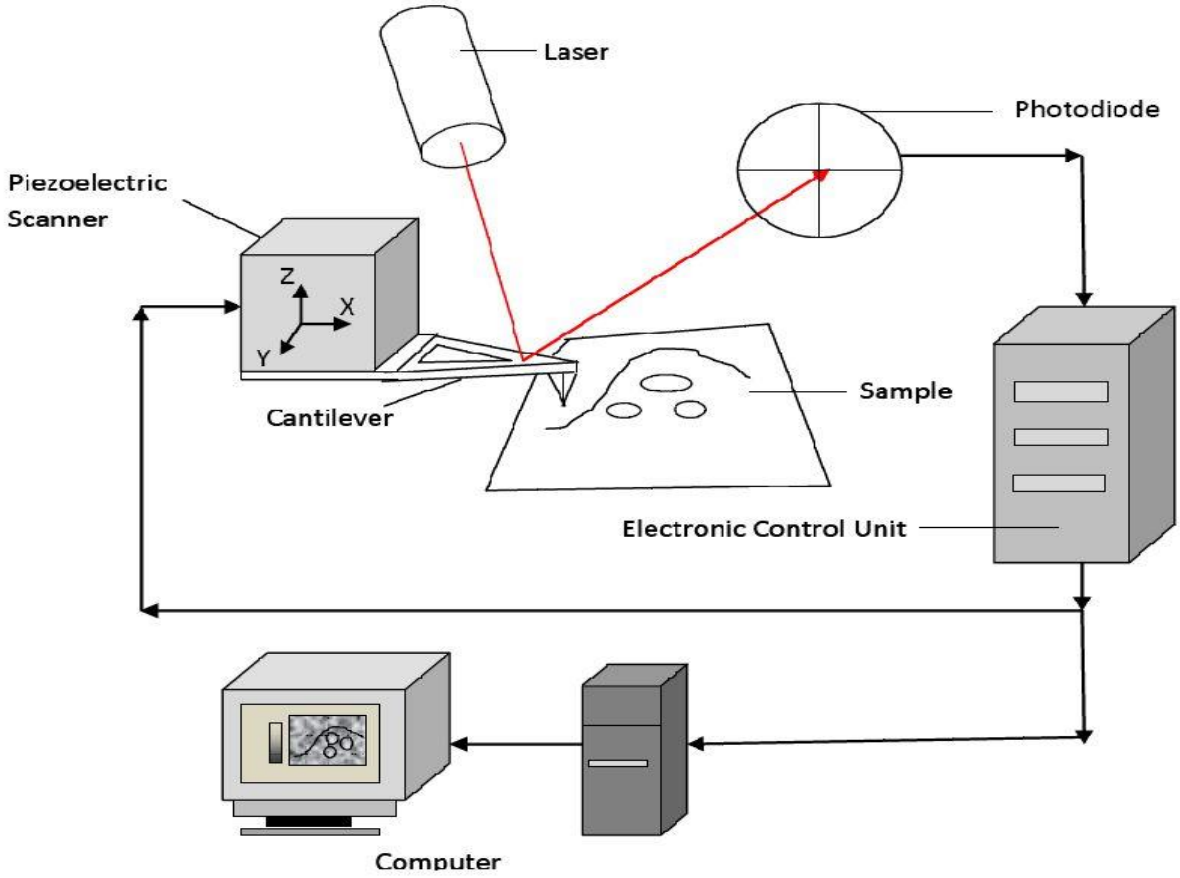

Figure 3.5 A schematic representation of the atomic force microscope. (Springer, USA) (Bhat et al., 2012), showing the main components for generating the 3D topographic image and topographic parameters of the sample surface.

The samples were imaged and characterised using <15 nm diamond-like coating multimode AFM tips at a scan rate of 2 µm/s over 20 µm square scan area, in the contact mode. For the purpose of statistical accountability, scan results were collected for 5 random areas on each sample surface. The experiment repeated n=5 times for each group of discs and the data pooled for each group for statistical accountability. The raw data was processed using Picoview

software (version 1.8) and the mean height parameters determined, together with standard deviation and error of means.

3.4.3. Profilometry

The 2D amplitude parameters or surface profile of the cpTi and the modified Ti surfaces were determined in addition to the 3D profile by means of a contact surface profilometer (Mitutoyo Surftest® SJ-400). This essentially involved dragging the measurement stylus across three random 2mm-length of the various Ti surfaces.

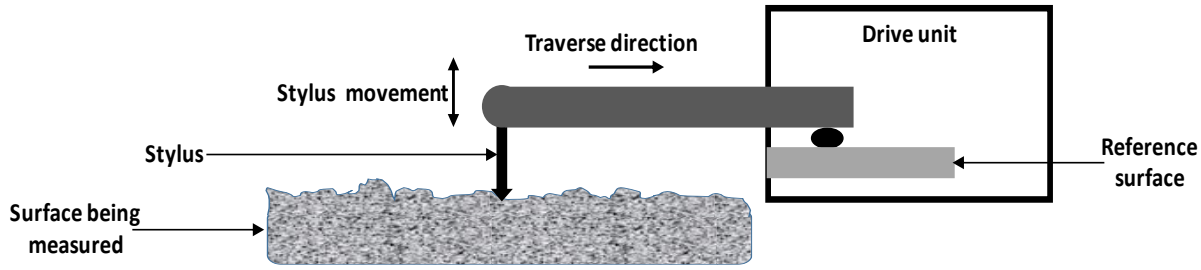

Figure 3.6 Schematic of a contact surface profilometer. The tip of the stylus directly touches the surface of the sample. As the stylus traces across the sample, it rises and falls together with the roughness on the sample surface. This movement in the stylus is picked up and used to measure surface roughness.

In principle, the profilometer (Figure 3.6) measures the sample surface features relative to the device's drive unit calibrated reference surface. This accurately measures the heights and depths or surface roughness of the sample. The measured features are reported in Ra, Rq, Rt and Rz, defined as

Arithmetical mean deviation of the roughness profile (Ra)

$$Ra = \frac{1}{L}\int_0^L |Z(x)|dx$$

Equation 3.1

Root mean square deviation of the roughness profile (Rq)

$$Rq = \sqrt{\frac{1}{L}\int_0^L |Z^2(x)|dx}$$

Equation 3.2

Maximum height of the roughness profile (Rt)

$$Rt = Rp + Rv$$ *Equation 3.3*

Rz: based on the five highest peaks and lowest valleys over the entire sampling length (L)

$$Rz = \frac{1}{n}\sum_{n=1}^{n} Rpn - Rvn$$ *Equation 3.4*

Where Rp = maximum peak height

Rv = maximum valley depth

L = evaluation length

Z(x) = the profile height function.

The clean, debris-free sample discs were firmly fixed onto the flat surface of the sample holder and secured from moving during testing. The contact stylus was then placed directly over the centre of the Ti disc sample, and gradually lowered until it came into contact with the sample surface. The stylus (minimum resolution 0.000125 µm (8 µm range), radius 5 µm, measuring force 4 mN, skid force less than 400 mN, and cut off 2.5 mm) was then set to drag along a 2.5 mm-length of the sample surface. This was repeated two more random 2.5mm-lengths, and the mean 2D profile parameters determined. The means of the line profile parameters are presented together with graphical representation of the surface peaks and valleys. For statistical accountability, three discs were profiled for each group of samples, representing n=9 reading for each surface under consideration.

3.4.4. Contact Angle Measurements

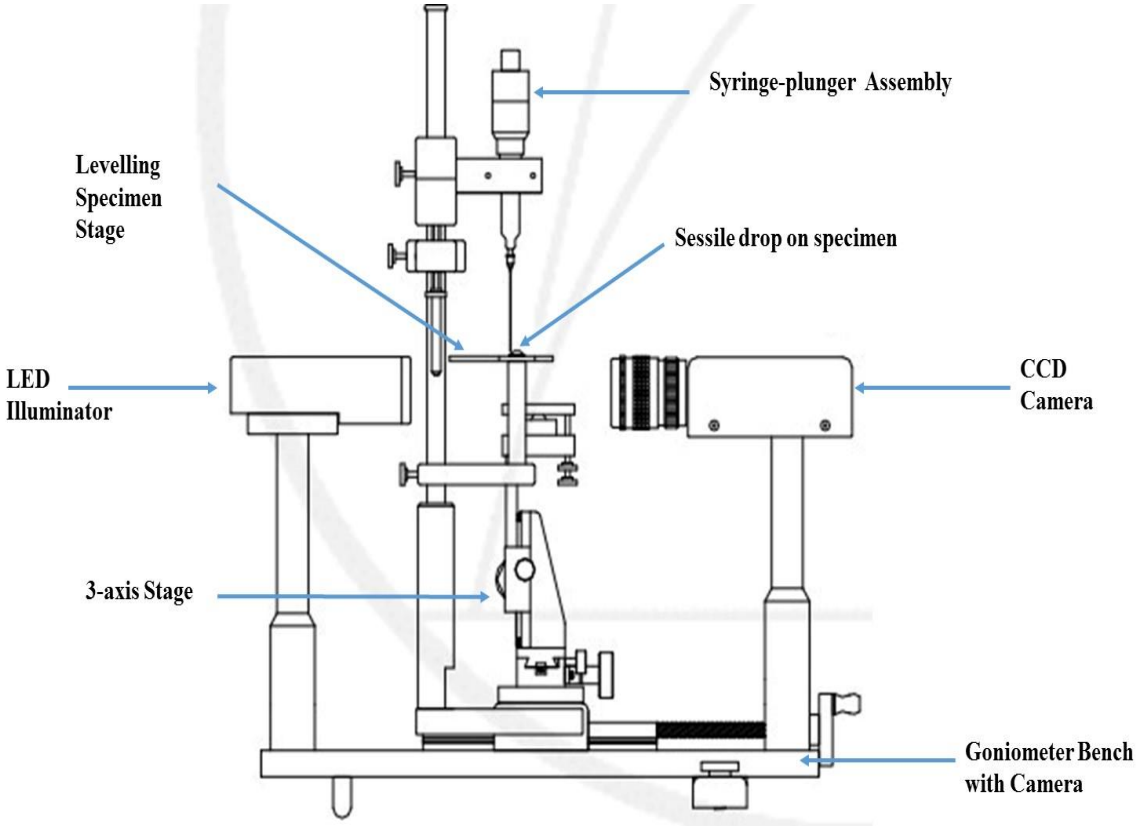

Figure 3.7 A schematic representation of the goniometer with camera. (Springer, USA), showing the position of the charge coupled device (CCD) camera, relative to the specimen and sessile drop position.

The contact angle, as a measure of the surface energy of the various titanium surfaces, were determined by the sessile drop method of advancing contact angle measurement, using the CAM 200 goniometer set-up (KSV Instruments Ltd., Finland). In doing this, a 2µl drop of the probe liquid (deionised water) was dispensed directly onto the titanium disc surface from a calibrated syringe-plunger system, as described by the manufacturer. The drop volume was calibrated to the profile of a calibration ball of know volume. An image of the drop was captured, by a distortion and degeneration proof telecentric lens and high-resolution charge-coupled device (CCD) camera with a frame grabber, and LED light source incorporated into the instrument, and transferred to an image analysis software (Figure 3.7). Images were captured at ambient conditions, at a rate of 1 image/s for 20 seconds. The software then extracts

the stored image with pixel accuracy, and the drop profile curve-fitted into the Young-Laplace equation to calculate the contact angle and/or surface tension/energy.

For statistical accountability, three random surface readings were taken for n=5 of the various titanium disc surfaces, and the mean parameters determined with standard deviations and errors.

3.5. Bacteria Culture

3.5.1. Anti-Microbial Suspension Assay

A preliminary assay to investigate the antimicrobial effects of the elements of interest incorporated onto the titanium surface, that is, calcium, zinc and silver was carried out. The implant related infection causing bacteria, *Staphylococcus aureus*, strain ATCC 6538, was cultured from beads stored at -20^{o}C. A bead of bacterial was aseptically transferred into 10ml of freshly prepared nutrient broth. This was incubated at 37^{o}C with shaking at 220rev/min for 24 hours in a shaker-incubator **(**Innova 44, New Brunswick Scientific**).** The freshly cultured bacteria suspension was then transferred into a 15ml centrifuge tube, and centrifuged at 3700rcf for 10min (Hettich Zentrifugen, model: Rotanta 460S), at the end of which the supernatant was then discarded and the bacteria pellets re-suspended in 10ml sterile distilled water ready for use.

1ml of this bacterial suspension was diluted with 9ml sterile distilled water to form a 10^{-1} dilution. Three such dilutions were prepared corresponding to the three elements of interest; calcium, silver and zinc, the combination of calcium-silver-zinc, the polished and unpolished Ti surface, and a control/reference sample of polycarbonate coupon. The appropriate treated and untreated discs, and control coupon were introduced into the 10^{-1} dilution bacterial suspension. At regular 10 min intervals, up till t=60 min, 1 ml bacterial suspension was taken and serially diluted 1in 10, four times. 50 µl triplicates of each dilution was plated on a 90 mm

Petri dish of nutrient agar medium (previously prepared and dried), using an automated spiral plater (Easyspiral pro, Interscience®). This was repeated for all three metallic elements and for the untreated polished titanium disc. The plated Petri dishes were then incubated at 37°C for 24 hours.

At the end of the incubation period, the Petri dishes were retrieved and the number of bacterial colony forming units (cfu) estimated using the Easyspiral counting kit as described by the manufacturer (Interscience®). The experiment was carried out n=7 times, and the mean counts of the most consistent five sets of results (in triplicates), representing n=15 plates for each sample surface, presented as a log graph of the number of colony forming units against time for the various modified surfaces, the commercially pure Ti surface, and the control disc.

3.5.2. Inhibition Zone: Modified Kirby-Bauer Test

A modified version of the Kirby-Bauer test (Reller et al., 2009) was used to ascertain the extent of the inhibitory ability of the modified titanium surfaces. 90mm nutrient agar plates were prepared and placed in a 37°C incubator for 10min to dry. Sectors were marked on each agar plate and labelled according to the treated/modified and control discs to be placed on. The *S. aureus* inoculum was prepared by inoculating 10ml nutrient broth with a single isolated colony of the bacteria and incubating at 37°C until a log phase bacteria suspension concentration of 1 x 10^8 to 2 x 10^8 cfu/ml corresponding to a 0.5 McFarland standard was attained. 50 µl of this bacterial suspension was uniformly spread on the 90mm nutrient agar by means of the automated spiral plater (Easyspiral pro, Interscience®), and allowed to set for up to 5min with the lid slightly opened for moisture escape.

Using flamed forceps (immersing the forceps in alcohol then igniting), the treated/modified discs and control coupons were carefully placed on the surface of correspondingly labelled sectors of the agar plate, one at a time, ensuring complete contact with the agar surface, each time. The plate lid was replaced in between each disc placement to minimise exposure to the

room air. With all the discs in place, the lid was replaced, the plates incubated at 37°C for 24 hours, following which the clear circular zones around the discs were measured. This was done using a pair of callipers, across the diameter of the disc, to the nearest millimetre (Figure 3.8). The measurements were made with the unaided eye, from the back of the Petri dish, a few inches above a black, non-reflecting surface, indirectly illuminated (Wayne, 2009). Bacterial growth up to the edge of a disc was reported as a zone of 0mm. Factors that could potentially influence the size of the inhibition zones include the rate of diffusion of the antimicrobial agent through the agar, the depth of the agar, and the sensitivity of the *S. aureus* to the antimicrobial agent(s) on the disc surface.

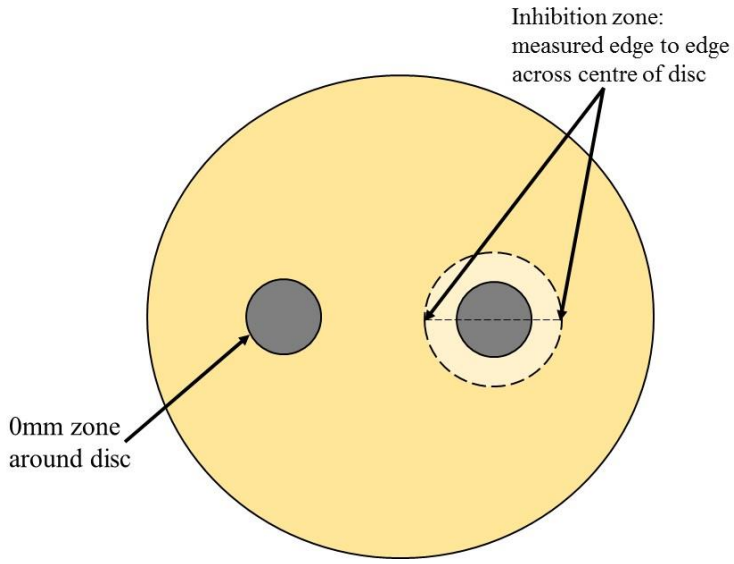

Figure 3.8 A schematic representation of the Ti disc, inhibition zone around disc, and measurement of inhibition zone

For statistical accountability, three measurements were taken for n=5 repeats of the various titanium disc and control surfaces, corresponding to 15 reading for each sample surface, and the mean inhibition zone determined with standard deviations and errors.

The above test was repeated for n=3 sets of modified discs leached in sterile deionised water in a shaker-incubator maintained at 37°C and 220 rev/min for 28 days. This was to test and

compare the growth/spread inhibitory effect of the freshly prepared discs and discs whose surface-active agents have been depleted over 4 weeks.

3.5.3. Biofilm Formation Assay

A number of researchers (Loza-Correa and Ramírez-Arcos, 2017, Ficai and Ficai, 2017, Ng et al., 2016, Bajpai, 2015) have demonstrated that, laboratory-grown biofilms may be engineered to respond a particular real-world environment. Alteration of parameters such as flow dynamics and reactor configuration, makes it possible to grow biofilms of different structure (e.g. thickness) and function (e.g. nutrient consumption) (Stoodley et al., 1998). This implies that the reactor choice affects the laboratory bio- film formed. Hence the selection of the appropriate reactor and growth conditions is important. The standardised design and protocol for the Centre for Disease Control (CDC) biofilm reactor (CBR) makes it an ideal tool for the repeatable growing of many different organisms under constant shear (Goeres et al., 2005). Flexibility in its operation (Gilmore et al., 2010) and room for modification (Williams et al., 2011) of it standard operating procedure (SOP) means it can be operated under a range of controllable conditions to repeatedly grow standard biofilms specific to an experimental design. Modification to the operation included replacing the polycarbonate coupons with the titanium discs, adjusting the stationary phase, baffle or sheer speed and nutrient in-flow rate to *S. aureus* doubling time. Other modifications included separate sterilization of the reactor vessel/content, and the reactor rods holding the samples, and time-interval sampling of the coupons/Ti discs.

To determine the effect of the Ti surface modifications, i.e. the effect the mirror-finished polished and the silver/zinc treatment have on bacterial colonization of the surfaces, biofilm formation experiments were carried out using a CDC biofilm reactor. The CDC Biofilm Reactor is made up of eight (8) polypropylene rods or coupon holders suspended from a polyethylene ported lid. Each reactor rod accommodates three (12.7 mm) diameter coupons, giving rise to 24 sampling opportunities. The lid with coupon holders and coupons/samples

surfaces is mounted in a 1L glass vessel with side-arm discharge port. The liquid growth media or biocide is circulated through the reactor vessel while mixing, the shear generated by a magnetic stir vane rotated by a magnetic stir plate. Sampling is conducted by aseptically removing individual coupon holders with accompanying (3) coupons or discs.

The underlying principles for the use of the CDC Biofilm Reactor include the understanding that biofilm bacteria exhibit a different phenotype from suspended bacterial cells of the same genotype (Donlan, 2001). In its use, a biofilm is grown under high shear and continuous flow conditions. The accumulated biofilm is quantified by recovering the biofilm from coupons/discs of a known surface area, breaking up the cells and polymer matrix in solution and estimating viable plate counts.

The density of the biofilm formed, estimated as the $\log_{10}$ density, is the key parameter. It is expressed in units of c.f.u. cm^2, calculated from

$$Log\ Density = log10(mean\ c.f.u.per\ plate) + log10(vol.scraped\ into) + log10(dilution) - log10(vol.plated) - log10(sample\ surface\ area) \quad \textit{Equation 3.5}$$

The CDC Biofilm Reactor (Figure 3.9) operates as a continuous flow stirred tank reactor (CFSTR). This means nutrients are steadily pumped into and flow out of the reactor at the same rate. This, together with the constant shear action, enables the reactor can achieve steady state conditions, eliminating all time-dependent terms in the mathematical model of the reactor, and the complexity of the mathematics involved in calculating the reduction in biofilm accumulation as a result of a treatment.

The nutrient flow rate is calculated by dividing the reactor volume by the residence time. The residence or generation time for *Staph. aureus* has been estimated as 30 minutes (Lindqvist, 2006, Nadkarni et al., 2002). This, together with reactor volume of approximately 350 ml, gives rise to a flow rate of approximately 12 ml/min. The flow rate is set based upon the measured fluid volume in the reactor when the reactor is completely set up: with baffle, rods, and coupons

in place, to achieve an exact 30-minute residence time. This is a critical parameter specific to the bacterial species used in the experiment, and must be less than the doubling time for the planktonic bacteria in order to select for biofilm growth in the reactor. This encourages the washing out of suspended cells, leaving only the biofilm.

In setting up for the experiment, the reactor components were thoroughly and rinsed with tap water, followed by reagent water and air-dried. Three discs of Ag, Zn, Ag/Zn, unpolished Ti, and polished Ti treated titanium, together with three polycarbonate coupons (as control) were inserted into the reactor rods and held in place by tightening the set screw adjacent to the hole, as described by the manufacturer. They were then placed in an autoclave bag, together with the titanium cured silicon tubing for operating the peristaltic pump.

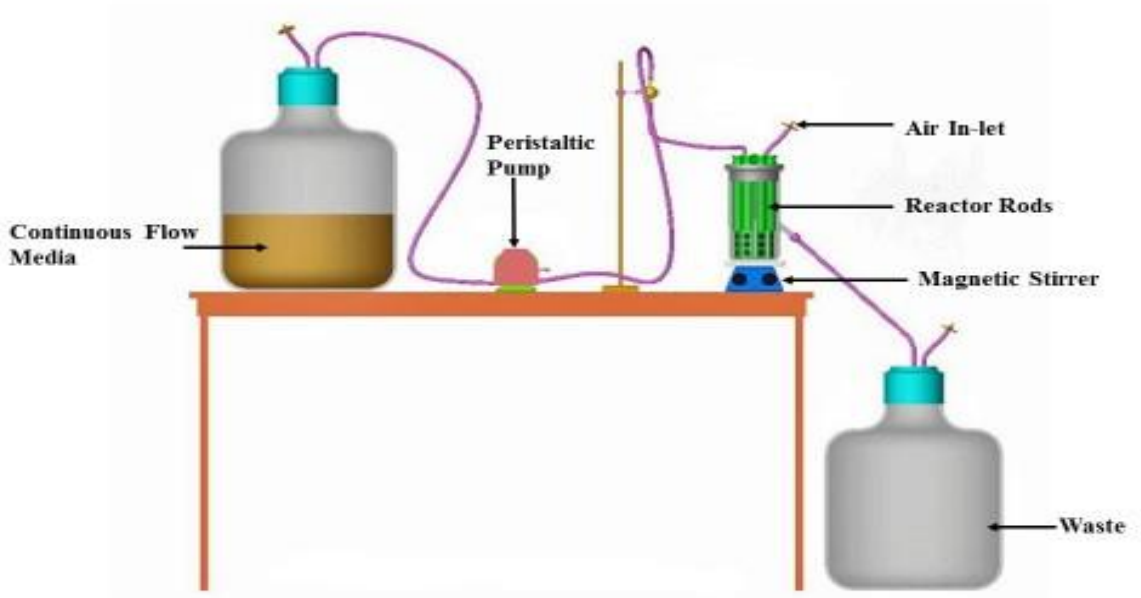

Figure 3.9. Schematic of the completely assembled CDC biofilm reactor system in operation. The peristaltic pump moves the nutrient through the system at a predetermined flow rate, characteristic of the residence time of the micro-organism. Shear is provided by the baffle rotating at a constant speed under the control of a magnetic stirrer,

25L of nutrient medium was prepared in an autoclavable carboy, together with 500ml of nutrient broth medium in the 1000 ml Pyrex beaker of the reactor, with the silicon tubing

attached to the spout and clamped shut. The reactor lid, together with the stirrer-baffle system in place, was placed over the beaker, and the reactor rod access holes in the lid sealed with oil paper and autoclave tape.

The 25L nutrient media in the carboy, together with the nutrient media in the reactor beaker, and the content of the autoclave bag were sterilised by steam autoclaving at 121^{o}C for 20 min.

10ml nutrient broth was inoculated with a single colony of *Staphylococcus aureus* from a bacteria isolation plate using sterile inoculating loop. This was incubated at 37^{o}C while shaking at 220 rev/min for 24 hours, until the inoculum of 10^{8} cfu/ml concentration (the viable bacterial density of the inoculum, confirmed by diluting and plating a sample from the inoculum flask) was attained.

1ml of the previously prepared inoculum was aseptically injected into the sterile medium in the reactor, and the stirrer/baffle operated at 125 rev/min (for a 30-min residence time) on a stir plate at room temperature, allowing air to pass freely through the bacterial air vent, and the effluent still clamped shut. This formed the batch phase of the set-up.

The reactor in batch phase was operated for 24 hours, with the rods holding the discs and coupons aseptically introduced into the reactor. The nutrient tubing line was subsequently aseptically connected to the carboy containing the sterile continuous flow nutrient broth, to allow for the continuous supply of nutrient media over the time course of biofilm formation. The foil at the end of the effluent tubing was removed and the tubing placed in a waste carboy and unclamped. The continuous flow media was then pumped into the reactor at a flow rate of 12ml/min, with the effluent collected in a waste carboy. This formed the continuous flow phase.

For the time course of bacterial cell attachment experiment, the discs corresponding to the various surfaces were retrieved at hourly interval, by aseptically removing the corresponding reactor rod, removing the disc from the reactor rod into a sterile Petri dish, and returning the

rod with remaining discs into the continuous flow phase. This was repeated hourly till all three discs/coupons held in a rod, corresponding to a surface, were all recovered from the reactor rod.

For the total biofilm formation experiments, the protocol was the same with the important variation of keeping the discs/coupons in place during the stationary and continuous phases, for 24 hours, at the end of which all three discs/coupons in a particular reactor rod, corresponding to a particular surface, were aseptically removed at the same time, and placed in sterile Petri dishes. Whereas the standard protocol allowed biofilm formation on the surfaces to be examined, this deviation from the standard protocol allowed for the rate of bacterial cells attachment to the sample surfaces (not biofilm formation) to be investigated. This however may have standardization and reproducibility implications, hence was carried out as preliminary investigation of the effect of the surface modifications on *S. aureus* propensity for biofilm formation in potentially hostile environment.

The discs/coupons were then briefly rinsed in sterile phosphate buffered saline (PBS). The biofilms formed on the various surfaces aseptically recovered by scraping motion, using sterile wooden sticks, and transferred into 9 ml of sterile distilled water, as described by the reactor manufacture. The disc surface was then rinsed with 1ml sterile distilled water to make the finale volume of bacteria biofilm suspension 10 ml. This was repeated for each disc/coupon. The final volume was then serially diluted three times. 50 µl of each dilution for each disc/coupon was then plated on nutrient agar, using an Interscience® automatic spiral plater. The plates were incubated at 37^{o}C for 24 hours, after which the bacteria colonies of the countable dilution plates were estimated using the Easyspiral counting kit as described by the manufacturer (Interscience®), as the number of colony forming units per ml for each treated, untreated and control surfaces.

The experiment was carried out n=8 times, and the mean counts of the most consistent five sets of results (representing n=15 plates for each sample surface) presented as a log reduction graph of the number of colony forming units against time for the various modified surfaces, with the commercially pure Ti surface, as the reference/control disc.

3.6. Atomic Absorption Spectrometer (AAS)

The amounts and rate of release of silver and zinc from the surface of the modified Ti surface were determined using the Perkin Elmer AAnalyst 200 (Beaconsfield, UK) atomic absorption spectrometer (Figure 3.10). This uses absorption spectrometry to determine the concentration of an analyte in a liquid sample. The technique uses are an acetylene fuelled flame to atomize the solution sample. The process of turning the liquid sample into atomic gas involves; desolvation, in which the liquid solvent is evaporated, vaporization, in which the solid left is vaporized to gas, and volatilization, in which the components of the sample are broken into free atoms. The variations in radiation flux emitted by the excited free atoms is measured by a detector as the absorbance, which is related to the analyte concentration or mass by the Beer-Lambert Law (García and Báez, 2011).

3.6.1. Silver and Zinc Release from Modified Ti Surface

A disc each from the treated disc batches (silver treated, zinc treated and silver/zinc treated) was placed in a 100 ml duran bottle containing 50 ml of double distilled water (ddH_2O). This was agitated in a shaker incubator (Innova 44, New Brunswick Scientific) maintained at 37^{o}C and 220 rev/min. 5 ml (10ml in the case of silver/zinc disc in ddH_2O) aliquots was withdrawn with a calibrated pipette into a clean scintillating vial at hourly intervals, for 10 hours (h), then daily for 7 days, then weekly for 3 weeks, making a total of 28 days sampling. The volume withdrawn was replaced with an equal volume of ddH_2O to maintain the starting reaction volume, and keep the volume influence on ionic release constant.

Separate calibration standards for silver (0.5, 1, 2, 5, and 10 ppm) and zinc (1, 2, 3, 4 and 5 ppm) were prepared from 1000 ppm stock (PerkinElmer), for analysing the release profile of silver and zinc on silver and zinc treated Ti surfaces respectively. A second set of separate calibration standards for silver (0.5, 1, 2, 5, and 10 ppm) and zinc (0.0625, 0.125, 0.25, 0.5, 1.0 and 2.0 ppm) was prepared for analysing the release profile of silver and zinc separately from the silver/zinc treated Ti.

With the exhaust venting system switched on, the burner fuel and oxidant turned on, and the outlet pressure adjusted to the recommended values (Table 3.1), the appropriate lamp for the analyte element was selected, and the spectrometer switched on via the AC power on/off switched. With the appropriate (silver or zinc) lumina hollow cathode lamp (PerkinElmer) installed and selected, the spectrometer was calibrated as instructed in the manufacturer's user guide, for the appropriate elements at the start of each analysis, at the optimal conditions suggested by the manufacturer. The ddH_2O was used as the calibration blank, and the calibration curves for the standards were constructed as a plot of absorbance against concentration. Every data point was obtained in triplicate and the mean value plotted. The midpoint standard for each range of standards was analysed as a quality control standard to verify the calibrations and check for memory effects.

The time series of unknown samples were sequentially analysed, and the result digitally presented for storage/analysis.

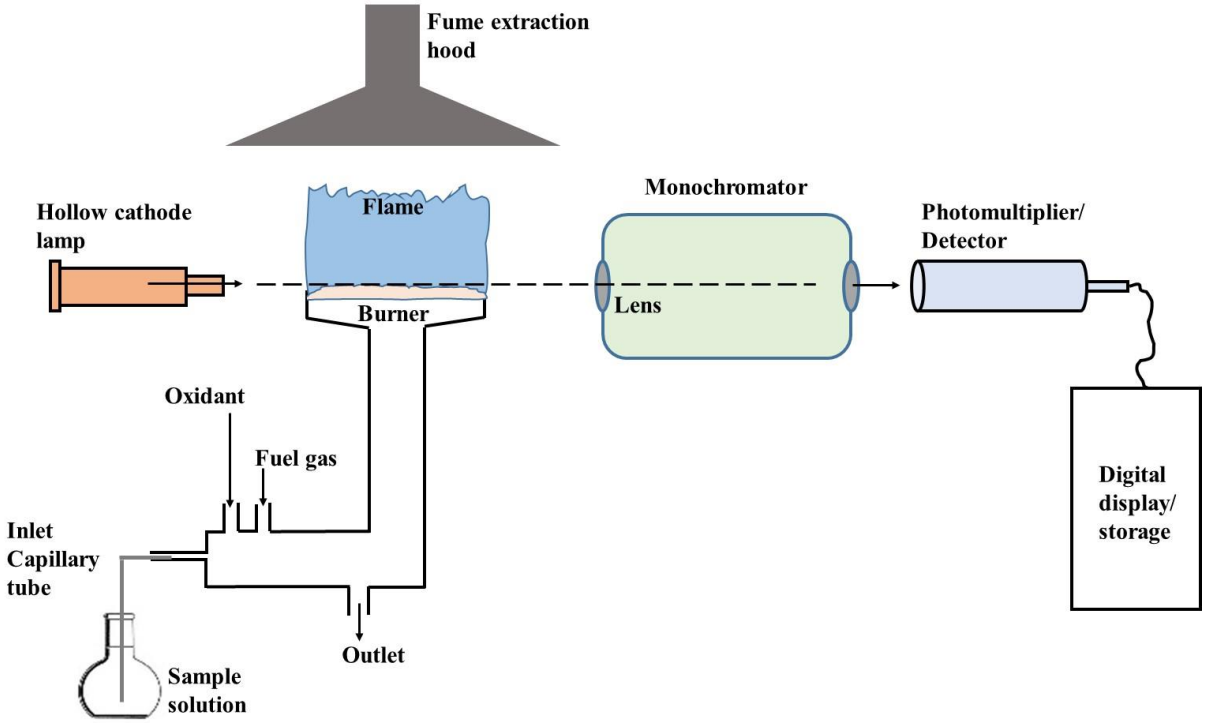

Figure 3.10 A schematic diagram of Atomic Absorption Spectrometry, showing the main components and operation.

Table 3.1 Operational values for Ag and Zn atomic absorption spectroscopy

	Element	
Parameter	Ag	Zn
Wavelength (nm)	328.07	213.86
Slit (mm)	2.7/0.8	2.7/1.8
Oxidant	Air	Air
Oxidant Flow (L/min)	10	10
Fuel (Acetylene) Flow (L/min)	2.5	2.5
Time (s)	3	3
Delay Time (s)	0	0

3.7. Interaction of Bone Cells with Modified Ti Surfaces

3.7.1. U2OS Cell Culture

A preliminary investigation of the effect of the surface modification on the ability of osteogenic cells to adhere to the modified surfaces was carried out.

Human OS cell line U2OS was obtained from the Toxicology Unit, MRC at University of Leicester (courtesy of Prof Andrew Tobin), maintained in McCoy's 5A (Modified) Medium, GlutaMAX™ (GIBCO® Life Technologies, GIBCO # 36600-021) growth medium, supplemented with 10% FBS plus 5% Penicillin/Streptomycin (GIBCO # 15140-122), and cultured in an incubator maintained at 37°C in the presence 5% CO_2 and 95% air (SANYO CO_2 Incubator Model MCO-18AIC(UV)).

Cells frozen in liquid nitrogen were thawed at room temperature and suspended in 10ml growth media. Typically, the medium was changed every 2-3 days and the cells were split in a ratio of 1:4 every 4 to 5 days or when a 85% confluence (1×10^7 cells/10sq.cm dish) was reached in a $25cm^2$ angled neck cell culture flask (Thermo Scientific Nunc Nunclon).

In sub-culturing the cells the growth media was aspirated away from the U2OS cells attached to the bottom of the flask. The cells were then washed with Dulbecco's Phosphate-Buffered Saline (GIBCO® Life Technologies) with 10% EDTA (DPBS –EDTA). 3mls of fresh DPBS –EDTA was added to the adherent cells in the flask and placed in the incubator for at least 5min to free cells from the flask. The flask was given several gentle firm taps to ensure all adherent cells are freed and resuspended. This was visually confirmed with an inverted optical microscope (Zeiss ID02) as free floating rounded cells.

3.7.2. Cell adhesion to Modified Ti Surfaces over 24 hours

The number of cells in the confluent population suspended in the growth medium was determined by means of a haemocytometer. To do this, 20µl of detached suspended confluent

cells was placed on the prepared haemocytometer or Neubauer chamber cell counter, and using an inverted optical microscope (Zeiss ID02), the number of cells in suspension was estimated as described by the cell counter manufacturer. The cell suspension was introduced to a space 0.1mm in depth beneath a coverslip and the count carried out within a grid of area $1mm^2$. Thus, the total count gives the number of cells per $0.1mm^3$ (or 0.1µL). This value, multiplied by 10 gives the number of cells per µL, and multiplying by 10,000 gives the number of cells per mL.

Prepared samples of Ti disc (12 mm in diameter), surface modified/thermochemical treated (as described in Section 3.3) were steam sterilized by autoclaving for 15min at 121°C. The respective sterilized discs (Table 3.2) were placed in the wells of a 24-well plate. 1ml of McCoy's 5A (Modified) Medium, GlutaMAX™ (GIBCO® Life Technologies, GIBCO # 36600-021) growth medium, supplemented with 10% FBS plus 5% Penicillin/Streptomycin (GIBCO # 15140-122), added onto the discs.

The volume of suspended cells equivalent to 2.5×10^5 osteoblast cells was seeded onto the Ti discs on 1ml of growth media under sterile conditions (Series Class II, Type A2 Biological Safety Cabinet, Thermo Scientific), and incubated, at 37°C in the presence 5% CO_2 and 95% air (SANYO CO_2 Incubator Model MCO-18AIC(UV)), for 24 hours. At the end of the incubation, the media surrounding the discs with planktonic cells were aspirated away. The U2OS cells attached and growing on the discs were gently washed with PBS and then teased off with DPBS-EDTA, by introducing 1ml DPBS –EDTA onto the discs and incubating at 37°C in the presence 5% CO_2 and 95% air for 30min. The well plates with discs were then examined under the microscope for cells floating from the surface.

The discs were agitated and the surrounding PBS re-suspended, to free all cells on discs' surfaces. The number of cells teased off the discs' surfaces were then estimated using the Scharfe System CASY Cell Counter + Analyzer System (Model TTC 301-3967). 100 µl of cell

suspension from each well was pipetted into a separate cell counter tube and appropriately labelled. 9900 µl of cell counter diluent was added to each counter tube to make 100 µl in 10 ml dilution, and the number of cells estimated for each tube (corresponding to a separate disc), as directed by the manufacturer. This preliminary cell adhesion experiment was repeated two more times and the mean values determined, together with the corresponding standard deviations and errors. The readings were then presented as a percentage increment/reduction column chart.

Table 3.2 Sample Discs Annotation

Ti Disc Treatment	Annotation
Polished silver treated	Ag
Polished Zinc treated	Zn
Polished Calcium treated	Ca
Polished Calcium and Zinc treated	CaZn
Polished Calcium and Silver treated	CaAg
Polished Calcium, Zinc and Silver treated	CaZnAg
Polished untreated	Pol or polTi
Unpolished untreated	Unpol or cpTi

3.7.3. Cell Response to Modified Ti Surfaces over 72 hours

To investigate the effect of the surface modifications on cell morphology, hence cytotoxicity, 10,000 U2OS cells were seeded into 1-1.5 ml growth medium over the different surface modifications in a 24-well plate; unpolished commercially pure surface, the polished surface, calcium-silver, calcium-zinc, calcium-silver-zinc and calcium treated surfaces, and incubated for up to 72 hours. With a mean population doubling time of 23.7±0.5 hours, 8 hours was allowed for planktonic cells to become adherent to the modified surfaces. The 8-hour mean counts and size of the adherent cells for the different modifications served as the baseline from which the interval cell counts and size changes were referenced.

Table 3.3 Sample Discs Annotation

Ti Disc Treatment	**Annotation**
Polished Calcium treated	Ca
Polished Calcium and Zinc treated	CaZn
Polished Calcium and Silver treated	CaAg
Polished Calcium, Zinc and Silver treated	CaZnAg
Polished untreated	Pol or polTi
Unpolished untreated	Unpol or cpTi

Four sets of sample discs (as annotated above) were sterilized by autoclaving (as described earlier), placed in four 24-well plates and appropriately labelled. The first set was to quantify the number of osteosarcoma cells that adhered to the disc surfaces as a baseline after 8 hours. The subsequent sets were to examine the cell proliferation after 24, 48 and 72 hours of incubation, in an incubator maintained at 37^{o}C with 5% CO_2 and 95% air.

1ml of sterile growth medium was pipetted onto each disc in the 8-hour and 24-hour well-plates, plus 1ml into an empty well. 1.5 ml of growth medium was pipetted onto each disc in the 48 and 72 hour well plates. A volume of cell suspension corresponding to 10,000 cells was sterilely inoculated into all the wells containing growth medium (Series Class II, Type A2 Biological Safety Cabinet, Thermo Scientific), and the four sets of well-plates placed in an incubator maintained at 37°C with 5% CO_2 and 95% air (SANYO CO_2 Incubator Model MCO-18AIC(UV)).

The first set of well plate discs were retrieved after 8 hours. The blank well (medium inoculated with 10,000 cells, and no sample disc) was examined under an inverted optical microscope (Zeiss ID02) for adherent or planktonic cells. On confirmation of cell adhesion, the well plates

were returned to the incubator and allowed to proceed. They were retrieved after 24, 48 and 72 hours.

3.7.4. Morphometric Analysis

For each set, the media and planktonic cells around the disc were aspirated away and gently rinsed three times with DPBS. The adherent cells were fixed on the disc surface with 4% paraformaldehyde (PFA), maintained at 4^{o}C for 2 hours. The fixed cells were then dehydrated with 40%, 50%, 60%, 70%, 80%, 90% and 100% ethanol, in series. The fixed, dried cells were then examined and photographed (Havrdova et al., 2014, Engel and Reichelt, 1984, McKinlay et al., 2004), using a scanning electron microscope (Carl Zeiss 'EVO HD' 15). Three random areas of size 2 mm by 1.5 mm were taken for each sample surface at 150x and 1000x magnifications, for numerical estimation and morphological characterisation, respectively. The number of cells attached to the various surfaces were digitally estimated and their morphology quantitatively analysis carried out using the image analysis software Pixcavator 5.1, set for semi-automatic analysis, with the maintenance of the same values for contrast, light intensity as well as dots size inclusion parameters (See Appendix 3). For statistical accountability, the experiment was repeated two more times and the mean parameters reported with standard deviations. Cell sizes are reported in pixels, (which may be calibrated say, in millimetres, by having an object in the image the actual size of which is known).

For statistical accountability. For statistical accountability, the experiment was repeated two more times. Three random surface areas were scanned for each sample surface, and the number of cells for each scan estimated the mean and standard deviation/error determined for each disc

3.8. Statistical Analysis

All numerical data were analyzed using Prism statistical software (GraphPad Inc. Version 6) and SPSS 22.0 (SPSS, Chicago, Il, USA). Error bars were calculated based on the standard

error of the mean for n-values ranging from 3 to 25. One-way analysis of variance (ANOVA) with a modified Bonferonni's post-hoc test, and the Student's t-test were used to determine statistical significance between groups, with a confidence interval of 95%.

The Sidak-Bonferroni test has a relatively simple modification that not only confers more statistical power to the traditional Bonferroni formula, but also retain much of the flexibility of the Bonferroni method (Wickens and Keppel, 2004). The slightly more complicated formula is:

$$\alpha_{S-B} = 1-\left(1-\alpha_{FWE}\right)^{1/c}$$

where $\alpha_{S\text{-}B}$ is the Sidak-Bonferroni alpha level used to determine significance, *c* is the number of comparisons or statistical tests conducted in the "family", and

α_{FWE} is the familywise error. The familywise error can be estimated with the following formula:

$$\alpha_{FWE} \leq 1-(1-\alpha_{EC})^{c}$$

where α_{FWE} is the familywise error rate, α_{EC} is the alpha rate for an individual test (almost always considered to be .05), and *c* is the number of comparisons (Šidák, 1967).

Assumption of normality was tested using the Kolmogorov-Smirnov test for sample sizes $\geq$50 or the ShapiroWilcox test used if samples were <50. For non-parametric data, the Kruskal Wallis test was used and well as the Mann-Whitney U test.

A p-value $\leq$0.05 was accepted as significant. In some cases, further robustness was introduced by setting confidence interval at 99%, with significance p-value of <0.01. Bar graph represents the mean ± standard error of means. In all cases, the experiments were carried out three or more times to ensure the results are reproducible. The data presented were from three or more comparable results for each parameter. Absolute baseline values however varied appropriately for each experiment (See Appendix 1).

Chapter 4 : Simple Surface Modifications Technique for Enhancing Implantable Titanium Surface

4.1. Introduction

It's been over 20 years since David F. Williams and Buddy Ratner attempted to highlight the importance and predict the trend of titanium as a metal of choice in biomedical applications (Williams, 2016). The perception is that, though a great deal of applications has been found for titanium, a great deal is still to be done in improving the current medical applications, particular in dental and orthopaedic medicine. With proven efficiency in replacing weight bearing tissue, largely as a result of its excellent mechanical properties and biocompatibility, a great deal of current research is centred on the interaction between the titanium material surface and the human tissue it is in direct contact with.

One of physics' many definitions of a surface is a sudden disruption of the atomic arrangement of a material. This disruption results in surface and bulk electronic properties differences, which in turn influence the varying physico-chemical behaviour of the surface and bulk regions of the material (Kittel, 2008). An extension of this theoretical view would suggest that, the means of disrupting the material atomic arrangement, leading to the introduction of a surface, i.e. the surface modification method, may result in different and peculiar surface properties. The suggestion is that, it is these physico-chemical properties that define the interaction between the host and the modified surface of the implant material. The uniqueness of the relationship between the means of surface modification and the resulting properties of the biomaterial surface has led to the suggestion that surfaces resulting from new surface modification strategies should be viewed and tested as new biomaterials (Albrektsson and Wennerberg, 2004a, Albrektsson and Wennerberg, 2004b, Coelho and Lemons, 2005).

After the introduction of the term ‘osseointegration’ by Per-Ingvar Brånemark of the Swedish group in 1952, implantology research focus shifted significantly from biocompatibility to integration with osseous tissue. The natural progression of this is the extensive research that is ongoing into the role of surfaces in the osseointegration process, and with this, improvement in surface properties to further enhance osseointegration performance of implants. Surface modification or texturing has thus become the most applied method of improving the host response to implants in the last decade (Coelho et al., 2009). It is evident from a review of current literature that, surface texturing by means of a variety of protocols including bioactive surface coating, post machining, as well as increasing surface biocompatibility and osseo-conductivity, and promoting bone healing, also enhances the anchorage and biomechanical stability of endosseous implants (Albrektsson and Wennerberg, 2004b, Albrektsson and Wennerberg, 2004a, Buser et al., 2004b).

In spite of the documented successes of the well-developed conventional methods of surface modifications, several problems still remain that make their general application problematic, and not entirely cost effective. Expensive large scale equipment is required for sputtering and plasma spraying, the effectiveness of which is limited by the complexity of the implant device shape. Strict control of atmospheric conditions is required in order to supress hydrolysis of reaction solutions during sol-gel method of surface modification. Very high temperatures are needed to encourage the formation of the all-important corrosive resistant oxides of titanium of the material surface, and the incorporation of other ions onto the surface of titanium (Ueda et al., 2009a).

Surface-tissue interaction studies in recent times, have adequately demonstrated that, cells in close proximity to implant surfaces are sensitive to their topographic features, and the features up regulate related gene expression, particularly of bone tissue in contact with titanium surface (Stanford, 2008). An exact understanding of the molecular mechanism of this is still lacking.

However, the role of the surface chemical and physical properties in modulating cell behaviour, instigating growth factor production, and encouraging osteogenic gene expression is well documented (Joseph et al., 2009b, Taloş et al., 2013, Kim et al., 1997b, Chen et al., 2007). An investigation into simple cost effective and efficient combination or independent additive or subtractive surface modification strategies to produce similar of improved osseointegration, along with other benefit(s), is therefore a worthwhile project.

4.1.1. Background: Oxide Formation

An examination of the surface of even the most carefully manufactured commercially pure titanium or fabricated titanium device indicates the surfaces are not entirely pure. This is because on exposure to air, an oxide layer of 5-100 Å thickness forms on the exposed surface. This surface adsorbed layer of oxygen is of critical importance to the formation of subsequent oxide layers and the physico-chemical properties and interactions of the titanium surface. Several surface oxide studies have demonstrated that the state of the oxide formed on the titanium surface depends on factors including the length of exposure, the temperature at the metal surface and the number of oxide monolayers formed on the surface, with evidence of both surface and subsurface oxygen absorption (Costerton et al., 1999a, Busscher et al., 2012a, Petrini et al., 2006). Carley et al identified three oxidized species: Ti^{2+} and, Ti^{3+} in the sub-monolayer, and Ti^{4+} mainly in the outermost layer. The stoichiometric oxidation states corresponding to these are TiO, Ti_2O_3 and TiO_2, with the dioxide TiO_2 the naturally abundant. The natural dioxide occurs in three crystalline forms; brookite which has an orthorhombic structure, anatase with a tetragonal structure and the most common rutile, also with a tetragonal structure (Busscher et al., 2012a, Jones, 2001). Following a study on the room temperature interactions between oxygen and titanium surfaces, Azoulay et al concluded that, the initial accumulation of oxygen is on the uppermost layer of titanium atoms. They also inferred that, the kinetics of oxygen accumulation on the surface conformed to an island or clustering model,

and depending on the characteristics of the metal surface on exposure, this presents as a mixture of 'patch-like' patterns of oxides of different valence states (Azoulay et al., 1997).

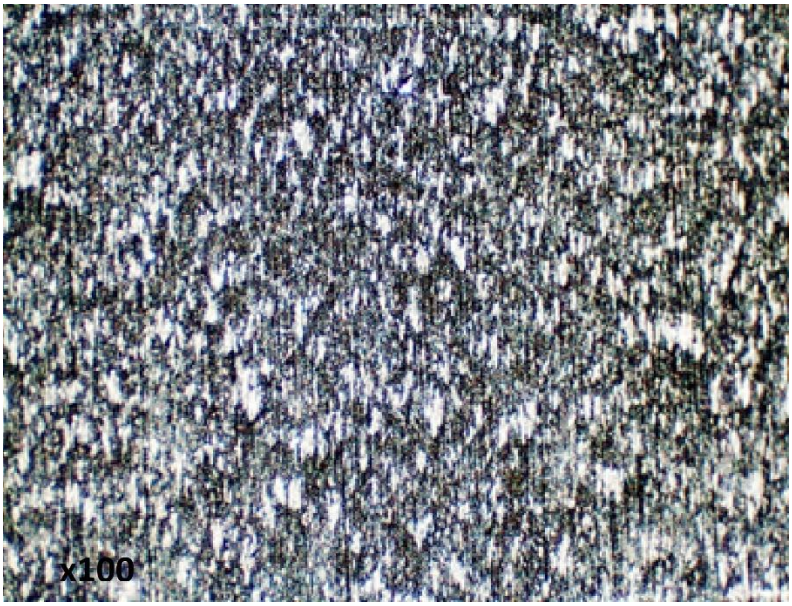

Figure 4.1. An optical microscope (x100) image of cpTi showing the microstructure and associated defects of the surface. These appear to direct oxide nucleation (as white patches) and confer oxidative protection to the Ti surface. These oxides have been shown to comprise mainly of TiO and TiO_2

It appears it is this original microstructure (Figure 4.1) and associated defects of the surface that direct oxide nucleation onto the surface, and ultimately confers the oxidative protection resulting from the formation of different oxides, mainly TiO and TiO_2. Consequently, the original and modifications to the microstructural details of the surface strongly influence the oxidation kinetics, i.e. the corrosion resistant property, and the osteo-integrative ability of titanium in close contact with the oxygen-rich *in situ* environment (Xu et al., 2010).

The rational thinking, inspired by the oxides of various elements that form on the Ti surface during manufacture, handling and storage suggests that these oxides form as layers of varying composition, thickness and structures. These in turn inform the surface features or topography of the exposed Ti surface. By this reasoning, the suggestion is that, the chemical modifications introduced onto the Ti surface are layered and influence the surface properties of the modified surface. However, it has been demonstrated that many important oxides on the Ti surface, such

as TiO2, MnO2, ZrO2, Nb2O5 do not exhibit layered structures, and are held together by strong ionic interactions (Sun and Li, 2003), which keep the metal cations and oxygen anions together

Modification of this oxide layer by both physical and chemical means has become popular in recent times. Machining or abrasive removal and chemical treatment with sodium hydroxide (NaOH) or hydrogen peroxide (H_2O_2) are the commonly employed techniques (Chrzanowski et al., 2008b). Wet processes such as the chemical modification with NaOH, which has been employed clinically, is suitable for surface modification of devices with large surface areas and or complex shapes (Fowler et al., 2000, Ueda et al., 2009b, Hamada et al., 2002).

The hydrothermal treatment technique is a wet chemical technique, widely used in creating nanocrystalline oxide surfaces (Armitage et al., 2008). The temperature employed is usually between the boiling and critical point of water. The usefulness and attraction of this technique in surface modification of biomaterials is in the ease of controlling the synthesis conditions such as treatment time, temperature and composition of the treatment solution. $CaTiO_3$, a favourable oxide for inducing bone formation on biomaterials, has been produced as a film on titanium substrate, by this process (Hamada et al., 2002, Wiff et al., 2007, Armitage et al., 2008). Calcium ions on the titanium surface encourages the formation of hydroxyapatite $Ca_{10}(PO_4)_6(OH)_2$, on the surface, and this precursor to bone material enhances the osteointegration process. Ueda et al concluded from their chemical-hydrothermal combined surface modification of titanium for improvement of osteointegration that, surface treatment with $Ca(OH)_2$ solution gives rise to the most structurally stable hydroxyapatite (HAp) in *in vitro* SBF conditions (Ueda et al., 2009a).

4.2. Method

Sample preparation involved cutting the commercially pure temper annealed titanium (cpTi) foil into precise 12mm (for use in the rods of the biofilm reactor and 24-well plate) discs, using

a Waterjet cutter. The discs were metallographically polished to a mirror-finish with a Labol 8-12 Convertible Grinding/Polishing Machine, water and silica carbide (SiC) emery paper of progressively reducing grit sizes. The resulting surfaces were characterised by means of scanning electron and atomic force microscopy, profilometry and goniometry. The detailed sample preparation and characterisation process is in sections 3.2 and 3.4. of chapter 3.

4.3. Results

4.3.1. Characterization and Comparison of Commercially Pure Titanium (cpTi) and Polished Titanium Surface (polTi)

Whereas the unpolished discs retain the natural dullness of the commercial titanium, the mirror-finished polished disc show a highly reflective mirror-like sheen (Figure 4.2). The attainment of the mirror-like reflective surface to the naked eye during the polishing process is an indication of the extent to which the surface defects retained post the manufacturing process, together with, dust, grease and oxides of other element layered on the surface during handling and storage, has been removed.

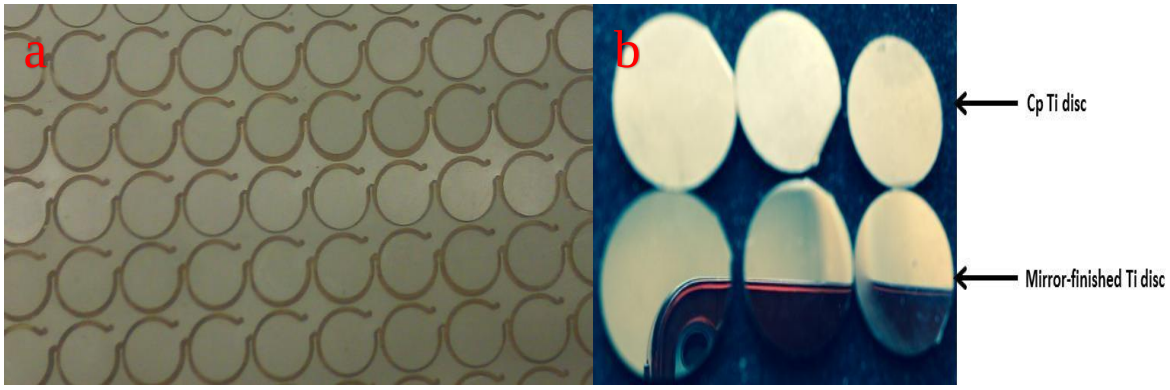

Figure 4.2. Flow-path drawn and Waterjet cut Titanium disc(a), and a comparison of the mechanically modified and unmodified Ti surfaces(b). Commercially pure unpolished (cpTi) and mirror-finished polished (polTi) and Yi surfaces show marked physical differences. Note the reflective/mirror-like surface of the polished titanium (second row of three) discs.

4.3.2. Surface Features and Composition of cpTi and polTi

In comparing the surface features of the commercially pure titanium (cpTi) with the mechanically modified titanium (polTi), scanning electron microscope images of the surfaces were taken at 500x magnification. Figure 4.3a/b shows the respective surfaces. The cpTi surface (Figure 4.3a) shows the characteristic groves/ridges left behind by the manufacturing machining process. These are also covered with oxygen as oxides, and other elements the surface become exposed to. An energy dispersal x-ray spectrum of the cpTi shows peaks for carbon and fluoride in addition to the Ti (Figure 4.3c). The polTi surface however shows the absence of the machining groves/ridges characteristic of the unpolished surface. At 500x magnification, the surface appears uniformly smooth and devoid of any defects or artifacts (Figure 4.3b). The EDS spectrum also shows the absence of fluoride, present prior to polishing to a mirror-finish.

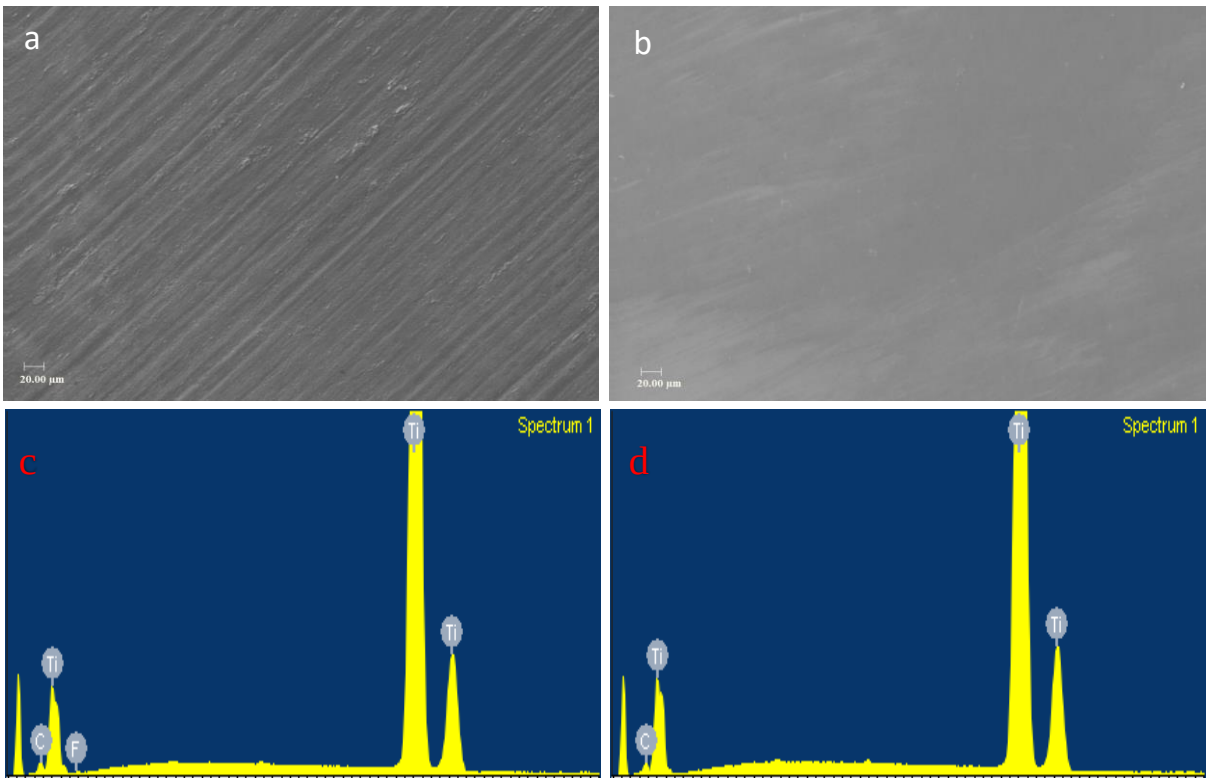

Figure 4.3. A comparison of the mechanically modified, polished Ti and unmodified Ti surfaces, with their corresponding surface elemental spectra (a) machined surface of cpTi showing the unidirectional machining groove artefact on the surface. (b) mirror-finished polTi, with uniformly smooth, mirror-like surface, devoid of artefacts even at 500x magnification. (c)EDS spectrum of cpTi, showing surface elemental composition peaks. Ti, along with carbon and fluoride are the main peaks for cpTi disc surface. (d) EDS spectrum of polTi. Ti, with carbon are the prominent peaks for polTi.

4.3.3. Surface Atomicity and Wettability of cpTi and polTi

The usefulness of titanium lies in the interaction between the Ti atoms at the surface of the metal, and other atoms or molecules it comes into contact with (Armitage and Grant, 2003). Therefore, any covering on the surface that reduces the number of Ti atoms available for a targeted interaction is undesirable. To examine the surfaces for improvement in the number of Ti, as a percentage of the total number of different atoms on the surface, an energy dispersal spectroscopic analysis of the surfaces was carried out.

Table 4.2 shows the number of different elements in addition to Ti on the surface. The table also shows the elemental atomic percentage composition for the cpTi surface (

Table 4.2a), and for the polTi surface (

Table 4.2b). A visual comparison of the percentage atomic composition of surface Ti of the two surfaces is depicted by Figure 4.4. The indications are that, the mechanical surface modifications of the cpTi improved the surface Ti composition from 55.96±1.88% to 95.91±0.63%.

The interaction leading to the formation of bonds between the titanium and surrounding tissue is influenced by the surface phenomenon such as wettability or surface energy. This is related to the contact angle (CA) of the surface by the Young-Dupre´ equation:

$$cos\theta = (\gamma SV - \gamma SL) \div \gamma LV \qquad \textit{Equation 4.1}$$

where θ is the contact angle, and γ is the interfacial energy/tension between the solid (S), liquid (L), and vapour (V) phases (Lai et al., 2010, Kim and Ramaswamy, 2009, Feng et al., 2002).

The surface energy of the solid substrate should be raised higher than the surface tension of the wetting liquid to improve wetting (Maddikeri et al., 2008).

Surface wettability was assessed by determining the water contact angle (CA) at the water-Ti interface (Menzies and Jones, 2010, Cheng et al., 2004). Fig 3.3b represent a comparison of

the contact angle measurements hence wettability of cpTi and polTi, determined by static sessile drop method using water as the wetting agent at standard conditions.

Table 4.1 A schematic of the static contact angle of a liquid droplet on an ideal solid surface and how it relates to the Young's equation (a), and the graphical relation between surface energy and the wetting of a solid (b).

(a)

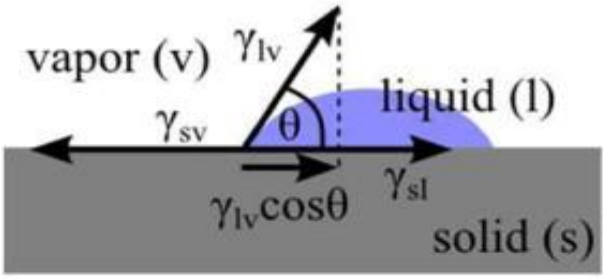

(b)

Energetic relationship	CA relationship	Optical representation	Macroscopic result
$\gamma_{sv} - \gamma_{sl} > 0$	$0° \leq \theta \leq 90°$		High wettability
$\gamma_{sv} - \gamma_{sl} > \gamma_{lv}$	$\theta = 0°$		Complete wetting (spreading)
$\gamma_{sv} - \gamma_{sl} < 0$	$90° \leq \theta \leq 180°$		Low wettability
$\gamma_{sl} - \gamma_{sv} > \gamma_{lv}$	$\theta = 180°$	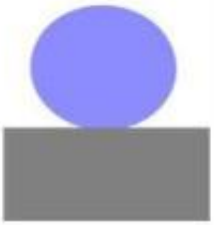	Non-wetting

Table 4.2 Showing the mean percentage atomic composition of (a) cpTi and (b) polTi for n=27 discs in each group. The polished surface appeared devoid of the common, fabrication, storage and handling surface oxides.

a Elements	Atomic %
O	21.9
Al, C, Ca, F, Si	22.2
Ti	56.0
Totals	100.1

b Elements	Atomic %
C	4.1
Ti	95.9
Totals	100.00

The cpTi shows a larger oxide surface component, together with other elements including calcium and silica. The polTi appears to have all the oxide surface component removed, with carbon consistently the only element present with Ti.

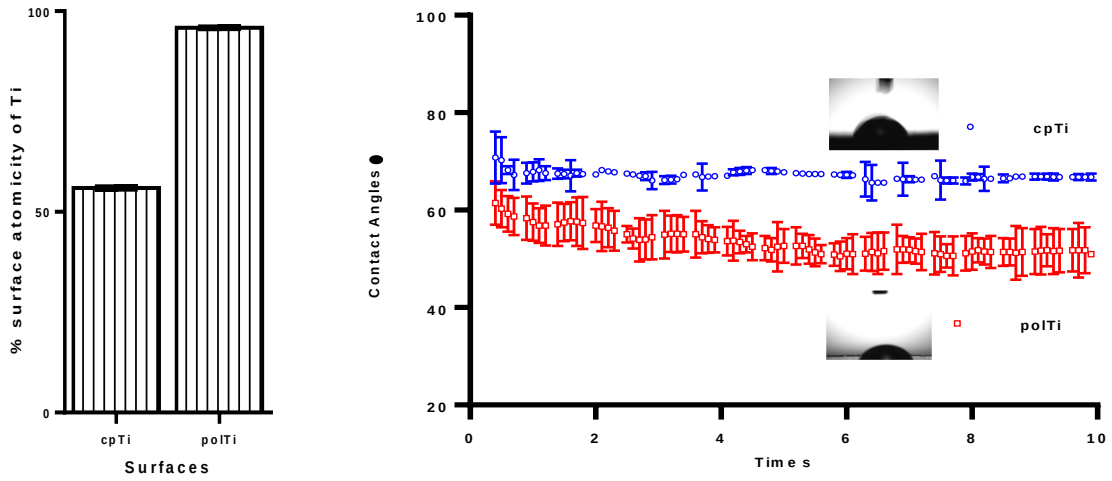

Figure 4.4 Comparing the surface titanium atomic composition and contact angle (measure of wettability) of the commercially pure Ti (cpTi) and mirror-finished Ti (polTi) surfaces. The surface composition of cpTi and polTi, determined by SEM/EDS shows 55.96±1.88% and 95.91±0.63% surface Ti atoms, for the respective surfaces, n=23. This suggests that, the polishing to a mirror-finish could enhance the surface interaction involving Ti atoms. The contact angles measurements of cpTi and polTi, determined by static sessile drop goniometry for n=3 surfaces, indicates a mean contact angle of 67.13±0.86o for cpTi and 53.49±2.65o for polTi. This suggests both have good with wetting properties (CA < 90o), with the mechanical surface modification marginally improving the wetting property. The error bars represent the mean ± S.E.M. A Welch-corrected two-tailed student t-test indicates a significant difference (p<0.01) between cpTi and polTi for both surface Ti composition and water contact angle.

Sessile drop contact angle measurement of the two surfaces suggests that, the cpTi surface has a mean contact angle of 67.1±0.9º. That for the polTi surface is 53.5±2.7º. This indicates both surfaces have good wetting properties (as is for surfaces with contact angle < 90º). The mirror-

finished surface however demonstrated a lower contact angle than the commercially pure surface, as shown in Figure 4.4.

4.3.4. Topography of cpTi and polTi

Another parameter that influences the interfacial response between the implantable titanium and the tissue it is in direct contact with is the topography of the solid material surface. A micro or nano-order topographic features may be the preferred scale depending on the application need of the implant. In characterising and comparing the topography of the cpTi and polTi, an atomic force microscope was employed to capture 3D images of the surfaces by the contact mode method. The ISO 25178 height parameters of interest for 3D surface texture analysis are the maximum height of peaks (Sp), the maximum height of valleys (Sv) and the arithmetic mean height of the surface (Sa). Figure 4.5 shows the scaled 3D image of cpTi and polTi surfaces. The cpTi surface shows different shades of peaks (lighter shades) and troughs (darker shades) of varying degree of heights/depths across the surface. The polTi surface however shows an almost uniformly smooth surface albeit of varying shades, implying differences in height parameters across the surface.

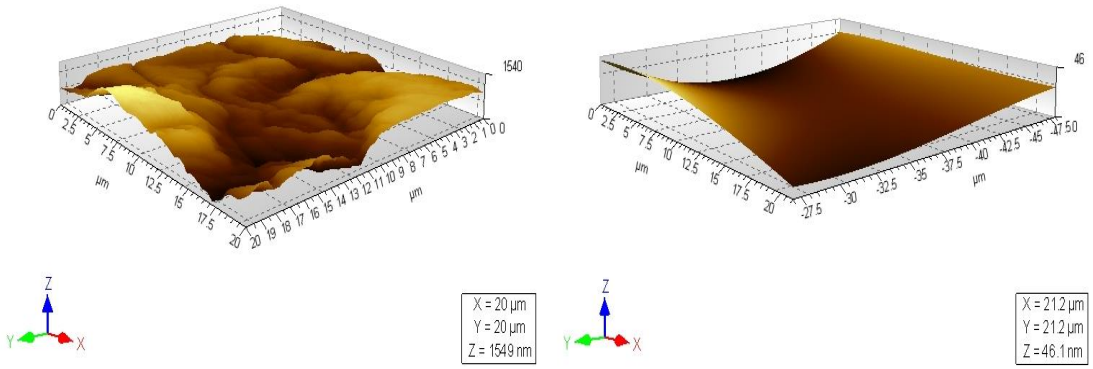

Figure 4.5 3D AFM topographic images of the cpTi surface (on the left), showing the undulating peaks (lighter shades) and troughs (darker shades) with the mean height scale (z) in the region of 1549 nm, and the polTi surface (on the right), showing the 'uniformly smooth' surface of the polTi disc, with z-scale in the region of 46.1 nm

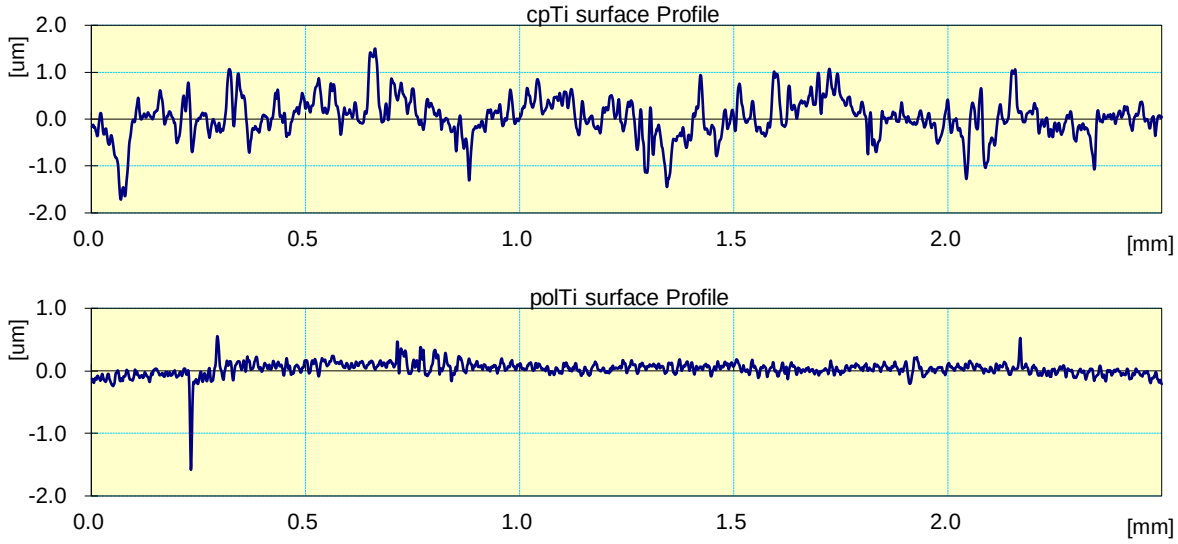

Figure 4.6. Profilometry display of cpTi (top)and polTi (bottom) showing the characteristic 'noisy' peaks and valleys of the rougher surface of the cpTi, and the relatively 'smoother' surface of the polTi surface.

An analysis of the surface texture of the 3D images was carried out using the Picoview software. The images suggest that, the cpTi surface consists of undulating peaks and valleys, as would be expected from the machining artefacts from the manufacturing process, and from the patchwork of oxides layers on the unmodified surface. The mirror-finished surface however appears uniformly smooth, with no visible characteristic features. The surface profile of the two surfaces is also shown in the profilometry display (Figure 4.6) shows the cpTi surface 'noisy' series of peaks and valleys, as previously suggested by the AFM image. The profile for the polTi, as also similarly suggested by the AFM image, confirmed a smoother surface, with tighter, narrower and smaller peaks and valleys.

Table 4.3 shows the height parameters in of the two surfaces. The mean roughness (for the 3D-image of the surfaces, Sa) values suggest that, the commercially pure surface cpTi has micro-scale topographic features. The modified polTi surface however appear to have nano-scale surface features. This appears to still hold true when other height parameters such as Sp and Sv are considered.

Table 4.3 Height and roughness parameters of cpTi and polTi surfaces, as determined by contact mode atomic force microscopy (top) and contact profilometry (bottom). In both cases (n=3), the parameters indicate the mirror-finished surface is comparatively better controlled than the commercially pure surface.

3D Roughness Parameters (nm)	cpTi	Stdev	polTi	Stdev
Sq	266.3	4.3	9.3	0.9
Ssk	-0.4	0.2	0.5	0.6
Sku	3.8	1.2	3.5	0.6
Sp	795.0	12.8	35.3	3.8
Sv	878.5	11.1	18.5	2.8
Sz	1673.0	9.3	53.8	3.0
Sa	204.5	7.0	7.4	2.8

Roughness Parameters (um)	cpTi (mean)	Stdev	polTi (mean)	Stdev
Ra	0.32	0.01	0.07	0.01
Rz	3.29	0.14	1.06	0.45
Rq	0.42	0.01	0.11	0.01
Rt	3.23	0.12	1.06	0.45

The cpTi has Sa of approximately 204.5±7 nm. This is approximately 9.3±0.9 nm for polTi. Similarly, the maxima heights of peaks (Sp) and valleys (Sv) are comparatively higher for cpTi than for polTi.

The 2D profile (stylus) parameters (Table 4.3), though less sensitive but more representative of the surfaces, also indicate, as before, that the cpTi surface is typically rougher, Ra of approximately 320±10 nm, than the polTi surface, Ra of approximately 70±10 nm. The Rz value, is also comparatively higher for the cpTi surface (approximately 3290±140 nm), than for the polTi surface (approximately 1060±450 nm). This is the average maximum profile height along (X, Y), derived from the average over the sampling lengths, of the difference between the highest peak and lowest valley. The Rt value represents the maximum profiler height along (X, Y), determined from the difference between the highest peak and lowest valley

along the evaluation length. The two values are similar here because a number of evaluation lengths was made up the sampling length.

4.4. Discussion

The surfaces of the mechanically modified or polished titanium (poTi) and that of the commercially pure titanium (cpTi), were characterised and compared by means of scanning electron microscopy, with energy dispersal spectroscopy for surface element composition. Goniometric contact angle measurements were also carried out to determine how the new surface compares to the old in terms of water contact angle and wettability. The surfaces were further characterised for their profile by means of an AFM and a stylus profilometer. The features of the two surfaces were then compared. The 3D images generated by the AFM facilitated characterising and comparing surface morphology of the modified and the commercially pure surfaces.

Waterjet cut discs of the commercially obtained 1mm thick titanium sheet formed the baseline sample or control of unmodified commercially pure Ti discs (cpTi). The hardness of titanium meant that a conventional cutter is not capable of cutting through the titanium into the desired precise 12mm diameter disc shape. A precision water-jet cutter, which employs water under high pressure was able to do this, with the added advantage of no involvement of heat or chemical, hence no heat or chemical affected zone, and the material surface remained as obtained without any modifications. The primary modification protocol during this phase of the study involved the use of reducing grit size SiC paper, a neoprene polishing cloth and ultrafine grain silicone suspension, on a rotating platen, to mechanically polish the Ti discs to a mirror finish. Figure 4.2 shows the cut discs and some discs before and after mechanically polishing to a mirror finish. The cpTi discs surfaces were dull and non-reflective. This is because the surface features retained from the manufacturing process did not allow the surface

to reflect light incident on it in an ordered unidirectional specular manner. Also, the cpTi surface is layered with oxides of titanium, and other atoms it has become exposed to during handling and storage. This readily formed titanate oxide layer however protects the surface from corrosive or oxidising agents. The thickness and morphology of this oxide layer depend on the duration of handling and storage, the prevailing storage conditions, and manufacturing artefacts retained on the surface of the Ti sheet. The relatively 'rough' surface of cpTi diffuses light incident on it hence not able to produce a virtual image of an object, such as a camera, held in front of it. The reverse is however true for the mirror-finished modified surface of the polished discs (polTi). The mechanical grinding and polishing process first removes the oxide layer on the disc surface, and smooth out all manufacturing defects on the surface, leaving a relatively 'smooth' surface capable of specular reflection of light incident on it.

The 500x SEM images, together with the EDS spectra of the surfaces provided a clearer picture of the two surface (Figure 4.3). The 'smooth' surface of the polTi suggests that the grinding and polishing process removed the oxide (impurities) layer on the cpTi, as well as the surface defects left by the sheet manufacturing process. This appears to confirm the initial observation that the specular refection observed with the polTi but not in the cpTi was as a result of the absence of microscopic peaks, troughs, grooves and ridges otherwise on the cpTi which diffuses light incident on it. The EDS spectra shows the presence of fluorine atoms on the cpTi surface, but absent after polishing. The spectra, together with the surface atomic composition data (

Table 4.2) gave further credence to the observation that, the mechanical grinding and polishing method developed enhanced the purity of the titanium foil surface. Contaminating elements found on the cpTi surface in addition to oxygen that forms oxide on the surface included Al, C, Ca, F, and Si. Though some of these results from the handling and storage of the Ti foil, the manufacturer reports the 99.6% tamper annealed Ti foil to contain traces in ppm of Al, Co, Cr,

Cu, Fe, Mg, Mn, Ni, Si, Sn, Ta, and V. All these elements, together with their oxides, were completely removed by the polishing process. The result is an approximately 40% increase, from shows 55.96±1.88% and 95.91±0.63% in surface Ti atomic composition (Figure 4.4), for n=23 samples. The process therefore led to an improved surface with more Ti atoms available for interaction with other agents to further improve the surface and/or interaction with living cells/tissues.

The surface water wettability of implant devices greatly influences the biological and non-biological event cascade at the host/implant interface. A review of literature suggests that, wetting is modulated by surface characteristics including surface topography and chemistry (Rupp et al., 2014, Elias et al., 2008, Ponsonnet et al., 2003, Janssen et al., 2006, Cho et al., 2012, Balaur et al., 2005, Vogler, 1999). Four major aspect of biological systems are affected by surface wettability: proteins and other macromolecules adhesion to surfaces during the conditioning process, hard and soft tissue interaction with the preconditioned surface, bacterial adhesion and biofilm formation, and speed of osseointegration (Maddikeri et al., 2008). To ascertain how the new modified surface performs with respect to contact angle and water wettability, parameters that will inform on the interaction between the surface and polar molecules it will come into contact with, static sessile drop contact angle measurements were carried out. These are related to the surface tensions or energies by the Young-Dupre´ equation

$$\cos\theta = \gamma SV - \gamma SL \div \gamma LV \qquad \text{Equation 4.1}$$

The measured contact angle values therefore yield an important parameter, i.e. the surface energy of the solid-vapour phase (γSV), which quantitatively represents the wetting characteristics of the solid material, the significance of which seen in the biocompatibility of medically applied materials. The evidence is well established that water-wettable surfaces (Table 4.1) response markedly differently to poorly-water-wettable surfaces, as the biological response to a given material is driven by the surface energy of the material (Vogler, 1999)

(Balaur et al., 2005). The mean contact angle readings for the surfaces were 67.1±0.9^{o} for cpTi and 53.5±2.7^{o} for polTi, showing only a marginal reduction in contact angle with polishing the commercially pure Ti surface. The indication from this is that, both surfaces have good water wetting capabilities as the mean contact angle for both is less than 90^{o} (Table 4.1). However, the approximately 14^{o} reduction in contact angle with the surface modification suggests an increase in the surface energy and reduction in hydrophobicity. The increased surface energy would suggest that a higher activation energy will be required for any biological interaction with the polTi surface, and that any bond so formed will required a higher amount of energy to disrupt. The chemical or biological bond formed will therefore be stronger for the polTi than for the cpTi surface. A paired sample analysis of the data suggests the difference in contact angle measurements was significant at 95% CI, with a positive correlation of 0.704 between the two samples for the modification applied to polTi.

Although the bacterial adhesion to surfaces mechanism is not fully understood as a result of the complexity of the different factors involved, making prediction of bacterial interfacial behaviour difficult, the general consensus on the material side is that, hydrophobicity (measure by water contact angle) and surface free energy, as well as the average surface roughness are crucial positive factors in the bacterial adhesion and biofilm formation process. The adhesion of human pathogens, particularly pathogens *S. aureus* and *S. epidermidis*, have been demonstrated to correlate to increased hydrophobicity, making it the main driving force for bacterial adhesion (Maddikeri et al., 2008, de Avila et al., 2015, Pjetursson et al., 2014, Simonis et al., 2010, Chen et al., 2014, Oliveira et al., 2015, Chug et al., 2013). The modification here therefore suggested that, the polTi surface will present a better opposition to bacteria adhesion than the cpTi.

A topographic comparison of the cpTi and polTi was carried out by the comparing the 3D and stylus profile images of the surfaces, and by comparing their height parameters. Whereas the

polTi surface appears uniformly ‘smooth’ with no apparent peaks and valleys, the cpTi shows a rougher texture, with numerous peaks and valleys as the various colour shades of the surface suggest. The mean surface roughness (Sa) of approximately 200±50 nm for cpTi and approximately 10±1 nm for polTi, together with the values for the maximum height of the surface (Sz), maximum height of valleys (Sv), and maximum height of peaks (Sp) (Table 4.3), collaborates the visual observation that the cpTi is more texturized or rougher than the polTi.

The symmetry of the surface height about the mean plane is represented by the skewness of height distribution (Ssk), the sign of which indicates the dominance of peaks (Ssk >0) or valleys (Ssk<0) on the surface. This would suggest that, the cpTi surface is valleys dominated, (Ssk of -0.4) as would be expected from the machining manufacturing process. The polTi surface appears peaks dominated, with Ssk of 0.51. The peak to valley ratio is represented by the kurtosis of height distribution (Sku). An Sku>3.00 represents a high peak to valley ratio, and the lack of Sku<3.00. Surfaces free of extreme peak or valley features tend to have Sku<3.00, and are described as gradually varying (Shi et al., 2008, Yamada et al., 2010). For both surfaces however, the similar Sku values (Sku<3.00) suggest both surfaces are free from extreme peaks and valleys, hence gradually varying.

Although the AFM provide more precise and sensitive data, the suggestion however, is that the dimensions analysed may not be representative of the total sample surface (Poon and Bhushan, 1995, Kakaboura et al., 2007). This, together with the stylus tips’ dimension and ability to deconvolute the surface morphology, introduce parameters that introduces difficulties in comparing the values provided by the two methods. However, general measures of roughness should be comparable for the two methods. In assessing the surface profiles of the cpTi and polTi using the stylus profile, which for the dimensions involved is more representative of the surface, the results (Table 4.3), again suggested correctly that the cpTi has more textured

surface than the polTi surface. The average roughness values Ra, were approximately 320±10 nm for the cpTi surface and approximately 70±10 nm for the polTi surface.

4.5. Conclusion

The values of the height parameters suggest that, though the surface features are gradually varying for both surfaces, the cpTi had more valleys or depth than peaks, from the grooves or artefacts left by the machining process. The surface modification method significantly reduces these till peaks dominate the surface. The measures for surface roughness (Sa and Ra) indicate that, the method in addition to removing the surface oxides and contaminants, also reduced the overall surface roughness from a micro scale to a nano scale. In the process the surface modification process also raised the water contact angle, thereby increasing water wettability and reducing the hydrophobicity of the surface.

Chapter 5 : Characterizing Ions Incorporated onto Modified Titanium

5.1. Introduction

Surface modification of the commonly used implant materials has become an important aspect of implantology studies. This is because most of the events leading to the body's acceptance of the implant device, and the eventual integration of the implant within the placement site tissue take place largely at the implant-tissue interface. Therefore, to enhance compatibility with the surrounding tissue, it is important to optimise surface characteristics such as surface energy, topography, roughness and chemistry (Howlett et al., 1999, Puleo and Nanci, 1999a). The modification of the surface chemistry of titanium has been extensively reported to influence the biocompatibility of implants, the attachment and proliferation of bone cells, promotion of osteogenic cell differentiation and signalling cascade of osteogenic cells (Zarb, 1985, Wall et al., 2009, Lee et al., 2010b).

Several surface chemistry modification methods have been developed, most of which are additive or ion implantation methods. Ion incorporation on the titanium surface may be carried out by an electro-chemical deposition, electrophoretic deposition, pulsed laser deposition, plasma spraying, sputtering method, biomimetic deposition and hydrothermal deposition (Armitage et al., 2008, Chrzanowski et al., 2008a). Advantages of the ion implantation methods include homogeneity and reproducibility of doping, speed, dosage control and high doping purity (Bosetti et al., 2001, Suchanek et al., 2015).

A modified, cost effective, hydrothermal deposition additive surface chemistry modification was employed here, aimed at introducing different metallic ions onto the titanium surface to achieve specific improvement on the function of the implantable titanium.

Calcium ions were introduced onto the surface to enhance the bone interaction with the material surface, as calcium implantation has been reported to encourage osteointegration by both *in*

vitro and *in vivo* models, and affect bone cells adhesion quantitative and qualitatively (Nayab et al., 2005, Le Guéhennec et al., 2007, Park et al., 2011, Kizuki et al., 2010, Velard et al., 2013, Wiff et al., 2007, Hamada et al., 2002). Silver ions was implanted onto the titanium surface to confer antimicrobial properties to the modified surface, as silver ion has been demonstrated in various studies to bring antibacterial capabilities to implant device surfaces (Ionita et al., 2011b, Juan et al., 2010, Whitehead et al., 2011, Ionita et al., 2011a, Ferraris et al., 2014, Wang et al., 2011, Sheehan et al., 2004).

5.2. Method

The ions of interest were incorporated onto the mirror-finished Ti surface in a two-step modified thermochemical wet treatment process. The novel surfaces were characterised for surface composition, thickness, topography and hydrophilicity by means of scanning electron and atomic force microscopy, profilometry and goniometry. The detailed ion-incorporation and surface characterisation processes are in sections 3.3 and 3.4. of chapter 3.

5.3. Results

5.3.1. Sodium Hydroxide Pre-treatment

Several techniques have been used to modify the surface of titanium to make it more bioactive. Heat treatment (HT) and treatment with sodium hydroxide (NaOH) are two common methods used in modifying the crystallinity and surface chemistry of titanium implants. However, no studies have systemically focused on combining these two techniques as a pre-treatment in functionalising the surface of implant grade Ti with bioactive agents such as calcium, silver and zinc.

In the alkali heat treatment developed in this study, the cpTi and the polTi surfaces were subjected to the aggressive oxidizing action of 10M NaOH solution at 80^{o}C for 24 hours (Figure 3.2).

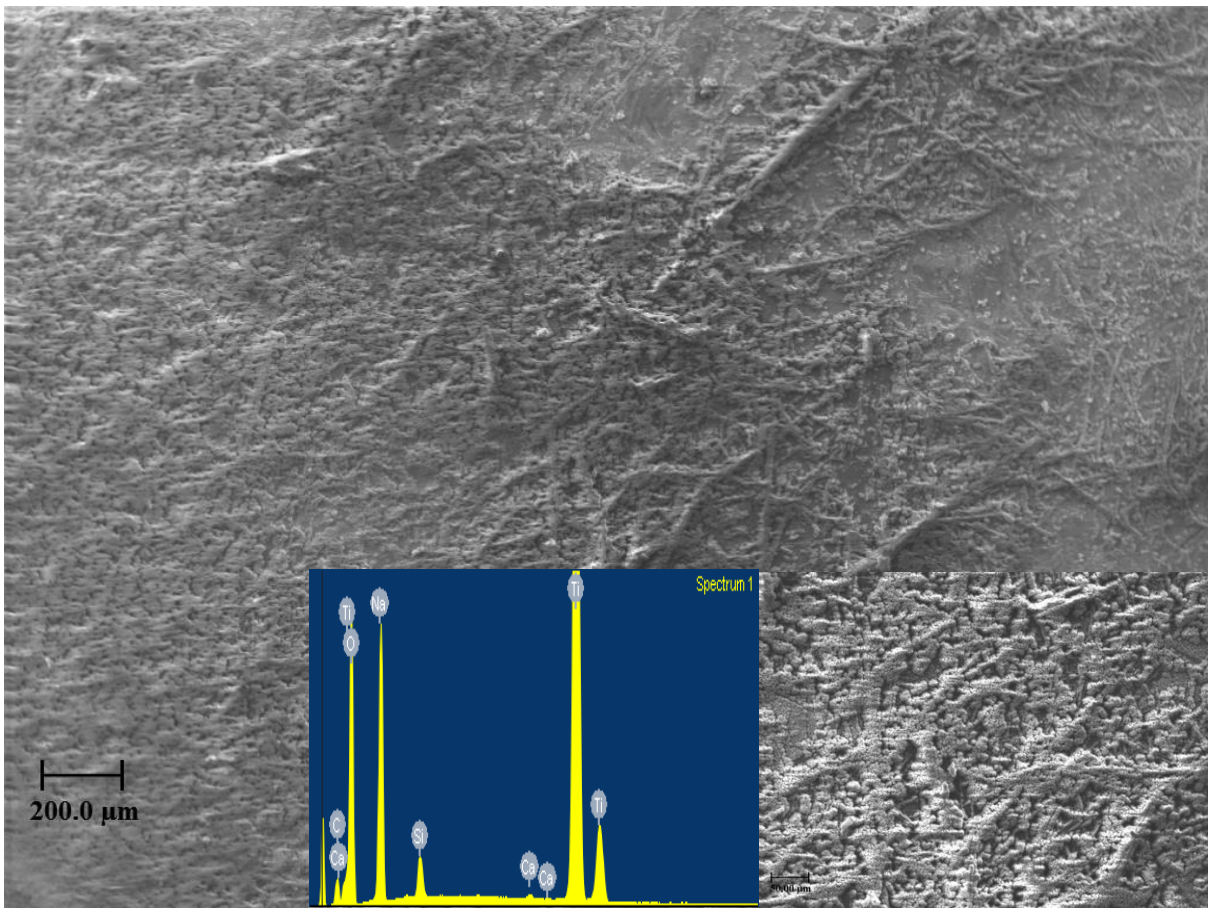

Figure 5.1. Scanning electron micrographs (main and insert) and EDS spectrum (insert) of the alkaline heat treated surface a Ti disc, showing an amorphous meshwork of sodium titanate fibres or 'nanorods'. The EDS spectrum shows peaks for silicon and calcium (impurities) as well as high peaks for sodium and oxygen.

The alkaline heat treatment of the Ti surface resulted in the formation of a hydrated amorphous layer of sodium titanate on the surface of the Ti disc. This appears as a meshwork of sodium titanate fibres or nanorods (Figure 5.1). The EDS spectrum (Figure 5.1 insert) and the composition indicate that the Ti disc surface if dominate by oxides, accounting for 64.3±1.6% of the surface components.

Table 5.1.. Showing the mean percentage atomic composition of the alkali heat treated Ti surface (n=23). The surface is predominantly covered with the resulting titanate sodium oxide, with traces of other atoms.

NaOH Pretreatment		
Element	**Atomic%**	**Stdev**
O K	64.29	1.58
Na K	11.60	0.46
Ti K	14.87	1.32
Others (Al, Ca, C, Cl, Si)	9.27	0.96

With sodium making 11.6±0.5% of the surface atoms, the deviation from the expected hydrated sodium titanate could be accounted for by oxides of other elements found on the Ti disc surface, which made up 9.3±0.9% of the atomic composition of the surface. An angled scan of the sodium titanate layer revealed that, this layer is approximately 821.1±9 nm thick across the Ti disc surface (Figure 5.2). This suggests that the alkali heat treatment transformed the nano-scale rough surface of the mirror-finished disc into the desirable for cell adhesion micro-scale rough surface. This micro-scale thick sodium titanate layer is the environment within which the exchangeable sodium of the titanate may be replaced with bioactive ions. Unlike the bioactive layer formed on the surface of Ti by other methods such as plasma spraying, the titanate layer formed by this method is chemically bound to the Ti surface, and appears not to delaminate, stays bound to the surface.

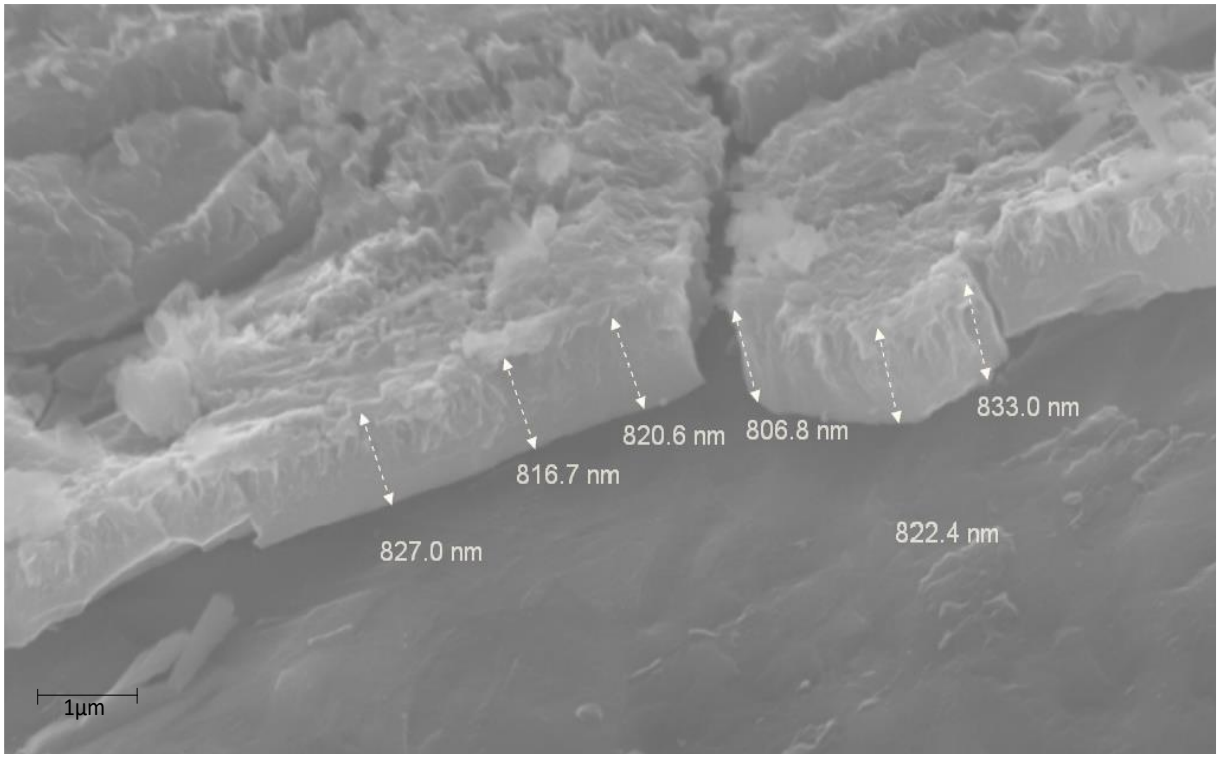

Figure 5.2. Cross-section SEM image of the sodium titanate layer formed on the surface of the alkali heat treated Ti disc. The thickness of the layer was found to be approximately 821.1±9 nm across the Ti disc surface, for n=3 discs.

In the presence of moisture, this transforms into a titanate sol-gel ion-exchange layer from which the sodium is readily available for exchange with other bioactive ions.

5.3.2. Incorporation of Calcium onto Titanium Surfaces

The hydrothermal incorporation of calcium ions was carried out for the unpolished commercially pure Ti discs (cpCa) and for the polished disc (polCa) to establish the need for the initial mechanical polishing of the Ti surface to a mirror-finish, prior to the ion incorporation. An SEM image of the surface showed the novel surface had a scar-like appearance that appeared stretched out and tightly bound to the surface (Figure 5.3). Analysis of the surface composition by SEM with EDS indicated the incorporation process was far more efficient for the polished surface than the unpolished surface. This was seen in the reduced peak intensity/height for the cpCa spectrum compared to the polCa surface. A quantification of the effectiveness of the surfaces in 'bonding' with Ca ions, measured as the surface

percentage atomic composition or proportion, indicates that 0.8±0.1%, Ca ions were incorporated on to the cpCa surface, as against 2.8±0.6% for the for the polCa surface (Figure 3.10 left). The EDS data of the calcium treated surface indicated that the surface is predominantly covered with the resulting titanate calcium oxide, with traces of Si, Al and Cl atoms. The absence of sodium from the sodium titanate formed from the initial pre-treatment with sodium hydroxide indicated that the sodium titanate sol-gel has effectively facilitated the exchange of Na^{+} with Ca^{2+} on the surface of the titanium. Also, the absence or trace Cl peaks/amounts (Table 5.2) indicated the Ca has been chemically incorporated onto the Ti surface, as against it being simply deposited on the surface, where the Cl atoms would have been expected to be twice the Ca component for the 1M $CaCl_2$ solution used. Na^{+} was therefore exchanged for Ca^{2+}, resulting in the formation of calcium titanate $CaTiO_3$, which in the presence of body fluids enhances the precipitation of hydroxyapatite(HAp) $Ca_{10}(PO_4)_6(OH)_2$, a precursor of bone tissue, on the titanium surface.

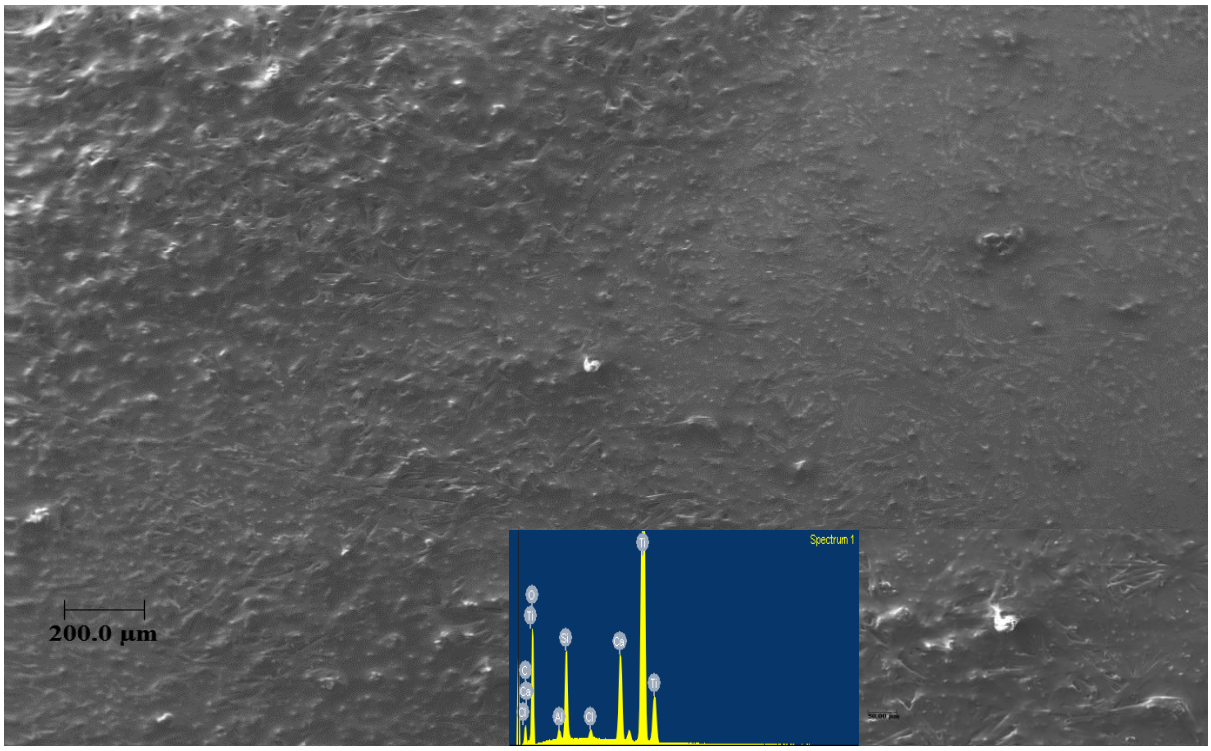

Figure 5.3. Scanning electron micrographs (main and insert) and EDS spectrum (insert) of the calcium treated surface of a Ti disc, post alkali heat treatment, showing scars-like strands and deposited of calcium incorporated onto the disc surface. The EDS spectrum shows peaks for silicon, and traces of Aluminium and chlorine, in addition to the calcium and titanium.

Table 5.2. Showing the percentage atomic composition of the post alkali heat treated calcium treated Ti surface (n=23). The surface is predominantly covered with the resulting titanate calcium oxide, with traces of Si, Al and Cl atoms

Ca Treatment		
Element	**Atomic%**	**Stdev**
O K	63.57	1.15
Ca K	2.76	0.56
Ti K	26.39	1.84
Cl	0.54	0.11
Others (Al, C, Si)	6.76	1.33

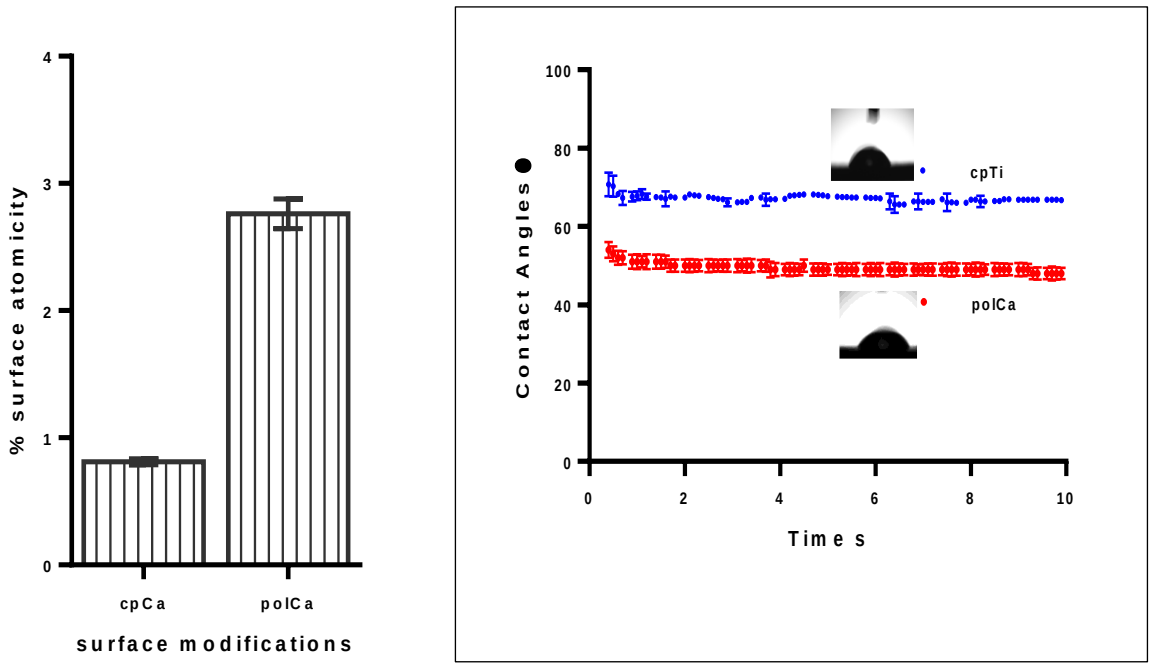

Figure 5.4. Showing a means comparison of Ca incorporation onto cpTi surface (cpCa) and the polished calcium-treated Ti (polCa) surface (left), n=23, and the water wetting abilities of polCa surface against the cpTi surface, n=3. The indication is that, polishing prior to calcium incorporation comparatively improves the calcium incorporation onto the disc surface. The calcium modified surface also shows an improvement in the water wetting capacity of the modified surface. The error bars represent the mean ± S.E.M. A Welch-corrected two-tailed student t-test indicates a significant difference ($p<0.01$) between cpTi and polTi for both surface Ca composition and water contact angle.

Water contact angle measurements for the Ca treated surface, as a measure of it water wettability also indicates that, the mean contact angels were 67.2±0.1^{o} for the cpTi surface and 50±0.1^{o} for the calcium modified surface (polCa). Although both surfaces appear to have good water wettability (contact angle <90^{o}), the calcium modification of the Ti surface appears to reduce the contact angle and further improves it water wetting capacities (Figure 5.4 right).

The mechanically modified and calcium treated surface's 3-dimentional (3D) height parameters, determined by contact mode atomic force microscopy indicates that, post treatment, the highest peaks (Sp) stands at 934.8±12 nm. The deepest valley (Sv) on the surface has a depth of 669.3±6 nm, with a positive height distribution skewness (Ssk) of 0.9±0.4. The arithmetic mean height of the surface (Sa), which is a measure of the roughness of the surface was 157±4 nm. These values (Table 5.3), derived from the 3D topographic image of the calcium treated surface (Figure 5.5 top), together with the kurtosis of height distribution (Sku) and the root mean square height of the surface (Sq), suggests the calcium modified surface has a peaks micro-scale rough surface. The more representative contact profilometry data indicates a roughness value Ra of 80±10 nm, which suggests the modified surface is minimally rough, as postulated by Winneberg and co (Wennerberg and Albrektsson, 2000). A profile of the minimally rough surface is shown in Figure 5.5 bottom.

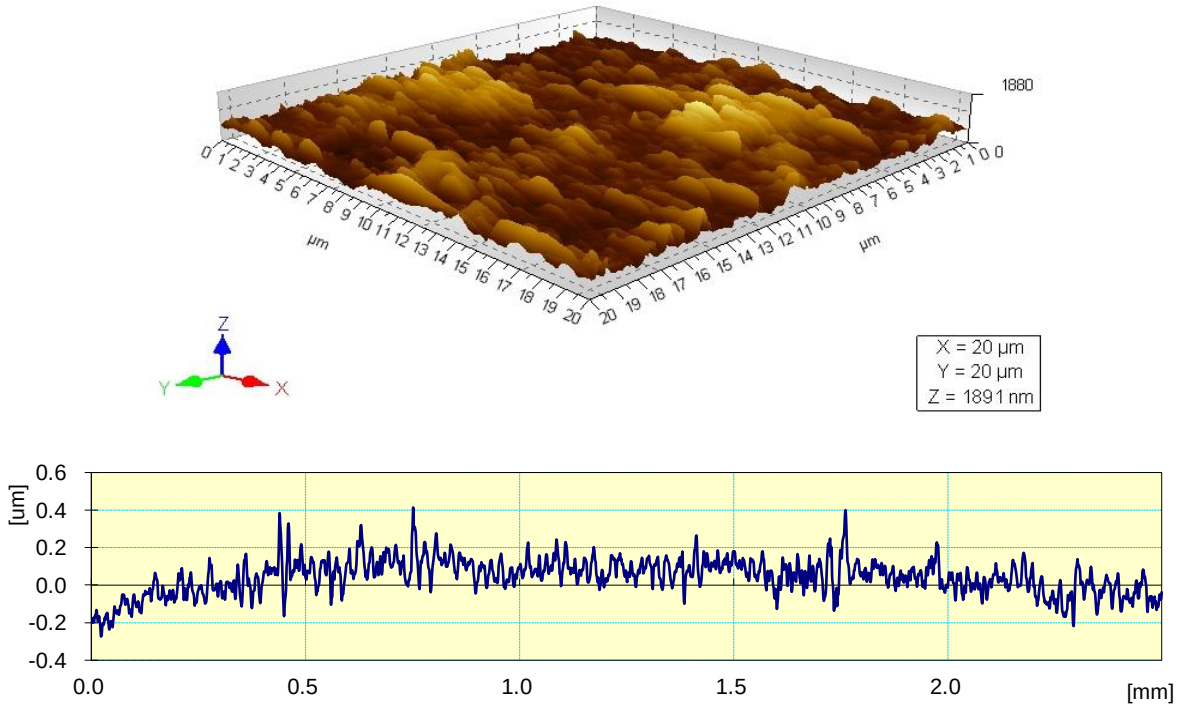

Figure 5.5. 3D AFM topographic characterisation image (top) and the contact profilometry display (bottom) of the Ca incorporated Ti surface, for n=3 surfaces. The topographic image shows the undulating peaks (lighter shades) and troughs (darker shades) of the surface roughness, with the mean height scale (z) in the region of 1891 nm. The profile shows the 'noisy' distribution of peaks and valleys about the reference point, characteristic of a micro-scale rough surface.

Table 5.3. Height and roughness parameters of the calcium treated Ti surface (polCa) surfaces, as determined by contact mode atomic force microscopy (left) and contact profilometry (right). Both approaches, for n=3 surfaces, together suggest the calcium modified surface tend towards a peaks dominated micro-rough surface.

3D Roughness Parameters (nm)	Mean	Stdev
Sq	203.8	5.4
Ssk	0.9	0.4
Sku	4.1	0.7
Sp	934.8	11.8
Sv	669.3	5.6
Sz	1604.3	8.1
Sa	157.0	4.3

Roughness Parameters (um)	Mean	Stdev
Ra	0.08	0.01
Rz	2.40	0.29
Rq	0.11	0.01
Rt	2.40	0.29

An angled SEM scan of the novel calcium treated surface (Figure 5.6) revealed that, the minimally rough calcium titanate layer formed on the Ti surface is approximately 1.75±0.06um thick.

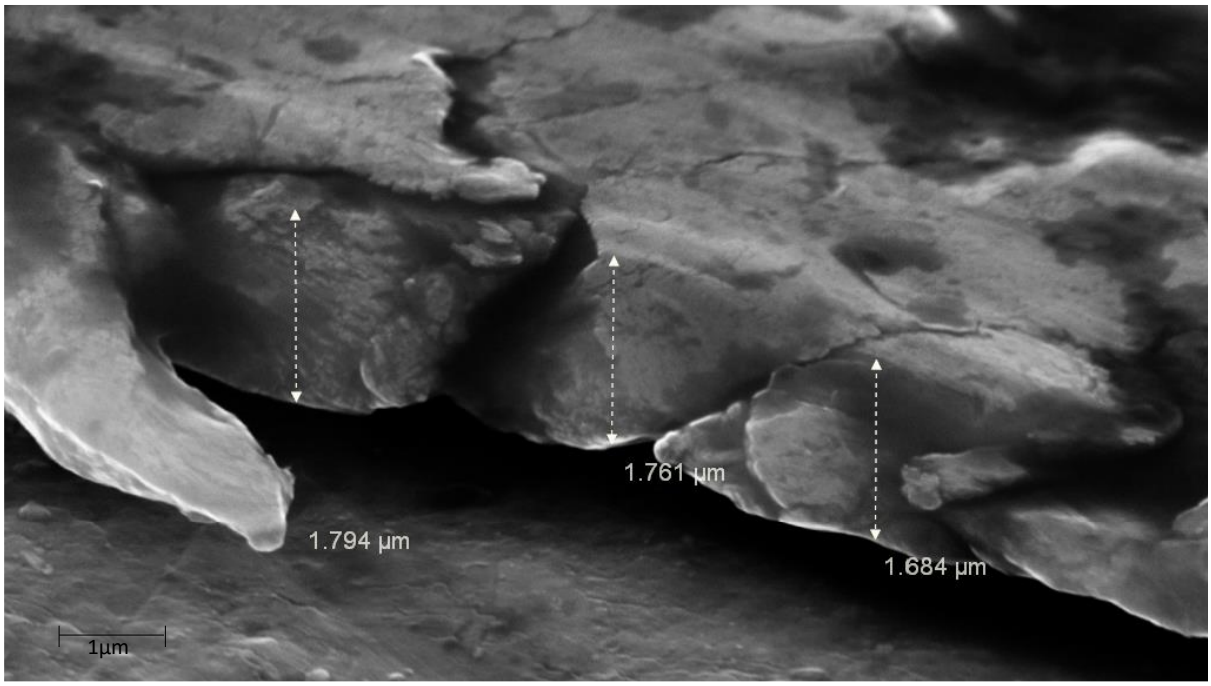

Figure 5.6. Cross-section SEM image of the post alkali heat treated calcium treated surface. The calcium titanate layer formed on the surface of the Ti disc was found to be approximately 1746.3±56.4 nm thick across the Ti disc surface for n=3 surfaces.

5.3.3. Implantation of Zinc on Titanium Surfaces

The incorporation of zinc ions onto the Ti surface was also carried out for both the unpolished commercially pure Ti discs (cpZn) and for the polished disc (polZn). The zinc treatment on the

Ti surface appeared as ‘embossed’ or ‘raised’ features on the SEM image of disc surface (Figure 5.7). Analysis of the surface composition by SEM with EDS indicated that the ion exchange with the sodium titanate formed from the pre-treatment with 10M NaOH, was again far more efficient for the polished surface than the unpolished surface, observed in the peak intensity from the spectrum produced. The spectra showed smaller Zn peaks for cpZn, than for the polZn. A quantification of the effectiveness of the surface bonding with Zn ions supports the peak intensities, that the modified surface is more effective in incorporating Zn ion (2.5±0.3%, polZn) than the unmodified surface (1.1±0.8%, cpZn). This is graphically represented in Figure 5.8 left.

The absence or much smaller Cl peaks again indicated the incorporation of Zn onto the Ti surface, as against simple deposition on the surface. The EDS data for the polZn surface shows the percentage atomic composition of the post alkali heat treated Zn treated Ti surface Table 5.4. This indicates that, the new surface is predominantly covered with the resulting titanate zinc oxide, the Na^{+} having been effectively exchanged for Zn^{2+}, with traces of Si and Cl atoms.

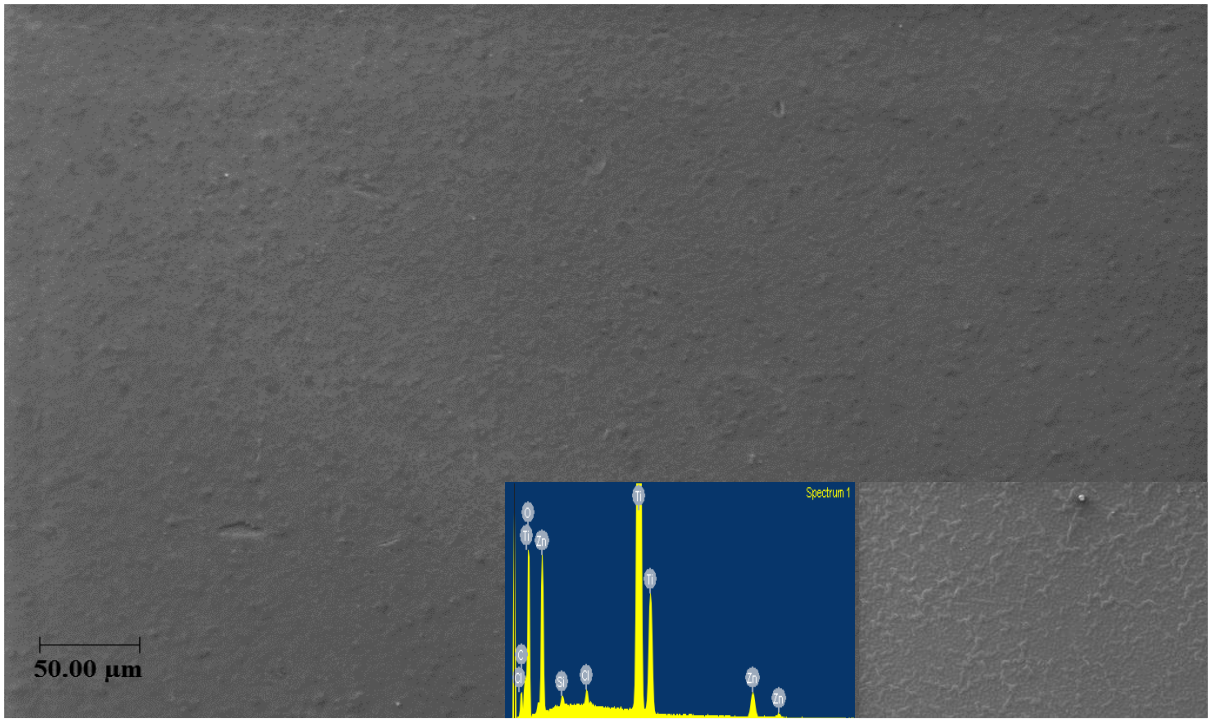

Figure 5.7. Scanning electron micrographs (main and insert) and EDS spectrum (insert) of the post alkali heat treated zinc treated Ti disc surface, showing an embossed appearance of zinc incorporated onto the disc surface. The EDS spectrum shows peaks for traces of silicon and chlorine, in addition to the zinc and titanium.

Table 5.4. Showing the percentage atomic composition of the post alkali heat treated Zn treated Ti surface for n=23 surfaces. The surface is predominantly covered with the resulting titanate zinc oxide, with traces of Si and Cl atoms

Zn Treatment		
Element	**Atomic%**	**Stdev**
O K	62.58	1.82
Zn K	2.49	0.25
Ti K	27.22	1.68
Cl	0.40	0.04
Others (Al, C, Si)	7.31	1.44

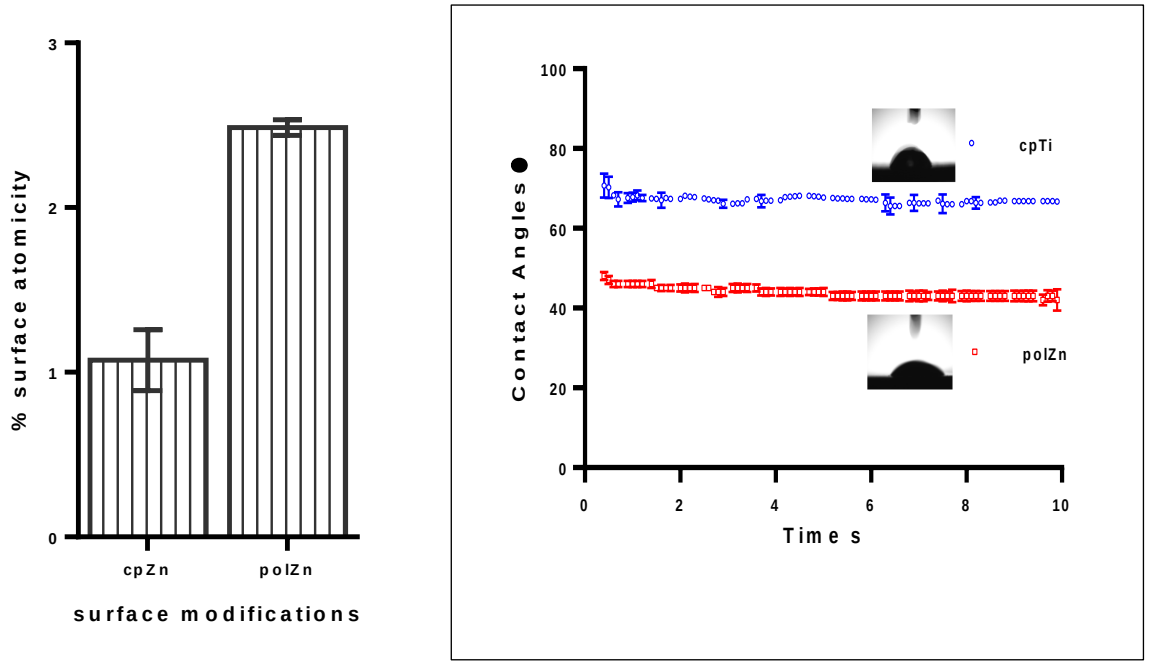

Figure 5.8. Showing a comparison of Zn incorporation onto cpTi surface (cpZn) and the polished zinc-treated Ti (polZn) surface (left)for n=23 surfaces, and the water wetting abilities of polZn surface against the cpTi surfacefor n=3 surfaces. The indication is that, polishing prior to Zn incorporation more than doubled that amount of Zn incorporated onto the disc surface. The Zn modified surface also shows an improvement in the water wetting capacity, compared to the commercially pure (cpTi) surface (right). A Welch-corrected two-tailed student t-test indicates a significant difference ($p<0.01$) between cpTi and polTi for both surface Zn composition and water contact angle.

The water contact angle measurements (Figure 5.8 right) for the zinc modified surface, compared with the commercially pure surface (cpTi) indicated that though have good water wetting capabilities (contact angles <90^o), the modification of the cpTi with the zinc ions further reduced the contact angle from 67.1±0.9^o to 44.4±1.2^o. This further improves the wetting performance of the new surface.

The surface features of the mechanically modified and zinc treated surface was also determined by contact mode atomic force microscopy and by stylus profilometry (Figure 5.9 top). The 3D image showed a peaks (lighter shades) dominated surface with very little extreme peaks or valleys (darker shades). These features were also shown by the stylus profile (Figure 5.9 bottom), which indicated a relatively finer, albeit wavy distribution of peaks and valleys about the reference point, characteristic of a controlled micro-scale rough surface. The AFM height parameters (Table 5.5) indicated that, the zinc modified surface's highest peaks (Sp) stood at 752±12.8 nm. The deepest valley (Sv) on the surface had a depth of 635±8.7 nm, with a positive

height distribution skewness (Ssk) of 0.8±0.2. The arithmetic mean height of the surface (Sa), which is a measure of the roughness of the surface was 113.3±4.7 nm. The stylus profilometer values indicated that, the surface roughness (Ra) was approximately 0.09±0.0 um. These values suggest that, the zinc modified Ti surface has topographic features on near nano-scale minimally rough characteristics.

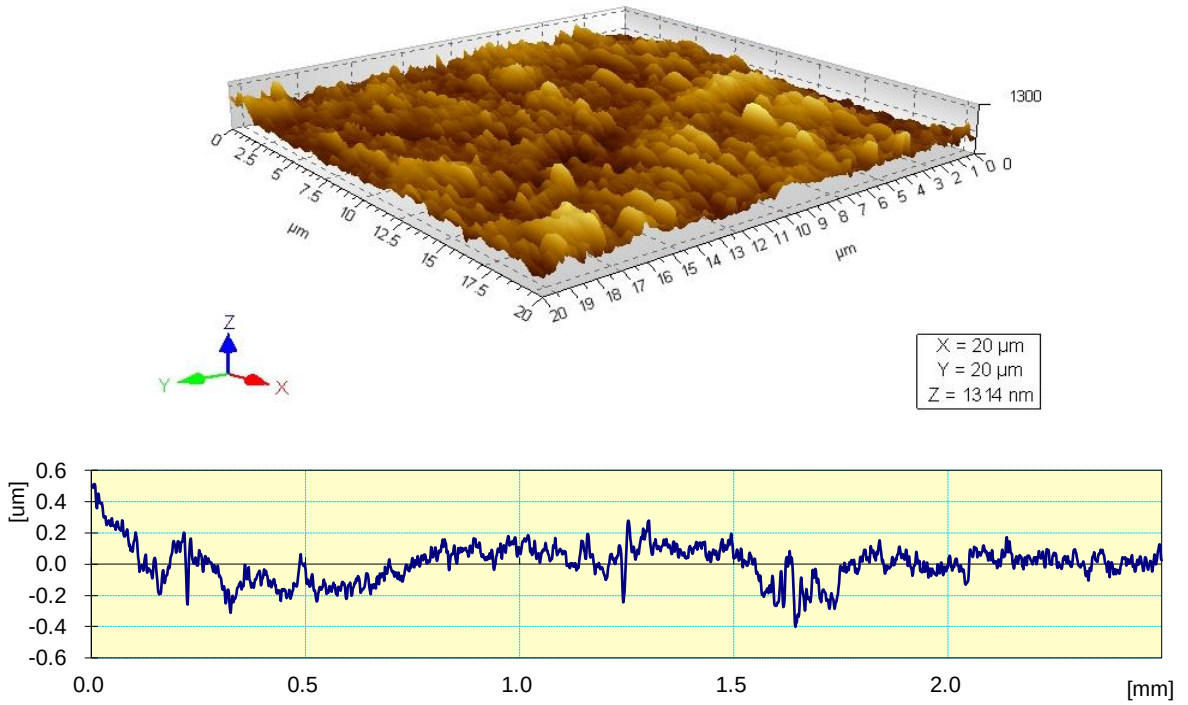

Figure 5.9. 3D AFM topographic characterisation image (top) and the contact profilometry display (bottom) of the Zn incorporated Ti surface, for n=3 surfaces. The topographic image shows the distinct peaks (lighter shades) and valleys (darker shades) of the surface roughness, with a mean height scale (z) of 1314 nm. The profile shows the finer, albeit wavy distribution of peaks and valleys about the reference point, characteristic of a relatively controlled micro-scale rough surface.

An angled SEM scan of the novel surface was carried out to determine the thickness of the zinc titanate layer formed on the polished Ti surface from the hydrothermal treatment. The resulting zinc titanate layer (Figure 5.10) was found to be approximately 979.1±25.7 nm thick across the Ti disc surface.

Table 5.5 . Height and roughness parameters of the zinc treated Ti (polZn) surfaces, as determined by contact mode atomic force microscopy (left) and contact profilometry (right) for n=3 surfaces. Together, both approaches suggest the novel Zinc modified surface tend towards a peaks dominated micro-rough surface.

3D Roughness Parameters (nm)	Mean	Stdev
Sq	149.5	7.3
Ssk	0.8	0.2
Sku	4.4	0.7
Sp	752.0	12.8
Sv	635.0	8.7
Sz	1387.3	9.4
Sa	113.3	4.7

Roughness Parameters (um)	Mean	Stdev
Ra	0.09	0.01
Rz	0.89	0.06
Rq	0.12	0.01
Rt	0.90	0.07

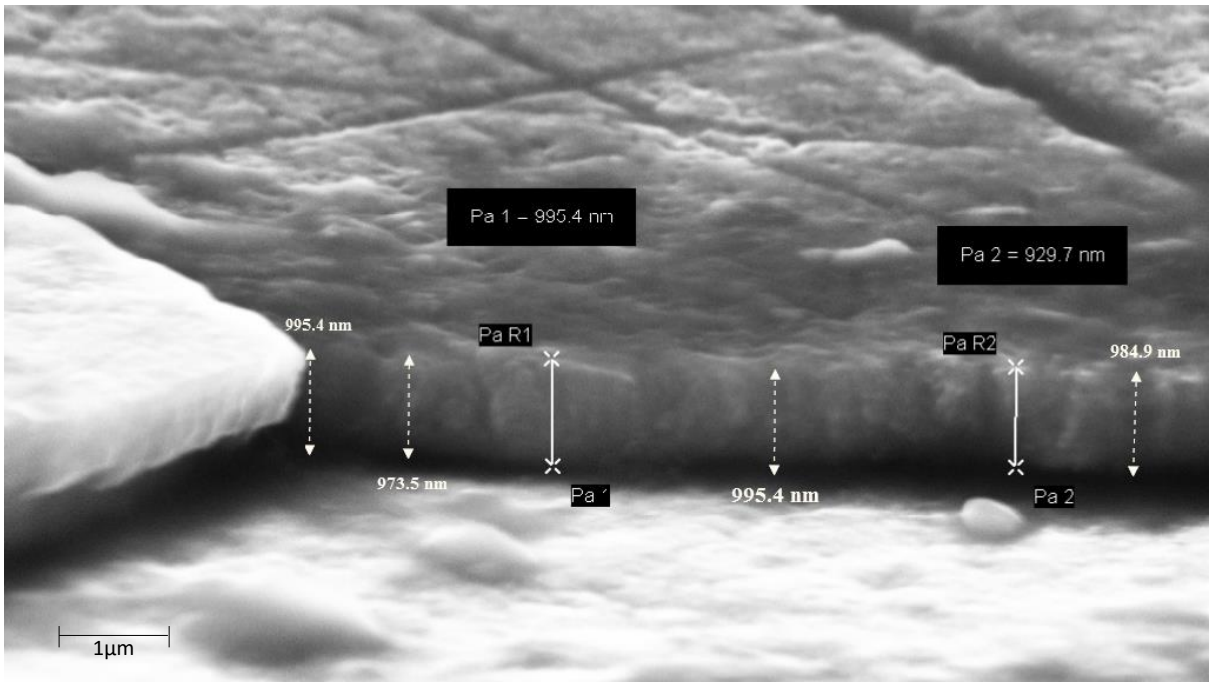

Figure 5.10. Cross-section SEM image of the Zinc treated Ti surface, post alkali heat treatment. The resulting Zinc titanate layer formed on the surface of the Ti disc was found to be approximately 979.1±25.7 nm thick across the Ti disc surface for n=3 surfaces.

5.3.4. Implantation of Silver on Titanium Surfaces

As with the other modified surfaces, silver incorporation onto the Ti surface was carried out for both the cpTi and designated cpAg, and for the polTi designated polAg. The resulting surface presented as a 'grainy' or specks spangled gritty surface (Figure 5.11). SEM with EDS spectra analysis again indicated that the sodium titanate sol-gel formed from the pre-treatment with NaOH effectively facilitated the exchange of Na^+ for Ag^+ on the Ti surface. The spectra

and associated data (Table 5.6) showed peaks for silver, titanium and oxygen, but no peaks for sodium or nitrogen. This suggests the sodium from the sodium titanate ($Na_2Ti_5O_{11}$) has been effectively replaced, and the silver ions are chemically incorporated onto the disc surface. A comparison of the cpAg and polAg surface silver composition (Figure 5.12 left) indicates that, the polishing prior to the hydrothermal chemical treatment, subsequent to alkali-heat pre-treatment, was more efficient than treating the cpTi surface. The surface composition of silver atoms was 4.79±1.3% for cpAg and 9.54±0.96% for polAg, indicating both surfaces have good water wetting profile. The values however, also indicate the silver incorporation onto the Ti surface are significantly improve the wettability of the surface (at 95% CI).

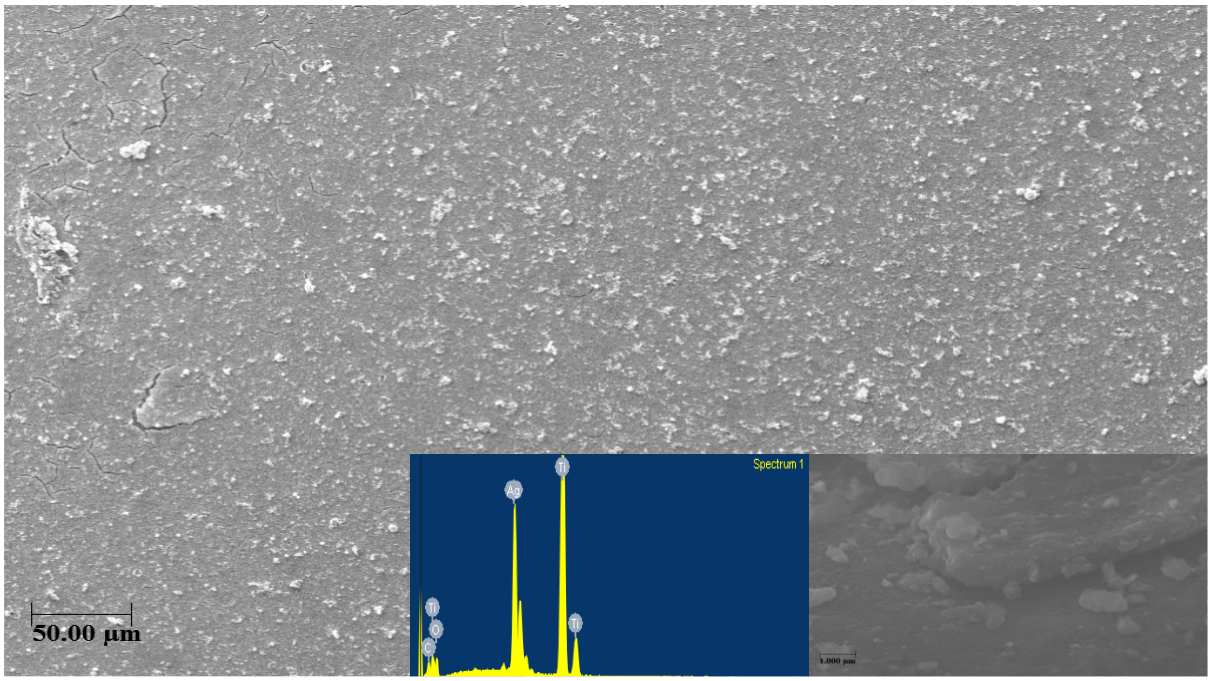

Figure 5.11. Scanning electron micrographs (main and insert) and EDS spectrum (insert) of the post alkali heat treated silver treated Ti disc surface, showing a 'grainy' appearance of silver incorporated onto the disc surface. The EDS spectrum shows peaks for oxygen. silver and titanium, but not for nitrogen, as would have been expected if the silver from $AgNO_3$ was simply deposited on the Ti surface.

The topography of the Ag treated surface was analysed as with the others by AFM (Figure 5.13 top) and stylus profilometry (Figure 5.13 bottom). The 3D AFM image shows dominant clusters of relatively low peaks (lighter shades) and intermittent valleys (darker shades) of a comparatively 'smooth' surface roughness, with a mean height scale (z) of 701 nm. This is

more clearly depicted in the stylus profile, which shows a 'smooth' surface with very little distinct peaks and valleys, which is characteristic of a well-controlled micro or nano-rough surface.

Table 5.6. Showing the percentage atomic composition of the post alkali heat treated silver treated Ti surface. The surface is predominantly covered with the resulting titanate silver oxide, with no nitrogen atoms, suggesting the silver is chemically incorporated onto the Ti surface.

Ag Treatment		
Element	**Atomic%**	**Stdev**
O K	62.90	1.49
Ag K	9.54	0.96
Ti K	15.84	2.47
N	0.00	0.00
Others (Al, C, Cl, Si)	11.73	2.18

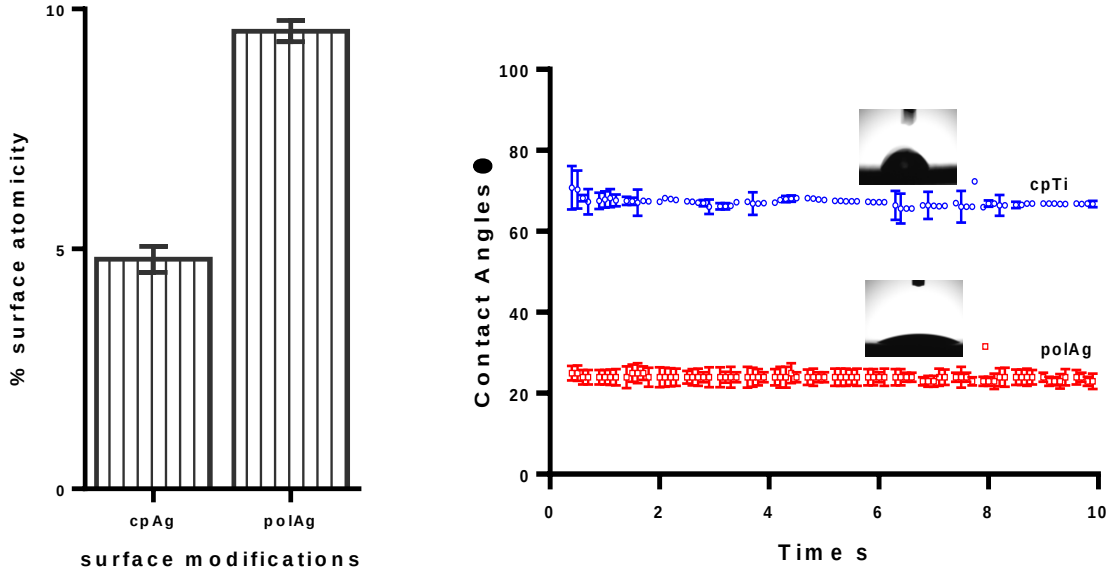

Figure 5.12. A comparison of Ag incorporation onto cpTi surface (cpAg) and the polished silver-treated Ti (polAg) surface (left), and the water wetting abilities of polAg surface against the cpTi surface. Polishing prior to Ag incorporation appears to increase the silver atoms incorporated onto the disc surface from 4.8±1.3% to 9.5±1.1%. The Ag modified surface also shows an improvement in the water wetting capacity, compared to the commercially pure (cpTi) surface (right). The error bars represent the mean ± S.E.M. A Welch-corrected two-tailed student t-test indicates a significant difference ($p<0.01$) between cpTi and polTi for both surface Ag composition and water contact angle.

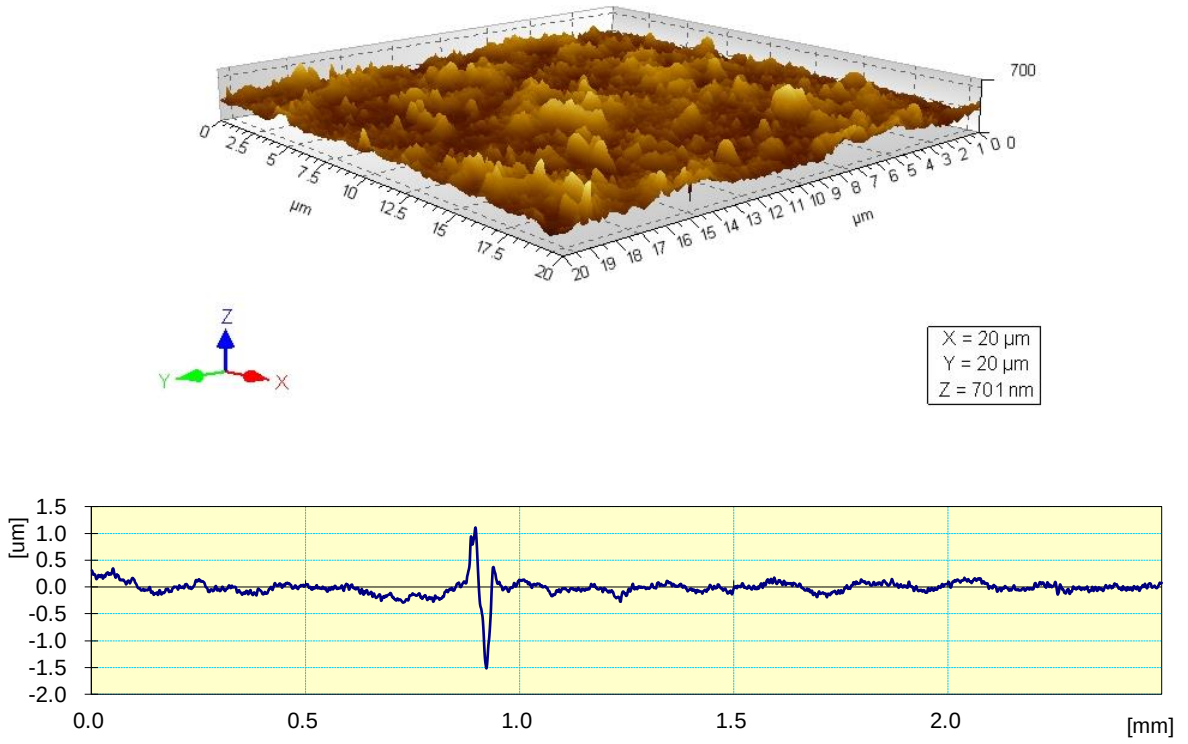

Figure 5.13. AFM topographic characterisation image (top) and the contact profilometry output (bottom) of the Ag incorporated Ti surface. The topographic image shows the clusters of peaks (lighter shades) and valleys (darker shades) of the surface roughness, with a mean height scale (z) of 701 nm. The profile display shows the comparatively smoother surface with very few distinct peaks or valleys, characteristic of a uniformly chemically modified surface.

The AFM height measures (Table 5.6 left) suggested that, the highest peak of the Ag modified surface (Sp) was 769.5±13.7 nm, and the deepest valley (Sv) was 639.5±11.1 nm, with a positive height distribution of (Ssk) 1.0±0.2, which suggest the surface is peaks dominated. The arithmetic mean height of the surface (Sa), a measure of the roughness of the surface was 83.3±8.5 nm, which suggests the Ag modified Ti surface has topographic features nano-rough characteristics. The stylus profile values (Table 5.6 right) indicated that the mean roughness (Ra) was 0.09±0.0 µm. This, together with the other stylus profile values, confirmed the initial AFM observation that the Ag treated surface was of nano-scale roughness.

Table 5.7 Height and roughness parameters of the calcium treated Ti surface (polAg) surfaces, as determined by contact mode atomic force microscopy (left) and contact profilometry (right). The surface roughness measure for both approaches Sa and Ra, indicate that the silver modified surface tends towards a nano-scale surface roughness (both measures showing <100 nm surface roughness).

3D Roughness Parameters (nm)	Mean	Stdev
Sq	107.9	13.0
Ssk	1.0	0.2
Sku	5.4	0.7
Sp	769.5	13.7
Sv	639.5	11.1
Sz	1409.5	7.0
Sa	83.3	8.5

Roughness Parameters (um)	Mean	Stdev
Ra	0.09	0.01
Rz	2.60	0.07
Rq	0.16	0.01
Rt	2.60	0.07

An angled SEM scan of the novel surface, carried out as with the other surfaces, to determine the thickness of the silver titanate layer indicated that this layer (Figure 5.14) was approximately 795±8.8 nm thick across the Ti disc surface.

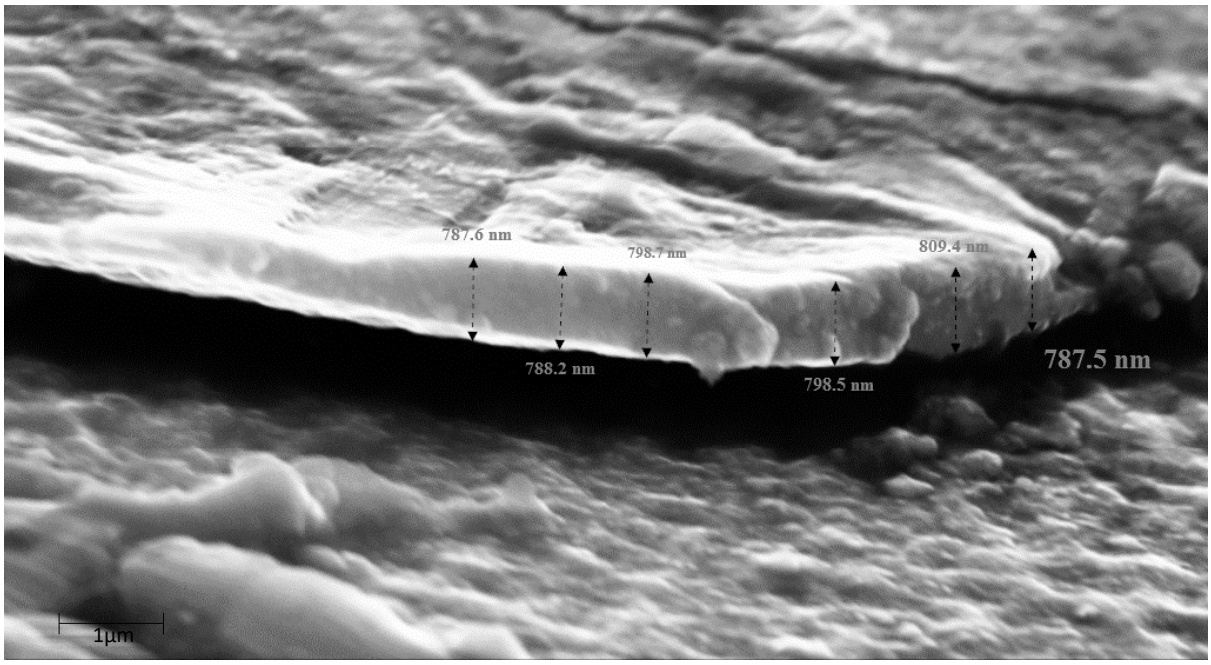

Figure 5.14. Angled SEM image of the Silver treated Ti surface, post alkali heat treatment. The resulting nano-topographic silver titanate layer formed on the surface of the Ti disc was found to be approximately 795±8.8 nm thick across the Ti disc surface.

5.3.5. Implantation of Calcium-Zinc-Silver on Titanium Surfaces

The final phase of the alkali heat, hydrothermal chemical modification of the cpTi involves the incorporation of calcium, silver and zinc ions onto the Ti surface. The resulting surface was designated polCaAgZn. This surface showed what appeared as a combination of the characteristic appearance of the three individual ions' surfaces; a varied 'grainy, flaky and raised' appearance of ions incorporated onto the disc surface (Figure 5.15) Analysis of the surface composition by SEM with EDS revealed distinct peaks for Ti, Ca, Zn and O, together with trace peaks for Al, Cl and Si. Ag peaks, if present, were indistinguishable, neither were the peaks for N. The EDS data (Table 5.8) however, indicated Ag was present on the modified surface, with the other elements. N was conspicuously absent, again suggesting the elements presents on the surface of the Ti disc were exchanged with Na from the sodium titanate sol-gel ion-exchanger, and not merely deposited on the Ti surface. The composition of the various elements on the Ti surface were 2.8±0.3% for silver, 1.1±0.1% for calcium and 1.1±0.3% for zinc. On comparing these values with that from the treated cpTi surface, whose composition was 1.1±0.2% for silver, 0.4±0.0% for calcium and 0.5±0.0% for zinc, the indications are that, the initial polishing to a mirror finish improved the incorporation of the target ions on to the Ti surface (Figure 5.16 left).

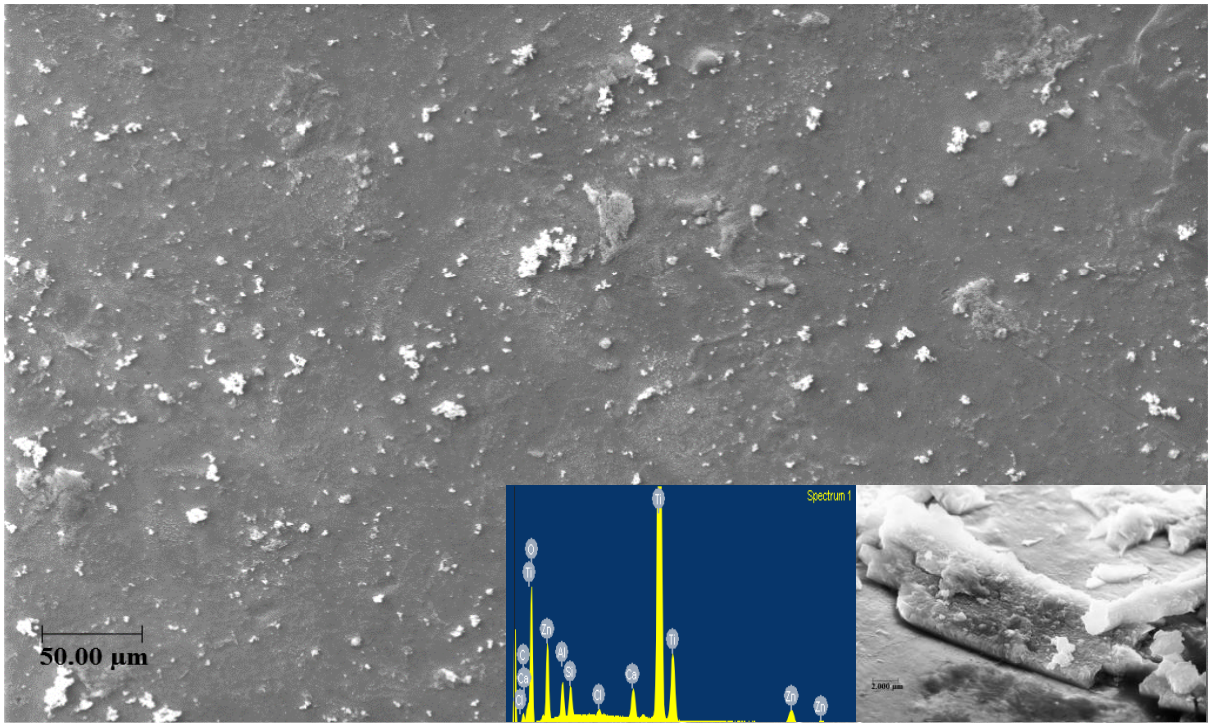

Figure 5.15 Scanning electron micrographs (main and insert) and EDS spectrum (insert) of the calcium-silver-zinc treated Ti disc surface after pre-treatment with 10M NaOH treatment, showing the varied 'grainy, flaky and raised' appearance of ions incorporated onto the disc surface. The EDS spectrum shows peaks for zinc, calcium, titanium and oxygen, in addition to traces of chlorine, aluminium and silicon. Silver peaks are not represented, but captured on elemental analysis.

The water contact angle measurements (Figure 5.16 right) for this new modified surface, on comparing with the cpTi surface indicated that both have good water wetting capabilities (contact angles <90^{o}). The modification of the cpTi with the calcium, silver and zinc ions however, further reduced the contact angle from 67.1±0.9^{o} to 27.4±0.9^{o}, suggesting a significant (P< 0.0001) improvement in the wetting performance of the new surface.

Table 5.8. Showing the percentage atomic composition of the calcium-silver-zinc treated Ti surface. The surface is predominantly covered with the resulting titanate oxides of calcium, silver and zinc, with no nitrogen atoms, suggesting the individual ions are chemically incorporated onto the Ti surface, via the sodium titanate sol-gel ion-exchanger.

CaAgZn Treatment		
Element	**Atomic%**	**Stdev**
O K	63.02	1.10
Ca K	1.08	0.14
Ag K	2.83	0.30
Zn K	1.05	0.26
Ti K	23.15	1.04
Others (Al, C, Cl, Si)	8.91	0.75

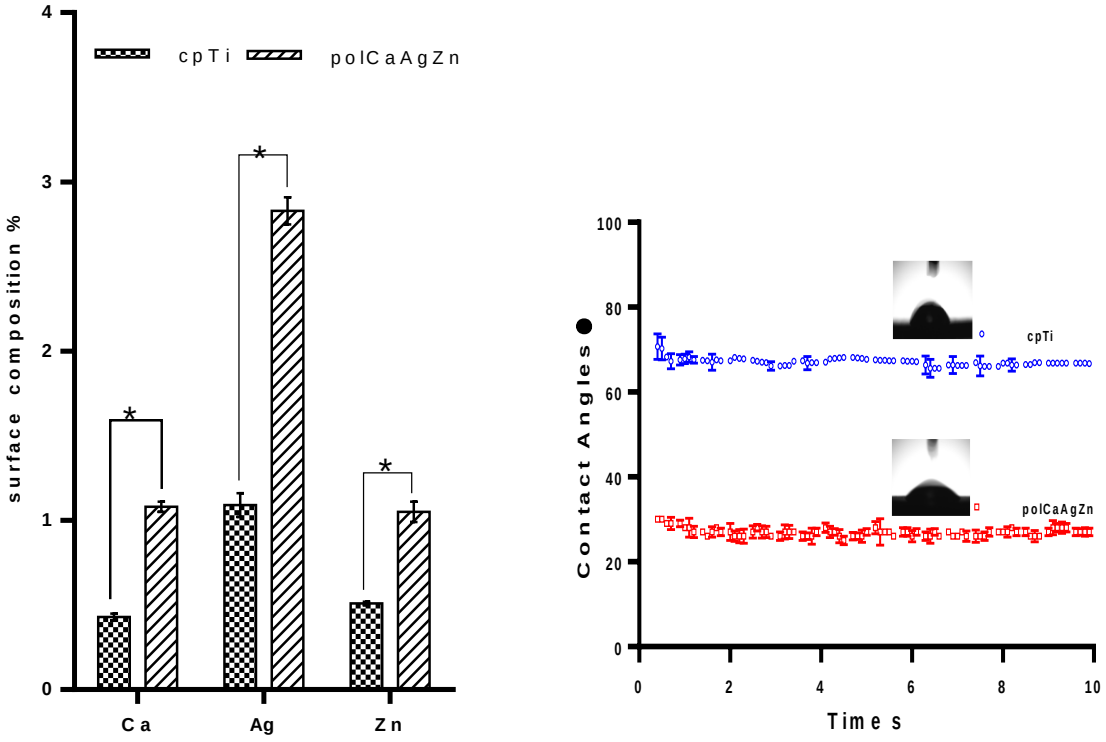

Figure 5.16. A comparison of Ca, Ag and Zn incorporation onto cpTi surface and the polished calcium-silver-zinc treated Ti (polCaAgZn) surface (left), and the water wetting capacities of the novel surface against the cpTi surface (right), for n=6 discs. Polishing prior to ion incorporation appears to dramatically increase the number of atoms making up the surface composition of the disc surface. Statistical significance (with $p<0.01$) for the surface composition for the multi-ion incorporation was determined using the Holm-Sidak method, with alpha=1.000% A Welch-corrected two-tailed student t-test indicates a significant difference ($p<0.01$) between the mean water contact angle of the cpTi and polCaAgZn. This suggests a significant improvement in the water wetting property of the novel surface, compared to the commercially pure (cpTi) surface. The error bars represent the mean ± S.E.M.*

The surface profile of this new mechanically modified and calcium, silver and zinc treated surface was also investigated using the two approached previously employed for the other surfaces; contact mode AFM (Figure 5.17 top) and by stylus profilometry (Figure 5.17 bottom). The 3D image showed 'large' areas of darker shades (valleys) in the middle of the micrograph, and 'few' distinct peaks (lighter shades) in the middle and towards the edges of the micrograph, with a mean height scale (z) is in the region of 1314 nm. The profilometry display shows a finer surface, with the few peaks in the middle and towards the edges duly represented, on an otherwise 'smooth' surface.

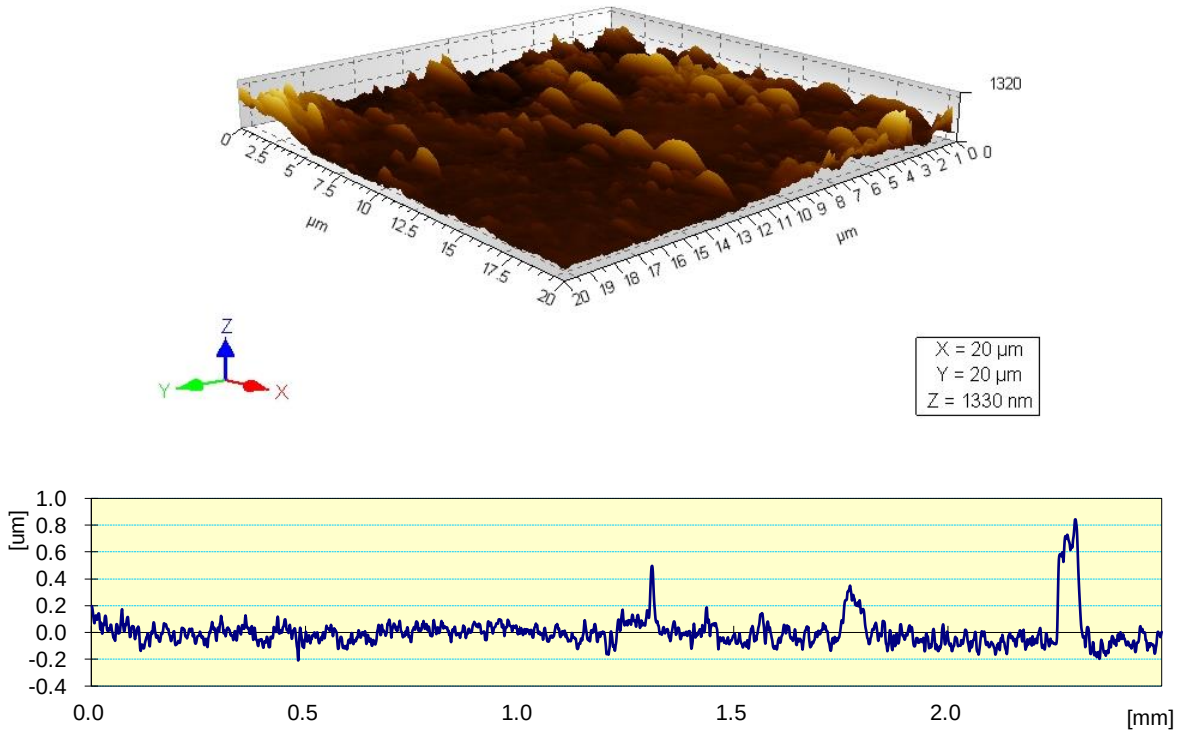

Figure 5.17. 3D AFM topographic characterisation image (top) and the contact profilometry output (bottom) of the calcium-silver-zinc incorporated Ti surface. The topographic image shows 'large' areas of darker shades (valleys) in the middle of the micrograph, and 'few' distinct peaks (lighter shades) in the middle and towards the edges of the micrograph. The mean height scale (z) is in the region of 1314 nm. The profile shows a finer surface, with the few peaks in the middle and towards the edges duly represented, on an otherwise 'smooth' surface.

The AFM height parameters (Table 5.5 left) indicated that, the new CaAgZn surface's highest peaks (Sp) stood at 1027±6.7 nm. The deepest valley (Sv) on the surface had a depth of 838±3.6 nm, with a positive height distribution skewness (Ssk) of 0.5±0.3. Its arithmetic mean height

of the surface (Sa), an indication of the roughness of the surface, was 236±4.8 nm. The stylus profilometer value suggested the surface roughness (Ra) was 0.09±0.0 µm. By both the more representative stylus profilometer readings and the more sensitive AFM values, the CaAgZn surface may be described as having topographic features of micro-scale characteristics.

Table 5.9. Height and roughness parameters of the calcium-silver-zinc treated Ti (polCaAgZn) surfaces, as determined by contact mode atomic force microscopy (left) and contact profilometry (right). The novel surface, tends towards a peaks dominated micro-rough surface with regards to the AFM approach, but minimally rough when considered by the profilometry method, which is less sensitive but more representative of the surface.

3D Roughness Parameters (nm)	Mean	Stdev
Sq	291.8	4.6
Ssk	0.5	0.3
Sku	3.4	1.8
Sp	1027.0	6.7
Sv	838.0	3.6
Sz	1865.3	3.8
Sa	236.0	4.8

Roughness Parameters (um)	Mean	Stdev
Ra	0.09	0.01
Rz	1.10	0.09
Rq	0.12	0.01
Rt	1.10	0.09

The cross-sectional SEM scan (Figure 5.18)of the novel surface to determine the thickness of the new calcium-silver-zinc titanate layer formed on the surface suggested this layer is approximately 1030.2±26.3 nm thick across the Ti disc surface.

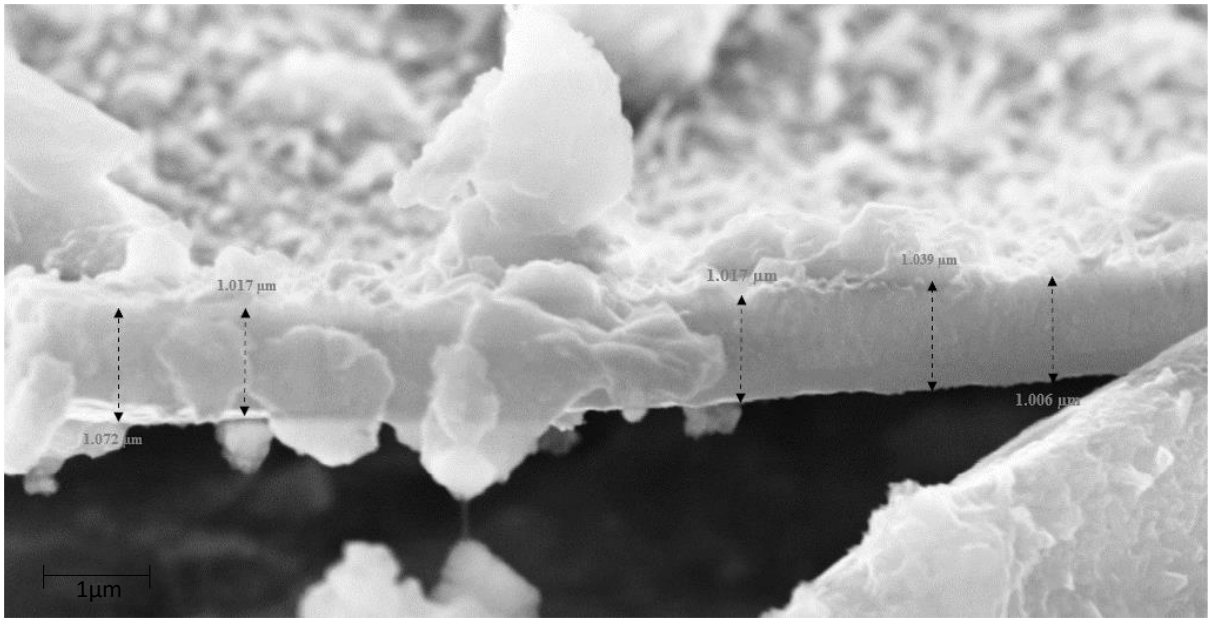

Figure 5.18. A cross-section SEM image of the calcium-silver-zinc treated Ti surface, post alkali heat treatment. The resulting micro-topographic calcium-silver-zinc titanate oxide layer formed on the surface of the Ti disc appeared to be approximately 1030.2±26.3 nm thick across the Ti disc surface.

5.4. Discussion

Surface modification strategies have become key means of improving the performance of implant devices, because of the significance of the events at the device-tissue interface leading to the integration or rejection of the implant device. Optimisation of the surface energy via the water contact angle, roughness or topography and surface chemistry carried out in this work.

The chemical modification of the Ti surface started with the pre-treatment of the disc surface with 10M NaOH, after mechanical polishing of the cpTi to a mirror finish. The alkali heat treatment of the Ti surface resulted in the formation of an amorphous meshwork of sodium titanate ($Na_2Ti_5O_{11}$) fibres or 'nano-rods' firmly bound on to the Ti surface, per the mechanism outline in section 3.2.2. The SEM/EDS examination of the surface suggested that, 11.6±0.46% of sodium made up the surface elemental composition of the resulting hydrated sodium titanate sol-gel, together with 64.29±1.58% of oxygen as oxide of all the elements present on the Ti disc surface. The dehydrated sodium titanate layer was found to be 821.1±9 nm thick across the disc surface.

Calcium, silver and zinc (as chlorides, nitrates and hydroxides) were then incorporated onto the pre-treated Ti surface based on evidence from other works (Sun and Li, 2003, Ravelingien et al., 2009, Papp et al., 2005, Li et al., 2012, Lee et al., 2010a, Kizuki et al., 2010, Akieh et al., 2008) that the sodium titanate formed on the Ti surface is an excellent ion-exchanger. SEM/EDS analysis of the individual resulting ion-incorporated surfaces indicated that the initial percentage composition of oxygen remained relatively constant throughout the subsequent treatment with the target ions. This was the first indication that the sodium titanate sol-gel has effectively facilitated the exchange of ions, leading to the incorporation of the target ions onto the Ti surface. A confirmation of this was provided by the absence of (or only trace amounts) peaks and percentage composition values of the respective chlorine and nitrogen from the 1M aqueous solutions used in the chemical treatments. these two indicators suggested the target ions had been chemically incorporated onto the Ti surface, and not simply deposited on the surface.

A comparison of the hydrothermal chemical incorporation process was carried out for the cpTi and polTi surface to establish whether time and labour-intensive polishing to a mirror finish was critical to the number of ions incorporated onto the Ti surface. The results suggest that, for the various ions, polishing to a mirror finish prior to treatment led to between two- and three-fold increase in the amounts of ions incorporated onto the Ti surface, across all the surfaces developed, with the resulting oxides layers ranging from 800 nm to 1700 nm in thickness. It appeared however that the thickness of the respective titanate oxide of the ion incorporated onto the Ti surface was dependent on the ionic radius and charge of the ion. Consequently, the Ca^{2+} formed the thickest layer, followed by Zn^{2+}, before the Ag^{+} titanate layer. The layer on Ti surface treated with all three ions was thicker that thinnest of the three, but thinner than the thickest of the three.

The surface profiles of the new surfaces were characterised by contact mode AFM, and by stylus contact profilometry. Though the AFM provided more sensitive and precise data for the surface, the scan dimension of 20 µm by 20 µm over many random areas on the 12-mm diameter disc surface, was considered not representative enough of the surfaces under examination. The resulting data was however useful in classifying the surface as either nano- or micro-topographic. The stylus profilometer, scanning several 2.5 mm lengths on the disc surface provided data that was more representative of the surface, though less sensitive, particularly in resolving sub-micro features on the disc surface. The combination of the two therefore provided enough reliable information to appropriately characterise the surfaces.

As would be expected, on the assumption that the mirror-finished polished Ti surfaces treated with the various ions were of similarly uniform topography, the surface profiles of the resulting ion-treated surfaces followed the same trend as the thickness of the titanate layer on the Ti surface, per the Sa value of the AFM micrographs of the surfaces. The smoothest surface was the Ag^{+} treated surface with nano-scale features, followed by the Zn^{2+} and then the Ca^{2+} treated surfaces, before the three-ions treated surface with micro-scale topographies. Per the more representative stylus profilometer values however, the surfaces are of identical micro-scale topographies.

Another characteristic of the modified Ti surfaces that appeared to be closely related to the ionic charge and radius of the incorporated ions, as well as the surface height parameters, was the water contact angle, hence wettability of the surfaces. A comparison of each with that of the cpTi suggests that, though all the surfaces have good water wetting properties, the introduction of ions onto the Ti surface generally reduces the water contact angle, thus increasing the wettability. The lowest contact angle was observed on the Ag^{+} treated surface, followed by the Zn^{2+} and then the Ca^{2+}. The contact angle of the three-ions treated surface was intermediate between the Ag^{+} and Zn^{2+} treated surfaces. This could be explained by the

presence of the comparatively two-folds more hydrating effect of Ag^{+} as a component of the three-ions treatment, making the resulting surface better wetting than the Zn^{2+} and Ca^{2+} surfaces.

5.5. Conclusion

The initial mechanical surface modification that resulted in the mirror-finish surface gave rise to the removal of oxides, grease, dust particles and moisture from the Ti surface, and the exposure of Ti surface atoms/oxides for interaction with other elements. On exposure to 10M NaOH for 24 hours, an 800-nm thick sodium titanate layers forms on the Ti surface, which in the sol-gel form, served as an effective ion-exchanger for the introduction of calcium, silver and zinc onto the Ti surface. SEM/EDS analyses of the resulting surfaces indicated that the elements introduced onto the Ti surface are chemically bound onto the surface, as opposed to mere physical deposition on the surface, and polishing the surfaces prior to treatment more than doubled the number of elements incorporated onto the Ti surface. It was also observed that the introduction of the target elements onto the Ti surface lowered the water contact angle, that is, improved its water wetting properties. Topographic analysis of the resulting surfaces suggested that the surfaces were mostly peaks dominated, consistent with surfaces subjected to additive treatment processes, and were of the micron-scale roughness postulated to be ideal for interaction with mammalian cells.

Chapter 6 : Effect of Sterilization by Autoclaving on Metal Ion Incorporation onto Ti Surface

6.1. Introduction

In investigating biofilm formation on the modified titanium surfaces using a biofilm reactor, there is the need to achieve and maintain sterility of the ensemble (Qiu et al., 2011). In most reported studies, autoclaving was used (Brammer et al., 2009, Park et al., 2009, Oh et al., 2006, Das et al., 2009, Bjursten et al., 2010, Yao et al., 2008). However, ultraviolent (UV) irradiation (Peng et al., 2009) and ethanol immersion (Popat et al., 2007a, Peng et al., 2009, Popat et al., 2007b) have also been employed. The sterilization methods have been reported to influence the surface properties of biomaterials, consequently affecting cell interaction with the surface (Serro and Saramago, 2003, Park et al., 2012, Mauerer et al., 2015, El-Wassefy et al., 2014). The belief is that the sterilization methods influence the bioactivity of titanium surfaces and the different sterilization methods in use may account for the conflicting biological behaviour reported. Dry heat sterilization has a long history compared to other methods. However, steam heat sterilization is more efficient in terms of heat transfer. Therefore, autoclaving was chosen as the method of sterilization in study. This was despite the suggestion that cleaning and sterilization by autoclaving affected hydrophobicity and roughness, modifying the surface properties, which has been demonstrated to affected osteogenic differentiation of human MG63 osteoblast-like cells (Park et al., 2012). The rational for choosing this method of sterilization is that the material being sterilized is not sensitive to heat and/or hydrolysis (Dion and Parker, 2013). It is also a chemical-free process, hence no residue from the process is left on the product.

This study aimed at investigating the influence of the autoclave sterilization on the ions incorporated onto the Ti surface.

The ensemble consisted of the biofilm reactor and the associated tubing, the coupon holders, the coupons or their replacements (in this case the modified/treated titanium discs), and the nutrient medium for the cultivation of the biofilm. The need to achieve and maintain sterility of the modified Ti discs surfaces was also paramount in the investigation of the mammalian cell attachment to and proliferation on the Ti disc surface. Achieving sterility in these cases involved autoclaving. The drawback with this however, was the danger that the process, which involved high temperatures and moisture, may affect the number of ions incorporated onto the Ti disc surface. An investigation into the extent of ion loss was therefore carried out, using the silver treatment, as this treatment demonstrated the highest level of ion incorporation onto and release from the Ti surface, thus ideal for assessing the worst-case scenario extrapolation to other ions incorporated onto the disc surface.

Twelve titanium discs (12 mm in diameter), were cut and polished to a mirror finish, cleaned and silver incorporated onto the surfaces as described earlier. The treated discs were then separated into four groups of three discs for autoclaving. The first group of three discs were immersed in sterile distilled water in a scintillating vial and kept at room temperature for 1 hour. The second group were placed in a dry and empty scintillating vial and autoclave on a cycle lasting 1 hour. The third group were placed in a scintillating vial containing sterile distilled water and autoclaved on a 1-hour cycle. The final group provided the baseline reading for silver deposited on the discs during the treatment process, and were not subjected to any further treatment.

6.2. Method

Twelve Ag^{+} incorporated discs then briefly washed in distilled water, air-dried and separated into four groups of three discs for autoclaving. The first group of three discs were immersed in

sterile distilled water in a scintillating vial and kept at room temperature for 1 hour. The second group were placed in a dry and empty scintillating vial and autoclave on a cycle lasting 1 hour. The third group were placed in a scintillating vial containing sterile distilled water and autoclaved on a 1 hour cycle. The final group provided the baseline reading for silver deposited on the discs during the treatment process, and were not subjected to any further treatment.

The features and amount of silver on the disc surfaces after the various treatments were then determined using a Carl Zeiss SMT Evo Series scanning electron microscope. The amount of silver deposited was represented as a percentage of silver atoms on the disc surface.

6.3. Results

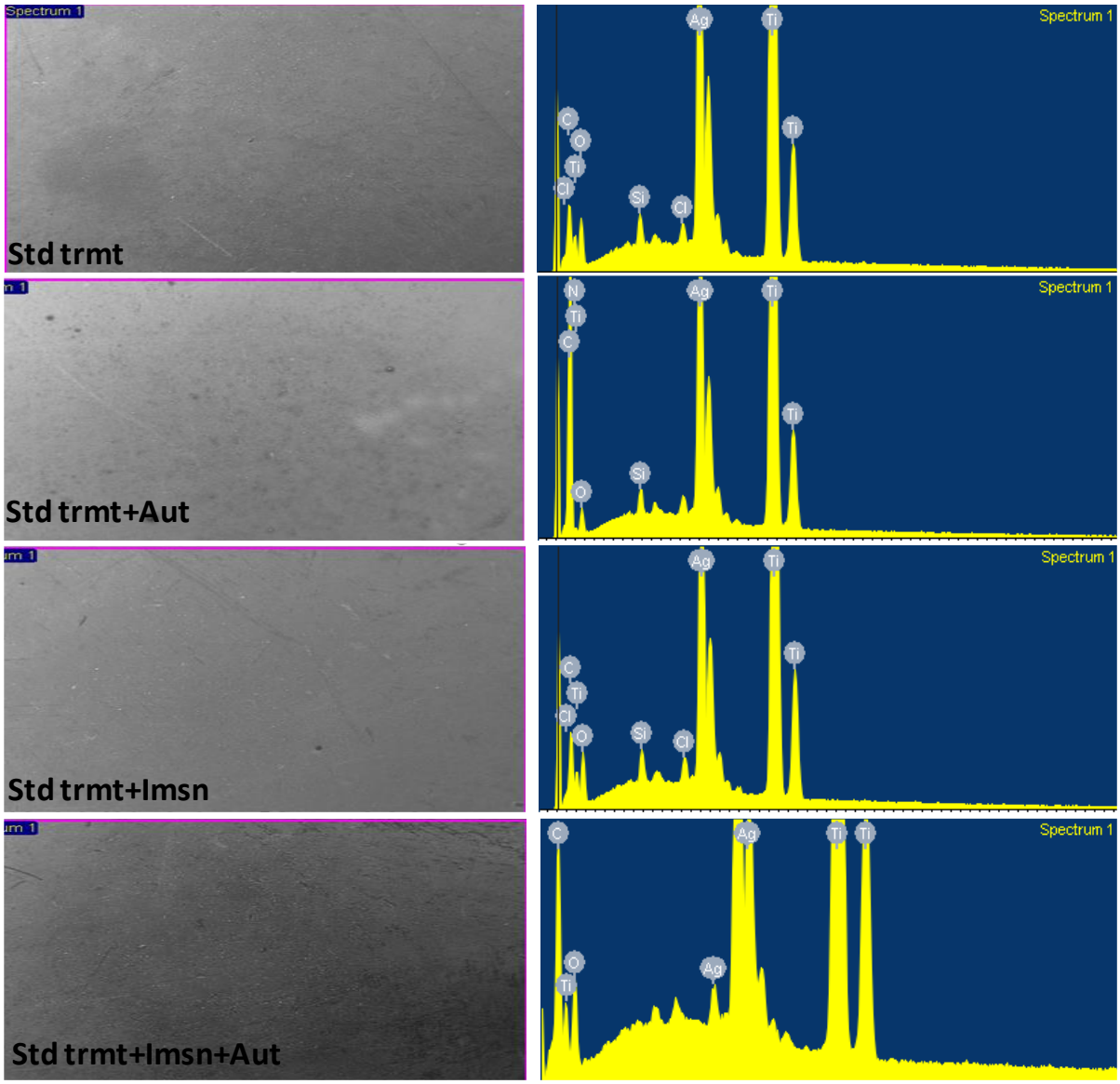

Figure 6.1. SEM/EDS micrographs of the Ag-treated surface after standard treatment (std trmt), standard treatment plus steam autoclaving (std trmt+aut), standard treatment plus immersion in deionised water (std trmt+imsn), and standard treatment plus immersion in deionised water plus autoclaving (std trmt+imsn+aut).

The features and amount of silver deposited on the discs' surfaces after the various treatments were then determined by means of scanning electron microscopy (SEM), with energy dispersive X-ray spectroscopy (EDS), and reported as a percentage of silver atoms composition on the sample disc surface (Figure 6.1).

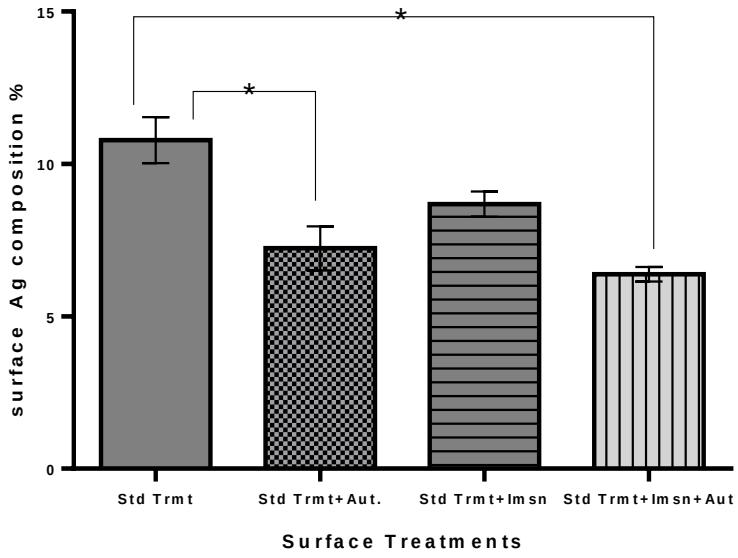

*Figure 6.2. Surface Ag composition on the various surfaces, showing the effect of the treatment on the amounts of Ag left on the surfaces after steam and water immersion sterilization, prior to use in antimicrobial and cell culture assays. The std trmt surface was the reference surface. The std trmt+imsn surface was the control. Error bars represents the mean ± S.E.M. for n=9 discs in each surface treatment group. * represents statistically significant variance (P < 0.05) from the standard treatment, as determined by a one-way ANOVA with Bonferonni's post-hoc test.*

6.4. Discussion

The wet chemical synthesis (WCS) treatment of the titanium discs leading to the incorporation of silver on the surface involves two processes; an initial pre-treatment with 10M sodium hydroxide and subsequent treatment with 1M silver nitrate. The pre-treatment with sodium hydroxide leads to the formation of sodium titanate. This involves the formation of intermediate TiO_2 which then reacts spontaneously with NaOH in the concentrated NaOH solution. The sodium titanate was therefore an effective intermediate ion-exchanger, via which other ions were introduced onto the surface.

Figure 6.2 is a plot of the mean percentage surface composition of silver on the various surface of the titanium discs, as a measure of the amount of silver remaining on the disc surfaces after the various treatments, for the various treatments the discs were exposed to. This plot indicates that the treatment process used led to the deposition of silver equivalent to an average of

10.8±2.3% of the total number of atoms found on the disc surface. On immersing the silver treated disc in sterile distilled water for 1 hour, the amount of atomic silver on the disc surface reduced to 8.7±1.3%. For the discs subjected to steam autoclaving after the standard treatment, the surface atomicity of silver was 7.2±2.2%. A slightly higher reduction is observed in the samples treated by immersion in water and then autoclaving. With an average deposition of 6.4±0.7% atomicity. An analysis of the variance suggests that the differences in mean silver deposition are statistically significant with a $p<0.0001$, at 95% CI. A comparison of the means with the standard treatment indicate that the mean differences of 2.10, 3.55 and 4.40 for the water-immersion, steam-autoclaving, and immersion-steam-autoclaving respectively, were also statistically significant, with p-values of 0.0147, 0.0001 and < 0.0001 respectively. The difference between the stean-autoclave and the immersion-steam-autoclave was however not significant.

These results appear to indicate that all the treatments implemented after the standard deposition treatment led to some loss of incorporated silver. The highest loss of silver was observed in the batch subjected to immersion in sterile deionised water and subsequently autoclaved. Although reports (Vetten et al., 2014, van Hengel et al., 2017) have indicated no significant change in size or morphology of silver nanoparticles incorporated onto Ti surfaces after wet autoclave sterilization, no report using EDX to date has quantified the effect on the surface composition.

For sterilising the silver incorporated discs prior to use in the biofilm reactor for biofilm experimentation, the new question is whether the amount of silver remaining on the surface after the two autoclaving processes is sufficient to demonstrably influence the extent of biofilm formed on the disc surface. This is 7.3% (0.7 SEM) atomicity for the autoclaving without immersion in water batch, and 6.4% (0.2 SEM) atomicity for the autoclaving with immersion in water batch.

The water-immersed-steam-autoclaved batch will provide a simpler and more reliable means of setting up the ensemble for the biofilm formation experiment, as this allows for the discs replacing the coupons to be mounted in the coupon holders, together with the nutrient medium in the reactor, and the unit sterilised by autoclaving as a single unit. The problem with this however is that, whereas the loss of surface silver observed in the batch immersed in water without autoclaving was over a period of 1 hour, a repeat of the process with the assembled unit may last considerable longer, and silver loss may be correspondingly higher.

The steam-autoclaved without immersing in water batch provides an alternative with a higher starting concentration of surface silver as the results above indicate. The application of the set up in the biofilm formation experimentation will involve setting up the reactor, with the discs in the coupon holder and sterilising by autoclaving without the nutrient broth. The nutrient broth is to be sterilised separately and aseptically transferred into the reactor. This can also be done via the peristaltic pump. This alternate set up process though allows for a higher starting surface silver concentration, requires a lot more care in maintaining the aseptic integrity of the set up.

6.5. Conclusion

In designing a means to sterilise the ion-incorporated titanium discs by autoclaving for subsequent use in biofilm formation experiments, two conditions were designed to simulate autoclaving the discs in the nutrient broth, and without the nutrient broth. Discs autoclaved while in deionised water represented the nutrient broth environment, and discs autoclaved without water represented the no nutrient broth environment. After analysing the disc surfaces by SEM/EDS, the latter condition showed a lesser loss/higher retention of the incorporated element relative to the average starting surface composition for all the discs.

Though the later process presents a greater challenge to maintaining aseptic integrity compared to the former, when the two conditions are applied in setting up the biofilm formation experiment protocol, the higher surface element retention allowed by the latter process makes it a better process for extrapolation into setting up the biofilm formation experiment.

Chapter 7 : Release Profile of Incorporated Ions

7.1. Introduction

Metallic implants placed in the electrolytic environment of the human body, undergo a number of electrochemical surface reactions that lead to the release of metal ions from the implant surface into the electrolytic physiologic environment. This release is coupled with a corresponding reduction reaction of constituents in the immediate environment to maintain charge neutrality (Bruschi et al., 2015, Zhao et al., 2009). The amount of metal ions released is therefore a function of a number of factors. These include the corrosion resistance of the metal surface, the physiological conditions (pH, Cl^- concentration, temperature,), electrochemical effects, mechanical factors (surface topography: pitting or crevices, pre-existing cracks, surface abrasion), thickness of the oxide layer, film adhesion, and the dense cell concentrations surrounding the implants (Joseph et al., 2009a, Solar et al., 1979, Advincula et al., 2007).

The mechanism underlying metal ions release from the metallic implant surface suggests that the surface oxide film or passive film formed on the material surface plays a critical role in the release process (Okazaki and Gotoh, 2008). As an inhibitor, this oxide layer regulates *in vivo* ion release (Hanawa, 2004). It has been reported that, strong passive layers release lower quantities of ions from the metal surface (Browne and Gregson, 1994). This however does not take cognisance of the presence of an active layer of the incorporated metallic oxide, whose release may be influenced primarily be thickness and solvation of this layer.

For the second generation (Figure 2.4) antimicrobial biomaterial agents, whose mechanism involves interaction with and subsequent disruption of bacterial cell wall and organelles, their release, is critical to their function.

In order to study the release of ions incorporated onto the Ti surfaces, the various treated discs were immersed in deionised water for 28 days.

7.2. Method

A Perkin Elmer AAnalyst 200 (Beaconsfield, UK) atomic absorption spectrometer, with a hollow cathode Ag and Zn lamp, was used in this study to investigate the amounts and rate of silver and zinc ions release from the modified Ti surfaces. The detail method is outlined in Section 3.6.1 of Chapter 3.

7.3. Results

7.3.1. Silver Release from Silver Modified Titanium Surfaces

The release profile of silver ions implanted onto the surface of the modified titanium was determined by immersing the modified silver treated discs in deionized water, maintained at 37^{o}C and 5ml sample volume taken periodically with replacement for 28 days. The cumulative concentration of silver ions released into solution, measured using flame atomic absorption spectroscopy, as a function of the immersion time is depicted in Figure 7.1. In the first 24 hours of immersion, concentration, hence the release rate of silver ions stood at 48 µg/L/h. In the following 7 days, a steadier decline in ion concentration or release rate of 15 µg/L/h was observed, after which the release of ions from the titanium surface appears to plateau, and then remains approximately constant through to the 4 weeks' immersion time at 3 µg/L/h.

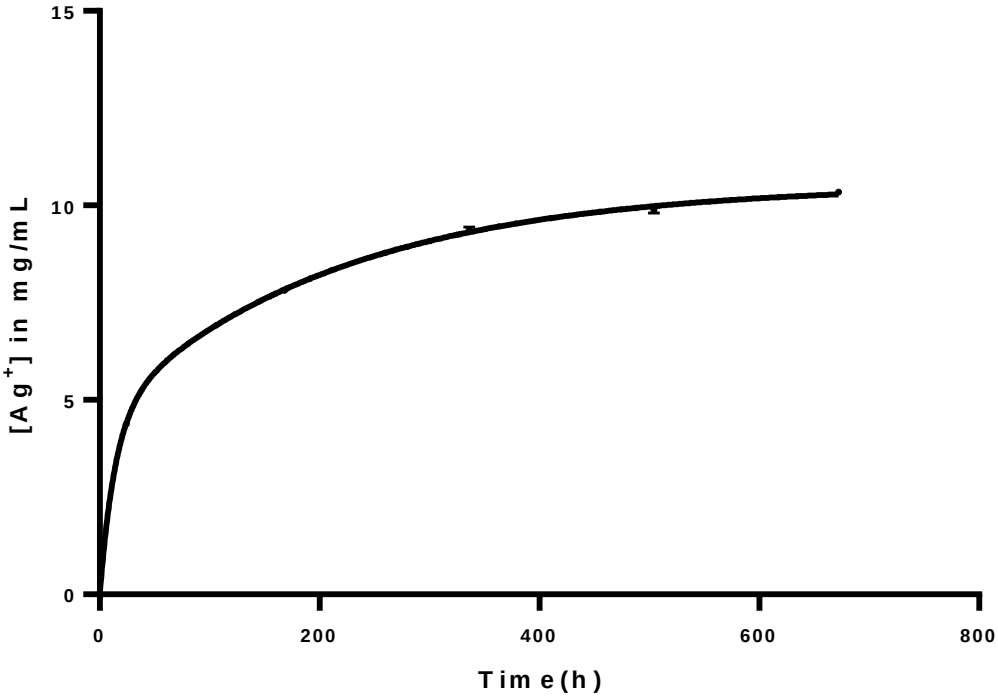

Figure 7.1 Cumulative release profile of silver from the modified silver treated Ti surface during 28days immersion in deionised water. Error bars represents the mean ± S.E.M. for n=3 repeats.

7.3.2. Zinc Release from Zinc Modified Titanium Surfaces

Zinc ions release from the surface of the modified titanium was determined as previously by immersing the modified zinc treated discs in deionized water, maintained at 37°C. 5 ml samples were taken periodically with replacement for 28 days. The cumulative zinc ions released into solution, measured using flame atomic absorption spectroscopy, as a function of the immersion time is depicted in Figure 7.2. In the first 24 hours of immersion, concentration, hence the release rate of zinc ions stood at 5.4 µg/L/h. In the following 7 days, a steadier decline in ion concentration or release rate of 2.71 µmg/L/h was observed, after which the release of ions from the titanium surface appears to plateau, and then remains approximately constant through to the 4-weeks' immersion time at 0.33 µg/L/h.

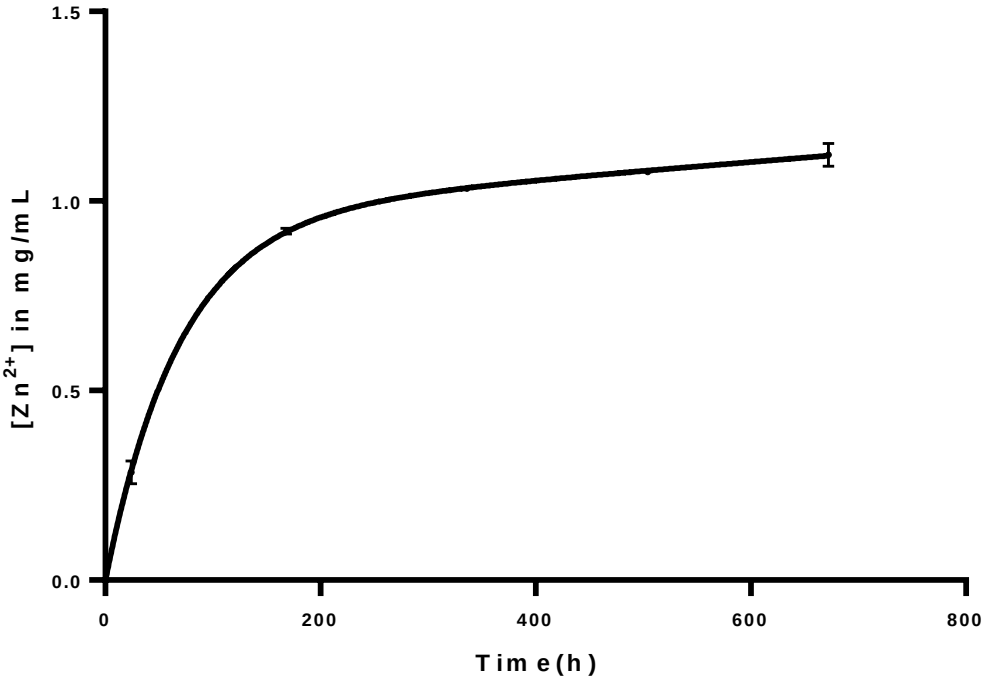

Figure 7.2 Cumulative release profile of zinc from the modified zinc treated Ti surface during 28 days immersion in deionised water. Error bars represents the mean ± S.E.M. for n=3 repeats.

7.3.3. Silver Release from Silver-Zinc Composite Modified Titanium Surfaces

The release profile of silver ions incorporated with calcium and zinc onto the surface of the modified titanium was determined as before, by immersing treated discs in deionized water, kept at 37^{o}C for 28 days. 5ml sample volume were taken periodically with replacement, and the cumulative concentrations of silver ions released into solution, measured using flame atomic absorption spectroscopy, as a function of the immersion time. This is shown in Figure 7.3. In the first 24 hours of immersion, concentration, hence the release rate of silver component ions stood at 3.3 µg/L/h. In the following 7 days, there was a steady decline in ion concentration or release rate of 0.86 µmg/L/h, after which the release of ions from the titanium surface appears to plateau, and then remains approximately constant through to the 4-weeks' immersion time at 0.1 µg/L/h.

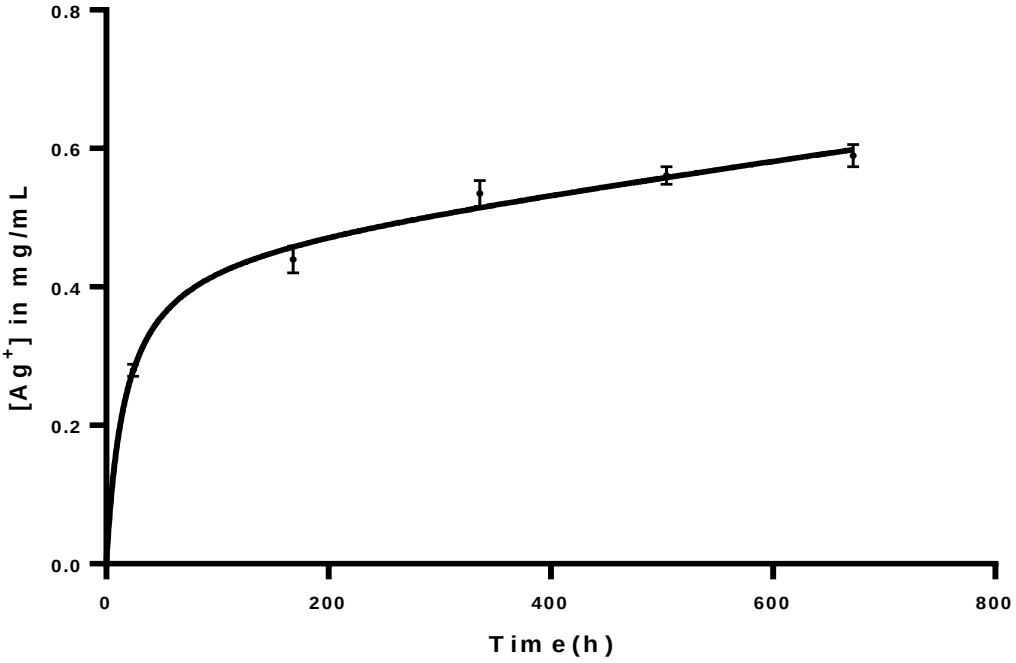

Figure 7.3 Cumulative release profile of silver from the modified silver-zinc composite treated Ti surface during 28 days immersion in deionised water. Error bars represents the mean ± S.E.M. for n=3 repeats.

7.3.4. Zinc Release from Silver-Zinc Composite Modified Titanium Surfaces

The release of the zinc ions moiety of the calcium-silver-zinc incorporated onto the surface of the modified titanium was also determined by immersing treated discs in deionized water, maintained at 37^{o}C. and 5 ml replacement volumes were drawn for 28 days. The cumulative concentrations of zinc ions released into solution was determined by means of a flame atomic absorption spectroscopy, as a function of the immersion time, as shown in Figure 7.4. In the first 24 hours of immersion, concentration, hence the release rate of zinc component ions stood at 2 µg/L/h. In the following 7 days, a steady decline in ion concentration or release rate of 0.64 µg/L/h was observed, after which the release of ions from the titanium surface appears to plateau, and then remains approximately constant through to the 4-weeks' immersion time at 0.1µg/L/h.

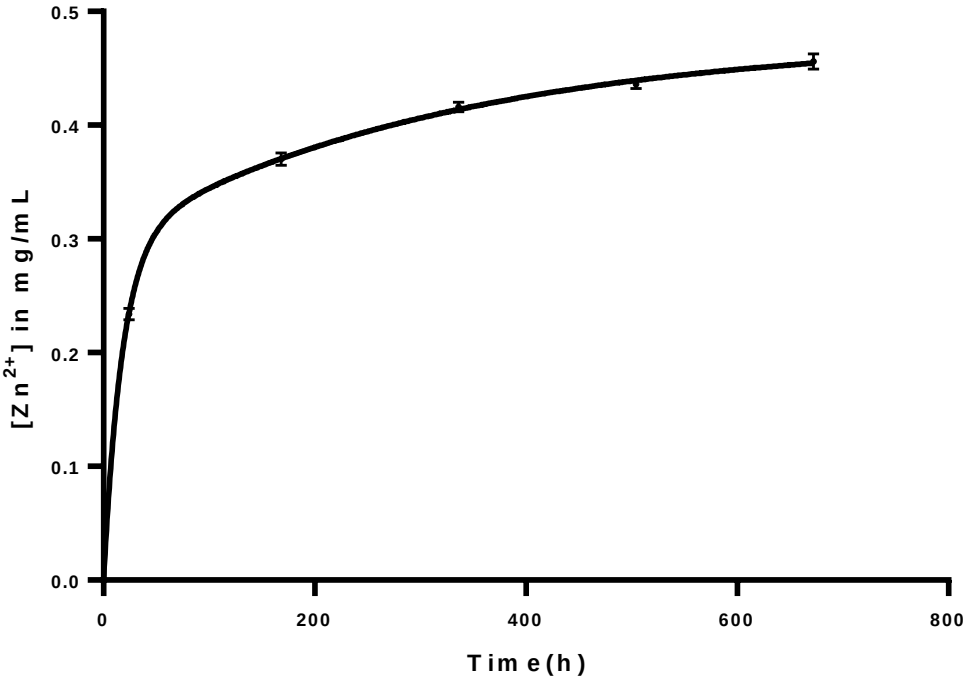

Figure 7.4 Release profile of zinc from the modified silver-zinc composite treated Ti surface during 28days immersion in deionised water. Error bars represents the mean ± S.E.M. for n=3 repeats.

Table 7.1 Summary of the time concentrations and time release rates of silver and zinc as 'mono' ion oxide layers, and as 3-ion oxide layer (*) from the modified surfaces.

Time/h	[Ag] mg/ml	Ag Rate mg/ml/h	[Zn] mg/ml	Zn Rate mg/ml/h	[Ag]* mg/ml	Ag Rate* mg/ml/h	[Zn]* mg/ml	Zn Rate* mg/ml/h
0	0.00E+00	8.00E-01	0.00E+00	4.00E-02	0.00E+00	4.00E-02	0.00E+00	3.00E-02
24	4.38E+00	4.80E-02	2.85E-01	5.40E-03	2.80E-01	3.30E-03	2.34E-01	2.00E-03
168	8.83E+00	1.50E-02	9.21E-01	2.71E-03	4.40E-01	8.57E-04	3.70E-01	6.36E-04
336	9.37E+00	6.00E-03	1.03E+00	3.33E-04	5.35E-01	4.29E-04	4.16E-01	2.14E-04
504	9.88E+00	4.00E-03	1.08E+00	3.33E-04	5.61E-01	1.67E-04	4.36E-01	1.00E-04
672	1.03E+01	3.00E-03	1.12E+00	3.33E-04	5.90E-01	1.11E-04	4.56E-01	6.25E-05

7.4. Discussion

Metallic biomaterials in aqueous physiologic solutions are systems with both passive and active surfaces in simultaneous contact with their environment, according to the passivity theory (Hanawa, 2004, Scharnweber et al., 2002, Kelly, 1982). Thus, it is thought that the surface oxide film on the metallic implant surface undergoes a cyclical or reversible process of partial

dissolution or solvation and re-precipitation in the aqueous environment. The incorporated metal ions are released when the dissolution rate is higher than the re-precipitation rate. A departure from this however, is the expectation that in the dynamic physiological environment of the body, fluid transport or transport of the bathing physiological fluids around the implant device prevents re-precipitation on the device surface. This leads to continual release of the incorporated ions from the device surface until they are completely depleted.

The cumulative release of Ag^{+} from the modified treated surfaces over a 28-day period is illustrated in Figure 7.1 as a function of the concentration against the immersion time. The release curve shows a two-phase release profile, comprising an initial fast or burst release over the first 24 hours, followed by a slow and then constant release phase for the next 27 days (Figure 7.1). A measurable amount of Ag^{+} were detected in the surrounding deionized water within a few hours of the immersion. After 24 hours, the cumulative release rate of Ag^{+} stood at 48 µg/L/h. By the end of the first week, the rate had dropped by about a third, to 15 µg/L/h, after which the release of Ag^{+} reaches a plateau and remains approximately constant at 3 µg/L/h. This trend is repeated in the cumulative release of Zn^{2+} form the surface of the polished Zn^{2+} treated titanium disc (Figure 7.2). Similar comparatively high amounts of Zn^{2+} was detected in the deionized water with a few hours of immersion, and after 24 hours that rate was 5.4µg/L/h. By the end of the first week, the rate had halved to 2.71 µg/L/h, after which the release of Zn reaches a plateau and remains approximately constant at 0.33 µg/L/h. The release of Ag^{+} (Figure 7.3) and Zn^{2+} (Figure 7.4) from the Ag/Zn multi-ion treated surface follow a similar trend, albeit with smaller concentration magnitude (Table 7.1).

7.5. Conclusion

Solvation leading to the formation of a cationic titanate sol-gel complex layer on the titanium disc surface may account for the trend in ion release observed after 28 days of immersion in

deionized water, the constant agitation of the immersion system facilitating the gradual release of ions into solution until the system approaches equilibrium or a sampling incident takes place to shift the system towards the release of more ions. The cumulative effect of this is the continuing release of ions into solution with reducing release rate in a two-phase release profile. The rate however approaches a constant as the ions in solution approaches the theoretical exhaustion point. The suggesting by this in that, ions with potential antimicrobial properties, reproducibly incorporated onto the Ti surface, may reliably sustain the presence of antimicrobial agents in the immediate environs of the implant, over sufficient period of time, to prevent biofilm forming bacterial from colonizing the implant surface as osseointegration commences.

Chapter 8 : Effect of Surface Modifications on Microbial Activity and Biofilm Formation

8.1. Introduction

Advances in the biomaterial science has allowed for a myriad of combinations of polymers and metal alloys to be used for tissue replacements. This has also resulted in the increased complexity of devices fabricated for these replacements (Ratner, 1996b). However, a major issue with the extended application of implantable devices is the propensity of biofilm forming bacteria to adhere to device material surfaces, resulting in biomaterial-centred infections, disruption of successful tissue integration, and inflammation mediated biocompatibility problems (Subbiahdoss et al., 2010, Costerton et al., 1999b, Busscher et al., 2012b). This is because the interactions between tissues, biomaterials and bacteria are directed not only by specific receptors and molecules of host and bacterial cell surfaces, but also by topography, elemental or atomic composition and the electronic state of the biomaterial surface (Palmquist et al., 2010, Oliveira et al., 2015, Kokubo et al., 2010). The thinking is that, biomaterial surface modifications at the elemental/atomic level will facilitate the alteration of (host and bacterial) cell-to-substratum events, and in so doing enhance implant integration, tissue compatibility and diminish infection by directly inhibiting biofilm formation (Gristina, 2004b).

Biofilms have been described by the Centre for Disease Control and Prevention (CDC) as microorganisms living in a self-organized community attached to surfaces, interfaces, or each other, embedded in a matrix of extracellular polymeric substances of microbial origin, while exhibiting altered phenotypes with respect to growth rate and gene transcription (Mendonça et al., 2009, Karlsson et al., 2003). This makes the biofilm the metabolic or accumulative phase of the bacterial cycle during which the bacteria use their pheromone-based quorum sensing mechanism of inter-bacterial communication, to alter their behaviour (Jefferson, 2004a). The

expression of a cementing amorphous highly hydrated extracellular matrix substance in which they become encased allows the bacteria to maintain a low metabolic state, thus becoming insensitive to antibiotic concentration up to a third order magnitude. This to some extent accounts for the higher prevalence of antibiotic resistance associated with certain strains of biofilm forming bacteria (Arciola et al., 2005, Arciola et al., 2002, Anwar et al., 1990). The biofilm protects the bacteria colony from harmful conditions created by the host and medication. It can also facilitate colonisation of favourable nutrient-rich areas and make use of the cooperative benefits of the bacteria community as in sharing of metabolic load. The biofilm may also become the default growth mode when conditions are not favourable (Jefferson, 2004b). In most cases of orthopaedic biomaterial associated infections, the biofilm colony is mono-microbial. Poly-microbial biofilms are common in urinary and oral infection however, due to the so-called co-adhesion of other strains and species to an existing biofilm (Wagner et al., 2011, Violant et al., 2014, Trautner and Darouiche, 2004). The interaction between two surfaces in a biological bathing medium leading to the attachment of microbial organisms to a surface is therefore essential in the biofilm formation process; and the microbial and the substrata surface properties are important in the interaction. A surface that resists microbial adhesion without provoking extensive inflammatory response is therefore promising in the quest for antibacterial biomaterials (Gristina et al., 1987, Gristina, 1987).

A critical step in the biofilm formation sequence of events is the production of an exopolymer, the so-called glycocalix which is an accumulation of glycoprotein that enables microbial adhesion (Costerton et al., 1987, Gristina, 2004b). This polymer mediated adhesion at the onset is reversible, and is dependent on the physico-chemical properties of the biological environment, the microbial cell surface, and the implant surface (Neu and Marshall, 1990, Tang et al., 2013). Of these three, it is the implant surface property's ability to interfere with biofilm

forming bacteria adhesion process that is being exploited in this study, to confer antimicrobial properties to the implant surface.

In spite of the extensive understanding in recent years, the progress in the design of surface strategies to halt microbial colonisation has not matched expectations. Pivotal in this the failure of design technologies to prevent or disrupt the highly protective biofilm phenotype that allows colonizing bacteria to evade antibiotics treatment and host immune responses for prolonged periods, only to return in more virulent phenotypes (Costerton et al., 1999a). The successful technology must therefore selectively favour tissue integration over bacteria adhesion and biofilm formation. The difficulty with such technology lies in the fact that integrin receptor-binding motifs that facilitate host cell adhesion, spreading and growth are also recognised by biofilm forming bacteria (Fowler et al., 2000). Also surface technologies that reliably stop bacteria colonization also interfere with host tissue integration (Chrzanowski et al., 2010). This suggests a thinking away from mono to multi-functional surface strategies that reliably select host tissues over bacteria cells. This is the thinking informing this study in the development of novel simple surface modification strategies that confer antimicrobial as well as osteo-integrating surface characteristic to the commercially pure titanium available for biomedical application. The antimicrobial strategy involves the incorporation of silver and zinc to the commercially pure titanium surface. Such a surface could employ both surface chemistry and topography modifications to encourage the titanium biomedical implant to effectively distinguish friend from foe and respond accordingly (Wang et al., 2012, Maddikeri et al., 2008, Shi et al., 2008, Chrzanowski et al., 2010)

A number of hypotheses (Feng et al., 2000b) have been put forward to explain the antibacterial activity of silver nano particles. These include the breakdown release of ionic silver from the silver modified Ti surface (Armitage, 2009), which inactivates vital bacterial enzymes by disrupting essential thiol groups. Silver ions have also been suggested to damage bacterial

cytoplasmic membrane, deplete intracellular adenosine triphosphate (ATP) and cause cell death, all by inhibiting bacterial DNA replication (Priya et al., 2013).

In contrast to other antimicrobial agents, it has also been established that prolonged exposure of bacteria to silver nanoparticles has so far not led to the development of resistant bacteria strains (Salem et al., 2015). This is because silver nanoparticles have been hypothesized to target multiple sites on or within bacterial cells, resulting in a broad spectrum activity (Markowska et al., 2013). Thus, silver nanoparticles could find an effective application as an antimicrobial agent for long-term usage.

Similarly for zinc, the mechanism of its bactericidal and bacteriostatic activity proposed include the direct contact of zinc oxide nano particles (ZnO-NP) (Brayner et al., 2006, Zhang et al., 2007, Reddy et al., 2007), generation of reactive oxygen species (ROS) (Sirelkhatim et al., 2015, Adams et al., 2006b), such as peroxides and hydroxyl radicals. These are involved in ZnO-localized interaction mediated cell wall damage, enhanced membrane permeability and uptake of toxic dissolved zinc ions, leading to mitochondria weakness, intracellular outflow, and disruption of gene expression of oxidative stress . This results in the eventual cell growth inhibition and cell death.

In the quest to manage the outcome, Anthony Gristina (1987) coined the phrase the "race for the surface," suggesting the concept that the fate of internally implanted devices is dependent on a competition between host tissue integration and bacteria colonization at the implant surface (Gristina, 2004b, Busscher et al., 2012a). Even though the hope is that the host's robust immune competence will give it the upper hand, the reality is that sometimes bacteria wins the race with dire repercussions. In a similar quest, this chapter investigates the effects of the incorporation of the antimicrobial agents of interest, i.e. silver in zinc, on *S. aureus* adhesion, biofilm formation and colonization of the implantable titanium surface.

8.2. Method

A series of assays were carried out in this study to investigate the antimicrobial effects of the metal-ions of interest that is, calcium, zinc and silver, incorporated onto the titanium surface. Details of the methods employed in the anti-microbial suspension assay, (Section 3.5.1), the modified Kirby-Bauer test (Section 3.5.2) and the CDC biofilm formation assay (3.5.3) are found in Chapter 3.

8.3. Results

8.3.1. Anti-Microbial Suspension Assay

A plot of the log number of colony forming units (cfu) against the time of bacterial suspension exposure to the modified/treated Ti disc surfaces (Figure 8.1), shows marked variations in the effect of the treated discs on the bacterial survival in suspension. The figure indicates an approximate starting *S. aureus* concentration of $7.5\pm0.02\log_{10}$ cfu/mL for all the discs under considerations. A constant colony counts of $7.5\pm0.02\log_{10}$ cfu/ml at 10min intervals was observed for the calcium treated surface over a 60min period. A similar trend was observed for the polished (polTi), and the unpolished (cpTi) surfaces, as well as the control polycarbonate coupon surface. The silver (polAgTi), zinc (polZnTi) and the silver-zinc composite treated surfaces however demonstrated a significant reduction in the colony numbers all the way to 60min of incubation time. The log reduction was approximately 0.34 for silver, 0.11 for zinc, and 0.24 for the composite treated surface after 10min. After 30min, the log reduction was 1.57 ± 0.04 for the zinc treated surface, 1.93 ± 0.03 for the silver-zinc composite surface and 2.44 ± 0.04 for the silver treated surface.

Between the 30th and 60th minute points, the reduction approached a constant for the zinc and silver-zinc composite surfaces, levelling off at approximately 1.99Log_{10} or 99% and 2.37Log_{10}

or 99% reduction respectively for the zinc and the composite surfaces. During this same time, the silver treated surface continued to demonstrate a steady reduction in the number of bacteria able to survive in the suspension exposed to the treated surface. By the end of 60min, the reduction was approximately 3.26Log_{10} or 99.9% from the starting bacterial count.

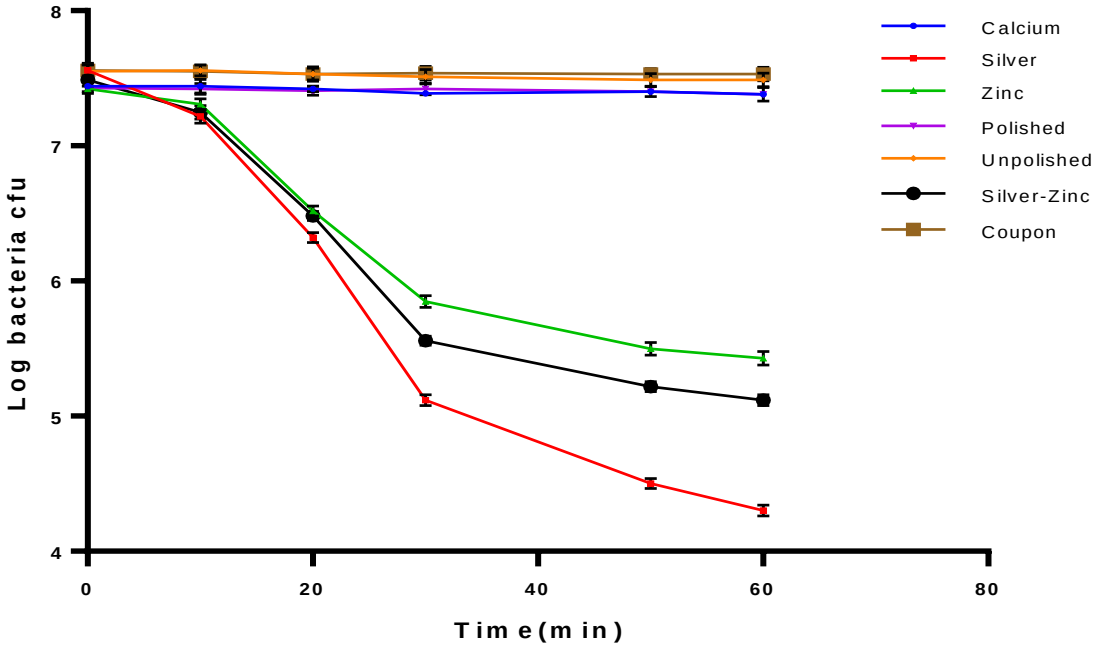

Figure 8.1. The effect of surface modifications on bacterial survival in a S. aureus suspension seeded with modified surfaces. A log10 of the number of colony forming units against the time of suspension exposure to the modified/treated surfaces shows variations in the effect of the treated discs on the bacterial survival in suspension. The plot shows a constant colony counts for the calcium treated surface, as well as for the polished (polTi), unpolished (cpTi) surfaces and the control coupon. Statistical analyses suggest that the reduction observed with silver and zinc treated surfaces are significant (P value of 0.0002, as determined by a one-way ANOVA with Bonferonni's post-hoc test). Error bars represents the mean ± S.E.M for n=5 samples.

8.3.2. Inhibition Zone: Modified Kirby-Bauer Test

A modified Kirby-Bauer test to demonstrate the effect of the surface modifications/treatments on *S. aureus* growth inhibition *Figure* 8.2, suggested the control polycarbonate coupon surface, the unmodified-untreated Ti surface, and the polished-untreated Ti surface had no inhibitory effect on the growth/spread of *S. aureus* on the solid agar medium. This is indicated by the absence of a clear zone of no bacteria growth/spread around these discs. The silver treated surface had the highest inhibitory effect, with an inhibitory zone diameter of approx.

18.23±0.12mm. The zone seen with of zinc is approximately 13.53±0.03mm. That of the silver-zinc composite of 15.27±0.15mm. The controls of polycarbonate coupon, polished and unpolished Ti demonstrated no inhibitory effect on the same solid medium, suggesting the inhibitory effect observed is due to the treatment/ion implanted on the disc surfaces.

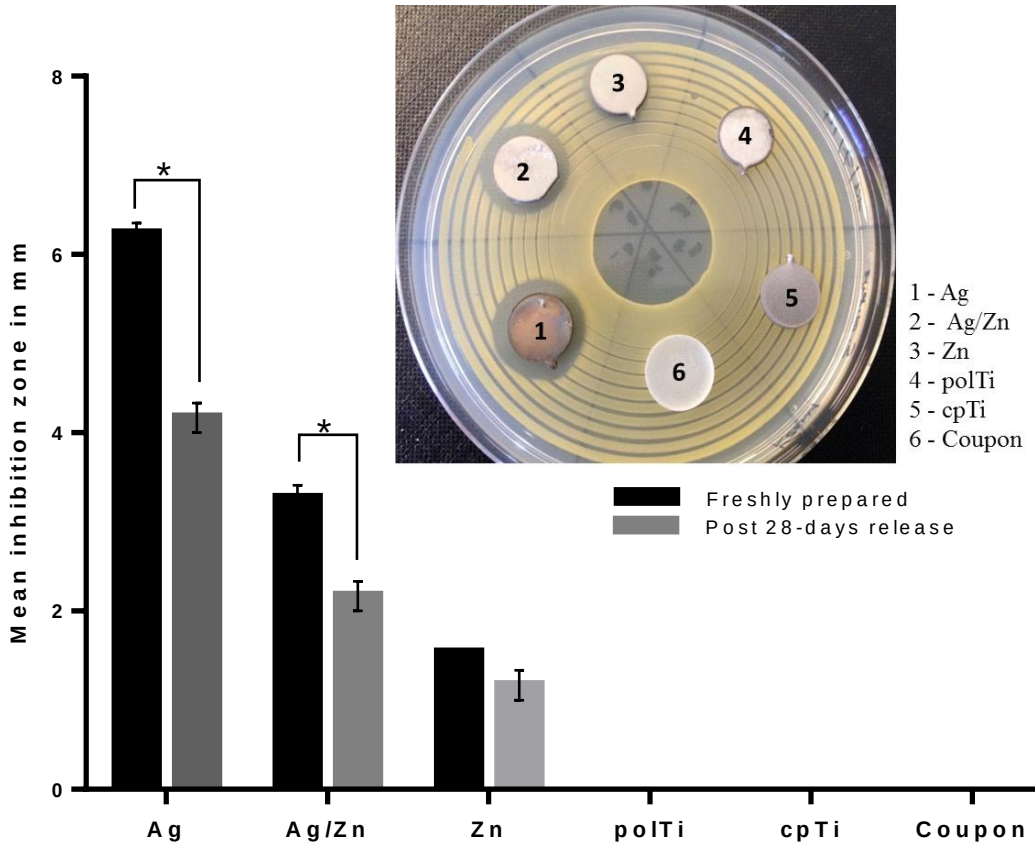

*Figure 8.2 Mean inhibition zones: effect of Ti surface modifications (undepleted and post 28-days depletion) on S. aureus strain ATCC6538 growth/spread on solid agar medium in a Petri dish, and (insert) an image of the presence/absence of inhibition zones around the various modified surfaces and controls. A paired t-test for the freshly prepared against the post 28-days release indicates that the overall differences observed are not statistically significant for a two-tailed p≤0.05, with a pairing correlation coefficient of 0.999. However, * indicates significant differences for each pairing surface. Error bars represents the mean ± S.E.M. for n=5 samples.*

The same modified Kirby-Bauer test was repeated, this time with similarly treated discs but leached or depleted for 28 days in sterile deionised water maintained at 37°C with shaking. The results show similar trend to the undepleted surfaces, albeit with statistically significant reduction in inhibition zone diameters. The zone around the silver treated surface was 16.17±0.29 mm in diameter. This was 14.17±0.29 mm for the silver-zinc surface, and

13.0±0mm for the zinc treated surface. The presence of inhibitory zones around the depleted silver and zinc treated discs suggests that the surfaces are still bacteriostatically active even after 4 weeks of continuous leaching or depleting.

8.3.3. CDC Biofilm Reactor – Biofilm Formation Test

The mean counts of *S. aureus* colony forming units recovered from biofilms formed on the control polycarbonate surface, the commercially pure Ti surface, and the modified Ti surfaces, subjected to the biofilm forming conditions of the biofilm reactor over 24 hours suggested the ability of the modified surface to resist bacteria attachment and colonization. The cpTi surface and the polycarbonate surface were the reference and the control surfaces respectively. As demonstrated previously by the suspension test and the modified Kirby-Bauer test, the silver treated surface supported the least number of bacterial colony forming units (approx. 4.17±0.06 log cells ml^{-1}), corresponding to the surface most resistant to bacteria attachment and colonization. The Ag/Zn treated surface again demonstrated an intermediary effect between the silver and zinc surfaces with a bacterial cells population of 4.30±0.05 log cells ml^{-1}. The polished, zinc treated Ti surface supported approx. 4.50±0.07 log cells ml^{-1}. The control polycarbonate coupon and cpTi supported highest number of colony forming units (4.72±0.06 log cells ml^{-1} and 4.63±0.02 log cells ml^{-1} respectively), representing the most favourable surfaces to bacteria biofilm formation. The polished, untreated Ti surface accommodated 4.60±0.06 log cells ml^{-1} of *S. aureus*.

Figure 8.3 is a plot of the log reduction in bacteria colony forming units, recovered from the 24h biofilm formation assay, against the various surfaces. With the commercially pure unpolished surface as the reference or baseline surface, the figure also suggests the polished silver treated surface exhibits the highest reduction, with a mean reduction of 0.46 log. This was followed by the zinc-silver surface at 0.34 log reduction. Of all the modified surfaces, the least reduction was in the polished untreated surface. The control polycarbonate coupon surface

did actually support biofilm formation with a negative log reduction of -0.08. A statistical analysis of the mean suggests the variance observed are due to the treatment the surfaces were subjected to and not a random outcome, with a p-value of 0.0001 at 95% CI.

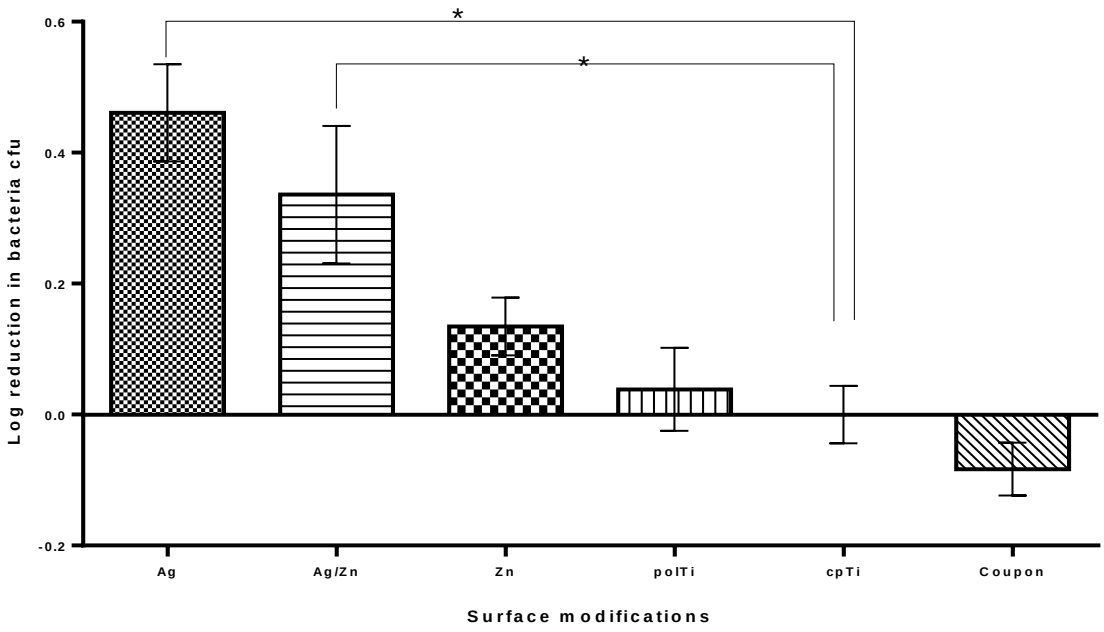

Figure 8.3. Log reduction in the number of S. aureus colonies units, hence biofilm, on the cpTi, modified Ti and polycarbonate control surfaces, as a measure of effectiveness at preventing bacteria adhesion or biofilm formation on the surfaces. The cpTi and polTi surfaces served as the reference surface, and the polycarbonate coupon surface as the control. The highest reduction is observed on the silver treated surface, and the least on the polished surface. The control polycarbonate coupon surface did not show a reduction but rather an increase in S. aureus colony numbers. Differences among means was statistically significant (P < 0.05), as determined by a one-way ANOVA with Bonferonni's post-hoc test. (*) indicates significant difference from the means of the cpTi surface. Error bars represents the mean ± S.E.M. for n=5 samples.

A comparatively marginal reduction in biofilm density is observed in the polished Ti surface. However, more significant reductions occurred in the ion-implanted surfaces. Bonferroni comparison of the surfaces suggests a statistically significant variance between the polished-silver-treated surface and all the other surfaces, except between the silver-zinc and the silver treated surfaces. Compared with the cpTi surface, the log reduction effect of polishing alone without treatment with either silver or zinc or both, was not statistically significant.

These suggest that, although the cpTi can reduce bacteria adhesion to its surface, it is the least effective compared to the modified surfaces. Polishing and chemical modification of the surfaces improved Ti interaction with biofilm forming bacteria, i.e. significantly reduced

bacteria adhesion or biofilm inhibition to the Ti surface. The silver treatment indicated the highest effectiveness in biofilm inhibition.

8.4. Discussion

A preliminary suspension test to determine the effect of the Ti surface modifications and treatments (mirror-finish polishing, and ion implantation) on bacteria growth and proliferation was carried out. The result (Figure 8.1), shows that approximately equal number of bacterial colonies were exposed to the surfaces at the start of the test, with marked variations in the effect of the treated discs on the bacterial survival in suspension.

For 60min, there was no change in the number of bacteria colony forming units for the polycarbonate (control) surface. The same was true for the cpTi (the reference) surface. This was also true for the calcium treated and the polished disc, suggesting that calcium incorporated on the disc surface has no antimicrobial effect on *S. aureus*. Likewise, the mirror-finished polished surface by itself has no antimicrobial properties on bacterial in suspension. To confer any antimicrobial or bacteriostatic effects, the elements incorporated onto the Ti surface must leach out into solution as ions or ionising agents. The silver and zinc implanted surfaces appear to achieve this. The results show the Ti surfaces implanted with silver and zinc have a similar reduction in number of bacteria in suspension just 10 min into the suspension test. After 30 min, a clear distinction between the effects of the silver, silver-zinc and zinc implanted surfaces begins to emerge; a sharp reduction in the number of bacteria in suspension. The reduction is however greatest in the silver implanted surface and least for the zinc implanted surface, with the silver-zinc surface's effect intermediary between the silver and zinc modified surfaces' effect. These differences in effect could be attributed to the empirical physico-chemical properties of the elements (Chrzanowski et al., 2010), and the amounts of the respective ions incorporated onto the surfaces, which influence the amounts released into solution.

The comparatively higher antimicrobial effect of the silver treated surface over the zinc treated surface could be attributed to the higher amounts incorporated on to the Ti surface, the subsequent higher amounts released into solution and the higher specific surface-to-volume ratio (Stobie et al., 2008) of silver nano particles from the surface characterisation. This promotes the dissolution of silver ions, and facilitates better contact with microorganisms and ease of bacterial cell wall permeability, hence augmenting bactericidal effectiveness. The release of silver and zinc incorporated into the Ti surface and their subsequent ionization are therefore key to their antibacterial activity.

The silver-zinc surface's effect was not additive on the silver surface's effect, but still an improvement on the zinc surface. This suggest that, the chemical reaction leading to the implantation of the ions is limited to the surface atomicity of the Ti disc, and the competition for the limited Ti surface atoms lead to the reduction in number of silver and zinc ions incorporated onto the Ti surface. Hence the reduction in the antimicrobial effect compare to the silver ion only incorporated surface. However, higher antimicrobial potency of silver over zinc augmented the antimicrobial effect of the silver-zinc surface over the zinc ion only incorporated surface. The reduction in bacteria numbers appears to taper off towards the 60min mark along the same trend for the zinc and silver-zinc surface. However, for the silver surface, the reduction continues steeply as the time approach the hour mark. By the end of the 60min, the bacteria load reduction was approximately 99% for both the zinc and zinc-silver treated surfaces, and approximately 99.9% for the silver treated surface. Statistical analyses suggest that the reduction observed with silver and zinc treated surfaces are significant (p-value of 0.0002, as determined by a one-way ANOVA with Bonferonni's post-hoc test).

The modified Kirby-Bauer Test was used to test the susceptibility of the *S. aureus* to the ions released from the disc surfaces, and the extent of diffusion of the released ions. This measured

the antimicrobial effect, of the modified Ti, as the diameter of the clear zone formed around the discs.

With no bactericidal or bacteriostatic agents incorporated on their surfaces, the control polycarbonate coupon surface, together with cpTi surface, and the polished-untreated (polTi) surface had no inhibitory effect on the growth/spread of *S. aureus* on the solid agar medium, has been previously demonstrated by work carried out by Deborah J Gorth et al (2012), investigating the effect of Ti, PEEK and silicon nitride (Si3N4) surface properties on *S. aureus* biofilm formation, colonization and growth. This was indicated by the absence of a clear zone of no bacteria growth/spread around these discs. The silver, zinc and silver-zinc composite surfaces however demonstrated bacterial growth inhibition, indicated by the presence of a clear region around the discs. The inhibition zone measurements indicate silver has the highest inhibitory effect, followed by the silver-zinc surface. The trend was broadly similar to that observed with suspension assay, and as in the suspension assay, may be attributable to the difference in specific surface-to-volume ratio of the silver and zinc nano particle on the surfaces. The trend observed may also be influenced by the amount of nano-particulate silver and zinc incorporated into the Ti disc surface, the amount of these released from the surface into the limited moisture of the solid agar and their subsequent ionization, and the ease of ion diffusion across the solid agar medium. These, together influence the amount of silver or zinc ions that come into contact with bacterial cell wall within the 24-hour period, leading to the subsequent peptidoglycan and intracellular organelle function disruption and eventual cell death. A similar trend was also observed when the surfaces were subjected to the modified Kirby-Bauer Test after the surface ions were controlled-leached into sterile de-ionised water over 28 days. The surfaces remained anti-microbially active even after 28 continuous days of controlled-leaching of the implanted ions from the surface. The observed inhibition was comparable to that seen in the ‘unleached’ surfaces. A paired t-test for the freshly prepared

surfaces against the post 28-days release surfaces indicates that the overall differences observed are not statistically significant for a two-tailed $p \leq 0.05$, with a pairing correlation coefficient of 0.999. However, the individual pairing surfaces indicate significant differences for the Ag and Ag/Zn pairing surfaces. As previously, the commercially pure Ti surface, together with the polished and polycarbonate control surfaces therefore showed no demonstrable bacteria inhibition activity.

One of the earliest events leading to bacteria colonization of an implant device *in situ* is the attachment of planktonic bacteria to the device surface and the subsequent formation of a bacterial biofilm. A surface capable of antimicrobial effect may do so by preventing bacterial adhesion and biofilm formation or release antimicrobial agents that antagonise bacterial proliferation and colonization. A biofilm formation assay was therefore carried out to determine how the modified/treated surfaces performed in a simulated biofilm forming environment of a CDC biofilm reactor.

The results suggested that, comparatively, the cpTi surface was the least effective at preventing bacterial adhesion of biofilm formation on the Ti surface, as has been demonstration by investigations on effect of surface topography on protein and bacteria adhesion, by other researchers (Gorth et al., 2012, Kang et al., 2012, Moriarty et al., 2011). Polishing and treating the surfaces improved Ti interaction with biofilm forming bacteria, i.e. significantly reduced bacteria adhesion to and chances of biofilm inhibition on the surface. The silver treatment demonstrated the highest effectiveness in biofilm inhibition. The differences in bacteria reduction or the various surfaces was statistically significant ($p < 0.05$), as determined by a one-way ANOVA with Bonferonni's post-hoc test.

The effect of the polished surface could be attributed to the reduced topographic features of the polished surface compared to the cpTi surface. The polishing removed the surface grooves,

peaks and valleys that provide anchorage sites for planktonic bacteria attachment. The suggestion here is that, although the polished surface has little or no inhibitory effect on bacterial growth and proliferation in solution, as demonstrated in the suspension and the Kirby-Bauer tests, the nano topographic features reduced bacteria cell adhesion to and biofilm formation on the surface.

8.5. Conclusion

The antimicrobial effects of the treated surfaces before and after 28 days of ion leaching into solution suggests that the potency of the treated surfaces in halting bacteria growth/spread reduces with depletion of the ions implanted on the Ti surfaces. That there was any inhibition effect at all after four weeks of continuous leaching suggests the treated surfaces can provide a sustained period of significant antimicrobial activity.

With regard to the prevention of biofilm formation, it is evident from the results that the mirror-finished polished surface performed demonstrably better than the unmodified commercially pure surface. This could be attributed to the reduced nano topographic features of the polished surface compared to the unpolished surface. The polishing removed the surface grooves, peaks and valleys that provide anchorage sites for planktonic bacteria attachment. This would suggest that, though the polished surface has little or no inhibitory effect on bacterial growth and proliferation, it is effective in preventing or reducing bacterial cell attachment and biofilm formation.

The Ag and Zn treated surfaces produced significant antimicrobial activity, i.e. effectively prevented bacteria cell attachment and biofilm formation on the treated Ti surfaces.

These results suggest that orthopaedic devices implanted with silver and zinc by the method developed here may provide durable antimicrobial protection against device-related infection.

Chapter 9 : Effect of Surface Modifications on Osteoblast-like Cell Adhesion and Proliferation

9.1. Introduction

Brånemark in 1990 redefined osseointegration as 'a continuing structural and functional coexistence, possibly in a symbolic manner, between differentiated, adequately remodelling, biologic tissues and strictly defined and controlled synthetic components providing lasting specific clinical functions without initiating rejection mechanism' (Albrektsson T, 2003). Since its introduction as a concept in 1950s, osseointegration become a significant dimension in the field of implantology, and in the treatment options for improving function and longevity of implant devices (Parithimarkalaignan and Padmanabhan, 2013, Zarb, 1985). The popularity of the use of implant devices in restorative medical/dental procedures is helped by the reported 98% initial success rate. Even the decline to the range of 90.1-95.4% after 5 years, and a further reduction to the range of 83-89% after 10 to 16 years (the longest current observation time reported) has only served to increase the use of implant devices. With the possible exception of co-morbidities and lifestyle choices, the other factors that affect the overall performance and longevity of implants are infections and insufficient osseointegration (de Avila et al., 2015, Pjetursson et al., 2014, Simonis et al., 2010).

One process critical to the establishment of a good bone-biomaterial integration or osteointegration is the retention of osteogenic cells on the surface of biomaterials. A good material is therefore one that readily recruits and retains bone cells from the surrounding bone tissues, in the case of material load-bearing and anchorage implant devices (Yamada et al., 2010), or mimics the natural osseous material to allow the cellular components to duplicate the natural response. This material surface enhances the attachment of osteoblast precursor cells, proliferation and differentiation into osteoblasts and accelerate the healing process in bone

replacement procedures (Chen et al., 2014). As the fundamental events leading to osseointegration occur at the implant surface, it is imperative that the surfaces of implants are optimized to foster biocompatibility with the surround tissues.

Surface characteristics, including micro and nano-scale topography and chemistry of the material surfaces are therefore important mediators of the initial interface interaction (Cyster et al., 2004, Ball et al., 2008). Aspects of cell behaviour such as cell adhesion, proliferation, differentiation, contact guidance, cell orientation, cell morphology, mechanical interlocking and the formation of the cell's microenvironment, are all to varying degree influenced by the physical and chemical properties of the material surface in contact with cells, all of which are relevant to the biological response to the surface (Anselme et al., 2000, Zinger et al., 2004). Changes in these parameters have been found to influence the attachment, spreading characteristics, signaling and maturity profile of bone cells and ultimately generate bone tissue around the implant (Braceras et al., 2005, Nayab et al., 2005). For weight bearing and permanent *in situ* implants particularly, the strength of the anchorage with the surrounding bone tissue (Schuler et al., 2006a, M, 2000) is of critical importance, as well as its ability to mimic the natural bone to allow the cellular components to perform in as similar manner as possible to the natural situation.

The behaviour of osteogenic cells, particularly the changes in morphology of the cells in an *in vitro* environment, provides an indication of the biocompatibility of the environment presented to the cells. For the various surface modifications under investigation, the number of U2OS cells adhering to the modified surfaces, and the cell morphological changes, assessed in relation to the extent of cell spreading or an estimate of the cell surface area, served as a useful means of comparing the effect of the different surfaces (Baxter et al., 2002).

9.1.1. Events at Bone-Implant Interface

An understanding of the event occurring at the bone-implant interface is therefore critical to modelling surfaces that best suit the desired outcome on implant devices. The sequence of events occurring at the interface starts with the formation of a water molecule layer around the implants within nano seconds of the implant placement in the prepared site. This water layer facilitates the adsorption of proteins and other molecules on the implant surface (Singhatanadgit, 2009, Shard and Tomlins, 2006, Thevenot et al., 2008b). The next event occurs with 30 seconds to hours of implant placement, when the implant surface becomes covered with a layer of extracellular matrix proteins, which come from the blood and tissue fluids at the insertion/wound site and later from the cellular activities at this site. Cells interact with the implant surface via the adsorbed protein layer, leading to cellular adhesion, migration and differentiation. This takes a few hours to several days, post implant placement to occur, and is rigorously regulated by implant topography, chemical characteristics, ion release form the implant surface, extracellular matrix (ECM) proteins, cell surface bound and cytoskeletal proteins (Puleo and Nanci, 1999a, Wilson et al., 2005, Ratner and Bryant, 2004).

Arginine-glycine-aspatate or RGD sequence containing molecule such as fibrin, collagen, fibronectin, bone sialoprotein, osteoprotein and vitronectin, present in some ECM protein are believed to be involved in the cell adhesion and mineral binding process (Schwartz et al., 1999, Puleo and Nanci, 1999a). Topography or rough guided cell adhesion occur through the actin rich cell extensions or filopodia which scan the surface for micro or sub-micrometer structures pores as anchorage points for the filipodia tips. On smooth surfaces however, focal adhesion mediates cell adhesion, resulting in more flattened cells with retracted extensions or filipodia (Adams, 2001, Singhatanadgit, 2009, Zhu et al., 2004). Most of the cells migrating to the implant surface with the adsorbed water molecules, and platelets are multipotent mesenchymal cell and not committed osteoblast. Factors such as the availability of nutrients, local oxygen

saturation and local regulatory growth factors, which also depend on the vascularity of the implant site and host physiology, dictate the differentiation product of the multipotent mesenchymal cell at the surface of the implant. Diminishing oxygen concentration gradient towards the centre of the wound resulting from cessation of circulation and local ischemia, leads to oxygen deprivation osteocytes and the aggregation of neutrophils and macrophages within 24-48 hours of implant placement. These cells are involved in clot and necrotic tissue formation (Davies, 2003). By 72-96 hours post implant placement, osteoblast related transcription factors are activated by the cells around the implant and necrotic bone around the implanted are resorbed, leading to the formation of a clearly defined interface boundary. Then onwards, alkaline phosphatase activity is detectable, suggesting the onset of mineralization and matrix remodeling by both contact and distance osteogenesis. By the end of the fourth week, the implant surface is in direct contact with the bone matrix, and osteoblasts form the bulk of tissue layer adjacent to the implant. In some cases, however, the implanted device may still be fibrin encapsulated. It takes 12 or more weeks for newly developed bone to formed on the implant surface to and become intimately integrated with mature lamella bone close to the implant (Depprich et al., 2008).

9.1.2. Calcium and Bone Mineralization

The bone mineralization and matrix remodeling process that occurs during osteogenensis is critically affected by Calcium ions (Ca^{2+}), as well as the entire cycle of bone from formation to repair (Habibovic and Barralet, 2011). On the implant surface, calcium facilitates the preferential electrostatic attachment of the different cells and mobilizing molecules needed for bio-mineralization. As major constituent of hydroxyapatite (Zhou and Lee, 2011), it encourages mineralization by attracting calcium-binding proteins, glycosaminoglycans and proteoglycans, to generate supersaturating conditions. This suggests that, calcium ions

incorporated onto biomaterial surfaces could enhance bone formation at the bone-implant interface (Anitua et al., 2015a).

9.1.3. Progression of Attachment of Cells to Surfaces

A review of the stages in the progression of cell attachment to surfaces, by comparing cell shapes, contact guidance and spreading cell extent of contact with different surfaces, has led to the identification of four distinctive events; : 1, initial contact via filopodia; 2, extension of lamellipodia; 3, spreading of the cytoplasm between the lamellipodia; and 4, full spreading to a round or polygonal shape (Iskandar et al., 2012, M, 2000, Payer et al., 2010), that occurs as cells become attached to surfaces without the formation of a fibrous encapsulation. The spread, shape or morphology of the cells on the implant device surface is therefore a good indication of the physical state of the cells, the cyto-compatibility or cytotoxicity, and hence a good indication of the biocompatibility of the cells and the surface under consideration.

9.1.4. U2OS Osteosarcoma Cell Line

To investigate the *in vitro* response of osteogenic cells on the modified/treated surfaces U2OS (U2OS ATCC® HTB-96™) osteosarcoma cell line was employed. The U2OS cell line is a human bone cells line derived from a 15-year-old female Caucasian osteosarcoma patient. Unlike other untransformed osteoblast-like cell lines, U2OS cell line show little variability in integrin expression, attachment and differentiation that would otherwise complicates the evaluation of results (Phinney et al., 1999, ter Brugge et al., 2002). Though most of their osteogenic features are lost, and they retain a low basal alkaline phosphatase activity, and no mineralization of the matrix, they still express characteristic osteoblast-like matrix, with very little variability (de Ruijter et al., 2001, Kostenuik et al., 1996). This osteosarcoma cell line is also suitable for studying some cell functions, including integrin expression or adhesion/attachment to surfaces and spreading characteristics (Clover and Gowen, 1994), binding to surfaces by means of focal contacts and adhesions (Wu et al., 2011).

U2OS cell lines therefore allowed the quantitative study of cell attachment/adhesion and differentiation/spreading out on the different types titanium surfaces investigated in this study. The quantitative analysis was carried out using the image analysis software Pixcavator 5.1. Cell sizes are reported in pixels.

9.2 Method

Investigations of the effect of the surface modifications on osteogenic cell adhesion and toxicity to the modified surfaces were carried out, using human osteosarcoma cell line U2OS, obtained from the Toxicology Unit, MRC at University of Leicester (courtesy of Prof Andrew Tobin), maintained in McCoy's 5A (Modified) Medium, GlutaMAX™ (GIBCO® Life Technologies, GIBCO # 36600-021) growth medium, supplemented with 10% FBS plus 5% Penicillin/Streptomycin (GIBCO # 15140-122), and cultured in an incubator maintained at 37°C in the presence 5% CO_2 and 95% air (SANYO CO_2 Incubator Model MCO-18AIC(UV)). The adherent cells were fixed on the disc surface with 4% paraformaldehyde (PFA), maintained at 4^{o}C for 2 hours. The fixed cells were then dehydrated with 40%, 50%, 60%, 70%, 80%, 90% and 100% ethanol, in series. The fixed, dried cells were then examined and photographed using a scanning electron microscope (Carl Zeiss 'EVO HD' 15). The procedures involved are detailed in Section 3.7 of Chapter 3.

9.3 Results

9.3.1. Confluent Time Cells on Modified Ti Surfaces

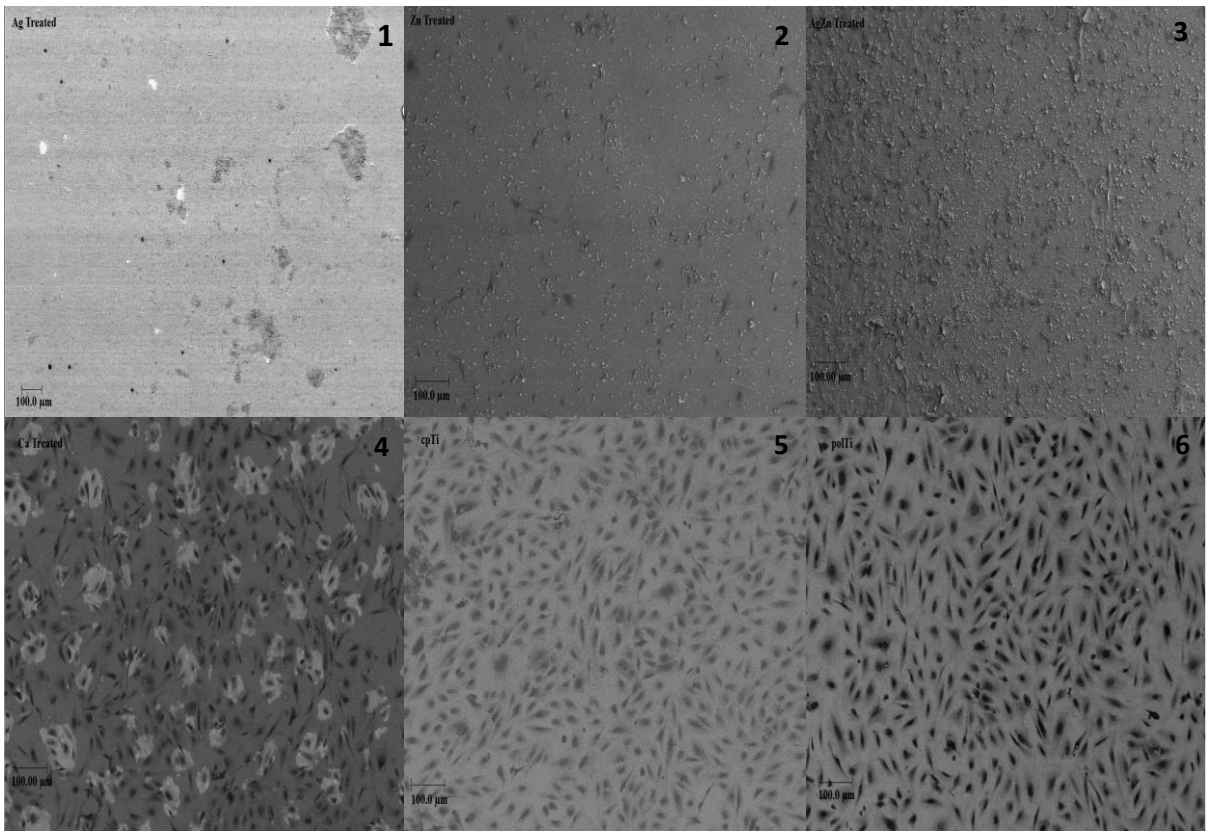

Figure 9.1. SEM micrographs of confluent time cell attachment to different Ti surfaces: 1-silver (Ag) treated surface, 2-zinc (Zn) treated surface, 3-silver-zinc (AgZn) treated surface, 4-calcium (Ca) treated surface, 5-commercially pure titanium (cpTi) surface and 5-polished titanium (polTi) surface.

U2OS cells were allowed to become attached and grow on the surface of the experimental discs in a 24-well plate under optimal conditions, until cell on the control surface (cpTi) have reached confluence (Figure 9.1). This was found to be within 24 hours.

A quantification of the confluent cells (Figure 9.2) suggested the polished (polTi) and commercially pure unpolished (cpTi) surfaces, with 1108±13 cells/ml and 1086±17cells/ml counts respectively had the highest cell counts, with very little variation in cell populations on their surfaces. The calcium treated surface however had a lower confluence population of 620 cells. The silver treated maintained surface supported very little cell adhesion and growth over the 24 hours' confluent period. 10±3 cells/ml were recorded for the surface. The zinc treated

surface recorded 105±65 cells/ml, whereas the silver-zinc surface had 58±2cells/ml on its surface at the same time it took for the U2OS cell on the control surface to reach confluence. Though all the surfaces supported U2OS cells to different extent, it appears the silver either did not support cell attachment or was toxic to the cells that were attached to its surface during the 24-hour period. The variation in the mean counts of cells on the various surfaces were found to be significant ($P < 0.05$).

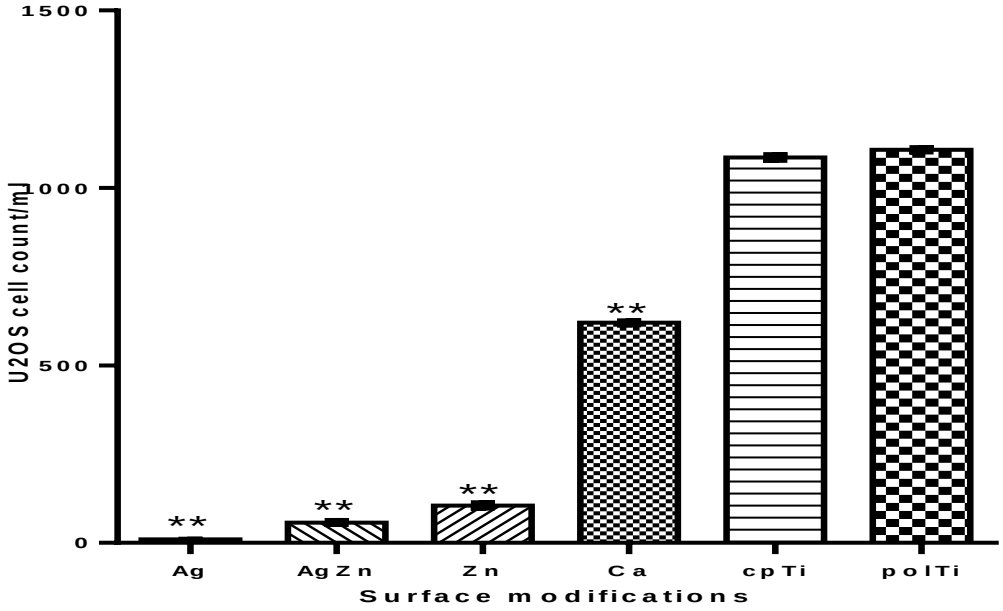

*Figure 9.2. Confluent time count of cells attached to the surfaces after 24 hours. Differences among the mean cell counts were statistically significant (P < 0.05), as determined by a one-way ANOVA with Bonferonni's post-hoc test. Error bars represents the mean ± S.E.M. for n=3 samples. ** represent significant variation (P < 0.0001) from the control poTi confluent cell count.*

To preliminarily ascertain the effect of silver and calcium on the U2OS cell attachment and growth, U2OS cells were incubated on a separate disc surface incorporated with calcium and silver (CaAg), and compared with the cpTi, the polTi (polTi), calcium treated Ti (Ca), the polished and calcium/silver treated Ti (CaAg) and the polished silver treated Ti (Ag). Figure 9.3 indicates that, the calcium treated surface (Ca) supported over 15200±17cells/ml, the most number of cells, while the silver surface (Ag) supported the least (975±8cells/ml) number of cells.

9.3.2. Effect of Calcium and Silver on Cell Adhesion and Proliferation

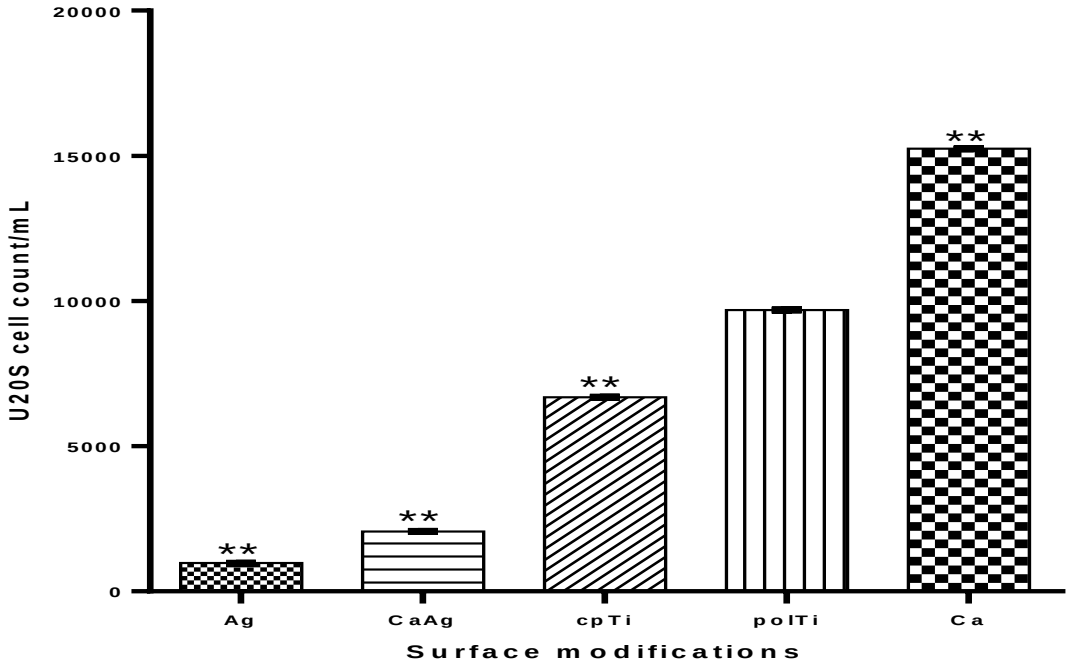

*Figure 9.3 Cell adhesion to modified Ti surfaces over 12 hours to investigate the effect of silver on U2OS cells' interaction. Differences among mean cell adhesion was statistically significant (P < 0.01), as determined by a one-way ANOVA with Bonferonni's post-hoc test. Similarly, comparison of the control polTi with the other surfaces indicate the differences in cell adhesion are significant (P < 0.0001), represented by **. Error bars represents the mean ± S.E.M. for n=3 samples.*

The polished surface performed better with over 9600±19 cells/ml, than the control commercially pure unpolished surface, which allowed the adhesion of and growth of over 6683±9 cells/ml. The CaAg surface accommodated 2065±8 cells/ml. More importantly however, U2OS do become attached to the silver treated surfaces in the 12-hour incubation period. It also appears calcium reduces the toxicity of silver on the Ti surface, as indicated by the higher counts on the CaAg surface, compared to the silver surface. This could however be as a result of the reduction in the amounts of silver on the CaAg surface. Similarly, the reduction in adherent cells compared to the Ca could be attributed to the reduced amount of Ca on the CaAg surface. However, on comparing with the cpTi and polTi surface, it can be inferred the presence of silver has deleterious effect on U2OS cell, but this is partially offset by calcium on the Ti surface, with the silver.

9.3.3. Adhesion and Proliferation of U2OS Cells to cpTi and Modified Titanium Surfaces

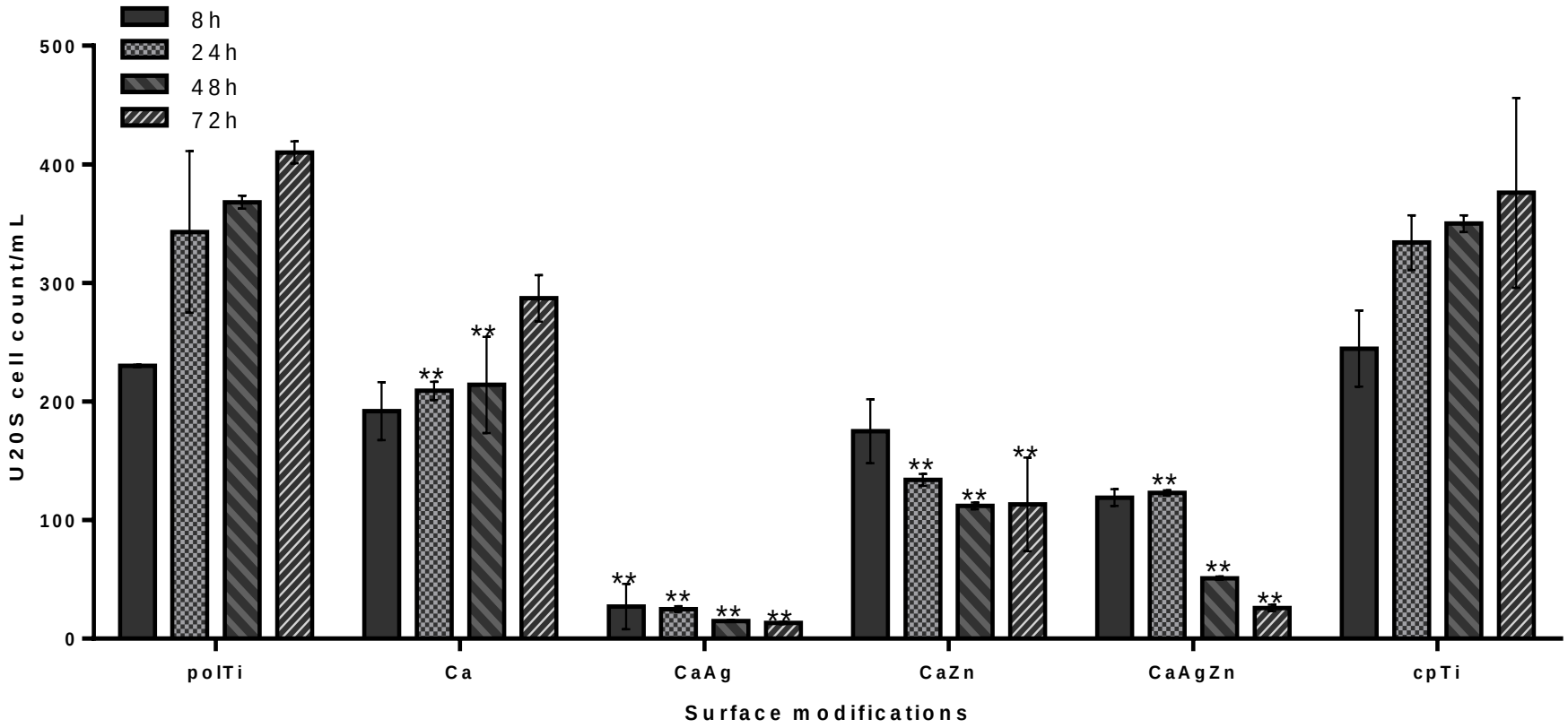

*Figure 9.4 showing cell adhesion (at 8 hours) and cell proliferation (up to 72 hours) counts on the cpTi, polTi and other Ti surfaces. The polTi and cpTi counts at the various time intervals are similar. Also, little or no statistically significant variation is observed in in the cell adhesion count (after 8 hours) for surface modifications except for the Ag+ treated surface. Comparisons of the mean cell counts for the various surfaces at the indicated time intervals, using the polTi as the control, suggests that, the differences in cell proliferation are generally significant at $p \leq 0.05$. * and ** represent $p \leq 0.01$ and $p \leq 0.001$ respectively. Error bars represents the mean ± S.E.M. for n=5 samples.*

9.3.4. Adhesion and Proliferation of U2OS Cells to cpTi and Modified Titanium Surfaces

After 8 hours of incubation, the data suggests that, the unpolished and polished surfaces encouraged the most cell adhesion, closely followed by the calcium treated surface. This agrees with the earlier observation in the Scharfe system and confluent counts. However, whereas the silver treated surface in the Scharfe count did not support any quantifiable number of cells, it appears the silver-calcium composite surface encourage some cell adhesion to the surface. Similarly, and more importantly, calcium in zinc and silver-zinc surfaces encouraged appreciable number of osteogenic cell adhesion to the modified surfaces. The order in numbers of adherent cells thus appears as cpTi>polTi>Ca >CaZn>CaAgZn>CaAg.

After initial adhesion to the material surface, cells under optimal condition, were expected to proliferate i.e. increase in cytoplasmic size and organelle numbers and divide, leading to increase in cell population. After 24 hours, there was there were distinct variations in the population of cells on the surfaces. Whereas the polished, unpolished and CaAgZn surfaces recorded approx. 49%, 37% and 4% increases respectively, the Ca, CaAg and CaZn surfaces recorded approx. 12%, 7% and 23% reduction in surface cell population from the adherent population.

After 48 hours, the proliferation continued for the Ca, polished and the unpolished surfaces. However large reduction in cell densities was observed for the Ag and Zn composite surfaces with Ca; approx. CaAgZn 57%, CaAg 44% and CaZn 36%, from the numbers at the time of adhesion to the surfaces. Growth in cell size however continued for all the surfaces with the exception of the calcium-silver surface which appears to have reduced in size by 88% from the 8-hour cell size.

By the end of 72 hours of cell adhesion and growth, the number of cells on the calcium surface has increase by approx. 50%. Similarly, the unpolished surface showed approx. 54% increase in cell numbers. The highest increase was in the polished surface, which was showing increase of 78%, from the 230 cells that adhered to the surface at 8 hours. For the silver component surfaces, however, the decline continued, albeit not to the point of total annihilation. After 72 hours only 13cells representing approx. 52% reduction, of the starting 27 cells were detectable on the CaAg surface. The figure was approx. -35% and approx. -78% for the CaZn and CaAgZn surfaces respectively. The data indicates that, post-adhesion to the surfaces, the cells on the polTi, cpTi and Ca treated surface increased in number, and that the increase from the adhesion count were significant. An analysis of the cell counts on the various surfaces with the control polTi surface suggests that, the cpTi had similar propensity for encouraging U2OS cells adhesion and proliferation on surface as the polTi. The CaAg, CaZn and CaAgZn surfaces however indicated significant reduction in the number of cells on the respective surfaces, compares to the control polTi, at the corresponding time intervals (Figure 9.4), even though an analysis of the counts at the various time internals for the individual surfaces suggests that the cell numbers are similar, that is, the reductions are not significant. This would suggest that, over 72 hours the CaAg, CaZn and CaAgZn surfaces retained similar number of surface that adhered to their surfaces after 8 hours of exposure to the osteogenic cells.

Analysis of the morphological sizes of the cells corresponding to the different surfaces, indicated a considerable variation in the ease of cellular attachment as a function of time, and subsequent growth as a function of cell size (Figure 9.5). As has been previously demonstrated by others (Nayab et al., 2005, Anitua et al., 2015a, Baxter et al., 2002, ter Brugge et al., 2002), cells attached to the Ca treated surface with a mean cell size of 2245±124 pixels, were the largest. This was followed by 1863±115 pixels for the polished surface. The calcium-zinc composite surface had cell with average size of 1394±127 pixels. An average size of 1304±132

pixels was recorded for the unpolished. However, a similar relatively smaller size of 1169±71 pixels and 1153±191 pixels was recorded for the calcium-silver-zinc and the calcium-silver surfaces respectively. Suggesting that the presence of Ag^+ ions on the Ti surface had an initial growth restrictive effect on the osteoblast-like cells.

The 24 hours cell morphology (Figure 9.5 and Figure 4.38a), also shows an appreciable size increases in the cells on all the surface modifications. A 64% increase to 2142±123 on the cpTi surface was the highest morphological size change recorded. A size increase of 60% to 1868±120 was recorded for CaAgZn, 53% reduction to 536±24 for CaAg, 21% increase to 2256±168 for the polTi, 18% increase to 1650±150 for CaZn and 6% increase to 2383±176 for the Ca treated surfaces. However, irrespective of the relatively small increase in the calcium treated surface, the mean size values show the calcium treated surface to have the largest cell size, after 24 hours, as observed after 8 hours. The cell size measurements also show that, the unpolished and polished surfaces supported cell growth better than surfaces with silver and/or zinc as components of the composite with calcium in their surface modification. The polTi surface was only marginally better at supporting cell growth on its surface than the commercially pure unpolished surface after 24 hours. More interestingly however, the CaAgZn demonstrated a better biocompatibility than the other multi-ion surfaces, with approx. 4% increase in cell numbers and 60% increase in cell size after 24 hours. The trend with the multi-ion surfaces has at this point changed from CaZn>CaAgZn >CaAg at 8 hours to CaAgZn>CaZn>CaAg after 24 hours.

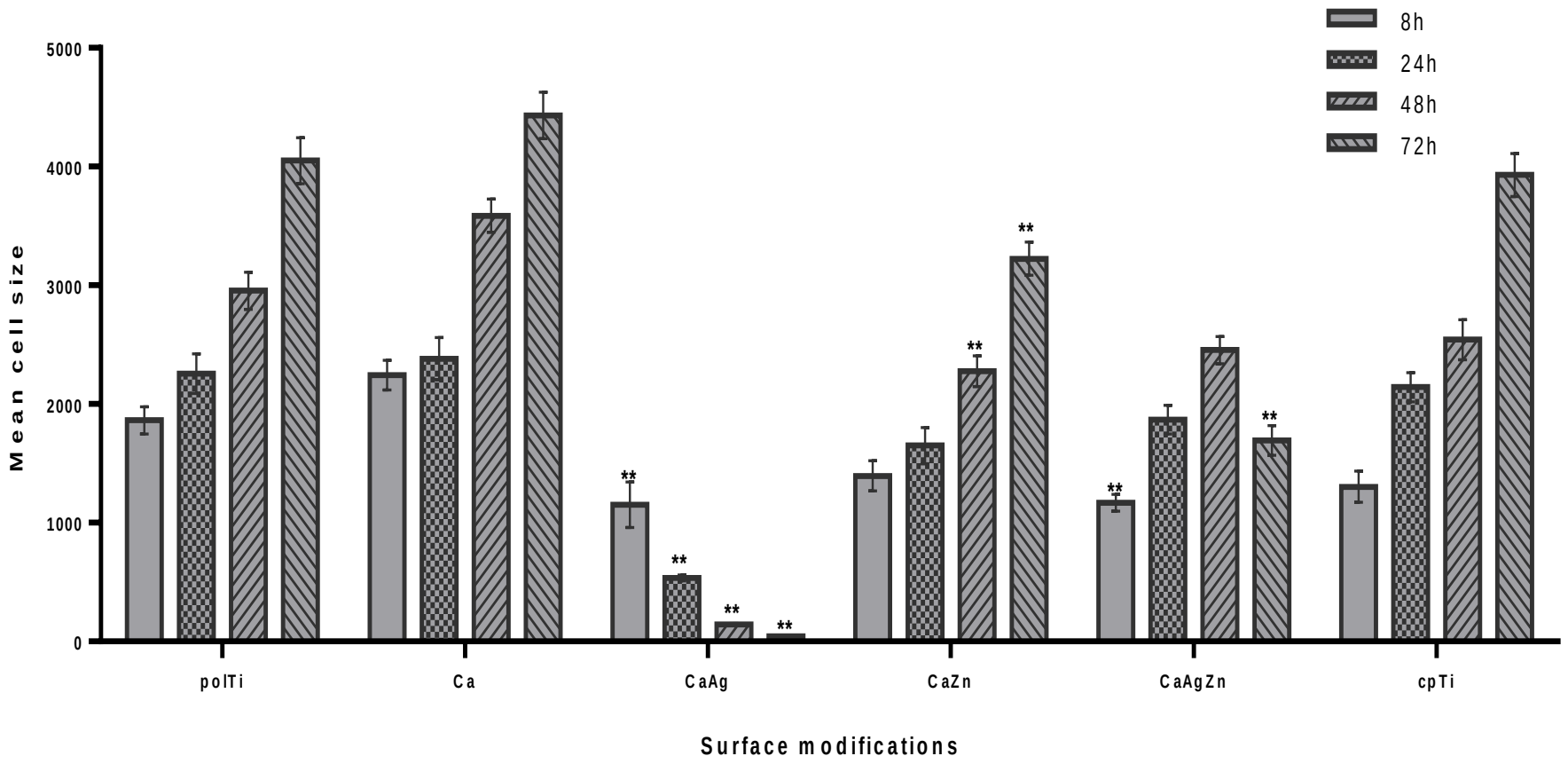

*Figure 9.5, showing the mean adherent cells' sizes/spread as a function of growth on the different titanium surface modifications over 72 hours. Similar cell sizes were recorded for the control polished surface, the unpolished surfaces, as well as the Ca treated surface, with the Ca treatment making the surface marginally superior at supporting cell growth. Ag+ ions on the surfaces however appear to adversely affect cell growth as early as within the first 24 hours. Comparative analysis of the cell sizes indicates that variations from the control polTi at the various time intervals were significant ($p \leq 0.01$). Error bars represents the mean ± S.E.M for n=5 samples. * and ** represent significant (at $p \leq 0.01$ and $p \leq 0.001$ respectively) variation in cell sizes from the adherent cells on the control polTi surface at the various time intervals.*

Calcium treatment enhances cell size growth as demonstrated by the surfaces with calcium. The calcium effect appears to more than compensating for the adverse effect of silver on the bone cells. The calcium treated surface remained the surface with the largest or healthiest cells. The cells on the calcium-zinc and calcium-silver-zinc surfaces were identical in size, 2279±129 pixels and 2455±115 pixels respectively after 48 hours. The polTi surface cell size at 2955±155 was now showing marked superiority to the cpTi surface cell size of 2542±170. The resulting trend after 48 hours suggests Ca>polished>unpolished>CaAgZn>CaZn>CaAg. An indication that Ca^{2+} ions on the Ti surface has a beneficial effect with regards to cell morphological increase or growth begins to emerge. Similarly, an Ag+ ion-related adverse effect on cell growth is established, after 48 hours. The presence of calcium appears to make the surface superior to the untreated and polished surfaces. Polishing to a mirror finish also made the Ti surface more favourable for the osteoblast cell growth than the commercially pure Ti. Also at 48 hours, the difference between the calcium, zinc and silver composite surfaces and the commercially pure surface was marginal, whereas a drastic adverse effect is observed with the silver-treated surfaces. This suggests the presence of calcium significantly offset the toxic effect of silver on the osteoblast-like cells.

After 72 hours, it is apparent that Ca^{2+} ions incorporate onto the Ti surface favours osteoblast cell morphological growth. Ag^{+} however appears to adversely affect cell growth, but not complete cell loss after 72 hours. This is indicated by the continued increase in cell size on the surfaces with calcium modification, while surfaces with silver modifications recorded marked reductions in cell size. The Ca treated surface had the largest cells, at 4430±195pixels. The cell on the polTi and cpTi surfaces had also increased to 4051±193 pixels and 3930±180 pixels respectively. The CaZn treated surface had increased from 1394±127 pixels at 8 hours to 3223±140 pixels at 72 hours. The CaAg surface however demonstrated a 96% reduction in morphological cell size from the 8-hour cell size. This suggest no viable cells on the CaAg

surface after 72 hours. Over the course of 72 hours, the overall trend for both morphological size or biocompatibility and proliferation of the osteoblast-like cells on the surfaces suggests Ca>polished>unpolished>CaZn>CaAgZn>CaAg.

The calcium, polished, unpolished and calcium-zinc composite surfaces showed a continuous growth over 72 hours, with the calcium treated surface having the largest cell size throughout. The silver multi-ion surfaces showed a cell size growth for 24 hours for the calcium-silver surface, and up till 48 hours for the calcium-silver-zinc surface, after which the cells stopped spreading and began to reduce in size. It thus appears the presence of calcium on the surface promoted cell morphological increase or growth, and the silver inhibited cell growth.

Statistical analysis of the mean cell sizes at the end of 72 hours indicated that, the variations in was significant for each surface compared to the poTi surface, except for the Ca and cpTi surface, at 95% confidence interval. comparing the mean adherent cells' sizes on the different titanium surface modifications for 8, 24, 48 and 72 hours. Ag^{+} and Zn^{2+} ions on the surfaces adversely affected cell growth, however Ca^{2+} promoted cell adhesion (at 8 hours) and growth (between 24-72 hours). After 48 hours, significant increases were observed for all the surface, except for the Ag treated surface, which showed significant reduction throughout, from the initial adhesive cells. Critically, the CaAgZn treated surface retained U2OS cells of sizes not significantly different from the adhesion cell sizes, on its surface at 72 hours.

9.3.5. Morphological Changes in U2OS Cells as a Measure of Biocompatibility on cpTi and Modified Titanium Surfaces

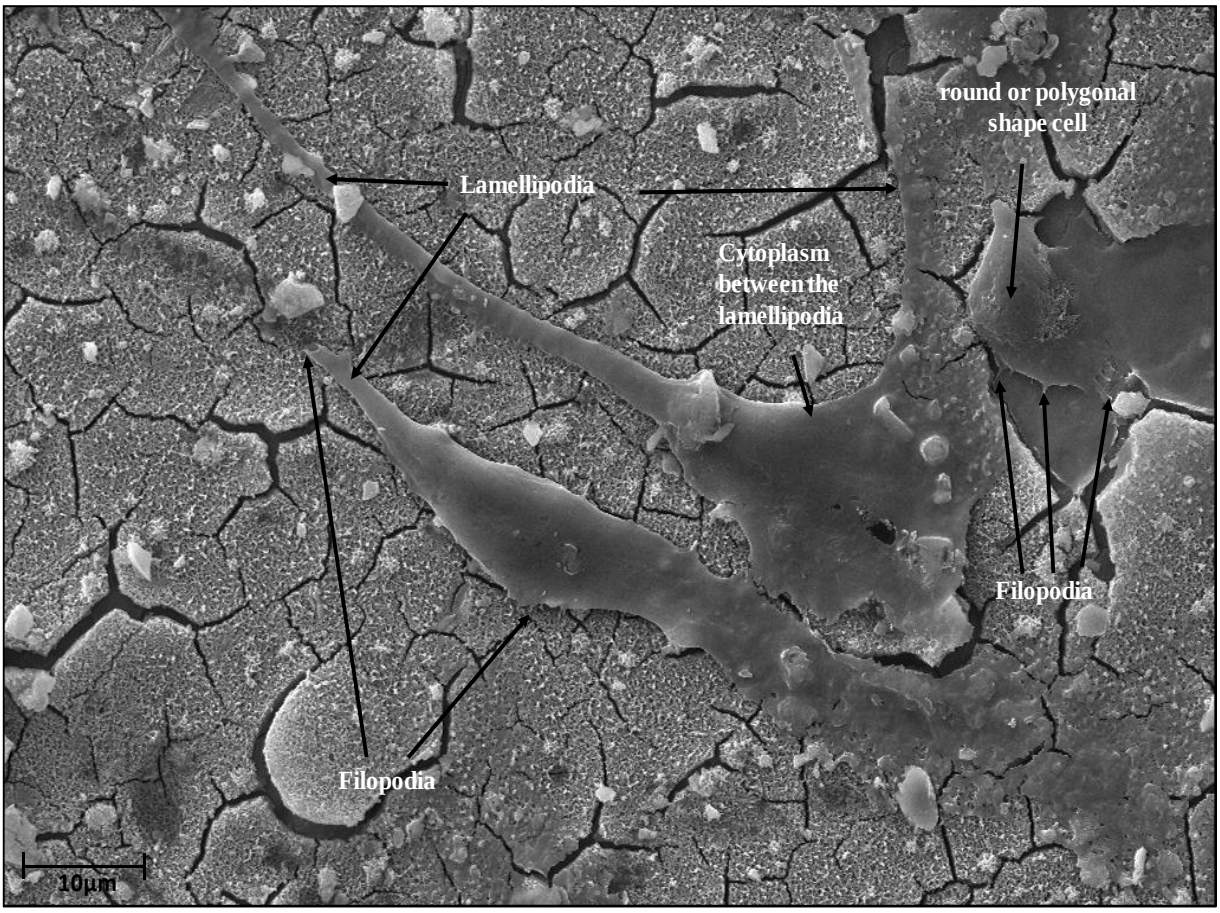

Figure 9.6 SEM micrograph of U2OS cells attached to and growing on calcium treated titanium surface. Both rounded and elongated or spreading0out cells with filopodia and lamellipodia extension are visible.

Figure 9.6 is ×3000 magnification SEM micrograph of osteosarcoma U2OS cells attached to and growing on the surface of a calcium-treated Ti surface. The image shows the four progressive events of cell attachment and spreading on a cyto-compatible surface: 1. initial contact via filopodia; 2. extension of lamellipodia; 3, spreading of the cytoplasm between the lamellipodia; and 4, full spreading to a round or polygonal shape cell.

Figure 9.7 shows cells on the cpTi, polTi and the polCa surfaces (a) after 8 hours (cell adhesion time), and (b) after 72 hours. On the commercially pure unpolished surface (cpTi), the U2OS cells after 8 hours appeared circular and embedded in the tamper annealed artefact topography of the material surface. They are not markedly larger, but of distinctly different irregular shapes

at 72 hours. Cells on the polished surface are mostly circular with distinct translucent regions around the cells. Cells are larger and elongated after 72 hours, with distinguishable nuclear materials as the cell appear thinly spread out on the nano-smooth polished surface, overlapping with adjacent cells. Cells on the calcium treated surface show a mixture of circular and elongated cells with distinct filopodia extensions at 8 hours. The cells appear larger and mostly elongated after 72 hours, without overlapping and clear junctions between adjacent individual growing cells. It thus appears calcium enhances the morphological spread and proliferation of U2OS cells on the modified surfaces.

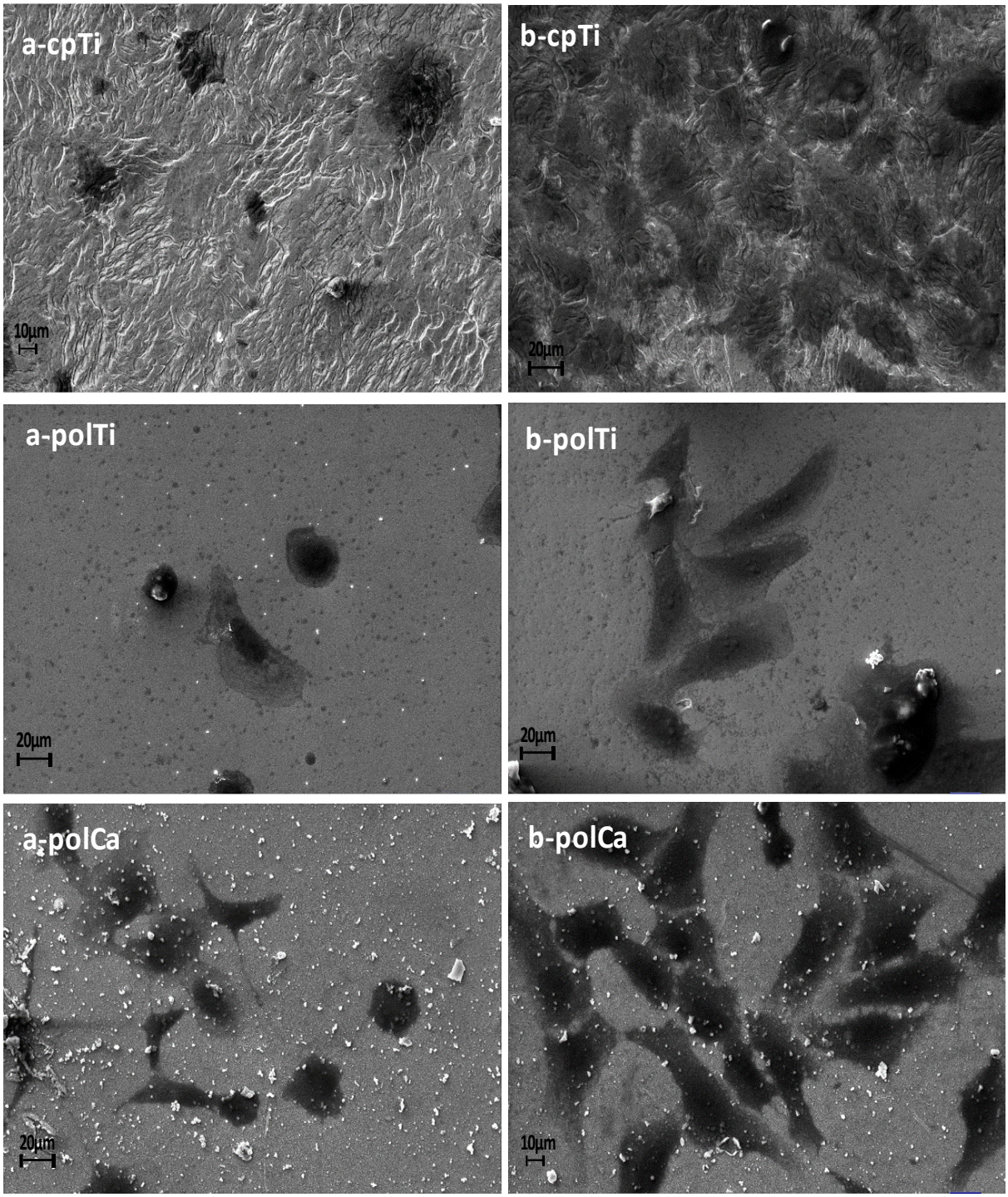

Figure 9.7. SEM micrographs showing the morphological state of U2OS osteosarcoma cells on the cpTi, polTi and the polCa surfaces at 8 hours (a) and after 72 hours (b).

Figure 9.8 also shows cell on the rest of the surfaces after (a) 8 hours and (b) 72 hours. Cells on the CaZn treated surface are all circular and of varied size that are altogether smaller than the calcium surface cells at 8 hours. After 72 hours, the cells appear larger and still mostly circular, with some showing filopodia extensions, characteristic of the calcium treated surface

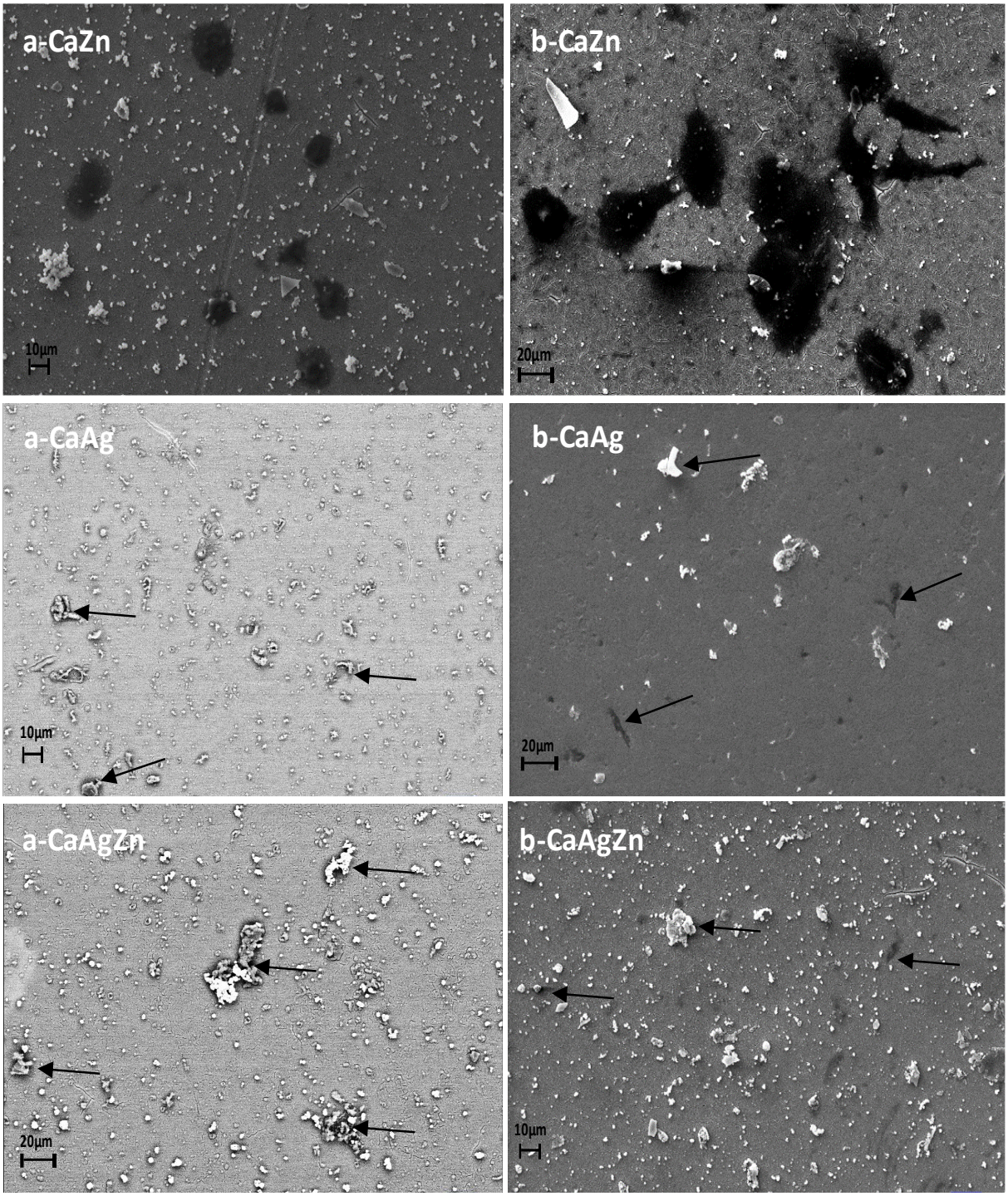

Figure 9.8 SEM micrographs showing the morphological state of U2OS osteosarcoma cells on the CaZn, CaAg and the CaAgZn surfaces at 8 hours (a) and after 72 hours (b).

cells. Cells on the CaAg composite surface appear barely visible, attached to calcium-rich spots of the surface as circular isolated patches beneath what appears as crystals on the implant surface at 8 hours. The attached cells appear much diminished in size and still in isolated

individual spots on the surface after 72 hours. Cells on the CaAgZn composite surface, like those on the CaAg surface, appear in isolated spots on the surface, beneath crystals of calcium, as circular dark spots at 8 hours. They are much smaller in size and spread than those on the previous surface, with no distinct features. They are however larger than those on the CaAg surface. After 72 hours, the cells appear much smaller and still in isolated spots on the modified surface, and just as in the Ag treated surface, impossible to identify any feature that suggest cell viability at time of fixing. It thus appears silver adversely affects the morphological growth and proliferation of U2OS cells on the modified surfaces.

9.4. Discussion

The goal of the use of external materials in biomaterial application, particularly in orthopaedics and dentistry, is the seamless, mechanically durable and functionally reliable integration of the exogenous material with the surrounding biologic tissue. Hence the usefulness and efficiency of any new device is assessed, amongst other parameters, on how it predictably integrates with the expected surrounding tissues, adapts to the body's defence mechanisms and resists colonization by biofilm forming bacteria, *in vitro* or *in vivo*.

It has been amply demonstrated that, all the events leading to osseointegration are intimately influenced by the characteristics of the device material surface. Modification of implant device material surface has therefore become paramount in the search for more efficient and more naturally adaptable implant materials and devices.

To investigate the surface modification developed here, i.e. the physical and chemical modification of implantable grade titanium, an *in vitro* model using U2OS osteogenic osteosarcoma cells was employed. This cell line is ideal for several reasons, including their ability to bind to surfaces by means of focal contacts, and their adhesion and spreading characteristics. They also express characteristic osteoblast-like matrix with little variability.

They therefore permitted the quantitative study of bone cell adhesion to the different modified surfaces, a pre-requisite to osseointegration.

A preliminary assay of the adhesion of the osteogenic cells to a selection of the modified surfaces was carried out. This was to ascertain the biocompatibility of the key modifications to the cpTi. The modifications examined were the mirror-finished polished surface, the calcium treated surface, the composite calcium-silver, calcium-zinc and calcium-silver-zinc treated surfaces, against the commercially pure Ti surface. In the biocompatibility assessment, changes in cell morphology or morphometric assays are used to provide qualitative indicators of cell health, growth and viability. This has the advantage of not requiring any label, and cells can be re-imaged and analysed over long periods (Rampersad, 2012). All the surface modifications supported the adhesion of U2Os cells, albeit to varying extent, as suggested by cells counts for each surface after 8 hours. The polished surface provided the most ideal surface for cell adhesion after 8 hours. These suggest that, polishing the surface to a mirror-finish may improve its interaction with bone cells. As has been demonstrated, the polishing conferred nano-scale surface topography to the titanium, which has been severally demonstrated to favour cell adhesion over the micro-scale surface of the commercially pure unpolished surface. Calcium, a major component of hydroxyapatite, and known to encourage biomineralization by attracting calcium-binding and other proteins (Zhou and Lee, 2011, Anitua et al., 2015a), on the polished titanium surface, improved U2OS cell adhesion and growth, compared to cpTi. *In vitro* cytocompatibility evaluations have demonstrate that the adhesion, proliferation and differentiation of rat osteogenic bMSC on Zn-incorporated coatings are significantly enhanced on the Zn-treated surface compared to the Zn-free and commercially pure Ti surface. Also, bMSC express higher level of alkaline phosphatase activity and differentiation into osteoblast cells on Zn-incorporated TiO_2 (Hu et al., 2012). Observations from this study appear to agree with these suggestions. It appears however, that the presence of Ag^+ ions on the modified

surface, previously demonstrated to confer anti-microbial propertied to the modified titanium surface, has a markedly deleterious effect on cell adhesion, even in combination with calcium. The presence of calcium however appeared to reduce the toxic effect of silver on the cells. This may be a concentration or biochemistry dependent effect, and appears to account for the adhesion and survival of some U2OS cells past 24 hours (Figure 9.2), when very few cells had not survived past 24 hours on the silver-only treated surfaces.

A visual and quantitative analysis of the confluent cells on the unpolished, polished and calcium treated surface suggests that, at confluence, there is no significant quantitative difference between the polished and unpolished surfaces. The calcium treated surface however had a comparatively lower confluent number of cells, supporting the argument that differences may be with the morphology and size of the cells adhering to the surfaces (Figure 9.1).

A cell adhesion and proliferation investigation was then carried out for the three previous antimicrobial surfaces, further incorporated with calcium to enhance their osseous interaction, i.e. calcium-silver (CaAg), calcium-zinc (CaZn) and calcium-silver-zinc (CaAgZn) composite surfaces, together with the calcium treated and polished surfaces, with the unpolished surface as the control. On enumeration of cells adherent to the surfaces after 8 hours, the data suggested similar results for the polished and unpolished surfaces. Similar numbers were also observed for the calcium and calcium-zinc surfaces with. It however appeared the silver-calcium surface encourage some cell adhesion to the surface. Similarly, and more significantly, the calcium in the zinc and the silver-zinc composites encouraged appreciable number of osteogenic cell adhesion to the modified surfaces. The order in numbers of adherent cells thus appears as unpolished>polished>calcium >calcium-zinc>calcium-silver-zinc>calcium-silver. These 8-hour adherent cells formed the baseline for the proliferation analysis.

After 24 hours, marked variations in the population of cells on the surfaces were observed. Whereas the polished, unpolished and Ca surfaces recorded approx. 49%, 37% and 9% increases respectively, the CaAg and CaZn surfaces recorded approx. 7%, and 23% reduction in surface cell population from the 8-hour adherent population. Interestingly, the CaAgZn recorded approx. 4% increase. The polished and unpolished surfaces though similar with adhesion number, were showing different proliferation rates, the polished surface being approx. 12% higher. The uniform nano-topographic surface of the polished surface thus appears to be more conducive for U2OS cell adhesion and proliferation than the micro-rough surfaces of the unpolished, and oxides incorporated modified surfaces. The relatively slow increment rate of the calcium treated surface's cells after 24 hours suggests that, in the presence of calcium, an osteogenic process beyond simple attachment to the surface occurs before cell division and proliferation. This may involve a preferential electrostatic attachment of the cells, and an attempt at mobilizing molecules and ions including amino acids, calcium and phosphates present in the growth medium, for bone biomineralization. As previously observed, the presence of silver appears to have a deleterious effect on U2OS cell adhesion and proliferation. This is suggested by the post 24-hours reduction in the cell numbers from the baseline numbers for all the surfaces that have silver as component of the surface modification (Zhou and Lee, 2011, Anitua et al., 2015a). Feng et al suggested that stress response become activated in cells exposed to Ag^{+}, leading to disruption in DNA function and detachment from cell wall (Feng et al., 2000a).

After 48 hours, the cell density on the calcium surface had increased by approx. 12%, and by 43% on the unpolished surface, and the polished surface by 60%. All the silver composite surfaces were by this time showing drastic reduction in cell numbers; CaAgZn 56%, CaAg 44% and CaZn 36% from the 8 hours' adhesion numbers (Figure 9.4). The cell size difference between the calcium, zinc and silver composite surfaces and the commercially pure surface

was marginal. However, a drastic adverse effect is observed with the silver-treated surfaces. This suggests the presence of calcium significantly offset the deleterious effect on silver on the osteoblast-like cells.

By the end of 72 hours of cell adhesion and growth, the number of cells on the calcium surface had shown an appreciable increase in population. This was however still well short of the confluent numbers after just 24 hours (Figure 9.2). There difference may be in the morphological spread of the cells on the Ti surfaces. The proliferation rate is at par with that of the unpolished surface, which stood at approx. 54%. This seem to support the earlier observation that the presence of calcium instigated other processes, such as bio-mobilization and mineralisation leading to cell attachment, before the initiation of proliferation. Differences in effect on the cells for these surfaces, if any, may as earlier suggested, lie in the cell morphology. At high SEM imaging magnification, the morphology of the cells remaining on the surfaces suggest that the cells selected for counting were viable at the time of fixing.

Over a period of 72 hours, cells on commercially pure unpolished surface, showed no distinct morphological shape, starting out as circular and embedded cells on the tamper annealed topography of the material surface. Some remained circular, others elongated, while others still showed filopodia extensions across the peaks and valleys of the surface. The cells however show clear contact boundaries, thus appearing to be closely packed together, yet distinctly separate from each other (Figure 9.7). This suggests the surface topography allows for individual cell anchorage to the commercially pure untreated surface.

The polished surface closely followed the calcium-only treated surface, in the morphological size of cells attached to its surface. The cells here appear circular with distinct translucent regions around the cells on attachment to the surface at 8 hours, and larger and elongated after 72 hours, with distinguishable nuclear materials, as the cell appear thinly spread out on the

nano-smooth polished surface, overlapping with adjacent cells. The nano topography thus appears to encourage cytoplasmic spread of the cells and clustering of the cells with thin cytoplasmic overlaps, and no distinct filopodia extensions seen in the commercially pure untreated surface (Figure 9.7). The polished surface thus provides little topography related sites for individual cell anchorage, but rather a more tightly packed and layered cell organisation on the modified surface. The calcium treated surface however, supported more proliferation and morphological growth than the other surfaces. The morphology of the cells on the calcium treated surfaces also suggested a more active filopodia extension. This is because in addition to increasing the surface roughness due to the calcium incorporation, calcium on the surface of the titanium disc facilitates the preferential electrostatic adhesion of the U2OS cells and mobilization of molecules needed for bio-mineralization. As major constituent of hydroxyapatite (Zhou and Lee, 2011), calcium encourages mineralization by attracting calcium-binding proteins, glycosaminoglycans and proteoglycans, to generate supersaturating conditions. The cells here therefore start as a mixture of circular dense cells, circular cells with overlapping translucent cytoplasmic boundaries, and elongated cells with distinct filopodia extensions. Over 72 hours, they appear as mostly elongated cells, with dense nuclear region that are closely packed with distinct cellular boundaries. The calcium surface modification thus appears to facilitate increased individual cell anchorage as observed in the commercially pure unmodified surface, as a result of the topographical advantage over the polished surface, as well as encourage healthier cell morphological increase and proliferation.

A mixture of effects is observed in the calcium-zinc treated surface. The cells though larger in size after 72 hours, were a mixture of circular, uniformly dense isolated and closely bound cells, some with filopodia extensions, and uniformly dense elongated cells (Figure 9.8). This is a reflection of the reduction in calcium content of the surface as a result of competition for surface occupation between zinc and calcium in the surface modification process. Cells of

drastically reduced size, appearing as distinct dark spots, are also observed on the calcium-zinc surface. This suggests zinc has some detrimental effect on the U2OS cells. This effect may however, over time, be overcome by the beneficial effects conferred by the presence of calcium as the surviving cells continue to increase and proliferate.

The calcium-silver and calcium-silver-zinc surfaces suggests the presence of silver has a deleterious effect on U2OS cell on the modified surfaces. After 8hours, it appeared cells adhered only to areas of the surface that had high aggregation of calcium ions/crystals, as dark spots beneath white crystals (Figure 9.8). These spots are also smaller in size on the CaAg surface, than on the CaAgZn surface, as the former has more Ag ions over the same surface area than the later. This appears to worsen the adverse effect silver has on cell adhesion to the surface. After 72 hours, the cells appear as smaller dark circular and elongated pits over the CaAg surface, and as dark circular and elongated regions on the CaAgZn surface, smaller than at 8 hours. It thus suggests that the silver has a concentration dependent adverse effect on the growth and proliferation of cells on the surface of the titanium discs. Considering the amount of silver and other ions leached from the disc surface into the surrounding media, in this case 1ml volume, resulting in a relatively high silver concentrated solution in contact with the cells, the adverse effect observed may not be as pronounced as suggested in a more dynamic *in vivo* environment.

The general trend thus suggests that, calcium treatment enhances cell adhesion, morphological growth and proliferation over the polished surface, which has marginal advantage over the unmodified surface. These appear to support other investigations that calcium enhances bone cell proliferation on calcium-treated surfaces (Nayab et al., 2005, Anitua et al., 2015a). Again as presented by other investigators (Greulich et al., 2012), the presence of zinc and silver have a concentration dependent adverse effect on cell growth and proliferation, compared to the unmodified commercially pure surface.

The number of cells on the silver composite surfaces continued to decline, albeit not to the point of total annihilation. After 72 hours only 13 cells, representing approx. 52% of the starting 27cells were detectable on the CaAg surface. Cell loss was comparatively more drastic for the other silver composite surface (CaAgZn), especially after 48 hours, from the comparatively higher cell adhesion and proliferation of the first 48 hours, facilitated by the calcium component of the composite. In addition to the well-established adhesion, differentiation and proliferation effect of calcium on bone cells, recent studies have indicated that, zinc stimulates osteoblast marker gene (type I collagen, alkaline phosphatase (ALP), and bone sialoprotein (BSP), osteocalcin (OCN) and Runx2) expression, vascular endothelial growth factor A (VEGF-A), and transforming growth factor-ß (TGF-beta) signalling pathway-related gene expression (Yusa et al., 2011, Yusa et al., 2016). Together on the Ti, the effect of the two may be synergistic or additive. Silver however, both as nano-particles and in its ionic, state has been shown to have cytotoxic and genotoxic effect on mammalian cells (including bone cells) via interaction with biological macromolecules and induction of oxidative stress, resulting in mitochondrial and DNA damage (Bartlomiejczyk et al., 2013, Mahmood et al., 2010, Alqahtani et al., 2016, Patlolla et al., 2015). The interaction of silver in this study supports these observations. Others studies however indicate that, the toxic effect of silver depends on the cell type involved in the interaction, and the silver nana-particle size (Carlson et al., 2008, Jiravova et al., 2016). On the contrary, others studies suggest that silver induces the proliferation and osteogenic differentiation of mesenchymal stem cells (MSCs) via induction/activation of TGF-β/BMP signalling in MSCs (Zhang et al., 2015, Xu et al., 2015). The consensus is therefore still not conclusive.

For the targeted novel CaAgZn treated Ti surface of this study, the cell size measurements, combined with the antimicrobial profiles of the surfaces (chapter 8), suggest that the CaAgZn surface promises the synergism of the favourable properties of all the ions incorporated onto

the Ti surface. This is supported by other recent studies that indicate Zn/Ag dual-ion co-implanted titanium shows good osseointegration, as well as good antibacterial properties through the formation of a Zn/Ag micro-galvanic couple (Cao et al., 2011, Jin et al., 2014, Jin et al., 2015).

9.5. Conclusion

Our findings suggest that the ions implanted onto the Ti surface produce a durable chemical and nano-topographical modification of the titanium oxide interface. This have implication on the Ti surface interaction with bone cells. The results suggest that calcium incorporated onto Ti surface by the method developed in this investigation modifies the adhesion and proliferation of osteogenic U2OS cells on the Ti surface both qualitatively and quantitatively.

The unpolished surface's micro-rough topography with higher peaks and deeper valleys providing numerous anchorage points, is the best suited for osteogenic cell adhesion. Followed closely by the polished surface, before the calcium treated surface. Over the course of a 72-hour attachment and proliferation period however, the polished surface of nano-scale topography was the most suitable, distantly followed jointly by the unpolished and calcium treated surfaces. Though to varying degree, it appears silver and zinc have toxic effect on cell adhesion and proliferation on surfaces, the effect of silver markedly more so.

Consequently, Ti implants surfaces modified with Ca^{2+} by the technique developed here represent an applicable, simple cost effective method to improve endosseous integration in titanium implantology.

The results also suggest the novel observation with regards to Zn^{2+} ions, together with Ag+ ion, that these ions have a concentration dependent toxic effect on bone (U2OS) cell attachment, differentiation, growth and proliferation on Ti surface.

A promising compromise between the beneficial effect of calcium ions and the toxic effect of zinc and silver is arrived at when the three ions are incorporated onto the Ti surface in approximately equal proportions. The resulting composite treated surface was found to support both cell proliferation in the first 24 hours, and exhibit a better biocompatibility profile over 72 hours. The CaAgZn composite treated surface thus combines the beneficial antimicrobial effect of silver-zinc, with the beneficial osseo-integrating effect of calcium.

Chapter 10 : General Discussion

Titanium has over the past several decades become the most useful mechanical support and weight bearing tissue replacement material in clinical applications. This is as a result of, amongst others, its excellent physical and chemical properties. These include an outstandingly high strength, low density (high specific strength), high corrosion resistance, complete inertness to body environment, enhanced biocompatibility (non-toxic and is not rejected by the body), low modulus and high capacity for osseointegration (to join with bone and other tissues) (Chua et al., 2008). Titanium thus meets the key requirements of resistance to oxidative stresses, adaptability and biocompatibility, and most of its applications are as a result of its excellent combination of high-strength and light-weight. Though 60% heavier than aluminium, it is 100% stronger, and as strong as steel, but 45% lighter. It is therefore ideal for applications where weight-bearing strength is required, light weight an advantage, and metal fatigue an issue (Asaoka et al., 1985).

In spite of it numerous beneficial attributes, titanium does not form an effective bond with bone tissue as does bioglass and bioglass-ceramics (Larsson et al., 1996). In response to this, various surface modification techniques have been developed (He et al., 2006, Rautray et al., 2010, Liu et al., 2004, Pohler, 2000), most of which involve some alterations to the material surface topography, in a bid to reduce the failure rates and increase the longevity of implants. It has also been demonstrated that a certain degree of surface roughening improves osseointegration and the strength of the bone-biomaterial interface (Khan et al., 2011). However, an increased rates of infection, incidence of stability issues related to surface alterations procedures such as coating, and their cost effectiveness vis-à-vis the related failure rate (Montali, 2006b, Wang et al., 2011), have necessitated the need to improve existing methods. It is in response to this; finding more cost-effective means of surface modifications that improves osseointegration, and confer antimicrobial properties to the novel surface, in a bid to improve the long-term titanium

implant stability, and reduce the implant surface bacteria colonization, thus reducing the incidence of secondary resection surgeries, and enhancing implant in situ longevity and performance, that this work was carried out. In this work, Ca, Zn and Ag are separately and co-incorporated onto titanium surfaces and the osteogenic activity and antibacterial ability are systematically investigated *in vitro*.

In the development of a cost-effective means of modifying implantable titanium surface to improve its osseointegration and confer antimicrobial properties to the novel surface, several techniques and procedures were carried out. Compared to the techniques currently in use, these processes and procedures were aimed at being readily replicable without specialist equipment and conditions of high temperature and pressure required by most of the techniques currently in use, and to overcome the common setbacks to the methods in present use, such the coating limitations associated with implant device conformations, and delamination.

The novel technique of surface modifications developed in this work consisted of an initial mechanical/physical topographic modification of the commercially pure titanium by abrasive grinding with silica carbide paper of reducing grit sizes, and polishing with colloidal silica suspension and OP-chem cloth on a rotating drum, to a mirror-finish. The polished surface was then pre-treated with 10M aqueous sodium hydroxide solution, for 24 hours, maintained at 80^{o}C in a shaking water bath. This lead to the formation of sodium titanate, an effective ion-exchanger on the titanium surface. Na^{+} was then replace with Ca^{2+}, Ag^{+}, and Zn^{2+} by treating with 1M aqueous solution of the osseointegration-enhancing calcium as calcium hydroxide or chloride, and antimicrobial activity-conferring silver and zinc as the nitrate or chloride, for 24 hours at 80^{o}C in an oven, in a thermochemical reaction. This wet chemical synthesis method differs significantly from the similar method in current use with regards to the temperatures at which the sodium titanate is formed. Other methods achieve this at temperature ranging from

170 °C to 800 °C (Ueda et al., 2009a, Liu et al., 2005a, Ravelingien et al., 2009, Razali et al., 2012, Aziz et al., 2013, Aniołek et al., 2015).

SEM analysis of surface modifications indicated that, the technique removed surface incorporated elements or impurities, comprising of Al, Co, Cr, Cu, Fe, Mg, Mn, Ni, Si, Sn, Ta, and V, from the commercially pure Ti surface, leading to a 40% improvement in Ti surface atomicity. This possibly significantly reduces adverse interaction with living tissues in close contact with the implant device. The mirror-finished surface topography was also within the nano-scale dimension regarded to best facilitate osteogenic cell attachment and proliferation, compared to the commercially pure surface.

It has been amply demonstrated that the surface wettability of implant devices, modulated by surface characteristics including surface topography and chemistry (Rupp et al., 2014, Elias et al., 2008, Ponsonnet et al., 2003, Janssen et al., 2006, Cho et al., 2012, Balaur et al., 2005, Vogler, 1999) greatly influence the biological event cascade at the host/implant interface. This include proteins and other macromolecules adhesion to surfaces during the conditioning process, hard and soft tissue interaction with the preconditioned surface, bacterial adhesion and biofilm formation, and speed of osseointegration (Maddikeri et al., 2008). A goniometric analysis of the polished surface indicated the techniques led to a significant approx. 5^{o} increase in water contact angle from the commercially pure surface. This translates to a substantial increase in the surface energy and hydrophobicity, which leads to the formation of stronger chemical and biological bond with the modified surface, than with the commercially pure, unmodified surface.

Though the process of adhesion of biological agents, including bacteria, to surfaces is yet to be fully elucidated, the consensus is that hydrophobicity (measure by water contact angle) and surface free energy, as well as the average surface roughness, are crucial positive factors in the

bacterial adhesion and biofilm formation process. The adhesion of biological molecules, including human pathogens, particularly *S. aureus* and *S. epidermidis*, have been demonstrated to correlate to increased hydrophobicity and roughness (Maddikeri et al., 2008, de Avila et al., 2015, Pjetursson et al., 2014, Simonis et al., 2010, Chen et al., 2014, Oliveira et al., 2015, Chug et al., 2013). The consensus at presents suggests that nano-scale topography is ideal for osteogenicity and resistance to bacterial adhesion (Mendonça et al., 2008, Arciola et al., 2012, Popat et al., 2007a, Juan et al., 2010, Díaz et al., 2011, Gittens et al., 2011, Wennerberg and Albrektsson, 2009, Webster and Ejiofor, 2004). A topographic analysis of the 3D AFM images of the modified surfaces suggests that, the mirror-finished surface is uniformly 'smooth' with no apparent peaks and valleys. In characterizing the topographic features of a device surface, Albrektsson and co suggested that, a surface with an arithmetic mean height <100 nm is classified as nano topographic. Surfaces >100 nm are micron-topographic (Wennerberg and Albrektsson, 2000). The arithmetic mean height of the surface (Sa) of 5.7 nm for polTi and 161.5 nm for cpTi, together with the maximum height of the surface (Sz), maximum height of valleys (Sv), and maximum height of peaks (Sp) values collaborates the visual observation that the cpTi is more texturized or rougher than the polTi. The profilometer surface roughness (Ra) value of 0.07±0.0 µm suggests that the polishing technique developed in this work yield a smoother surface than that other techniques reported in some recent literature that yielded Ra values ranging from 0.3 to 0.5 µm (He et al., 2008, Ozdemir et al., 2016), and 9.5 nm to 205 nm (Yan et al., 2017, Kulkarni et al., 2015, Ozdemir et al., 2016) for AFM determined surface roughness value (Sa). The results also indicated that, the mechanical modification of the cpTi surface also resulted in an improvement in the water wetting or surface energy properties of the Ti surface. Sessile drop contact angle measurement of the two surfaces indicated the mean contact angle improved from of 67.1±0.9^{o} to 53.5±2.7^{o}. This improvement in hydrophilicity is similar to the 84.4 ± 0.7^{o} to 45.6 ± 1.2^{o} reported in a similar recent study, in which this was

reported as critical factor on the effect of the polishing on ion incorporation onto the Ti surface (Ozdemir et al., 2016).

This suggests that, the surface modification developed here leads to surfaces with potential for greater bone response and less accommodating of bacteria adhesion due to fewer anchorage points, than the surface of the unmodified commercially pure Ti.

In developing the surface modification strategy, we also sought to incorporate Ca^{2+} onto the titanium surface to form calcium titanate $CaTiO_3$, which in the presence of body fluids encourages the precipitation of hydroxyapatite(HAp) $Ca_{10}(PO_4)_6(OH)_2$ (Anitua et al., 2015a), a precursor of bone tissue, as well as Ag^+ and Zn^{2+} which are known to have antimicrobial activity (Le Ouay and Stellacci, 2015). Hitherto, incubation of the Ti surface in SBF has been the main strategy for incorporating ions, particularly Ca^{2+}, on to the Ti surface. Other elements such as Cu, Ag and Zn have been deposited on Ti surfaces via highly specialised and expensive methods that mostly have line-of-vision limitation and delamination problems. The method developed in this study harnessed the passivating, ion-exchanging action of the sodium titanate sol-gel formed on Ti surface on treatment with sodium hydroxide. This allowed the introduction of various metallic ions in theory, and calcium, silver and zinc in particular, individually and in combinations, onto the Ti surface in a novel, consistent and cost-effective manner. The mechanism involved the hydrolysis of the sodium titanate sol-gel and the subsequent ionisation of the Na^+, which are exchanged for the available metallic ions in solution in a concentration and competition directed manner. Though it has not been previously established in literature, a quantitative analysis of SEM/EDS micrographs of the surfaces showed that, a mirror-finished modification of the surface prior to hydrothermal chemical treatment was more efficient than directly treating the commercially pure Ti surface, by 2-3.5-fold increase in surface atomicity of the incorporated elements. For both the mirror-finished and cpTi surfaces, the absence of peaks for nitrogen and chlorine in the micrograph from

$AgNO^3$ and $CaCl_2/ZnCl_2$ used in the surface treatment suggested that Ag^+, Ca^{2+} and Zn^{2+} were chemically implanted or incorporated, and not simply deposited, onto the Ti surface.

With Sa values of 157 nm for the calcium treated surface, 113.3 nm for the zinc treated surface and 83.3 nm for the silver treated surface, within Albrektsson micro and nano-topographic margins (Albrektsson and Wennerberg, 2004a), the indications are that the developed hydrothermal chemical modification resulted in surfaces sufficiently smooth to resist bacterial adhesion, as has been suggested (Anselme et al., 2011), and moderately rough enough to encourage favourable bone cell response (Andersson et al., 2003), in addition to the potential osteogenic and antimicrobial properties conferred by the implanted chemical agents (Juan et al., 2010, Jones et al., 2008, Reddy et al., 2007, Salem et al., 2015, Sirelkhatim et al., 2015, Xu et al., 2010).

A study of the 28-days release profile of ions incorporated on the modified surfaces shows that, measurable amounts of Ag^+ were detected in the surrounding deionized water within a few hours of the immersion. After 24 hours, the cumulative release rate stood at 48 µg/L/h. By the end of the first week, the rate had dropped by about a third, to 15 µg/L/h, after which the release of Ag^+ plateaued and remained approximately constant at 3 µg/L/h. The release mechanism suggests an early burst of Ag release, followed by a steady release, the rate and duration of which is dependent on the sample surface area, the amounts of Ag incorporated onto the sample surface, and the volume of surrounding media. This compared similarly to release mechanisms demonstrated in other studies (Mei et al., 2014, Kang et al., 2012). The cumulative amounts of Ag ions released however differed from results of other studies (Cao et al., 2011, Mei et al., 2014, Kang et al., 2012). This could arise from a myriad of factors including the sample surface area differences and the methods of determination; FAAS was used in this work, whereas most other studies employed ICP-MS.

The ions release trend observed with Ag is similarly observed in the release of Zn^{2+} from the surface of the polished Zn^{2+} treated titanium disc. An initial similarly high amount of Zn^{2+} was detected in the deionized water within a few hours of immersion, corresponding to a burst release profile observed with the Ag treated surface. After 24 hours, the rate was 5.4 µg/L/h. By the end of the first week, the rate had halved to 2.71 µg/L/h, after which the release of Zn plateaued and remained approximately steady at 0.33 µg/L/h. The comparatively low amounts of Zn ions released is in conformity with other study, where this slow and constant Zn ion release has been correlated to its simultaneous antibacterial effect and up-regulation of osteogenic gene expression (Hu et al., 2012, Yang et al., 2012, Hu et al., 2011, Zhang et al., 2016). The general release for all the surface incorporated ions indicates an initial burst release, followed by a sustained slow release that appears to continue past the 28-days experimental period. This collaborates others works that indicate that in aqueous solutions, Ti surfaces treated with calcium release 2/3 of the total measured Ca^{2+} within the first minute, and the rest over the following 85 days (Ozdemir et al., 2016). Although the measurements were carried on for 28 days in this study, the hypothesis is that the calcium release continues in the same sustained pattern, until the surface and surrounding medium calcium concentrations reach an equilibrium.

To understand the relationship between the Zn and Ag ions on the multi-ion samples, and their biological effects, the number of ions released from the samples were measured by FAAS. The release of Ag^{+} and Zn^{2+} from the Ag/Zn multi-ion treated surface follow a similar trend to that of the mono-ion treated surfaces, albeit with smaller concentration. It has been suggested that Ag and Zn in a surface in an electrolytic solution form a micro-galvanic couple (Jin et al., 2014), in which the release of Zn^{2+} and consumption of protons occur at the same time on the Zn/Ag co-implanted titanium. This leads to a higher ionic release of Zn ions, at the expense of

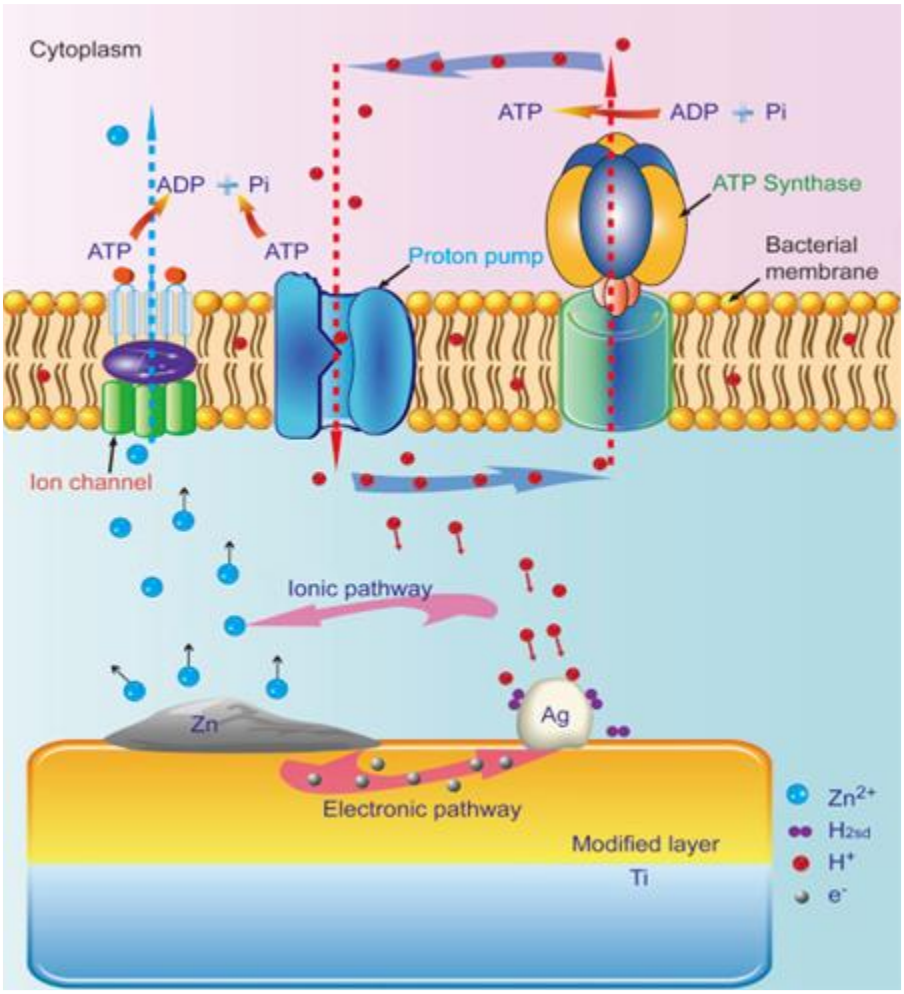

Figure 10.1 Schematic illustration of the possible antibacterial mechanism on the Zn/Ag co-implanted titanium surface(Jin et al., 2014).

Ag ion release. In this study, however, the release of Ag ions remained comparatively higher than Zn ions throughout. This could arise from the higher amounts of Ag ions originally incorporated onto the Ti surface in the 3-ion co-incorporation onto the Ti surface. The presence of similarly charged Ca ions in the microenvironment could also interfere with the Zn ion release, hence the lower than expected values. The Zn^{2+} ions released to the microenvironment play a long-range role in enhancing the antimicrobial ability, while the incorporated Ag NPs play a short-range antibacterial role in *vitro* and *in vivo*, as illustrated in Figure 10.1.

Also, an appropriate amount of released Zn^{2+} from the Zn/Ag co-implanted titanium can improve the osteogenic activity of osteogenic cells *via* the long-range interactions.

Concurrently, the embedded Ag NPs in the Zn/Ag co-incorporated titanium surface creates a microenvironment between the biomaterials and cells beneficial to osteogenic cells *via* short-range interactions. Overall, the synergism of the long-range and short-range interactions reduces the potential toxic effect of Ag, and enhances the osteogenic activity on the Zn/Ag co-incorporated Ti surface (Cao et al., 2011).

An assay of the antimicrobial effect of the surface modifications, first by means of modified suspension and inhibition zone tests, and then by biofilm formation assays using the CDC biofilm reactor suggested that, the mirror-finished surface is significantly more resistant to *S. aureus* biofilm formation and surface colonization than the commercially pure untreated surface. The antimicrobial effect is further enhanced when the polished surface is treated with Ag^{+} and Zn^{2+}, and composites with Ca^{2+}, even though the Ti surface implantation with these elements alters the nano-scale topography of the polished surface. This is particularly so for the $Ca^{2+}/Zn^{2+}/Ag^{+}$ composite treated surfaces. A Bonferroni comparison of the surfaces, at 95% CI, suggests a statistically significant variance in antimicrobial effect between the polished Ca^{2+}/Ag^{+} treated surface and all the other surfaces, except for the composite $Ca^{2+}/Zn^{2+}/Ag^{+}$ surface. Compared with the commercially pure unmodified, untreated surface, although the polished surface performed better than the commercially pure surface, the analysis indicated that the antimicrobial effect of polishing alone without treatment with either silver or zinc or both, was not statistically significant.

The mechanism of the antibacterial effect of Ag is related to Ag release followed by increased cell membrane permeability and loss of the proton motive force, including de-energization of cells and efflux of phosphate, leakage of cellular contents, and disruption of DNA replication. Many studies demonstrated that Ag particles could kill bacteria as well as other microorganisms such as fungi, yeast, and viruses (Marambio-Jones and Hoek, 2010).

It is generally accepted that, the interactions between Ag^+ and bacteria (cells) are short-range, as the embedded Ag NPs can interact with bacteria *via* the micro-galvanic effects without release of Ag^+ (Agarwal et al., 2010, Ochoa and Mow, 2008). The micro-galvanic effect in which other metallic ions on a surface are released or 'corroded' in preference to silver, derives from the micro-galvanic couples between the silver nano-particles and titanium substrate, due to the marked electronegativity difference between standard electrode potential of titanium ($E°Ti = -1.630$ V) and that of silver ($E°Ag = 0.7996$ V) (Cao et al., 2011, Vanysek, 1998). This becomes activated in aqueous conditions where they become conductive (Arslan et al., 2008).

The interactions between Zn^{2+} and bacteria (cells) are however, long-range ones. This is because the proposed interactions are based on the uptake of Zn^{2+} present in the microenvironment between the Zn-treated biomaterial surface and or bacteria (Chen and Schluesener, 2008). But the exact toxicity mechanism is still being debated, as there are some queries within the spectrum of antibacterial activity requiring further explanations. Proposed distinctive mechanisms in the literature include: direct contact of ZnO-NPs with cell walls, resulting in bacterial cell wall integrity disruption (Brayner et al., 2006, Zhang et al., 2007, Adams et al., 2006a), the liberation of antimicrobial ions mainly Zn^{2+} ions (Kasemets et al., 2009, Brunner et al., 2006, Li et al., 2011), and the generation of reactive oxygen species (ROS) (Lipovsky et al., 2011, Zhang et al., 2008b, Jalal et al., 2010). The toxicity mechanism at play may however vary depending on the physiological media as the species of dissolved Zn may change per the medium components besides the physicochemical properties of ZnO-NPs (Li et al., 2011).

The long-range interactions of Zn^{2+} stimulate both the osteogenic activity and antibacterial ability (Barrena et al., 2009), whereas the short-range interactions of Ag NPs can efficiently kill bacteria. Interestingly, ZnO-NPs have been reported by several studies as non-toxic to

human cells (Colon et al., 2006), necessitating their usage as antibacterial agents; noxious to microorganisms, but with good biocompatibility to human cells (Padmavathy and Vijayaraghavan, 2008). Therefore, the reproducible simultaneous incorporation of Zn and Ag into Ti may yield promising osteogenic and antimicrobial activity.

Hitherto, pulsed Plasma immersion ion implantation (pulsed-PIII) has been deemed a suitable and versatile method that can introduce nearly any elements into different types of substrates and biomedical components without the line-of-sight limitation (Pelletier and Anders, 2005, Huang et al., 2004). The simple and effective technique that introduces both Zn and Ag into implantable titanium surfaces developed in this study is therefore highly desirable.

To investigate the osteogenic effect of the surface modification developed here, an *in vitro* model using U2OS osteogenic osteosarcoma cells was employed. This cell line is ideal because of its ability to bind to surfaces by means of focal contacts, and its adhesion and spreading characteristics. It also expresses characteristic osteoblast-like matrix with little variability, and therefore permits the quantitative study of bone cell adhesion (a pre-requisite to osseointegration) to the different surfaces (de Ruijter et al., 2001, Musa et al., 2013, ter Brugge et al., 2002, Niforou et al., 2008). For the first 8-hour cell adhesion period, the unpolished surface's micron-rough topography with higher peaks and deeper valleys providing numerous anchorage points, was the best suited for osteogenic cell adhesion. Over the course of a 72 hours cell adhesion and proliferation period however, the polished surface of nano-scale topography was the most suitable, distantly followed jointly by the unpolished and calcium treated surfaces. Though not to the same degree, it appears silver and zinc have an untoward effect on cell adhesion and proliferation on surfaces, with the effect of silver markedly more so. This is however in opposition to other studies that have suggested that *in vitro* cell culture assay show no significant cytotoxicity, and even good cytocompatibility on the Ag-PIII treated Ti samples (Cao et al., 2011), the caveat being the high concentration of silver and zinc ions in

the limited volume of the 24-well plate. The results indicate that, presence of calcium, by itself and in combination with other ions on the Ti surface, improved osteoblast-like cell adhesion to the Ti surface, as also demonstrated by other recent studies (Oshiro et al., 2015, Valanezahad et al., 2011, Park et al., 2011), via the formation of a calcium ionic-bridge between the Ti (implant) surface and the Ca^{2+} -binding biomolecule of the surrounding osseous tissue (Anitua et al., 2015a).

An examination of the qualitative changes in the cell morphology of U2OS cells exposed to the modified surfaces was used to determine how the various modification altered the cell morphology, hence the health and growth promotion or cytotoxic effect of the surface modifications. Over a period of 72 hours, all the surfaces supported morphometric cell growth, albeit to varying extents. Cells on commercially pure unpolished surface, showed no distinct morphological shape, starting out as circular cells embedded on the tamper annealed micron-topography of the material surface. Some remained circular, others elongated, while others still showed lamellipodia extensions across the peaks and valleys of the surface. The cells however show clear contact boundaries, thus appearing to be closely packed together, yet distinctly separate from each other. This suggests the surface topography allows for individual cell anchorage to the commercially pure untreated surface. The polished surface closely followed the calcium-only treated surface, in the morphological size of cells attached to its surface. The cells here appeared circular with distinct translucent regions around the cells on attachment to the surface at 8 hours, and larger and elongated after 72 hours, with distinguishable raised nuclear materials. They appeared thinly spread out on the nano-smooth polished surface, overlapping with adjacent cells. The nano topography thus appears to encourage cytoplasmic spread and clustering of the cells, with thin cytoplasmic overlaps, and no distinct lamellipodia extensions seen in the commercially pure untreated surface. The polished surface thus provides

little topography related sites for individual cell anchorage, but rather a more tightly packed and layered cell organisation on the modified surface.

The calcium treated surface on the other hand, supported more proliferation and morphological growth than the other surfaces. The morphology of the cells on the calcium treated surfaces also suggested a more active lamellipodia/filopodia extensions. This is because in addition to increasing the surface roughness because of the calcium incorporation, calcium on the surface of the titanium disc facilitates the preferential electrostatic adhesion of the U2OS cells and mobilization of molecules needed for bio-mineralization. (Anitua et al., 2015a, Ozdemir et al., 2016, Anitua et al., 2015b). The cells here therefore start as a mixture of circular dense cells, circular cells with overlapping translucent cytoplasmic boundaries, and elongated cells with distinct lamellipodia/filopodia extensions. Over 72 hours, they appear as mostly elongated cells, with dense nuclear region that are closely packed with distinct cellular boundaries. The calcium surface modification thus appears to facilitate increased individual cell anchorage as observed in the commercially pure unmodified surface, because of the topographical advantage over the polished surface, as well as encourage healthier cell morphological increase and proliferation.

The morphometric changes observed on calcium-silver, calcium-zinc and calcium-silver-zinc composite surfaces again suggest the presence of silver has a deleterious effect on U2OS cell on the modified surfaces. After 8 hours, it appeared cells adhered only to areas of the surface with high aggregation of calcium ions/crystals. They were also smaller in size on the calcium-silver surface, than on the calcium-silver-zinc surface, as the former has more silver ions over the same surface area than the later. After 72 hours, the cells appeared as smaller dark circular pits and elongated groves over the calcium-silver surface, and as dark circular and elongated regions on the calcium-silver-zinc surface, smaller than at 8 hours. This suggests that silver has a concentration dependent adverse effect on the growth and proliferation of cells on the surface

of the titanium discs. Considering the amount of silver and other ions leached from the disc surface into the surrounding media, in this case 1 ml volume, the adverse effect observed may not be as pronounced as suggested, in the more dynamic *in vivo* environment.

The general trend thus suggests that, the surface modification strategy developed here facilitated a cost-effective incorporation of bioactive calcium, silver and zinc and their composites onto the commercially pure Ti surface. Also, the bioactivity profile of the resulting modified surfaces suggests, calcium treatment better enhances cell adhesion, morphological growth and proliferation over the polished surface, which has marginal advantage over the unmodified surface. The co-incorporation of calcium, silver and zinc onto the titanium surface by the techniques developed in this work promises a potentially efficient means of harnessing the synergistic short-term antimicrobial ability of silver and the long-term osteogenic activity of zinc and calcium to improve the performance of titanium biomaterials, Finally, zinc and silver, while conferring potent antimicrobial properties to the modified surfaces, also indicate a potential concentration-dependent adverse effect on cell growth and proliferation, compared to the unmodified commercially pure surface.

Chapter 11 : Critical evaluation, conclusion and future directions

The goal of biomaterial science application, particularly in orthopaedics and dentistry, is the seamless, mechanically durable and functionally reliable integration of the exogenous material with the surrounding biologic tissue. Hence the usefulness and efficiency of any new device is assessed, amongst other parameters, on how it predictably integrates with the expected surrounding tissues, *in vitro*, and then *in vivo*. Several both *in vitro* and *in vivo* models have been used to assess and predict the performance of new orthopaedic devices, particularly about osseointegration.

It has been demonstrated that events leading to osseointegration are intimately influenced by the physical and chemical characteristics of the device material surface. Modification of implant device material surface therefore presents a strategic means of influencing osseointegration, in the search for more efficient and more naturally adaptable implant materials and devices.

Over the years, several methods (A and C, 2004, Albrektsson and Wennerberg, 2004b, Albrektsson and Wennerberg, 2004a, Glinel et al., 2012, Fadeeva et al., 2011, Lavenus et al., 2010, Bruellhoff et al., 2010) have been proposed and used to alter the material surface of implantable weight-bearing devices in a bid to improve biocompatibility, confer properties that reduce or eliminated implant related infections and reduce implant failure (Armitage et al., 2003). To achieve Ti implant surface with these ideal properties, the continued introduction of new strategies and modification of existing techniques, together with contributing to existing knowledge on the interaction of biological systems (bone and microbial cells) with implant material surface is important.

The surface wettability of implant devices has been shown to greatly influence the biological event cascade at the host/implant interface. Wetting is modulated by surface characteristics including surface topography and chemistry (Rupp et al., 2014, Elias et al., 2008, Ponsonnet et al., 2003, Janssen et al., 2006, Cho et al., 2012, Balaur et al., 2005, Vogler, 1999). Critical biological events affected by surface wettability include proteins and other macromolecules adhesion to surfaces during the conditioning process, hard and soft tissue interaction with the preconditioned surface, bacterial adhesion and biofilm formation, and speed of osseointegration (Maddikeri et al., 2008). The mechanisms of bacterial and other biomolecules adhesion to surfaces however remains unclear. This is mostly as a result of the complexity of the different factors involved, thus making prediction of bacterial interfacial behaviour difficult. The consensus, thermodynamically, is that, hydrophobicity (measured by water contact angle) and surface free energy, as well as the average surface roughness are crucial positive factors in the bacterial adhesion and biofilm formation process. The adhesion of human pathogens, particularly the biofilm forming *S. aureus* and *S. epidermidis*, have been demonstrated to correlate with increased hydrophobicity.

The mechanical surface modification protocol developed in this study, to attain a mirror-finished Ti surface, resulted in a surface more thermodynamically suitable for interaction with chemical, and biological molecules, compared with the commercially pure surface. This was suggested by the contact angle and water wettability measurements. In further thermochemical modification of the mirror-finished surface, to introduce bone cells activating calcium and antimicrobial property conferring silver and zinc onto the Ti surface, it has been demonstrated that, the mirror-finished surface is superior in the incorporation of ions onto its surface, compared to the commercially pure surface. The SEM micrograph of the surface showing the absence oxygen peaks suggests the mechanical surface modification technique employed effectively removed most of the oxides and other elements deposited on the Ti surface because

of the manufacturing process, handling and exposure to atmospheric and storage conditions. The SEM analysis of the further thermochemically treated Ti surfaces, employed for the first time here, indicates peaks for calcium from calcium hydroxide and chloride, silver from silver nitrate and zinc from zinc hydroxide and chloride, without the corresponding nitrogen and chloride peaks. This suggests that, the initial sodium titanate formed in the pre-treatment was an effective ion-exchanger on solvation, and effectively exchanged Na^+ for Ca^{2+}, Ag^+ and Zn^{2+}. The absence of nitrogen and chloride peaks in the EDS profile indicates the ions of interest were chemically incorporated into the Ti surface, and not present as passive residue of the novel surface treatment protocol developed.

It's been severally reported that, generally, the implant surface roughness plays a significant role in the anchoring of bone and connective tissues to the implant surface, thereby influencing healing time (Györgyey et al., 2013), shear bond strength and tensile bond strength (Elias et al., 2008, Moussa et al., 2015, Akiyama et al., 2013), by providing enlarged contact area through micro- and nano-structuring of the surface (Puckett et al., 2007, Yan et al., 2017, Kulkarni et al., 2015, Parithimarkalaignan and Padmanabhan, 2013, Chug et al., 2013, Gittens et al., 2011, Alla et al., 2011). The traditional method of quantifying surface finish is through the profile roughness parameter Ra, which characterises the surface by the average vertical deviation from the mean line (i.e. arithmetical average roughness). In this study, this was determined by means of a profilometer and atomic force microscopy.

In characterizing the topographic features of a device surface, the standards established by Albrektsson and co suggest that, a surface with an arithmetic mean height Sa <100 nm is classified as a nano topographic. Surfaces >100 nm are micron-topographic (Wennerberg and Albrektsson, 2000). The debate as to which is more favorable for osseointegration is still ongoing. The general consensus appear to be that, moderately rough surfaces show greater bone responses than rough surfaces (Wennerberg and Albrektsson, 2009). It has also been

suggested by some researchers that proteins typically respond to surface of about 1–10 nm, while cells, including human primary osteoblast cells, are sensitive to Ti surface of structural features on the nano-scale of Ra 0.015–100 μm (Vorobyev and Guo, 2007, Györgyey et al., 2013).

The height parameters values obtained with the surface modification and ion implantation methods developed in this study suggest that, the methods, in addition to removing the surface oxides and contaminants, also reduced the overall surface roughness from a micro-scale, to the osteoblast mechanical interlocking preferred (Cochran et al., 1998, Joob-Fancsaly et al., 2004, De Santis et al., 1996) peaks dominated nano-scale surface.

Though silver has been the main experimental element employed in the attempt to confer antibacterial properties to implant device surfaces, it has also been shown that high concentrations of zinc, as in Ti surfaces chemically modified with ZnO, reduce *in vitro* viability of some bacteria (Xu et al., 2010, Petrini et al., 2006). This study further established this existing knowledge and understanding.

The release profile shows that measurable amounts of both Ag^{+} and Zn^{2+} were detected in the surrounding deionized water within a few hours of immersion in deionized water. After the initial burst of Ag^{+} and Zn^{2+} release within the first 24 hours, the cumulative release continued steadily for 28 days. This indicates an initial rapid release of Ag and Zn ions, followed by a maintained release of lower concentration of ions over the next 28 days. This initial burst of ions may be critical to the antibacterial properties of the modified Ti surface (Hetrick and Schoenfisch, 2006, Jamuna-Thevi et al., 2011), as is required to achieve immediate antibacterial concentrations in contact with implants, tissues and body fluids, to be followed by a sustained release of lower concentration of ions over a period of time to kill or inhibit bacteria growth (Burrell and Morris, 2001). A comparison of the antimicrobial effects of the

'freshly treated' surfaces with the 28-day-leached surfaces suggests that the modified surfaces remained antimicrobially active past four weeks of continuous ion release from the surface. However, the potency reduces with depletion of the implanted ions. This suggests that orthopaedic devices implanted with silver and zinc by the method developed here may provide durable antimicrobial protection against device-related infection. This, together with good tolerability by osteoblast cells have been documented (Cao et al., 2011).

The overall Ag ion release from all the modified surfaces was measured between 0.029 ppm and 10.34 ppm which is higher than the minimum concentration required for antimicrobial efficacy (0.1 ppb) and within the maximum toxic concentration (10 ppm) for human cells (Jamuna-Thevi et al., 2011). Similarly, the Zn ion release of between 0.234 ppm and 1.122 ppm was above the reported 0.0653 ppm (Coughlan et al., 2008, Hu et al., 2012) minimum zinc concentration required for bacterial inhibition.

We also found that, polishing the surface may improve its interaction with bone cells. The polishing conferred nano-scale surface topography to the titanium and enhance its surface wettability, which have been severally demonstrated to favour cell adhesion over the micro-scale surface of the commercially pure unpolished surface (Anselme et al., 2010, Anselme et al., 2011, Brunette, 1996, Bucci-Sabattini et al., 2010). Calcium, a major component of hydroxyapatite and known to encourage bio-mineralization by attracting calcium-binding and other proteins (Zhou and Lee, 2011, Anitua et al., 2015a), on to the polished titanium surface, further improved the adhesion and growth of bone cells. Previous attempts to introduce calcium unto Ti surfaces have employed the use of simulated body fluids (Takadama et al., 2001, Kokubo and Takadama, 2006, Jonášová et al., 2004, Jonášová et al., 2002, Cho et al., 2012, Becker et al., 2007). The novelty of the approach developed here lies in the direct introduction of calcium onto the Ti surface, without the other ions of the simulated body fluid. This is done by employing the effective ion-exchange capacity of the alkali titanate formed on the Ti surface

on interaction with strong alkali. This chemistry was utilised again in introducing silver and zinc ions onto the Ti surface.

It appears however, that the presence of Ag^+ ions on the modified surface, previously demonstrated to confer anti-microbial propertied to the modified titanium surface, adversely affected osteoblast-like U2OS cell adhesion to the modified surface, even in combination with calcium. However, not all the U2OS cells attached were wiped out, and some survived past 24 hours. A quantitative analysis of the confluent cells on the unpolished, polished and calcium treated surface suggests that, at confluence, there is no significant quantitative difference between the polished and unpolished surfaces. There were however marked morphological differences in cells on the various surfaces. The results suggest that although the three-ion calcium-silver-zinc surface was preferable for cell adhesion over two-ion calcium-silver surface, the latter was better suited to osteoblast cells proliferation than the former.

In the assessment of the cytotoxic effect of the implanted ions, changes in cell morphology or morphometric assays were used to provide qualitative indicators of cell health, growth and viability. (Rampersad, 2012). The results indicated that, calcium treatment significantly enhanced cell adhesion, morphological or size growth, and proliferation, over the polished surface, which has marginal advantage over the commercially pure unmodified surface, as previously demonstrated by other researchers (Nayab et al., 2005, Anitua et al., 2015a). In combination with either and both silver and zinc, there is a concentration dependent (directly with regard to calcium, and inversely with silver and zinc) effect on osteosarcoma U2OS cell attachment and proliferation. This supports similar finding involving the use of osteogenic MG-63 cells (Nayab et al., 2005, Greulich et al., 2012). The resulting multi-ion treated surface therefore combines the beneficial antimicrobial effect of silver/zinc with the beneficial osseo-integrating effect of calcium.

The suggestion therefore is that, antimicrobial agents can be directly incorporated onto the Ti implant surface, by the protocols developed in this study, to facilitate the localized delivery of a therapeutic agents, to prevent bacterial colonization and threat of infection at implant device sites. Similarly, osteogenic agents can be more efficiently incorporated onto Ti implant devices by this protocol, to encourage the osseointegration process.

The Ti surface modification method developed in this study therefore present a more efficient, more consistent, and a better controlled means of presenting therapeutic agents directly onto the Ti implant surface, to provide effective and prolonged antibacterial action, and a good bone integration ability and stability in the physiological environment. Thus, representing a promising solution to the problems of implant related infections and osseointegration related implant failures

11.1. Future Direction

It has been demonstrated in this work that a simpler, cost effective means of incorporating bioactive ions onto the surface of implant grade Ti is possible. This was however done using a uniform one-dimensional surface of a disc. It will therefore be interesting to investigate how this method holds up when applied to an actual 3-dimensional implant device of irregular surface such as a dental implant, a bone screw or an internal fixation. The main problem associated with this surface modification strategy is the relatively rapid initial release of the antibacterial agent. This coupled with the cytotoxic behaviour at the highest concentration may present tolerability issues over a larger implant device surface area. This has been cited by some researchers (Ferraris and Spriano, 2016) as the reason for the absence of Ti based implant with antimicrobial properties of the medical device market currently. The presence of active principles released from the material surface also poses a complication with classification of the device, thus increasing commercialisation time and cost.

Future work may therefore be carried out

To examine the application of the surface modification method developed here to an actual multifaceted implant device, and ascertain its antimicrobial profile and tissue compatibility *in vivo* using animal models.

To investigate the release profile of the implanted ions on a larger representative surface area, and how the amounts of ions released affect surrounding tissues and cells.

To investigate the antimicrobial action of the implanted silver and zinc ion on *S. aureus* and other biofilm forming bacterial using *in vivo* animal models.

To explore the involvement of the intracellular signal transduction pathways in the effects reported here. Integrins, together with fibronectins, are known to play a major role in the cellular adhesion signal transduction process (de Ruijter et al., 2001, Kostenuik et al., 1996, Fowler et al., 2000). How these are affected by ions implanted on the Ti surface will elucidate the mechanism of the interaction between the modified Ti surface and the surrounding cells.

To investigate the involvement of some novel genes possibly implicated in the cell response to the silver, zinc and calcium modification of the Ti surface. This will measure and quantify the genes expressed in the interaction, and provide a comprehensive picture of the modified Ti-cell interaction at the gene level.

To investigate, using animal models, the *in vivo* effects of the implanted ions on osseointegration and biofilm formation.

To examine the effects of the multi-ions incorporated Ti surface on the mineralisation of newly-formed bones around the implant surface, using *in vitro* and/or *in vivo* animal models.

References:

A, B. & C, D. B. 2004. Surface treatments and roughness properties of Ti-based biomaterials. *J Mater Sci Mater Med. 2004 Sep;15(9):935-49.*, T - ppublish.

ADAMS, J. C. 2001. Cell-matrix contact structures. *Cell Mol Life Sci,* 58**,** 371-92.

ADAMS, L. K., LYON, D. Y. & ALVAREZ, P. J. 2006a. Comparative eco-toxicity of nanoscale TiO 2, SiO 2, and ZnO water suspensions. *Water Res,* 40**,** 3527-3532.

ADAMS, L. K., LYON, D. Y. & ALVAREZ, P. J. J. 2006b. Comparative eco-toxicity of nanoscale TiO2, SiO2, and ZnO water suspensions. *Water Res,* 40**,** 3527-3532.

ADVINCULA, M. C., PETERSEN, D., RAHEMTULLA, F., ADVINCULA, R. & LEMONS, J. E. 2007. Surface analysis and biocorrosion properties of nanostructured surface sol–gel coatings on Ti6Al4V titanium alloy implants. *Journal of Biomedical Materials Research Part B: Applied Biomaterials,* 80B**,** 107-120.

AGARWAL, A., WEIS, T. L., SCHURR, M. J., FAITH, N. G., CZUPRYNSKI, C. J., MCANULTY, J. F., MURPHY, C. J. & ABBOTT, N. L. 2010. Surfaces modified with nanometer-thick silver-impregnated polymeric films that kill bacteria but support growth of mammalian cells. *Biomaterials,* 31**,** 680-690.

AGGARWAL, V. K., BAKHSHI, H., ECKER, N. U., PARVIZI, J., GEHRKE, T. & KENDOFF, D. 2014. Organism profile in periprosthetic joint infection: pathogens differ at two arthroplasty infection referral centers in Europe and in the United States. *J Knee Surg,* 27**,** 399-406.

AKIEH, M. N., LAHTINEN, M., VÄISÄNEN, A. & SILLANPÄÄ, M. 2008. Preparation and characterization of sodium iron titanate ion exchanger and its application in heavy metal removal from waste waters. *Journal of Hazardous Materials,* 152**,** 640-647.

AKIYAMA, H., YAMAMOTO, K., KANEUJI, A., MATSUMOTO, T. & NAKAMURA, T. 2013. In-vitro characteristics of cemented titanium femoral stems with a smooth surface finish. *Journal of Orthopaedic Science,* 18**,** 29-37.

ALATORRE-MEDA, M. & MANO, J. F. 2016. General Characterization of Chemical Properties of Natural-Based Biomaterials. *Biomaterials from Nature for Advanced Devices and Therapies***,** 517-531.

ALBREKTSSON T, B. T., LINDHE J. 2003. Osseointegration: historic background and current concepts. *Clinical periodontology and implant dentistry,* 4**,** 809–820.

ALBREKTSSON, T. & WENNERBERG, A. 2004a. Oral implant surfaces: Part 1--review focusing on topographic and chemical properties of different surfaces and in vivo responses to them. *Int J Prosthodont,* 17**,** 536-43.

ALBREKTSSON, T. & WENNERBERG, A. 2004b. Oral implant surfaces: Part 2--review focusing on clinical knowledge of different surfaces. *Int J Prosthodont,* 17**,** 544-64.

ALLA, R. K., GINJUPALLI, K., UPADHYA, N., SHAMMAS, M., RAVI, R. K. & SEKHAR, R. 2011. Surface Roughness of Implants: A Review. *Trends Biomater. Artif. Organs,* 25**,** 112-8.

ALLEN, B. 2011. The eleven most implanted medical devices in America. *24/7 Wallst*.

ALQAHTANI, S., PROMTONG, P., OLIVER, A. W., HE, X. T., WALKER, T. D., POVEY, A., HAMPSON, L. & HAMPSON, I. N. 2016. Silver nanoparticles exhibit size-dependent differential toxicity and induce expression of syncytin-1 in FA-AML1 and MOLT-4 leukaemia cell lines. *Mutagenesis***,** gew043.

ANDERSON, J. M., RODRIGUEZ, A. & CHANG, D. T. 2008a. Foreign body reaction to biomaterials. *Innate and Adaptive Immune Responses in Tissue Engineering,* 20**,** 86-100.

ANDERSON, J. M., RODRIGUEZ, A. & CHANG, D. T. 2008b. Foreign body reaction to biomaterials. *Semin Immunol,* 20**,** 86-100.

ANDERSSON, A.-S., BÄCKHED, F., VON EULER, A., RICHTER-DAHLFORS, A., SUTHERLAND, D. & KASEMO, B. 2003. Nanoscale features influence epithelial cell morphology and cytokine production. *Biomaterials,* 24**,** 3427-3436.

ANIOŁEK, K., KUPKA, M., BARYLSKI, A. & DERCZ, G. 2015. Mechanical and tribological properties of oxide layers obtained on titanium in the thermal oxidation process. *Applied Surface Science,* 357, Part B**,** 1419-1426.

ANITUA, E., PIÑAS, L., MURIAS, A., PRADO, R. & TEJERO, R. 2015a. Effects of calcium ions on titanium surfaces for bone regeneration. *Colloids and Surfaces B: Biointerfaces,* 130**,** 173-181.

ANITUA, E., PRADO, R., ORIVE, G. & TEJERO, R. 2015b. Effects of calcium-modified titanium implant surfaces on platelet activation, clot formation, and osseointegration. *Journal of Biomedical Materials Research Part A,* 103**,** 969-980.

ANSELME, K., BIGERELLE, M., NOEL, B., DUFRESNE, E., JUDAS, D., IOST, A. & HARDOUIN, P. 2000. Qualitative and quantitative study of human osteoblast adhesion on materials with various surface roughnesses. *J Biomed Mater Res,* 49**,** 155-66.

ANSELME, K., DAVIDSON, P., POPA, A. M., GIAZZON, M., LILEY, M. & PLOUX, L. 2010. The interaction of cells and bacteria with surfaces structured at the nanometre scale. *Acta Biomaterialia,* 6**,** 3824-3846.

ANSELME, K., DAVIDSON, P., POPA, A. M., GIAZZON, M., LILEY, M. & PLOUX, L. 2011. Response to comment on “The interaction of cells and bacteria with surfaces structures at the nanoscale”. *Acta Biomaterialia,* 7**,** 1936-1937.

ANWAR, H., DASGUPTA, M. K. & COSTERTON, J. W. 1990. Testing the susceptibility of bacteria in biofilms to antibacterial agents. *Antimicrob Agents Chemother,* 34**,** 2043-6.

ARCIOLA, C. R., CAMPOCCIA, D., GAMBERINI, S., DONATI, M. E., PIRINI, V., VISAI, L., SPEZIALE, P. & MONTANARO, L. 2005. Antibiotic resistance in exopolysaccharide-forming Staphylococcus epidermidis clinical isolates from orthopaedic implant infections. *Biomaterials,* 26**,** 6530-5.

ARCIOLA, C. R., CAMPOCCIA, D. & MONTANARO, L. 2002. Effects on antibiotic resistance of Staphylococcus epidermidis following adhesion to polymethylmethacrylate and to silicone surfaces. *Biomaterials,* 23**,** 1495-1502.

ARCIOLA, C. R., CAMPOCCIA, D., SPEZIALE, P., MONTANARO, L. & COSTERTON, J. W. 2012. Biofilm formation in Staphylococcus implant infections. A review of molecular mechanisms and implications for biofilm-resistant materials. *Biomaterials,* 33**,** 5967-5982.

ARENS, S., HANSIS, M., SCHLEGE, U., EIJER, H., PRINTZEN, G., ZIEGLER, W. J. & PERREN, S. M. 1996a. Infection after open reduction and internal fixation with dynamic compression plates â€" Clinical and experimental data. *Injury,* 27, Supplement 3**,** S/C27-S/C33.

ARENS, S., HANSIS, M., SCHLEGE, U., EIJER, H., PRINTZEN, G., ZIEGLER, W. J. & PERREN, S. M. 1996b. Infection after open reduction and internal fixation with dynamic compression plates â€" Clinical and experimental data. *Implants and Infection in Fracture Fixation,* 27, Supplement 3**,** S/C27-S/C33.

ARMITAGE, D. 2009. Therapeutic ion release from modified-titanium surfaces. *Journal of Pharmacy and Pharmacology,* 61**,** A15-A16.

ARMITAGE, D. A. & GRANT, D. M. 2003. Characterisation of surface-modified nickel titanium alloys. *Materials Science and Engineering: A,* 349**,** 89-97.

ARMITAGE, D. A., MIHOC, R. I., JONES, F. H., TATE, T. J. & KNOWLES, J. C. 2008. Calcium-enriched titanium surfaces via a hydrothermal process. *Journal of Pharmacy and Pharmacology,* 60**,** A2-A3.

ARMITAGE, D. A., PARKER, T. L. & GRANT, D. M. 2003. Biocompatibility and hemocompatibility of surface-modified NiTi alloys. *Journal of Biomedical Materials Research Part A,* 66**,** 129-137.

ARSLAN, H., ÇELIKKAN, H., ÖRNEK, N., OZAN, O., ERSOY, A. E. & AKSU, M. L. 2008. Galvanic corrosion of titanium-based dental implant materials. *Journal of Applied Electrochemistry,* 38**,** 853-859.

ASAOKA, K., KUWAYAMA, N., OKUNO, O. & MIURA, I. 1985. Mechanical properties and biomechanical compatibility of porous titanium for dental implants. *Journal of Biomedical Materials Research,* 19**,** 699-713.

AZIZ, R. A., MISNON, I. I., CHONG, K. F., YUSOFF, M. M. & JOSE, R. 2013. Layered sodium titanate nanostructures as a new electrode for high energy density supercapacitors. *Electrochimica Acta,* 113**,** 141-148.

AZOULAY, A., SHAMIR, N., FROMM, E. & MINTZ, M. H. 1997. The initial interactions of oxygen with polycrystalline titanium surfaces. *Surface Science,* 370**,** 1-16.

BAGNO, A. & DI BELLO, C. 2004. Surface treatments and roughness properties of Ti-based biomaterials. *Journal of Materials Science: Materials in Medicine,* 15**,** 935-949.

BAHAR, A. A. & REN, D. 2013. Antimicrobial Peptides. *Pharmaceuticals,* 6**,** 1543-1575.

BAJPAI, P. 2015. Chapter 4 - Factors Affecting Biofilm Development. *Pulp and Paper Industry.* Elsevier.

BAKIR, M. 2012. Haemocompatibility of titanium and its alloys. *J Biomater Appl,* 27**,** 3-15.

BALAUR, E., MACAK, J. M., TAVEIRA, L. & SCHMUKI, P. 2005. Tailoring the wettability of TiO2 nanotube layers. *Electrochemistry Communications,* 7**,** 1066-1070.

BALL, M., GRANT, D. M., LO, W.-J. & SCOTCHFORD, C. A. 2008. The effect of different surface morphology and roughness on osteoblast-like cells. *Journal of Biomedical Materials Research Part A,* 86A**,** 637-647.

BARRENA, R., CASALS, E., COLÓN, J., FONT, X., SÁNCHEZ, A. & PUNTES, V. 2009. Evaluation of the ecotoxicity of model nanoparticles. *Chemosphere,* 75**,** 850-857.

BARTLOMIEJCZYK, T., LANKOFF, A., KRUSZEWSKI, M. & SZUMIEL, I. 2013. Silver nanoparticles–allies or adversaries? *Annals of Agricultural and Environmental Medicine,* 20.

BAXTER, L. C., FRAUCHIGER, V., TEXTOR, M., AP GWYNN, I. & RICHARDS, R. G. 2002. Fibroblast and osteoblast adhesion and morphology on calcium phosphate surfaces. *Eur Cell Mater,* 4**,** 1-17.

BECKER, I., HOFMANN, I. & MÜLLER, F. A. 2007. Preparation of bioactive sodium titanate ceramics. *Journal of the European Ceramic Society,* 27**,** 4547-4553.

BELT, H. V. D., NEUT, D., SCHENK, W., HORN, J. R. V., MEI, H. C. V. D. & BUSSCHER, H. J. 2001. Infection of Orthopedic Implants and The Use of Antibiotic-loaded Bone cCments: A Review. *Acta Orthop Scand,* 72**,** 557-571.

BERBARI, E. F., OSMON, D. R., CARR, A., HANSSEN, A. D., BADDOUR, L. M., GREENE, D., KUPP, L. I., BAUGHAN, L. W., HARMSEN, W. S., MANDREKAR, J. N., THERNEAU, T. M., STECKELBERG, J. M., VIRK, A. & WILSON, W. R. 2010. Dental Procedures as Risk Factors for Prosthetic Hip or Knee Infection: A Hospital-Based Prospective Case-Control Study. *Clinical Infectious Diseases,* 50**,** 8-16.

BESSHO, K., FUJIMURA, K. & IIZUKA, T. 1995. Experimental long-term study of titanium ions eluted from pure titanium miniplates. *Journal of Biomedical Materials Research,* 29**,** 901-904.

BHASKAR, B., ARUN, S., SREEKANTH, P. R. & KANAGARAJ, S. 2016. Biomaterials in Total Hip Joint Replacements: The Evolution of Basic Concepts, Trends, and Current Limitations—A Review. *Trends in Biomaterials.* Pan Stanford.

BHAT, S., JUN, D., BIPLAB, P. C. & DAHMS, T. E. S. 2012. *Viscoelasticity in Biological Systems: A Special Focus on Microbes*.

BHAT, V. & BALAJI, S. S. 2014. Surface topography of dental implants. *Nitte University Journal of Health Science,* 4**,** 46.

BJURSTEN, L. M., RASMUSSON, L., OH, S., SMITH, G. C., BRAMMER, K. S. & JIN, S. 2010. Titanium dioxide nanotubes enhance bone bonding in vivo. *Journal of Biomedical Materials Research Part A,* 92**,** 1218-1224.

BOLLEN, C. M., PAPAIOANNO, W., VAN ELDERE, J., SCHEPERS, E., QUIRYNEN, M. & VAN STEENBERGHE, D. 1996. The influence of abutment surface roughness on plaque accumulation and peri-implant mucositis. *Clin Oral Implants Res,* 7**,** 201-11.

BONGARTZ, T., HALLIGAN, C. S., OSMON, D. R., REINALDA, M. S., BAMLET, W. R., CROWSON, C. S., HANSSEN, A. D. & MATTESON, E. L. 2008. Incidence and risk factors of prosthetic joint infection after total hip or knee replacement in patients with rheumatoid arthritis. *Arthritis Care & Research,* 59**,** 1713-1720.

BOSETTI, M., MASSE, A., TOBIN, E. & CANNAS, M. 2001. In vivo evaluation of bone tissue behavior on ion implanted surfaces. *Journal of Materials Science: Materials in Medicine,* 12**,** 431-435.

BOWERS, K. T., KELLER, J. C., RANDOLPH, B. A., WICK, D. G. & MICHAELS, C. M. 1991. Optimization of surface micromorphology for enhanced osteoblast responses in vitro. *Int J Oral Maxillofac Implants,* 7**,** 302-310.

BOYNE, P. & JONES, S. D. 2004. Demonstration of the osseoinductive effect of bone morphogenetic protein within endosseous dental implants. *Implant Dentistry,* 13**,** 180-184.

BOZIC, K. J. & RIES, M. D. 2005. The impact of infection after total hip arthroplasty on hospital and surgeon resource utilization. *Journal of Bone and Joint Surgery - Series A,* 87**,** 1746-1751.

BRACERAS, I., ONATE, J. I., GOIKOETXEA, L., VIVIENTE, J. L., ALAVA, J. I. & DE MAEZTU, M. A. 2005. Bone cell adhesion on ion implanted titanium alloys. *Surface and Coatings Technology,* 196**,** 321-326.

BRAMMER, K. S., OH, S., COBB, C. J., BJURSTEN, L. M., HEYDE, H. V. D. & JIN, S. 2009. Improved bone-forming functionality on diameter-controlled TiO2 nanotube surface. *Acta Biomaterialia,* 5**,** 3215-3223.

BRAYNER, R., FERRARI-ILIOU, R., BRIVOIS, N., DJEDIAT, S., BENEDETTI, M. F. & FIÉVET, F. 2006. Toxicological impact studies based on Escherichia coli bacteria in ultrafine ZnO nanoparticles colloidal medium. *Nano Lett,* 6**,** 866-870.

BRÉMAUD, D., RUDMANN, D., KAELIN, M., ERNITS, K., BILGER, G., DÖBELI, M., ZOGG, H. & TIWARI, A. N. 2007. Flexible Cu(In,Ga)Se2 on Al foils and the effects of Al during chemical bath deposition. *Thin Solid Films,* 515**,** 5857-5861.

BRETT, P., HARLE, J., SALIH, V., MIHOC, R., OLSEN, I., JONES, F. & TONETTI, M. 2004. Roughness response genes in osteoblasts. *Bone,* 35**,** 124-133.

BROWNE, M. & GREGSON, P. J. 1994. Surface modification of titanium alloy implants. *Biomaterials,* 15**,** 894-898.

BRUCK, S. D. 1980. The role of biomaterials in insulin delivery systems. *Int J Artif Organs,* 3**,** 299-304.

BRUELLHOFF, K., FIEDLER, J., MÃ¶LLER, M., GROLL, J. & BRENNER, R. E. 2010. Surface coating strategies to prevent biofilm formation on implant surfaces. *International Journal of Artificial Organs,* 33**,** 646-653.

BRUNETTE, D. 1996. Effects of surface topography of implant materials on cell behavior in vitro and in vivo. *Nanofabrication and biosystems: integrating materials science, engineering, and biology***,** 335-355.

BRUNETTE, D. M., TENGVALL, P., TEXTOR, M. & THOMSEN, P. 2012. *Titanium in medicine: material science, surface science, engineering, biological responses and medical applications*, Springer Science & Business Media.

BRUNNER, T. J., WICK, P., MANSER, P., SPOHN, P., GRASS, R. N., LIMBACH, L. K., BRUININK, A. & STARK, W. J. 2006. In vitro cytotoxicity of oxide nanoparticles: comparison to asbestos, silica, and the effect of particle solubility. *Environ Sci Technol,* 40**,** 4374-4381.

BRUSCHI, M., STEINM, #XFC, LLER-NETHL, D., GORIWODA, W. & RASSE, M. 2015. Composition and Modifications of Dental Implant Surfaces. *Journal of Oral Implants,* 2015**,** 14.

BUCCI-SABATTINI, V., CASSINELLI, C., COELHO, P. G., MINNICI, A., TRANI, A. & EHRENFEST, D. M. D. 2010. Effect of titanium implant surface nanoroughness and calcium phosphate low impregnation on bone cell activity in vitro. *Oral Surgery, Oral Medicine, Oral Pathology, Oral Radiology, and Endodontology,* 109**,** 217-224.

BUNKER, J. P. 2001. The role of medical care in contributing to health improvements within societies. *International Journal of Epidemiology,* 30**,** 1260-1263.

BURNS, J. W. 2009. Biology takes centre stage. *Nat Mater,* 8**,** 441-443.

BURRELL, R. E. & MORRIS, L. R. 2001. Anti-microbial coating for medical devices. Google Patents.

BUSER, D., BROGGINI, N., WIELAND, M., SCHENK, R., DENZER, A., COCHRAN, D., HOFFMANN, B., LUSSI, A. & STEINEMANN, S. 2004a. Enhanced bone apposition to a chemically modified SLA titanium surface. *Journal of Dental Research,* 83**,** 529-533.

BUSER, D., BROGGINI, N., WIELAND, M., SCHENK, R. K., DENZER, A. J., COCHRAN, D. L., HOFFMANN, B., LUSSI, A. & STEINEMANN, S. G. 2004b. Enhanced Bone Apposition to a Chemically Modified SLA Titanium Surface. *Journal of Dental Research,* 83**,** 529-533.

BUSSCHER, H. J., VAN DER MEI, H. C., SUBBIAHDOSS, G., JUTTE, P. C., VAN DEN DUNGEN, J. J., ZAAT, S. A., SCHULTZ, M. J. & GRAINGER, D. W. 2012a. Biomaterial-associated infection: locating the finish line in the race for the surface. *Sci Transl Med,* 4**,** 153rv10.

BUSSCHER, H. J., VAN DER MEI, H. C., SUBBIAHDOSS, G., JUTTE, P. C., VAN DEN DUNGEN, J. J. A. M., ZAAT, S. A. J., SCHULTZ, M. J. & GRAINGER, D. W. 2012b. Biomaterial-Associated Infection: Locating the Finish Line in the Race for the Surface. *Science Translational Medicine,* 4**,** 153rv10.

CAMPOCCIA, D., MONTANARO, L. & ARCIOLA, C. R. 2006. The significance of infection related to orthopedic devices and issues of antibiotic resistance. *Biomaterials,* 27**,** 2331-2339.

CAMPOCCIA, D., MONTANARO, L. & ARCIOLA, C. R. 2013. A review of the biomaterials technologies for infection-resistant surfaces. *Biomaterials,* 34**,** 8533-8554.

CAMPOCCIA, D., MONTANARO, L., SPEZIALE, P. & ARCIOLA, C. R. 2010. Antibiotic-loaded biomaterials and the risks for the spread of antibiotic resistance following their prophylactic and therapeutic clinical use. *Biomaterials,* 31**,** 6363-6377.

CAO, H., LIU, X., MENG, F. & CHU, P. K. 2011. Biological actions of silver nanoparticles embedded in titanium controlled by micro-galvanic effects. *Biomaterials,* 32**,** 693-705.

CARLSON, C., HUSSAIN, S. M., SCHRAND, A. M., K. BRAYDICH-STOLLE, L., HESS, K. L., JONES, R. L. & SCHLAGER, J. J. 2008. Unique cellular interaction of silver nanoparticles: size-dependent generation of reactive oxygen species. *The journal of physical chemistry B,* 112**,** 13608-13619.

CARLSSON, L. V., ALBREKTSSON, T. & BERMAN, C. 1989. Bone response to plasma-cleaned titanium implants. *International Journal of Oral & Maxillofacial Implants,* 4.

CATS-BARIL, W., GEHRKE, T., HUFF, K., KENDOFF, D., MALTENFORT, M. & PARVIZI, J. 2013. International Consensus on Periprosthetic Joint Infection: Description of the Consensus Process. *Clinical Orthopaedics and Related Research®,* 471**,** 4065-4075.

CHEN, F.-M. & LIU, X. 2016. Advancing biomaterials of human origin for tissue engineering. *Progress in polymer science,* 53**,** 86-168.

CHEN, H., ZHANG, M., LI, B., CHEN, D., DONG, X., WANG, Y. & GU, Y. 2015. Versatile antimicrobial peptide-based ZnO quantum dots for in vivo bacteria diagnosis and treatment with high specificity. *Biomaterials,* 53**,** 532-544.

CHEN, Q. & THOUAS, G. 2015a. *Biomaterials: A Basic Introduction*, CRC Press.

CHEN, Q. & THOUAS, G. A. 2015b. Metallic implant biomaterials. *Materials Science and Engineering: R: Reports,* 87**,** 1-57.

CHEN, W.-C., CHEN, Y.-S., KO, C.-L., LIN, Y., KUO, T.-H. & KUO, H.-N. 2014. Interaction of progenitor bone cells with different surface modifications of titanium implant. *Materials Science and Engineering: C,* 37**,** 305-313.

CHEN, W., GUO, X., ZHANG, S. & JIN, Z. 2007. TEM study on the formation mechanism of sodium titanate nanotubes. *Journal of Nanoparticle Research,* 9**,** 1173-1180.

CHEN, W., LIU, Y., COURTNEY, H. S., BETTENGA, M., AGRAWAL, C. M., BUMGARDNER, J. D. & ONG, J. L. 2006. In vitro anti-bacterial and biological properties of magnetron co-sputtered silver-containing hydroxyapatite coating. *Biomaterials,* 27**,** 5512-5517.

CHEN, X. & SCHLUESENER, H. 2008. Nanosilver: a nanoproduct in medical application. *Toxicology letters,* 176**,** 1-12.

CHENG, L., MULLER, S. J. & RADKE, C. J. 2004. Wettability of silicone-hydrogel contact lenses in the presence of tear-film components. *Current Eye Research,* 28**,** 93-108.

CHO, S. K., PARK, I. S., LEE, S. J., KIM, K. A., PARK, J. M., AHN, S. G., SONG, K. Y., YOON, D. J. & LEE, M. H. 2012. Surface characteristics of Ti-10Ta-10Nb alloy modified by hydrogen peroxide treatment for dental implants. *Surface and Interface Analysis,* 44**,** 114-120.

CHOSA, N., TAIRA, M., SAITOH, S., SATO, N. & ARAKI, Y. 2004. Characterization of Apatite Formed on Alkaline-heat-treated Ti. *Journal of Dental Research,* 83**,** 465-469.

CHRZANOWSKI, W., NEEL, E. A., ARMITAGE, D. & KNOWLES, J. 2008a. Surface preparation of bioactive Ni–Ti alloy using alkali, thermal treatments and spark oxidation. *Journal of Materials Science: Materials in Medicine,* 19**,** 1553-1557.

CHRZANOWSKI, W., NEEL, E. A. A., ARMITAGE, D. A., LEE, K., WALKE, W. & KNOWLES, J. C. 2008b. Nanomechanical evaluation of nickel–titanium surface properties after alkali and electrochemical treatments. *Journal of the Royal Society Interface,* 5**,** 1009-1022.

CHRZANOWSKI, W., VALAPPIL, S. P., DUNNILL, C. W., NEEL, E. A. A., LEE, K., PARKIN, I. P., WILSON, M., ARMITAGE, D. A. & KNOWLES, J. C. 2010. Impaired bacterial attachment to light activated Ni–Ti alloy. *Materials Science and Engineering: C,* 30**,** 225-234.

CHU, P. K., CHEN, J. Y., WANG, L. P. & HUANG, N. 2002. Plasma-surface modification of biomaterials. *Materials Science and Engineering: R: Reports,* 36**,** 143-206.

CHUA, P.-H., NEOH, K.-G., KANG, E.-T. & WANG, W. 2008. Surface functionalization of titanium with hyaluronic acid/chitosan polyelectrolyte multilayers and RGD for promoting osteoblast functions and inhibiting bacterial adhesion. *Biomaterials,* 29**,** 1412-1421.

CHUG, A., SHUKLA, S., MAHESH, L. & JADWANI, S. 2013. Osseointegration—Molecular events at the bone–implant interface: A review. *Journal of Oral and Maxillofacial Surgery, Medicine, and Pathology,* 25**,** 1-4.

CLEARFIELD, A. & LEHTO, J. 1988. Preparation, structure, and ion-exchange properties of Na4Ti9O20 · xH2O. *Journal of Solid State Chemistry,* 73**,** 98-106.

CLOVER, J. & GOWEN, M. 1994. Are MG-63 and HOS TE85 human osteosarcoma cell lines representative models of the osteoblastic phenotype? *Bone,* 15**,** 585-591.

COCHRAN, D. L. 1999. A Comparison of Endosseous Dental Implant Surfaces. *J Periodontol,* 70**,** 1523-1539.

COCHRAN, D. L., SCHENK, R. K., LUSSI, A., HIGGINBOTTOM, F. L. & BUSER, D. 1998. Bone response to unloaded and loaded titanium implants with a sandblasted and acid-etched surface: a histometric study in the canine mandible. *J Biomed Mater Res,* 40**,** 1-11.

COELHO, P. & LEMONS, J. 2005. IBAD nanothick bioceramic incorporation on metallic implants for bone healing enhancement. From physico/chemical characterization to in-vivo performance evaluation. *ISBN, editor. Anaheim, CA: NSTI***,** 316-319.

COELHO, P. G., GRANJEIRO, J. M., ROMANOS, G. E., SUZUKI, M., SILVA, N. R. F., CARDAROPOLI, G., THOMPSON, V. P. & LEMONS, J. E. 2009. Basic research methods and current trends of dental implant surfaces. *Journal of Biomedical Materials Research Part B: Applied Biomaterials,* 88B**,** 579-596.

COLON, G., WARD, B. C. & WEBSTER, T. J. 2006. Increased osteoblast and decreased Staphylococcus epidermidis functions on nanophase ZnO and TiO2. *Journal of Biomedical Materials Research Part A,* 78**,** 595-604.

COMMISSION, J. E. 2009. ETN nanomedicine: roadmaps in nanomedicine towards 2020. Expert Report 2009. 1.0 ed.

CONNER, K. A., SABATINI, R., MEALEY, B. L., TAKACS, V. J., MILLS, M. P. & COCHRANN, D. L. 2003. Guided Bone Regeneration Around Titanium Plasma-Sprayed, Acid-Etched, and Hydroxyapatite-Coated Implants in the Canine Model. *J Periodontol,* 74**,** 658-668.

COOPER, L. F. 1998. Biologic determinants of bone formation for osseointegration: Clues for future clinical improvements. *J Prosthet Dent,* 80**,** 439-449.

COOPER, L. F. 2000. A role for surface topography in creating and maintaining bone at titanium endosseous implants. *J Prosthet Dent,* 84**,** 522-534.

CORDERO, J., MUNUERA, L. & FOLGUEIRA, M. D. 1994. Influence of metal implants on infection. An experimental study in rabbits. *The Journal of bone and joint surgery British volume,* 76**,** 717-20.

COSTERTON, J. W., CHENG, K. J., GEESEY, G. G., LADD, T. I., NICKEL, J. C., DASGUPTA, M. & MARRIE, T. J. 1987. Bacterial biofilms in nature and disease. *Annu Rev Microbiol,* 41**,** 435-64.

COSTERTON, J. W., MONTANARO, L. & ARCIOLA, C. R. 2005. Biofilm in implant infections: its production and regulation. *Int J Artif Organs,* 28**,** 1062-8.

COSTERTON, J. W., STEWART, P. S. & GREENBERG, E. P. 1999a. Bacterial biofilms: a common cause of persistent infections. *Science,* 284**,** 1318-22.

COSTERTON, J. W., STEWART, P. S. & GREENBERG, E. P. 1999b. Bacterial Biofilms: A Common Cause of Persistent Infections. *Science,* 284**,** 1318-1322.

COUGHLAN, A., BOYD, D., DOUGLAS, C. & TOWLER, M. 2008. Antibacterial coatings for medical devices based on glass polyalkenoate cement chemistry. *Journal of Materials Science: Materials in Medicine,* 19**,** 3555-3560.

CYSTER, L., PARKER, K., PARKER, T. & GRANT, D. 2004. The effect of surface chemistry and nanotopography of titanium nitride (TiN) films on primary hippocampal neurones. *Biomaterials,* 25**,** 97-107.

DALE, H., HALLAN, G., ESPEHAUG, B., HAVELIN, L. I. & ENGESÆTER, L. B. 2009. Increasing risk of revision due to deep infection after hip arthroplasty. *Acta Orthopaedica,* 80**,** 639-645.

DANIELS, S. L., SPRUNGER, P. T., KIZILKAYA, O., LYTLE, D. A. & GARNO, J. C. 2013. Nanoscale surface characterization of aqueous copper corrosion: Effects of immersion interval and orthophosphate concentration. *Applied Surface Science,* 285, Part B**,** 823-831.

DAROUICHE, R. O. 2004. Treatment of Infections Associated with Surgical Implants. *New England Journal of Medicine,* 350**,** 1422-1429.

DAS, K., BOSE, S. & BANDYOPADHYAY, A. 2009. TiO2 nanotubes on Ti: influence of nanoscale morphology on bone cell–materials interaction. *Journal of Biomedical Materials Research Part A,* 90**,** 225-237.

DAVIES, J. E. 2003. Understanding peri-implant endosseous healing. *J Dent Educ,* 67**,** 932-49.

DAVIS, J. R. 2000. *Corrosion: understanding the basics*, ASM International.

DE AVILA, E. D., LIMA, B. P., SEKIYA, T., TORII, Y., OGAWA, T., SHI, W. & LUX, R. 2015. Effect of UV-photofunctionalization on Oral Bacterial Attachment and Biofilm Formation to Titanium Implant Material. *Biomaterials*.

DE RUIJTER, J. E., TER BRUGGE, P. J., DIEUDONNE, S. C., VAN VLIET, S. J., TORENSMA, R. & JANSEN, J. A. 2001. Analysis of integrin expression in U2OS cells cultured on various calcium phosphate ceramic substrates. *Tissue Eng,* 7**,** 279-89.

DE SANTIS, D., GUERRIERO, C., NOCINI, P., UNGERSBOCK, A., RICHARDS, G., GOTTE, P. & ARMATO, U. 1996. Adult human bone cells from jaw bones cultured on plasma-sprayed or polished surfaces of titanium or hydroxylapatite discs. *Journal of Materials Science: Materials in Medicine,* 7**,** 21-28.

DEEKSHA ARYA, S. T., RAMESH BHARTI 2012. Role of surface topography of titanium endosseous implants for improved osseointegration. *Journal of Dental Implants* Vol 2 93-96.

DEPPRICH, R., ZIPPRICH, H., OMMERBORN, M., MAHN, E., LAMMERS, L., HANDSCHEL, J., NAUJOKS, C., WIESMANN, H.-P., KÜBLER, N. R. & MEYER, U. 2008. Osseointegration of zirconia implants: an SEM observation of the bone-implant interface. *Head & Face Medicine,* 4**,** 25-25.

DÍAZ, C., FERNÁNDEZ LORENZO DE MELE, M. A. & SCHILARDI, P. L. 2011. Comment on "The interaction of cells and bacteria with surfaces structured at the nanometre scale". *Acta Biomaterialia,* 7**,** 1934-1935.

DIEBOLD, U. 2003. The surface science of titanium dioxide. *Surface Science Reports,* 48**,** 53-229.

DION, M. & PARKER, W. 2013. Steam Sterilization Principles. *Pharmaceutical Engineering,* 33.

DM, B. 2001. *Mechanical, Thermal, Chemical and Electrochemical Surface Treatment of Titanium,* Berlin Heidelberg, Springer-Verlang.

DOHAN EHRENFEST, D. M., COELHO, P. G., KANG, B.-S., SUL, Y.-T. & ALBREKTSSON, T. 2010. Classification of osseointegrated implant surfaces: materials, chemistry and topography. *Trends Biotechnol,* 28**,** 198-206.

DONDOSSOLA, E., HOLZAPFEL, B. M., ALEXANDER, S., FILIPPINI, S., HUTMACHER, D. W. & FRIEDL, P. 2016. Examination of the foreign body response to biomaterials by nonlinear intravital microscopy. *Nature Biomedical Engineering,* 1**,** 0007.

DONLAN, R. M. 2001. Biofilm Formation: A Clinically Relevant Microbiological Process. *Clinical Infectious Diseases,* 33**,** 1387-1392.

EL-WASSEFY, N., EL-FALLAL, A. & TAHA, M. 2014. Effect of different sterilization modes on the surface morphology, ion release, and bone reaction of retrieved micro-implants. *Angle Orthod,* 85**,** 39-47.

ELIAS, C. N., OSHIDA, Y., LIMA, J. H. C. & MULLER, C. A. 2008. Relationship between surface properties (roughness, wettability and morphology) of titanium and dental implant removal torque. *Biological Materials Science,* 1**,** 234-242.

ELLINGSEN, J. E., THOMSEN, P. & LYNGSTADAAS, S. P. 2006a. Advances in dental implant materials and tissue regeneration. *Periodontol 2000,* 41**,** 136-56.

ELLINGSEN, J. E., THOMSEN, P. & LYNGSTADAAS, S. P. 2006b. Advances in dental implant materials and tissue regeneration. *Periodontol 2000,* 41**,** 136-156.

ENGEL, A. & REICHELT, R. 1984. Imaging of biological structures with the scanning transmission electron microscope. *Journal of Ultrastructure Research,* 88**,** 105-120.

EVERAERT, E. P., MAHIEU, H. F., WONG CHUNG, R. P., VERKERKE, G. J., VAN DER MEI, H. C. & BUSSCHER, H. J. 1997. A new method for in vivo evaluation of biofilms on surface-modified silicone rubber voice prostheses. *Eur Arch Otorhinolaryngol,* 254**,** 261-3.

FADEEVA, E., TRUONG, V. K., STIESCH, M., CHICHKOV, B. N., CRAWFORD, R. J., WANG, J. & IVANOVA, E. P. 2011. Bacterial Retention on Superhydrophobic Titanium Surfaces Fabricated by Femtosecond Laser Ablation. *Langmuir,* 27**,** 3012-3019.

FENG, B., CHEN, J. Y., QI, S. K., HE, L., ZHAO, J. Z. & ZHANG, X. D. 2002. Characterization of surface oxide films on titanium and bioactivity. *Journal of Materials Science: Materials in Medicine,* 13**,** 457-464.

FENG, Q. L., WU, J., CHEN, G. Q., CUI, F. Z., KIM, T. N. & KIM, J. O. 2000a. A mechanistic study of the antibacterial effect of silver ions on Escherichia coli and Staphylococcus aureus. *J Biomed Mater Res,* 52**,** 662-8.

FENG, Q. L., WU, J., CHEN, G. Q., CUI, F. Z., KIM, T. N. & KIM, J. O. 2000b. A mechanistic study of the antibacterial effect of silver ions on Escherichia coli and Staphylococcus aureus. *Journal of Biomedical Materials Research,* 52**,** 662-668.

FERNÁNDEZ-LIMA, F., BAPTISTA, D. L., ZUMETA, I., PEDRERO, E., PRIOLI, R., VIGIL, E. & ZAWISLAK, F. C. 2002. Structural analysis of TiO2 films grown using microwave-activated chemical bath deposition. *Thin Solid Films,* 419**,** 65-68.

FERRARIS, S. & SPRIANO, S. 2016. Antibacterial titanium surfaces for medical implants. *Materials Science and Engineering: C,* 61**,** 965-978.

FERRARIS, S., VENTURELLO, A., MIOLA, M., COCHIS, A., RIMONDINI, L. & SPRIANO, S. 2014. Antibacterial and bioactive nanostructured titanium surfaces for bone integration. *Applied Surface Science,* 311**,** 279-291.

FICAI, D. & FICAI, A. 2017. 7 - Prevention of biofilm formation by material modification A2 - Deng, Ying. *In:* LV, W. (ed.) *Biofilms and Implantable Medical Devices.* Woodhead Publishing.

FITZGERALD, J. R. 2014. Evolution of Staphylococcus aureus during human colonization and infection. *Infection, Genetics and Evolution*.

FORDHAM, R., SKINNER, J., WANG, X., NOLAN, J. & GROUP, T. E. P. O. S. 2012. The economic benefit of hip replacement: a 5-year follow-up of costs and outcomes in the Exeter Primary Outcomes Study. *BMJ Open,* 2.

FOWLER, T., WANN, E. R., JOH, D., JOHANSSON, S., FOSTER, T. J. & HOOK, M. 2000. Cellular invasion by Staphylococcus aureus involves a fibronectin bridge between the bacterial fibronectin-binding MSCRAMMs and host cell beta1 integrins. *Eur J Cell Biol,* 79**,** 672-9.

FRAKER, A., RUFF, A., SUNG, P., VAN ORDEN, A. & SPECK, K. 1983. Surface preparation and corrosion behavior of titanium alloys for surgical implants. *Titanium alloys in surgical implants.* ASTM International.

FRANZ, S., RAMMELT, S., SCHARNWEBER, D. & SIMON, J. C. Immune responses to implants â€“ A review of the implications for the design of immunomodulatory biomaterials. *Biomaterials,* 32**,** 6692-6709.

FRÖHLICH, E. 2012. The role of surface charge in cellular uptake and cytotoxicity of medical nanoparticles. *International journal of nanomedicine,* 7**,** 5577-5591.

GAGGL, A., SCHULTES, G., MÃ¼LLER, W. D. & KÃ¤RCHER, H. 2000. Scanning electron microscopical analysis of laser-treated titanium implant surfaces-a comparative study. *Biomaterials,* 21**,** 1067-1073.

GAHARWAR, A. K., DETAMORE, M. S. & KHADEMHOSSEINI, A. 2016. Emerging Trends in Biomaterials Research. *Ann Biomed Eng,* 44**,** 1861-1862.

GALLO, J., HOLINKA, M. & MOUCHA, C. S. 2014. Antibacterial surface treatment for orthopaedic implants. *Int J Mol Sci,* 15**,** 13849-80.

GAO, G., LANGE, D., HILPERT, K., KINDRACHUK, J., ZOU, Y., CHENG, J. T. J., KAZEMZADEH-NARBAT, M., YU, K., WANG, R., STRAUS, S. K., BROOKS, D. E., CHEW, B. H., HANCOCK, R. E. W. & KIZHAKKEDATHU, J. N. 2011. The biocompatibility and biofilm resistance of implant coatings based on hydrophilic polymer brushes conjugated with antimicrobial peptides. *Biomaterials,* 32**,** 3899-3909.

GARCÍA, R. & BÁEZ, A. 2011. Atomic Absorption Spectrometry (AAS). *Atomic Absorption Spectroscopy***,** 1.

GEETHA, M., SINGH, A. K., ASOKAMANI, R. & GOGIA, A. K. 2009a. Ti based biomaterials, the ultimate choice for orthopaedic implants Ã¢â‚¬â€œ A review. *Progress in Materials Science,* 54**,** 397-425.

GEETHA, M., SINGH, A. K., ASOKAMANI, R. & GOGIA, A. K. 2009b. Ti based biomaterials, the ultimate choice for orthopaedic implants â€“ A review. *Progress in Materials Science,* 54**,** 397-425.

GIAVARESI, G., FINI, M., CIGADA, A., CHIESA, R., RONDELLI, G., RIMONDINI, L., TORRICELLI, P., ALDINI, N. N. & GIARDINO, R. 2003. Mechanical and histomorphometric evaluations of titanium implants with different surface treatments inserted in sheep cortical bone. *Biomaterials,* 24**,** 1583-1594.

GILBERT, P., DAS, J. & FOLEY, I. 1997. Biofilm susceptibility to antimicrobials. *Adv Dent Res,* 11**,** 160-7.

GILMORE, B. F., HAMILL, T. M., JONES, D. S. & GORMAN, S. P. 2010. Validation of the CDC biofilm reactor as a dynamic model for assessment of encrustation formation on urological device materials. *Journal of Biomedical Materials Research Part B: Applied Biomaterials,* 93B**,** 128-140.

GITTENS, R. A., MCLACHLAN, T., OLIVARES-NAVARRETE, R., CAI, Y., BERNER, S., TANNENBAUM, R., SCHWARTZ, Z., SANDHAGE, K. H. & BOYAN, B. D. 2011. The effects of combined micron-/submicron-scale surface roughness and nanoscale features on cell proliferation and differentiation. *Biomaterials,* 32**,** 3395-3403.

GLINEL, K., THEBAULT, P., HUMBLOT, V., PRADIER, C. M. & JOUENNE, T. 2012. Antibacterial surfaces developed from bio-inspired approaches. *Acta Biomaterialia,* 8**,** 1670-1684.

GOERES, D. M., LOETTERLE, L. R., HAMILTON, M. A., MURGA, R., KIRBY, D. W. & DONLAN, R. M. 2005. Statistical assessment of a laboratory method for growing biofilms. *Microbiology,* 151**,** 757-762.

GÖKÇEN, A., VILCINSKAS, A. & WIESNER, J. 2013. Methods to identify enzymes that degrade the main extracellular polysaccharide component of Staphylococcus epidermidis biofilms. *Virulence,* 4**,** 260-270.

GORTH, D. J., PUCKETT, S., ERCAN, B., WEBSTER, T. J., RAHAMAN, M. & BAL, B. S. 2012. Decreased bacteria activity on Si(3)N(4) surfaces compared with PEEK or titanium. *International journal of nanomedicine,* 7**,** 4829-4840.

GREULICH, C., BRAUN, D., PEETSCH, A., DIENDORF, J., SIEBERS, B., EPPLE, M. & KOLLER, M. 2012. The toxic effect of silver ions and silver nanoparticles towards bacteria and human cells occurs in the same concentration range. *RSC Advances,* 2**,** 6981-6987.

GRISTINA, A. 2004a. Biomaterial-centered infection: microbial adhesion versus tissue integration. 1987. *Clinical orthopaedics and related research***,** 4-12.

GRISTINA, A. 2004b. Biomaterial-centered infection: microbial adhesion versus tissue integration. 1987. *Clin Orthop Relat Res***,** 4-12.

GRISTINA, A. G. 1987. Biomaterial-centered infection: microbial adhesion versus tissue integration. *Science,* 237**,** 1588-95.

GRISTINA, A. G., HOBGOOD, C. D., WEBB, L. X. & MYRVIK, Q. N. 1987. Adhesive colonization of biomaterials and antibiotic resistance. *Biomaterials,* 8**,** 423-6.

GUTWEIN, L. G. & WEBSTER, T. J. 2004. Increased viable osteoblast density in the presence of nanophase compared to conventional alumina and titania particles. *Biomaterials,* 25**,** 4175-4183.

GYÖRGYEY, Á., UNGVÁRI, K., KECSKEMÉTI, G., KOPNICZKY, J., HOPP, B., OSZKÓ, A., PELSÖCZI, I., RAKONCZAY, Z., NAGY, K. & TURZÓ, K. 2013. Attachment and proliferation of human osteoblast-like cells (MG-63) on laser-ablated titanium implant material. *Materials Science and Engineering: C,* 33**,** 4251-4259.

HABIBOVIC, P. & BARRALET, J. E. 2011. Bioinorganics and biomaterials: Bone repair. *Acta Biomaterialia,* 7**,** 3013-3026.

HAFNER, A., LOVRIĆ, J., LAKOŠ, G. P. & PEPIĆ, I. 2014. Nanotherapeutics in the EU: an overview on current state and future directions. *Int J Nanomedicine,* 9**,** 1005-1023.

HALLAB, N., MERRITT, K. & JACOBS, J. J. 2001. Metal Sensitivity in Patients with Orthopaedic Implants. *The Journal of Bone and Joint Surgery (American),* 83**,** 428-428.

HAMADA, K., KON, M., HANAWA, T., YOKOYAMA, K. I., MIYAMOTO, Y. & ASAOKA, K. 2002. Hydrothermal modification of titanium surface in calcium solutions. *Biomaterials,* 23**,** 2265-2272.

HAMDAN, M., BLANCO, L., KHRAISAT, A. & TRESGUERRES, I. F. 2006. Influence of titanium surface charge on fibroblast adhesion. *Clin Implant Dent Relat Res,* 8**,** 32-38.

HANAWA, T. 2004. Metal ion release from metal implants. *Materials Science and Engineering: C,* 24**,** 745-752.

HANSON, S. 2016. Blood–material Interactions. *Handbook of Biomaterial Properties.* Springer.

HAVRDOVA, M., POLAKOVA, K., SKOPALIK, J., VUJTEK, M., MOKDAD, A., HOMOLKOVA, M., TUCEK, J., NEBESAROVA, J. & ZBORIL, R. 2014. Field emission scanning electron microscopy (FE-SEM) as an approach for nanoparticle detection inside cells. *Micron,* 67**,** 149-154.

HE, H. W., LIU, M. L., ZHU, Z. L., YANG, M. Z., LI, Q. L. & CHEN, Z. Q. 2008. Influence of surface morphology of cpTi on the adsorption and attachment of collagen/chitosan. *Applied Surface Science,* 255**,** 509-511.

HE, L., ZHANG, X. & TONG, C. 2006. Surface modification of pure titanium treated with B4C at high temperature. *Surface and Coatings Technology,* 200**,** 3016-3020.

HEALY, K. & DUCHEYNE, P. 1993. Passive dissolution kinetics of titanium in vitro. *Journal of Materials Science: Materials in Medicine,* 4**,** 117-126.

HENCH, L. & WILSON, J. 1984. Surface-active biomaterials. *Science,* 226**,** 630-636.

HENCH, L. L. 1980. Biomaterials. *Science,* 208**,** 826-31.

HENCH, L. L. 1998. Biomaterials: a forecast for the future. *Biomaterials,* 19**,** 1419-1423.

HENCH, L. L. & POLAK, J. M. 2002. Third-generation biomedical materials. *Science,* 295**,** 1014-7.

HENCH, L. L. & THOMPSON, I. 2010. *Twenty-first century challenges for biomaterials*.

HENDRIKS, M. & CAHALAN, P. 2016. Historical Perspectives on Biomedical Coatings in Medical Devices. *Medical Coatings and Deposition Technologies***,** 1-25.

HETRICK, E. M. & SCHOENFISCH, M. H. 2006. Reducing implant-related infections: active release strategies. *Chemical Society Reviews,* 35**,** 780-789.

HILAL, N., BOWEN, W. R., ALKHATIB, L. & OGUNBIYI, O. 2006. A Review of Atomic Force Microscopy Applied to Cell Interactions with Membranes. *Chemical Engineering Research and Design,* 84**,** 282-292.

HOLZAPFEL, B. M., REICHERT, J. C., SCHANTZ, J.-T., GBURECK, U., RACKWITZ, L., NÖTH, U., JAKOB, F., RUDERT, M., GROLL, J. & HUTMACHER, D. W. 2013. How smart do biomaterials need to be? A translational science and clinical point of view. *Advanced Drug Delivery Reviews,* 65**,** 581-603.

HOWLETT, C. R., ZREIQAT, H., WU, Y., MCFALL, D. W. & MCKENZIE, D. R. 1999. Effect of ion modification of commonly used orthopedic materials on the attachment of human bone-derived cells. *Journal of biomedical materials research,* 45**,** 345-354.

HU, H., ZHANG, W., QIAO, Y., JIANG, X., LIU, X. & DING, C. 2011. Antibacterial activity and increased bone marrow stem cell functions of Zn-incorporated TiO2 coatings on titanium. *Acta Biomaterialia,* 8**,** 904-915.

HU, H., ZHANG, W., QIAO, Y., JIANG, X., LIU, X. & DING, C. 2012. Antibacterial activity and increased bone marrow stem cell functions of Zn-incorporated TiO2 coatings on titanium. *Acta Biomaterialia,* 8**,** 904-915.

HUANG, N., YANG, P., LENG, Y., WANG, J., SUN, H., CHEN, J. & WAN, G. 2004. Surface modification of biomaterials by plasma immersion ion implantation. *Surface and Coatings Technology,* 186**,** 218-226.

HUEBSCH, N. & MOONEY, D. J. 2009. Inspiration and application in the evolution of biomaterials. *Nature,* 462**,** 426-32.

HUTMACHER, D. W. 2006. Regenerative medicine will impact, but not replace, the medical device industry. *Expert Review of Medical Devices,* 3**,** 409-412.

IONITA, D., GRECU, M., UNGUREANU, C. & DEMETRESCU, I. 2011a. Antimicrobial activity of the surface coatings on TiAlZr implant biomaterial. *Journal of bioscience and bioengineering,* 112**,** 630-634.

IONITA, D., GRECU, M., UNGUREANU, C. & DEMETRESCU, I. 2011b. Modifying the TiAlZr biomaterial surface with coating, for a better anticorrosive and antibacterial performance. *Applied Surface Science,* 257**,** 9164-9168.

ISKANDAR, M. E., CIPRIANO, A. F., LOCK, J., GOTT, S. C., RAO, M. P. & HUINAN, L. Improved bone marrow stromal cell adhesion on micropatterned Titanium surfaces. Engineering in Medicine and Biology Society (EMBC), 2012 Annual International Conference of the IEEE, Aug. 28 2012-Sept. 1 2012. 5666-5669.

ISKANDAR, M. E., CIPRIANO, A. F., LOCK, J., GOTT, S. C., RAO, M. P. & LIU, H. 2012. Improved bone marrow stromal cell adhesion on micropatterned titanium surfaces. *Conf Proc IEEE Eng Med Biol Soc,* 2012**,** 5666-9.

JAFARI, S. M., COYLE, C., MORTAZAVI, S. M. J., SHARKEY, P. F. & PARVIZI, J. 2010. Revision Hip Arthroplasty Infection is the Most Common Cause of Failure. *Clinical orthopaedics and related research,* 468**,** 2046-2051.

JALAL, R., GOHARSHADI, E. K., ABARESHI, M., MOOSAVI, M., YOUSEFI, A. & NANCARROW, P. 2010. ZnO nanofluids: green synthesis, characterization, and antibacterial activity. *Materials Chemistry and Physics,* 121**,** 198-201.

JALILI, N. & LAXMINARAYANA, K. 2004. A review of atomic force microscopy imaging systems: application to molecular metrology and biological sciences. *Mechatronics,* 14**,** 907-945.

JAMBURE, S. B., PATIL, S. J., DESHPANDE, A. R. & LOKHANDE, C. D. 2014. A comparative study of physico-chemical properties of CBD and SILAR grown ZnO thin films. *Materials Research Bulletin,* 49**,** 420-425.

JAMUNA-THEVI, K., BAKAR, S. A., IBRAHIM, S., SHAHAB, N. & TOFF, M. R. M. 2011. Quantification of silver ion release, in vitro cytotoxicity and antibacterial properties of nanostuctured Ag doped TiO2 coatings on stainless steel deposited by RF magnetron sputtering. *Vacuum,* 86**,** 235-241.

JANDT, K. D. 2007. Evolutions, Revolutions and Trends in Biomaterials Science ? A Perspective. *Advanced Engineering Materials,* 9**,** 1035-1050.

JANSSEN, D., DE PALMA, R., VERLAAK, S., HEREMANS, P. & DEHAEN, W. 2006. Static solvent contact angle measurements, surface free energy and wettability determination of various self-assembled monolayers on silicon dioxide. *Thin Solid Films,* 515**,** 1433-1438.

JEFFERSON, K. K. 2004a. What drives bacteria to produce a biofilm? *FEMS microbiology letters,* 236**,** 163-173.

JEFFERSON, K. K. 2004b. What drives bacteria to produce a biofilm? *FEMS Microbiol Lett,* 236**,** 163-73.

JEONG, K. S., CH, C., SEDLMAYR, E. & SÜLZLE, D. 2000. Electronic structure investigation of neutral titanium oxide molecules Ti x O y. *Journal of Physics B: Atomic, Molecular and Optical Physics,* 33**,** 3417.

JIANG, Z., DAI, X. & MIDDLETON, H. 2011. Investigation on passivity of titanium under steady-state conditions in acidic solutions. *Materials Chemistry and Physics,* 126**,** 859-865.

JIN, G., QIN, H., CAO, H., QIAN, S., ZHAO, Y., PENG, X., ZHANG, X., LIU, X. & CHU, P. K. 2014. Synergistic effects of dual Zn/Ag ion implantation in osteogenic activity and antibacterial ability of titanium. *Biomaterials,* 35**,** 7699-7713.

JIN, G., QIN, H., CAO, H., QIAO, Y., ZHAO, Y., PENG, X., ZHANG, X., LIU, X. & CHU, P. K. 2015. Zn/Ag micro-galvanic couples formed on titanium and osseointegration effects in the presence of S. aureus. *Biomaterials,* 65**,** 22-31.

JIRAVOVA, J., TOMANKOVA, K. B., HARVANOVA, M., MALINA, L., MALOHLAVA, J., LUHOVA, L., PANACEK, A., MANISOVA, B. & KOLAROVA, H. 2016. The effect of silver nanoparticles and silver ions on mammalian and plant cells in vitro. *Food and Chemical Toxicology,* 96**,** 50-61.

JONÁŠOVÁ, L., MÜLLER, F. A., HELEBRANT, A., STRNAD, J. & GREIL, P. 2002. Hydroxyapatite formation on alkali-treated titanium with different content of Na+ in the surface layer. *Biomaterials,* 23**,** 3095-3101.

JONÁŠOVÁ, L., MÜLLER, F. A., HELEBRANT, A., STRNAD, J. & GREIL, P. 2004. Biomimetic apatite formation on chemically treated titanium. *Biomaterials,* 25**,** 1187-1194.

JONES, F. H. 2001. Teeth and bones: applications of surface science to dental materials and related biomaterials. *Surface Science Reports,* 42**,** 79-205.

JONES, N., RAY, B., RANJIT, K. T. & MANNA, A. C. 2008. Antibacterial activity of ZnO nanoparticle suspensions on a broad spectrum of microorganisms. *FEMS microbiology letters,* 279**,** 71-76.

JOOB-FANCSALY, A., HUSZAR, T., DIVINYI, T., ROSIVALL, L. & SZABO, G. 2004. [The effect of the surface morphology of Ti-implants on the proliferation activity of fibroblasts and osteoblasts]. *Fogorv Sz,* 97**,** 251-5.

JOSEPH, L. A., ISRAEL, O. K. & EDET, E. J. 2009a. Comparative evaluation of metal ions release from titanium and Ti-6Al-7Nb into bio-fluids. *Dental Research Journal,* 6.

JOSEPH, L. A., ISRAEL, O. K. & EDET, E. J. 2009b. Comparative Evaluation of Metal Ions Release from Titanium and Ti-6Al-7Nb into Bio-Fluids. *Dental Research Journal,* 6**,** 7-11.

JUAN, L., ZHIMIN, Z., ANCHUN, M., LEI, L. & JINGCHAO, Z. 2010. Deposition of silver nanoparticles on titanium surface for antibacterial effect. *International journal of nanomedicine,* 5**,** 261-267.

KAKABOURA, A., FRAGOULI, M., RAHIOTIS, C. & SILIKAS, N. 2007. Evaluation of surface characteristics of dental composites using profilometry, scanning electron, atomic force microscopy and gloss-meter. *Journal of Materials Science: Materials in Medicine,* 18**,** 155-163.

KANG, M.-K., MOON, S.-K., KWON, J.-S., KIM, K.-M. & KIM, K.-N. 2012. Antibacterial effect of sand blasted, large-grit, acid-etched treated Ti–Ag alloys. *Materials Research Bulletin,* 47**,** 2952-2955.

KARLSSON, M., PÅLSGÅRD, E., WILSHAW, P. R. & DI SILVIO, L. 2003. Initial in vitro interaction of osteoblasts with nano-porous alumina. *Biomaterials,* 24**,** 3039-3046.

KASEMETS, K., IVASK, A., DUBOURGUIER, H.-C. & KAHRU, A. 2009. Toxicity of nanoparticles of ZnO, CuO and TiO 2 to yeast Saccharomyces cerevisiae. *Toxicology in vitro,* 23**,** 1116-1122.

KAWAHARA, H., SOEDA, Y., NIWA, K., TAKAHASHI, M., KAWAHARA, D. & ARAKI, N. 2004. In vitro study on bone formation and surface topography from the standpoint of biomechanics. *Journal of materials science.Materials in medicine,* 15**,** 1297-1307.

KELLY, E. J. 1982. Electrochemical behavior of titanium. *Modern aspects of electrochemistry.* Springer.
KHAN, M. R., DONOS, N., SALIH, V. & BRETT, P. M. 2011. The enhanced modulation of key bone matrix components by modified Titanium implant surfaces. *Bone,* 50**,** 1-8.
KIM, H., MIYAJI, F., KOKUBO, T. & NAKAMURA, T. 1997a. Effect of heat treatment on apatite-forming ability of Ti metal induced by alkali treatment. *Journal of Materials Science: Materials in Medicine,* 8**,** 341-347.
KIM, H. M., MIYAJI, F., KOKUBO, T. & NAKAMURA, T. 1996. Preparation of bioactive Ti and its alloys via simple chemical surface treatment. *Journal of Biomedical Materials Research,* 32**,** 409-417.
KIM, H. M., MIYAJI, F., KOKUBO, T. & NAKAMURA, T. 1997b. Effect of heat treatment on apatite-forming ability of Ti metal induced by alkali treatment. *Journal of Materials Science: Materials in Medicine,* 8**,** 341-347.
KIM, H. M., MIYAJI, F., KOKUBO, T. & NAKAMURA, T. 1997c. Effect of heat treatment on apatite-forming ability of Ti metal induced by alkali treatment. *Journal of materials science.Materials in medicine,* 8**,** 341-347.
KIM, K. H. & RAMASWAMY, N. 2009. Electrochemical surface modification of titanium in dentistry. *Dental Materials Journal,* 28**,** 20-36.
KIM, S. 2008. Changes in surgical loads and economic burden of hip and knee replacements in the US: 1997–2004. *Arthritis Care & Research,* 59**,** 481-488.
KITTEL, C. 2008. *Introduction to Solid State Physics,* Hoboken, NJ, Wiley.
KIZUKI, T., TAKADAMA, H., MATSUSHITA, T., NAKAMURA, T. & KOKUBO, T. 2010. Preparation of bioactive Ti metal surface enriched with calcium ions by chemical treatment. *Acta Biomaterialia,* 6**,** 2836-2842.
KOH, J.-W., YANG, J.-H., HAN, J.-S., LEE, J.-B. & KIM, S.-H. 2009. Biomechanical evaluation of dental implants with different surfaces: Removal torque and resonance frequency analysis in rabbits. *The Journal of Advanced Prosthodontics,* 1**,** 107-112.
KOHLES, S. S., CLARK, M. B., BROWN, C. A. & KENEALY, J. N. 2004. Direct assessment of profilometric roughness variability from typical implant surface types. *Int J Oral Maxillofac Implants,* 19**,** 510-6.
KOKUBO, T., MIYAJI, F., KIM, H. M. & NAKAMURA, T. 1996. Spontaneous formation of bonelike apatite layer on chemically treated titanium metals. *Journal of the American Ceramic Society,* 79**,** 1127-1129.
KOKUBO, T., PATTANAYAK, D. K., YAMAGUCHI, S., TAKADAMA, H., MATSUSHITA, T., KAWAI, T., TAKEMOTO, M., FUJIBAYASHI, S. & NAKAMURA, T. 2010. Positively charged bioactive Ti metal prepared by simple chemical and heat treatments. *Journal of the Royal Society, Interface / the Royal Society,* 7 Suppl 5**,** S503-13.
KOKUBO, T. & TAKADAMA, H. 2006. How useful is SBF in predicting in vivo bone bioactivity? *Biomaterials,* 27**,** 2907-2915.
KOSTENUIK, P., SANCHEZ-SWEATMAN, O., ORR, F. W. & SINGH, G. 1996. Bone cell matrix promotes the adhesion of human prostatic carcinoma cells via the α2β1 integrin. *Clinical & Experimental Metastasis,* 14**,** 19-26.
KU, Y., CHUNG, C.-P. & JANG, J.-H. 2005. The effect of the surface modification of titanium using a recombinant fragment of fibronectin and vitronectin on cell behavior. *Biomaterials,* 26**,** 5153-5157.
KULKARNI, M., MAZARE, A., SCHMUKI, P. & IGLIČ, A. 2014. Biomaterial surface modification of titanium and titanium alloys for medical applications. *Nanomedicine,* 5**,** 112-130.
KULKARNI, M., PATIL-SEN, Y., JUNKAR, I., KULKARNI, C. V., LORENZETTI, M. & IGLIČ, A. 2015. Wettability studies of topologically distinct titanium surfaces. *Colloids and Surfaces B: Biointerfaces,* 129**,** 47-53.
KUMAR, P. S., RAJ, A. D., MANGALARAJ, D. & NATARAJ, D. 2008. Growth and characterization of ZnO nanostructured thin films by a two step chemical method. *Applied Surface Science,* 255**,** 2382-2387.

KURODA, D., NIINOMI, M., MORINAGA, M., KATO, Y. & YASHIRO, T. 1998. Design and mechanical properties of new Î² type titanium alloys for implant materials. *Materials Science and Engineering: A,* 243**,** 244-249.

KURTZ, S. M., LAU, E., SCHMIER, J., ONG, K. L., ZHAO, K. & PARVIZI, J. 2008. Infection Burden for Hip and Knee Arthroplasty in the United States. *Journal of Arthroplasty,* 23**,** 984-991.

KURTZ, S. M., LAU, E., WATSON, H., SCHMIER, J. K. & PARVIZI, J. 2012. Economic Burden of Periprosthetic Joint Infection in the United States. *J Arthroplasty,* 27**,** 61-65.e1.

KURTZ, S. M., ONG, K. L., SCHMIER, J., MOWAT, F., SALEH, K., DYBVIK, E., KÄRRHOLM, J., GARELLICK, G., HAVELIN, L. I., FURNES, O., MALCHAU, H. & LAU, E. 2007. Future clinical and economic impact of revision total hip and knee arthroplasty. *Journal of Bone and Joint Surgery - Series A,* 89**,** 144-151.

LACEFIELD, W. R. 1999. Materials Characteristics of Uncoated/Ceramic-Coated Implant Materials. *Advances in Dental Research,* 13**,** 21-26.

LAI, H.-C., ZHUANG, L.-F., LIU, X., WIELAND, M., ZHANG, Z.-Y. & ZHANG, Z.-Y. 2010. The influence of surface energy on early adherent events of osteoblast on titanium substrates. *Journal of Biomedical Materials Research Part A,* 93A**,** 289-296.

LAMAGNI, T. 2014. Epidemiology and burden of prosthetic joint infections. *Journal of Antimicrobial Chemotherapy,* 69**,** i5-i10.

LANDOLT, D., CHAUVY, P. F. & ZINGER, O. 2003. Electrochemical micromachining, polishing and surface structuring of metals: fundamental aspects and new developments. *Electrochimica Acta,* 48**,** 3185-3201.

LANGER, R. & PEPPAS, N. A. 2003. Advances in biomaterials, drug delivery, and bionanotechnology. *AIChE Journal,* 49**,** 2990-3006.

LARRY L. HENCH, S. M. B. 2013. A History of Biomaterials. *In:* LEMONS, B. D. R., ALLAN S. HOFFMAN, FREDERICK J. SCHOEN, JACK E. (ed.) *Biomaterials Science (Third Edition).* Academic Press.

LARSSON, C., THOMSEN, P., ARONSSON, B. O., RODAHL, M., LAUSMAA, J., KASEMO, B. & ERICSON, L. E. 1996. Bone response to surface-modified titanium implants: studies on the early tissue response to machined and electropolished implants with different oxide thicknesses. *Biomaterials,* 17**,** 605-616.

LATOUR, R. A., JR. & BLACK, J. 1992. Development of FRP composite structural biomaterials: ultimate strength of the fiber/matrix interfacial bond in in vivo simulated environments. *J Biomed Mater Res,* 26**,** 593-606.

LAUSMAA, J. 2001. Mechanical, Thermal, Chemical and Electrochemical Surface Treatment of Titanium. *Titanium in Medicine.* Springer Berlin Heidelberg.

LAVENUS, S., LOUARN, G. & LAYROLLE, P. 2010. Nanotechnology and dental implants. *International journal of biomaterials,* 2010**,** 915327.

LE GUEHENNEC, L., LOPEZ-HEREDIA, M. A., ENKEL, B., WEISS, P., AMOURIQ, Y. & LAYROLLE, P. 2008. Osteoblastic cell behaviour on different titanium implant surfaces. *Acta Biomater,* 4**,** 535-43.

LE GUEHENNEC, L., SOUEIDAN, A., LAYROLLE, P. & AMOURIQ, Y. 2007. Surface treatments of titanium dental implants for rapid osseointegration. *Dent Mater,* 23**,** 844-54.

LE GUÉHENNEC, L., SOUEIDAN, A., LAYROLLE, P. & AMOURIQ, Y. 2007. Surface treatments of titanium dental implants for rapid osseointegration. *Dental Materials,* 23**,** 844-854.

LE OUAY, B. & STELLACCI, F. 2015. Antibacterial activity of silver nanoparticles: A surface science insight. *Nano Today,* 10**,** 339-354.

LEE, B. A., KANG, C. H., VANG, M. S., JUNG, Y. S., PIAO, X. H., KIM, O. S., CHUNG, H. J. & KIM, Y. J. 2012. Surface characteristics and osteoblastic cell response of alkali-and heat-treated titanium-8tantalum-3niobium alloy. *J Periodontal Implant Sci,* 42**,** 248-55.

LEE, K. & YOO, D. 2015. Large-area sodium titanate nanorods formed on titanium surface via NaOH alkali treatment. *Archives of Metallurgy and Materials,* 60**,** 1371-1374.

LEE, S.-B., OTGONBAYAR, U., LEE, J.-H., KIM, K.-M. & KIM, K.-N. 2010a. Silver ion-exchanged sodium titanate and resulting effect on antibacterial efficacy. *Surface and Coatings Technology,* 205, Supplement 1**,** S172-S176.

LEE, Y.-H., BHATTARAI, G., ARYAL, S., LEE, N.-H., LEE, M.-H., KIM, T.-G., JHEE, E.-C., KIM, H.-Y. & YI, H.-K. 2010b. Modified titanium surface with gelatin nano gold composite increases osteoblast cell biocompatibility. *Applied Surface Science,* 256**,** 5882-5887.

LI, M., ZHU, L. & LIN, D. 2011. Toxicity of ZnO nanoparticles to Escherichia coli: mechanism and the influence of medium components. *Environ Sci Technol,* 45**,** 1977-1983.

LI, N., ZHANG, L., CHEN, Y., FANG, M., ZHANG, J. & WANG, H. 2012. Highly Efficient, Irreversible and Selective Ion Exchange Property of Layered Titanate Nanostructures. *Advanced Functional Materials,* 22**,** 835-841.

LINCKS, J., BOYAN, B. D., BLANCHARD, C. R., LOHMANN, C. H., LIU, Y., COCHRAN, D. L., DEAN, D. D. & SCHWARTZ, Z. 1998. Response of MG63 osteoblast-like cells to titanium and titanium alloy is dependent on surface roughness and composition. *Biomaterials,* 19**,** 2219-2232.

LINDEQUE, B., HARTMAN, Z., NOSHCHENKO, A. & CRUSE, M. 2014. Infection after primary total hip arthroplasty. *Orthopedics,* 37**,** 257-65.

LINDQVIST, C. & SLATIS, P. 1985. Dental bacteremia--a neglected cause of arthroplasty infections? Three hip cases. *Acta Orthop Scand,* 56**,** 506-8.

LINDQVIST, R. 2006. Estimation of Staphylococcus aureus Growth Parameters from Turbidity Data: Characterization of Strain Variation and Comparison of Methods. *Appl Environ Microbiol,* 72**,** 4862-4870.

LIPOVSKY, A., NITZAN, Y., GEDANKEN, A. & LUBART, R. 2011. Antifungal activity of ZnO nanoparticles—the role of ROS mediated cell injury. *Nanotechnology,* 22**,** 105101.

LIU, F., SONG, Y., WANG, F., SHIMIZU, T., IGARASHI, K. & ZHAO, L. 2005a. Formation characterization of hydroxyapatite on titanium by microarc oxidation and hydrothermal treatment. *Journal of bioscience and bioengineering,* 100**,** 100-104.

LIU, X., CHU, P. K. & DING, C. 2004. Surface modification of titanium, titanium alloys, and related materials for biomedical applications. *Materials Science and Engineering: R: Reports,* 47**,** 49-121.

LIU, Y., DE GROOT, K. & HUNZIKER, E. B. 2005b. BMP-2 liberated from biomimetic implant coatings induces and sustains direct ossification in an ectopic rat model. *Bone,* 36**,** 745-757.

LOSINA, E., BARRETT, J., MAHOMED, N. N., BARON, J. A. & KATZ, J. N. 2004. Early failures of total hip replacement: Effect of surgeon volume. *Arthritis & Rheumatism,* 50**,** 1338-1343.

LOZA-CORREA, M. & RAMÍREZ-ARCOS, S. 2017. 8 - Detection of bacterial adherence and biofilm formation on medical surfaces A2 - Deng, Ying. *In:* LV, W. (ed.) *Biofilms and Implantable Medical Devices.* Woodhead Publishing.

LU, X., ZHAO, Z. & LENG, Y. 2005. Calcium phosphate crystal growth under controlled atmosphere in electrochemical deposition. *Journal of Crystal Growth,* 284**,** 506-516.

LYDEN, J. R. & DELLINGER, E. P. 2016. Surgical site infections. *Hospital Medicine Clinics,* 5**,** 319-333.

M, S. 2000. - The development of the ITI DENTAL IMPLANT SYSTEM. Part 1: A review of the. - *Clin Oral Implants Res. 2000;11 Suppl 1:8-21.***,** T - ppublish.

MACK, D., BECKER, P., CHATTERJEE, I., DOBINSKY, S., KNOBLOCH, J. K. M., PETERS, G., ROHDE, H. & HERRMANN, M. 2004. Mechanisms of biofilm formation in Staphylococcus epidermidis and Staphylococcus aureus: functional molecules, regulatory circuits, and adaptive responses. *International Journal of Medical Microbiology,* 294**,** 203-212.

MADDIKERI, R., TOSATTI, S., SCHULER, M., CHESSARI, S., TEXTOR, M., RICHARDS, R. & HARRIS, L. 2008. Reduced medical infection related bacterial strains adhesion on bioactive RGD modified titanium surfaces: a first step toward cell selective surfaces. *Journal of Biomedical Materials Research Part A,* 84**,** 425-435.

MAHMOOD, M., CASCIANO, D. A., MOCAN, T., IANCU, C., XU, Y., MOCAN, L., IANCU, D. T., DERVISHI, E., LI, Z. & ABDALMUHSEN, M. 2010. Cytotoxicity and biological effects of functional nanomaterials delivered to various cell lines. *Journal of Applied Toxicology,* 30**,** 74-83.

MARAMBIO-JONES, C. & HOEK, E. M. 2010. A review of the antibacterial effects of silver nanomaterials and potential implications for human health and the environment. *Journal of Nanoparticle Research,* 12**,** 1531-1551.

MARKOWSKA, K., GRUDNIAK, A. M. & WOLSKA, K. I. 2013. Silver nanoparticles as an alternative strategy against bacterial biofilms. *Acta Biochimica Polonica,* 60**,** 523-530.

MAUERER, A., HENKEL, M., WELSCH, G., FORST, R., RICHTER, R. & HEIDENAU, F. 2015. Effects of different sterilisation methods on antibacterial Cu–TiO2 coatings. *Surface Engineering,* 31**,** 757-762.

MAVROGENIS, A., DIMITRIOU, R., PARVIZI, J. & BABIS, G. 2009. Biology of implant osseointegration. *J Musculoskelet Neuronal Interact,* 9**,** 61-71.

MCKINLAY, K., SCOTCHFORD, C., GRANT, D., OLIVER, J., KING, J. R. & BROWN, P. D. 2004. Scanning electron microscopy of biomaterials.

MEI, S., WANG, H., WANG, W., TONG, L., PAN, H., RUAN, C., MA, Q., LIU, M., YANG, H., ZHANG, L., CHENG, Y., ZHANG, Y., ZHAO, L. & CHU, P. K. 2014. Antibacterial effects and biocompatibility of titanium surfaces with graded silver incorporation in titania nanotubes. *Biomaterials,* 35**,** 4255-4265.

MENDONÃ§A, G., MENDONÃ§A, D. B. S., ARAGÃ£O, F. J. L. & COOPER, L. F. 2008. Advancing dental implant surface technology â€“ From micron- to nanotopography. *Biomaterials,* 29**,** 3822-3835.

MENDONÇA, G., MENDONÇA, D. B. S., ARAGÃO, F. J. L. & COOPER, L. F. 2008. Advancing dental implant surface technology – From micron- to nanotopography. *Biomaterials,* 29**,** 3822-3835.

MENDONÇA, G., MENDONÇA, D. B. S., SIMÕES, L. G. P., ARAÚJO, A. L., LEITE, E. R., DUARTE, W. R., ARAGÃO, F. J. L. & COOPER, L. F. 2009. The effects of implant surface nanoscale features on osteoblast-specific gene expression. *Biomaterials,* 30**,** 4053-4062.

MENZIES, K. L. & JONES, L. 2010. The Impact of Contact Angle on the Biocompatibility of Biomaterials. *Optometry & Vision Science,* 87**,** 387-399 10.1097/OPX.0b013e3181da863e.

MERRITT, K., HITCHINS, V. M. & NEALE, A. R. 1999. Tissue colonization from implantable biomaterials with low numbers of bacteria. *Journal of Biomedical Materials Research,* 44**,** 261-265.

MIRON, R. J. & BOSSHARDT, D. D. 2016. OsteoMacs: Key players around bone biomaterials. *Biomaterials,* 82**,** 1-19.

MIRON, R. J., ZOHDI, H., FUJIOKA-KOBAYASHI, M. & BOSSHARDT, D. D. 2016. Giant cells around bone biomaterials: Osteoclasts or multi-nucleated giant cells? *Acta Biomaterialia,* 46**,** 15-28.

MIRZA, S. B., DUNLOP, D. G., PANESAR, S. S., NAQVI, S. G., GANGOO, S. & SALIH, S. 2010. Basic science considerations in primary total hip replacement arthroplasty. *The open orthopaedics journal,* 4**,** 169-80.

MOHAMMED, M. T., KHAN, Z. A. & SIDDIQUEE, A. N. 2014. Surface Modifications of Titanium Materials for developing Corrosion Behavior in Human Body Environment: A Review. *Procedia Materials Science,* 6**,** 1610-1618.

MONTALI, A. 2006a. Antibacterial coating systems. *Injury,* 37**,** S81-S86.

MONTALI, A. 2006b. Antibacterial coating systems. *Injury,* 37**,** S81-S86.

MOONEY, D. J. 2016. Engineering the microenvironment with biomaterials. *European Cells and Materials,* 32**,** 17.

MORIARTY, T. F., POULSSON, A. H. C., ROCHFORD, E. T. J. & RICHARDS, R. G. 2011. Bacterial Adhesion and Biomaterial Surfaces A2 - Ducheyne, Paul. *Comprehensive Biomaterials.* Oxford: Elsevier.

MORRA, M. 2006. Biochemical modification of titanium surfaces: peptides and ECM proteins. *Eur Cell Mater,* 12.

MORRA, M., CASSINELLI, C., CASCARDO, G. & BOLLATI, D. 2009. Collagen I-coated titanium surfaces for bone implantation. *Biological Interactions on Materials Surfaces.* Springer.

MORRA, M., CASSINELLI, C., CASCARDO, G., BOLLATI, D. & RODRIGUEZ Y BAENA, R. 2010. Multifunctional implant surfaces: Surface characterization and bone response to acid-etched Ti implants surface-modified by fibrillar collagen I. *Journal of Biomedical Materials Research Part A,* 94**,** 271-279.

MOUSSA, R. M., AWADALLA, M. A., MAREI, M. K. & NASSEF, T. M. 2015. A Computerized Tomographic Data Analysis System to Evaluate the Dental Implant Surface Roughness. *Procedia Computer Science,* 61**,** 472-477.

MURDOCH, D. R., ROBERTS, S. A., FOWLER JR, V. G., JR., SHAH, M. A., TAYLOR, S. L., MORRIS, A. J. & COREY, G. R. 2001. Infection of orthopedic prostheses after Staphylococcus aureus bacteremia. *Clinical infectious diseases : an official publication of the Infectious Diseases Society of America,* 32**,** 647-9.

MUSA, M., KANNAN, T. P. & MUSTAFA, S. 2013. Cell Proliferation Study of Human Osteosarcoma Cell Line (U2OS) using Alamar Blue Assayand Live Cell Imaging.

NADKARNI, M. A., MARTIN, F. E., JACQUES, N. A. & HUNTER, N. 2002. Determination of bacterial load by real-time PCR using a broad-range (universal) probe and primers set. *Microbiology,* 148**,** 257-266.

NAMBA, R. S., INACIO, M. C. & PAXTON, E. W. 2013. Risk factors associated with deep surgical site infections after primary total knee arthroplasty. *J Bone Joint Surg Am,* 95**,** 775-782.

NANCI, A., WUEST, J. D., PERU, L., BRUNET, P., SHARMA, V., ZALZAL, S. & MCKEE, M. D. 1998. Chemical modification of titanium surfaces for covalent attachment of biological molecules. *Journal of Biomedical Materials Research,* 40**,** 324-335.

NANOMEDICINE–NANOMED, E. 2013. Contribution of nanomedicine to horizon 2020. NanoMedicine European technology platform.

NAYAB, S. N., JONES, F. H. & OLSEN, I. 2005. Effects of calcium ion implantation on human bone cell interaction with titanium. *Biomaterials,* 26**,** 4717-4727.

NEU, T. R. & MARSHALL, K. C. 1990. Bacterial polymers: physicochemical aspects of their interactions at interfaces. *J Biomater Appl,* 5**,** 107-33.

NG, T. S., DESA, M. N. M., SANDAI, D., CHONG, P. P. & THAN, L. T. L. 2016. Growth, biofilm formation, antifungal susceptibility and oxidative stress resistance of Candida glabrata are affected by different glucose concentrations. *Infection, Genetics and Evolution,* 40**,** 331-338.

NIFOROU, K. N., ANAGNOSTOPOULOS, A. K., VOUGAS, K., KITTAS, C., GORGOULIS, V. G. & TSANGARIS, G. T. 2008. The Proteome Profile of the Human Osteosarcoma U2OS Cell Line. *Cancer Genomics - Proteomics,* 5**,** 63-77.

NING, R., WANG, F. & LIN, L. 2016. Biomaterial-based microfluidics for cell culture and analysis. *TrAC Trends in Analytical Chemistry,* 80**,** 255-265.

O'CONNOR, D. T., CHOI, M. G., KWON, S. Y. & SUNG, K. L. P. 2004. New insight into the mechanism of hip prosthesis loosening: effect of titanium debris size on osteoblast function. *Journal of Orthopaedic Research,* 22**,** 229-236.

OCHOA, R. A. T. & MOW, C. S. 2008. Deep infection of a total knee implant as a complication of disseminated pneumococcal sepsis. A case report and review of literature. *The Knee,* 15**,** 144-147.

OH, S.-H., FINÃµNES, R. R., DARAIO, C., CHEN, L.-H. & JIN, S. 2005. Growth of nano-scale hydroxyapatite using chemically treated titanium oxide nanotubes. *Biomaterials,* 26**,** 4938-4943.

OH, S., DARAIO, C., CHEN, L. H., PISANIC, T. R., FINONES, R. R. & JIN, S. 2006. Significantly accelerated osteoblast cell growth on aligned TiO2 nanotubes. *Journal of Biomedical Materials Research Part A,* 78**,** 97-103.

OHTAKI, T., AJIMA, M., ITO, S., ONUMA, M. & OMACHI, A. 2014. Scanning electron microscope. Google Patents.

OKAZAKI, Y. & GOTOH, E. 2008. Metal release from stainless steel, Co–Cr–Mo–Ni–Fe and Ni–Ti alloys in vascular implants. *Corrosion Science,* 50**,** 3429-3438.

OLIVEIRA, D. P., PALMIERI, A., CARINCI, F. & BOLFARINI, C. 2015. Gene expression of human osteoblasts cells on chemically treated surfaces of Ti–6Al–4V–ELI. *Materials Science and Engineering: C,* 51**,** 248-255.

OSHIRO, W., AYUKAWA, Y., ATSUTA, I., FURUHASHI, A., YAMAZOE, J., KONDO, R., SAKAGUCHI, M., MATSUURA, Y., TSUKIYAMA, Y. & KOYANO, K. 2015. Effects of CaCl2 hydrothermal treatment of titanium implant surfaces on early epithelial sealing. *Colloids and Surfaces B: Biointerfaces,* 131**,** 141-147.

OTTO, M. 2008. Staphylococcal biofilms. *Curr Top Microbiol Immunol,* 322**,** 207-28.

OZDEMIR, Z., OZDEMIR, A. & BASIM, G. B. 2016. Application of chemical mechanical polishing process on titanium based implants. *Materials Science and Engineering: C,* 68**,** 383-396.

PADMAVATHY, N. & VIJAYARAGHAVAN, R. 2008. Enhanced bioactivity of ZnO nanoparticles—an antimicrobial study. *Science and Technology of Advanced Materials,* 9**,** 035004.

PALMQUIST, A., OMAR, O. M., ESPOSITO, M., LAUSMAA, J. & THOMSEN, P. Titanium oral implants: Surface characteristics, interface biology and clinical outcome. *Journal of the Royal Society Interface,* 7**,** S515-S527.

PALMQUIST, A., OMAR, O. M., ESPOSITO, M., LAUSMAA, J. & THOMSEN, P. 2010. Titanium oral implants: Surface characteristics, interface biology and clinical outcome. *Journal of the Royal Society Interface,* 7**,** S515; Technical Research Institute of Sweden, BorÃƒÂ¥s, Sweden-S527.

PAPP, S., KÕRÖSI, L., MEYNEN, V., COOL, P., VANSANT, E. F. & DÉKÁNY, I. 2005. The influence of temperature on the structural behaviour of sodium tri- and hexa-titanates and their protonated forms. *Journal of Solid State Chemistry,* 178**,** 1614-1619.

PARAMESWARAN, S. & VERMA, R. S. 2011. Scanning electron microscopy preparation protocol for differentiated stem cells. *Anal Biochem,* 416**,** 186-190.

PARITHIMARKALAIGNAN, S. & PADMANABHAN, T. V. 2013. Osseointegration: An Update. *The Journal of the Indian Prosthodontic Society,* 13**,** 2-6.

PARK 2003. *Biomaterials : principles and applications,* Boca Raton [Fla.] :, CRC Press.

PARK, J.-W., TUSTUSMI, Y., LEE, C. S., PARK, C. H., KIM, Y.-J., JANG, J.-H., KHANG, D., IM, Y.-M., DOI, H., NOMURA, N. & HANAWA, T. 2011. Surface structures and osteoblast response of hydrothermally produced CaTiO3 thin film on Ti–13Nb–13Zr alloy. *Applied Surface Science,* 257**,** 7856-7863.

PARK, J., BAUER, S., SCHLEGEL, K. A., NEUKAM, F. W., VON DER MARK, K. & SCHMUKI, P. 2009. TiO2 Nanotube Surfaces: 15 nm—An Optimal Length Scale of Surface Topography for Cell Adhesion and Differentiation. *Small,* 5**,** 666-671.

PARK, J. & LAKES, R. S. 2007a. *Biomaterials: an introduction*, Springer Science & Business Media.

PARK, J. & LAKES, R. S. 2007b. Metallic Implant Materials. *Biomaterials.* Springer New York.

PARK, J. B. & BRONZINO, J. D. 2003. *Biomaterials : principles and applications,* Boca Raton, Fl., CRC Press.

PARK, J. H., OLIVARES-NAVARRETE, R., BAIER, R. E., MEYER, A. E., TANNENBAUM, R., BOYAN, B. D. & SCHWARTZ, Z. 2012. Effect of cleaning and sterilization on titanium implant surface properties and cellular response. *Acta Biomaterialia,* 8**,** 1966-1975.

PARVIZI, J., PAWASARAT, I. M., AZZAM, K. A., JOSHI, A., HANSEN, E. N. & BOZIC, K. J. 2010a. Periprosthetic Joint Infection: The Economic Impact of Methicillin-Resistant Infections. *J Arthroplasty,* 25**,** 103-107.

PARVIZI, J., PAWASARAT, I. M., AZZAM, K. A., JOSHI, A., HANSEN, E. N. & BOZIC, K. J. 2010b. Periprosthetic joint infection: The economic impact of methicillin-resistant infections. *Journal of Arthroplasty,* 25**,** 103-107.

PATLOLLA, A. K., HACKETT, D. & TCHOUNWOU, P. B. 2015. Genotoxicity study of silver nanoparticles in bone marrow cells of Sprague–Dawley rats. *Food and Chemical Toxicology,* 85**,** 52-60.

PATTANAYAK, D. K., YAMAGUCHI, S., MATSUSHITA, T. & KOKUBO, T. 2011. Effect of heat treatments on apatite-forming ability of NaOH- and HCl-treated titanium metal. *Journal of Materials Science: Materials in Medicine,* 22**,** 273-278.

PAWAR, S. M., PAWAR, B. S., KIM, J. H., JOO, O.-S. & LOKHANDE, C. D. 2011. Recent status of chemical bath deposited metal chalcogenide and metal oxide thin films. *Current Applied Physics,* 11**,** 117-161.

PAYER, M., LORENZONI, M., JAKSE, N., KIRMEIER, R., DOHR, G., STOPPER, M. & PERTL, C. 2010. Cell growth on different zirconia and titanium surface textures: A morphologic in vitro study. *J Dental Implant (in German),* 4**,** 338-51.

PEEL, T. N., DOWSEY, M. M., DAFFY, J. R., STANLEY, P. A., CHOONG, P. F. M. & BUISING, K. L. 2011. Risk factors for prosthetic hip and knee infections according to arthroplasty site. *Journal of Hospital Infection,* 79**,** 129-133.

PELLETIER, J. & ANDERS, A. 2005. Plasma-based ion implantation and deposition: A review of physics, technology, and applications. *IEEE Transactions on Plasma Science,* 33**,** 1944-1959.

PENG, L., ELTGROTH, M. L., LATEMPA, T. J., GRIMES, C. A. & DESAI, T. A. 2009. The effect of TiO 2 nanotubes on endothelial function and smooth muscle proliferation. *Biomaterials,* 30**,** 1268-1272.

PENNSYLVANIA, R. C. F. A. P. S. S. U. & INSTITUTE, J. P. S. P. T. A. 1992. *Spare Parts : Organ Replacement in American Society: Organ Replacement in American Society*, Oxford University Press, USA.

PETRINI, P., ARCIOLA, C. R., PEZZALI, I., BOZZINI, S., MONTANARO, L., TANZI, M. C., SPEZIALE, P. & VISAI, L. 2006. Antibacterial activity of zinc modified titanium oxide surface. *Int J Artif Organs,* 29**,** 434-42.

PHINNEY, D. G., KOPEN, G., RIGHTER, W., WEBSTER, S., TREMAIN, N. & PROCKOP, D. J. 1999. Donor variation in the growth properties and osteogenic potential of human marrow stromal cells. *J Cell Biochem,* 75**,** 424-36.

PIATTELLI, A. & IEZZI, G. 2016. MSCs and Biomaterials. *Dental Stem Cells: Regenerative Potential.* Springer.

PILLIAR, R. M., VOWLES, R. & WILLIAMS, D. F. 1987. Fracture toughness testing of biomaterials using a mini-short rod specimen design. *J Biomed Mater Res,* 21**,** 145-54.

PJETURSSON, B. E., ASGEIRSSON, A. G., ZWAHLEN, M. & SAILER, I. 2014. Improvements in implant dentistry over the last decade: comparison of survival and complication rates in older and newer publications. *Int J Oral Maxillofac Implants,* 29 Suppl**,** 308-24.

POHLER, O. E. M. 2000. Unalloyed titanium for implants in bone surgery. *Injury,* 31, Supplement 4**,** D7-D13.

POLLAK, D. & FLOMAN, Y. 1983. Late hematogenous infection: a constant threat to total joint replacement. *Isr J Med Sci,* 19**,** 206-8.

PONSONNET, L., REYBIER, K., JAFFREZIC, N., COMTE, V., LAGNEAU, C., LISSAC, M. & MARTELET, C. 2003. Relationship between surface properties (roughness, wettability) of titanium and titanium alloys and cell behaviour. *Materials Science and Engineering: C,* 23**,** 551-560.

POON, C. Y. & BHUSHAN, B. 1995. Comparison of surface roughness measurements by stylus profiler, AFM and non-contact optical profiler. *Wear,* 190**,** 76-88.

POPAT, K. C., ELTGROTH, M., LATEMPA, T. J., GRIMES, C. A. & DESAI, T. A. 2007a. Decreased Staphylococcus epidermis adhesion and increased osteoblast functionality on antibiotic-loaded titania nanotubes. *Biomaterials,* 28**,** 4880-4888.

POPAT, K. C., LEONI, L., GRIMES, C. A. & DESAI, T. A. 2007b. Influence of engineered titania nanotubular surfaces on bone cells. *Biomaterials,* 28**,** 3188-3197.

POPPER, K. R. 2002. *The Logic of Scientific Discovery*, Routledge.

PRIYA, R., GEETHA, D. & RAMESH, P. 2013. Antibacterial activity of nano-silver capped by β-cyclodextrin. *Carbon Sci. Technol.,* 1**,** 197-202.

PRUSI, A. & ARSOV, L. D. 1992. The growth kinetics and optical properties of films formed under open circuit conditions on a titanium surface in potassium hydroxide solutions. *Corrosion Science,* 33**,** 153-164.

PUCKETT, S., PARETA, R. & WEBSTER, T. 2007. Nano rough micron patterned titanium for directing osteoblast morphology and adhesion. *International journal of nanomedicine,* 3**,** 229-241.

PULEO, D. A. & NANCI, A. 1999a. Understanding and controlling the bone–implant interface. *Biomaterials,* 20**,** 2311-2321.

PULEO, D. A. & NANCI, A. 1999b. Understanding and controlling the boneâ€“implant interface. *Biomaterials,* 20**,** 2311-2321.

QIU, Q. Q., SUN, W. Q. & CONNOR, J. 2011. 4.410 - Sterilization of Biomaterials of Synthetic and Biological Origin A2 - Ducheyne, Paul. *Comprehensive Biomaterials.* Oxford: Elsevier.

QUIRYNEN, M. & BOLLEN, C. M. 1995. The influence of surface roughness and surface-free energy on supra- and subgingival plaque formation in man. A review of the literature. *J Clin Periodontol,* 22**,** 1-14.

QUIRYNEN, M., BOLLEN, C. M., PAPAIOANNOU, W., VAN ELDERE, J. & VAN STEENBERGHE, D. 1996. The influence of titanium abutment surface roughness on plaque accumulation and gingivitis: short-term observations. *Int J Oral Maxillofac Implants,* 11**,** 169-78.

RAJPUT, R., CHOUHAN, Z., SINDHU, M., SUNDARARAJAN, S. & CHOUHAN, R. R. S. 2016. A Brief Chronological Review of Dental Implant History. *International Dental Journal of Students Research,* 4.

RAMPERSAD, S. N. 2012. Multiple Applications of Alamar Blue as an Indicator of Metabolic Function and Cellular Health in Cell Viability Bioassays. *Sensors (Basel, Switzerland),* 12**,** 12347-12360.

RATNER, B. 2001. A Perspective on Titanium Biocompatibility. *Titanium in Medicine.* Springer Berlin Heidelberg.

RATNER, B. D. 1996a. *Biomaterials science : an introduction to materials in medicine,* San Diego, Academic Press.

RATNER, B. D. 1996b. *Biomaterials science : an introduction to materials in medicine,* San Diego, Academic Press.

RATNER, B. D. & BRYANT, S. J. 2004. BIOMATERIALS: Where We Have Been and Where We are Going. *Annual Review of Biomedical Engineering,* 6**,** 41-75.

RATNER, B. D., HOFFMAN, A. S., SCHOEN, F. J. & LEMONS, J. 2004. Biomaterials science: a multidisciplinary endeavor. *Biomaterials science: an introduction to materials in medicine***,** 1-9.

RATNER, B. D., HOFFMAN, A. S., SCHOEN, F. J. & LEMONS, J. E. 2012. *Biomaterials Science: An Introduction to Materials in Medicine*, Elsevier Science.

RAUTRAY, T. R., NARAYANAN, R., KWON, T. Y. & KIM, K. H. 2010. Surface modification of titanium and titanium alloys by ion implantation. *Journal of Biomedical Materials Research - Part B Applied Biomaterials,* 93**,** 581-591.

RAVELINGIEN, M., MULLENS, S., LUYTEN, J., MEYNEN, V., VINCK, E., VERVAET, C. & REMON, J. P. 2009. Thermal decomposition of bioactive sodium titanate surfaces. *Applied Surface Science,* 255**,** 9539-9542.

RAZALI, M. H., MOHD NOOR, A.-F., MOHAMED, A. R. & SREEKANTAN, S. 2012. Morphological and Structural Studies of Titanate and Titania Nanostructured Materials Obtained after Heat Treatments of Hydrothermally Produced Layered Titanate. *Journal of Nanomaterials,* 2012**,** 10.

REDDY, K. M., FERIS, K., BELL, J., WINGETT, D. G., HANLEY, C. & PUNNOOSE, A. 2007. Selective toxicity of zinc oxide nanoparticles to prokaryotic and eukaryotic systems. *Applied Physics Letters,* 90**,** 213902.

RELLER, L. B., WEINSTEIN, M., JORGENSEN, J. H. & FERRARO, M. J. 2009. Antimicrobial Susceptibility Testing: A Review of General Principles and Contemporary Practices. *Clinical Infectious Diseases,* 49**,** 1749-1755.

RING, M. E. 1995. A thousand years of dental implants: a definitive history--part 2. *Compend Contin Educ Dent,* 16**,** 1132, 1134, 1136 passim.

RUPP, F., GITTENS, R. A., SCHEIDELER, L., MARMUR, A., BOYAN, B. D., SCHWARTZ, Z. & GEIS-GERSTORFER, J. 2014. A review on the wettability of dental implant surfaces I: Theoretical and experimental aspects. *Acta Biomaterialia,* 10**,** 2894-2906.

SALEM, W., LEITNER, D. R., ZINGL, F. G., SCHRATTER, G., PRASSL, R., GOESSLER, W., REIDL, J. & SCHILD, S. 2015. Antibacterial activity of silver and zinc nanoparticles against Vibrio cholerae and enterotoxic Escherichia coli. *International Journal of Medical Microbiology,* 305**,** 85-95.

SALERNO, M., GIACOMELLI, L., DERCHI, G., PATRA, N. & DIASPRO, A. 2010. Atomic force microscopy in vitro study of surface roughness and fractal character of a dental restoration composite after air-polishing. *BioMedical Engineering OnLine,* 9**,** 59-59.

SAUVET, A. L., BALITEAU, S., LOPEZ, C. & FABRY, P. 2004. Synthesis and characterization of sodium titanates Na2Ti3O7 and Na2Ti6O13. *Journal of Solid State Chemistry,* 177**,** 4508-4515.

SCHARNWEBER, D., BEUTNER, R., RÖßLER, S. & WORCH, H. 2002. Electrochemical behavior of titanium-based materials–are there relations to biocompatibility? *Journal of Materials Science: Materials in Medicine,* 13**,** 1215-1220.

SCHIERHOLZ, J. M. & BEUTH, J. 2001. Implant infections: a haven for opportunistic bacteria. *Journal of Hospital Infection,* 49**,** 87-93.

SCHMALZRIED, T. P., AMSTUTZ, H. C., AU, M. K. & DOREY, F. J. 1992. Etiology of deep sepsis in total hip arthroplasty. The significance of hematogenous and recurrent infections. *Clin Orthop Relat Res***,** 200-7.

SCHNEIDER, G., PERINPANAYAGAM, H., CLEGG, M., ZAHARIAS, R., SEABOLD, D., KELLER, J. & STANFORD, C. 2003. Implant surface roughness affects osteoblast gene expression. *Journal of Dental Research,* 82**,** 372-376.

SCHOEN, F. J. & LEVY, R. J. 2005. Calcification of Tissue Heart Valve Substitutes: Progress Toward Understanding and Prevention. *The Annals of thoracic surgery,* 79**,** 1072-1080.

SCHULER, M., OWEN, G. R., HAMILTON, D. W., DE WILD, M., TEXTOR, M., BRUNETTE, D. M. & TOSATTI, S. G. P. 2006a. Biomimetic modification of titanium dental implant model surfaces using the RGDSP-peptide sequence: A cell morphology study. *Biomaterials,* 27**,** 4003-4015.

SCHULER, M., TRENTIN, D., TEXTOR, M. & TOSATTI, S. G. P. 2006b. Biomedical interfaces: titanium surface technology for implants and cell carriers. *Nanomedicine,* 1**,** 449-463.

SCHWARTZ, Z., LOHMANN, C. H., OEFINGER, J., BONEWALD, L. F., DEAN, D. D. & BOYAN, B. D. 1999. Implant surface characteristics modulate differentiation behavior of cells in the osteoblastic lineage. *Adv Dent Res,* 13**,** 38-48.

SCHWARTZ, Z., NASAZKY, E. & BOYAN, B. D. 2005. Surface microtopography regulates osteointegration: the role of implant surface microtopography in osteointegration. *The Alpha omegan,* 98**,** 9-19.

SCHWARZ, F., WIELAND, M., SCHWARTZ, Z., ZHAO, G., RUPP, F., GEIS-GERSTORFER, J., SCHEDLE, A., BROGGINI, N., BORNSTEIN, M. M., BUSER, D., FERGUSON, S. J., BECKER, J., BOYAN, B. D. & COCHRAN, D. L. 2009. Potential of chemically modified hydrophilic surface characteristics to support tissue integration of titanium dental implants. *Journal of Biomedical Materials Research - Part B Applied Biomaterials,* 88**,** 544-557.

SCOTCHFORD, C. A., EVANS, M. & VATS, A. 2016. Biomaterials, tissue engineering and their applications. *Basic Clinical Radiobiology,* 2**,** 1118.

SCULCO, T. P. 1993. The economic impact of infected total joint arthroplasty. *Instructional course lectures,* 42**,** 349-351.

SEDDIKI, O., HARNAGEA, C., LEVESQUE, L., MANTOVANI, D. & ROSEI, F. 2014. Evidence of antibacterial activity on titanium surfaces through nanotextures. *Applied Surface Science,* 308**,** 275-284.

SERRO, A. & SARAMAGO, B. 2003. Influence of sterilization on the mineralization of titanium implants induced by incubation in various biological model fluids. *Biomaterials,* 24**,** 4749-4760.

SHAH, S. R., TATARA, A. M., D'SOUZA, R. N., MIKOS, A. G. & KASPER, F. K. 2013. Evolving strategies for preventing biofilm on implantable materials. *Materials Today,* 16**,** 177-182.

SHALABI, M. M., GORTEMAKER, A., HOF, M. A. V. T., JANSEN, J. A. & CREUGERS, N. H. J. 2006a. Implant Surface Roughness and Bone Healing: a Systematic Review. *Journal of dental research,* 85**,** 496-500.

SHALABI, M. M., GORTEMAKER, A., VAN'T HOF, M. A., JANSEN, J. A. & CREUGERS, N. H. 2006b. Implant surface roughness and bone healing: a systematic review. *J Dent Res,* 85**,** 496-500.

SHARD, A. G. & TOMLINS, P. E. 2006. Biocompatibility and the efficacy of medical implants. *Regen Med,* 1**,** 789-800.

SHEEHAN, E., MCKENNA, J., MULHALL, K. J., MARKS, P. & MCCORMACK, D. 2004. Adhesion of Staphylococcus to orthopaedic metals, an in vivo study. *Journal of Orthopaedic Research,* 22**,** 39-43.

SHI, Z., NEOH, K., KANG, E., POH, C. & WANG, W. 2008. Bacterial adhesion and osteoblast function on titanium with surface-grafted chitosan and immobilized RGD peptide. *Journal of Biomedical Materials Research Part A,* 86**,** 865-872.

ŠIDÁK, Z. 1967. Rectangular confidence regions for the means of multivariate normal distributions. *Journal of the American Statistical Association,* 62**,** 626-633.

SIEVÄNEN, H., KANNUS, P. & JÄRVINEN, T. L. N. 2007. Bone Quality: An Empty Term. *PLoS Medicine,* 4**,** e27.

SIMONIS, P., DUFOUR, T. & TENENBAUM, H. 2010. Long-term implant survival and success: a 10-16-year follow-up of non-submerged dental implants. *Clin Oral Implants Res,* 21**,** 772-7.

SINGHATANADGIT, W. 2009. Biological Responses to New Advanced Surface Modifications of Endosseous Medical Implants. *Bone and Tissue Regeneration Insights,* 2**,** 1-11.

SIRELKHATIM, A., MAHMUD, S., SEENI, A., KAUS, N. H. M., ANN, L. C., BAKHORI, S. K. M., HASAN, H. & MOHAMAD, D. 2015. Review on zinc oxide nanoparticles: antibacterial activity and toxicity mechanism. *Nano-Micro Letters,* 7**,** 219-242.

SITTIG, C., TEXTOR, M., SPENCER, N. D., WIELAND, M. & VALLOTTON, P. H. 1999. Surface characterization of implant materials c.p. Ti, Ti-6Al-4V with different pre-treatments. *Journal of Materials Science: Materials in Medicine,* 10**,** 35-46.

SMITH, A. J., DIEPPE, P., VERNON, K., PORTER, M. & BLOM, A. W. 2012. Failure rates of stemmed metal-on-metal hip replacements: analysis of data from the National Joint Registry of England and Wales. *The Lancet,* 379**,** 1199-1204.

SOLAR, R. J., POLLACK, S. R. & KOROSTOFF, E. 1979. In vitro corrosion testing of titanium surgical implant alloys: An approach to understanding titanium release from implants. *Journal of Biomedical Materials Research,* 13**,** 217-250.

SORENSON, C., TARRICONE, R., SIEBERT, M. & DRUMMOND, M. 2011. Applying health economics for policy decision making: do devices differ from drugs? *Europace,* 13**,** ii54-ii58.

STANFORD, C. M. 2008. Surface modifications of dental implants. *Aust Dent J,* 53**,** S26-S33.

STECKELBERG, J. M. & OSMON, D. R. 2000. Prosthetic joint infections. *Infections associated with indwelling medical devices***,** 173-209.

STEINEMANN, S. G. 1998. Titanium — the material of choice? *Periodontol 2000,* 17**,** 7-21.

ŠTENGL, V., BAKARDJIEVA, S., ŠUBRT, J., VEČERNÍKOVÁ, E., SZATMARY, L., KLEMENTOVÁ, M. & BALEK, V. 2006. Sodium titanate nanorods: Preparation, microstructure characterization and photocatalytic activity. *Applied Catalysis B: Environmental,* 63**,** 20-30.

STINCHFIELD, F. E., BIGLIANI, L. U., NEU, H. C., GOSS, T. P. & FOSTER, C. R. 1980. Late hematogenous infection of total joint replacement. *J Bone Joint Surg Am,* 62**,** 1345-50.

STOBIE, N., DUFFY, B., MCCORMACK, D. E., COLREAVY, J., HIDALGO, M., MCHALE, P. & HINDER, S. J. 2008. Prevention of Staphylococcus epidermidis biofilm formation using a low-temperature processed silver-doped phenyltriethoxysilane sol–gel coating. *Biomaterials,* 29**,** 963-969.

STOODLEY, P., DODDS, I., BOYLE, J. & LAPPIN-SCOTT, H. 1998. Influence of hydrodynamics and nutrients on biofilm structure. *Journal of applied microbiology,* 85.

SUBBIAHDOSS, G., PIDHATIKA, B., COULLEREZ, G., CHARNLEY, M., KUIJER, R., VAN DER MEI, H. C., TEXTOR, M. & BUSSCHER, H. J. 2010. Bacterial biofilm formation versus mammalian cell growth on titanium-based mono-and bi-functional coating. *Eur Cell Mater,* 19**,** 205-13.

SUCHANEK, K., BARTKOWIAK, A., GDOWIK, A., PERZANOWSKI, M., KĄC, S., SZARANIEC, B., SUCHANEK, M. & MARSZAŁEK, M. 2015. Crystalline hydroxyapatite coatings synthesized under

hydrothermal conditions on modified titanium substrates. *Materials Science and Engineering: C,* 51**,** 57-63.

SUH, H. 1998. Recent advances in biomaterials. *Yonsei Med J,* 39**,** 87-96.

SUL, Y.-T. 2003. The significance of the surface properties of oxidized titanium to the bone response: special emphasis on potential biochemical bonding of oxidized titanium implant. *Biomaterials,* 24**,** 3893-3907.

SUN, X. & LI, Y. 2003. Synthesis and Characterization of Ion-Exchangeable Titanate Nanotubes. *Chemistry – A European Journal,* 9**,** 2229-2238.

SUN, X. & XI, T. 2006. Third-generation biomedical materials and regenerative medicine. *Zhongguo Xiu Fu Chong Jian Wai Ke Za Zhi,* 20**,** 189-93.

SURENDER, L., REKHA, R. K., VEERENDRA, N. R. P. & INDUMATHY, P. 2011. Surface characteristics of titanium dental implants for rapid osseointegration. *Indian Journal of Dental Advancements,* 3**,** 602-612.

TAKADAMA, H., KIM, H.-M., KOKUBO, T. & NAKAMURA, T. 2001. TEM-EDX study of mechanism of bonelike apatite formation on bioactive titanium metal in simulated body fluid. *Journal of Biomedical Materials Research,* 57**,** 441-448.

TAKEUCHI, M., ABE, Y., YOSHIDA, Y., NAKAYAMA, Y., OKAZAKI, M. & AKAGAWA, Y. 2003. Acid pretreatment of titanium implants. *Biomaterials,* 24**,** 1821-7.

TALOŞ, F., SENILĂ, M., FRENTIU, T. & SIMON, S. 2013. Effect of titanium ions on the ion release rate and uptake at the interface of silica based xerogels with simulated body fluid. *Corrosion Science,* 72**,** 41-46.

TAMBASCO DE OLIVEIRA, P. & NANCI, A. 2004. Nanotexturing of titanium-based surfaces upregulates expression of bone sialoprotein and osteopontin by cultured osteogenic cells. *Biomaterials,* 25**,** 403-413.

TANG, L., SCHRAMM, A., NEU, T. R., REVSBECH, N. P. & MEYER, R. L. 2013. Extracellular DNA in adhesion and biofilm formation of four environmental isolates: a quantitative study. *FEMS Microbiol Ecol*.

TAVARES, M. G., DE OLIVEIRA, P. T., NANCI, A., HAWTHORNE, A. C., ROSA, A. L. & XAVIER, S. P. 2007. Treatment of a commercial, machined surface titanium implant with H2SO4/H2O2 enhances contact osteogenesis. *Clin Oral Implants Res,* 18**,** 452-8.

TAYLOR, R., MARYAN, C. & VERRAN, J. 1998. Retention of oral microorganisms on cobalt-chromium alloy and dental acrylic resin with different surface finishes. *J Prosthet Dent,* 80**,** 592-7.

TENGVALL, P. 2001. Proteins at Titanium Interfaces. *Titanium in Medicine.* Springer Berlin Heidelberg.

TER BRUGGE, P. J., DIEUDONNE, S. & JANSEN, J. A. 2002. Initial interaction of U2OS cells with noncoated and calcium phosphate coated titanium substrates. *Journal of Biomedical Materials Research,* 61**,** 399-407.

THEVENOT, P., HU, W. & TANG, L. 2008a. Surface Chemistry Iinfluence Implant Biocompatibility. *Curr Top Med Chem,* 8**,** 270-280.

THEVENOT, P., HU, W. & TANG, L. 2008b. Surface chemistry influences implant biocompatibility. *Curr Top Med Chem,* 8**,** 270-80.

THOMAS, K. A. & COOK, S. D. 1985. An evaluation of variables influencing implant fixation by direct bone apposition. *J Biomed Mater Res,* 19**,** 875-901.

TRAMPUZ, A., GILOMEN, A., FLUCKIGER, U., FREI, R., ZIMMERLI, W. & WIDMER, A. 2006. Treatment outcome of infections associated with internal fixation devices: Results from a 5-year retrospective study (1999-2003). *International Journal of Infectious Diseases,* 10**,** S79-S79.

TRAMPUZ, A. & WIDMER, A. F. 2006. Infections associated with orthopedic implants. *Current opinion in infectious diseases,* 19**,** 349-356.

TRAMPUZ, A. & ZIMMERLI, W. 2006. Diagnosis and treatment of infections associated with fracture-fixation devices. *Injury,* 37**,** S59-S66.

TRAUTNER, B. W. & DAROUICHE, R. O. 2004. Role of biofilm in catheter-associated urinary tract infection. *American Journal of Infection Control,* 32**,** 177-183.

TRINDADE, R., ALBREKTSSON, T., TENGVALL, P. & WENNERBERG, A. 2014. Foreign Body Reaction to Biomaterials: On Mechanisms for Buildup and Breakdown of Osseointegration. *Clin Implant Dent Relat Res*.

TRISI, P., RAO, W. & REBAUDI, A. 1999. A histometric comparison of smooth and rough titanium implants in human low-density jawbone. *Int J Oral Maxillofac Implants,* 14**,** 689-98.

TSAI, C.-C. & TENG, H. 2006. Structural Features of Nanotubes Synthesized from NaOH Treatment on TiO2 with Different Post-Treatments. *Chemistry of Materials,* 18**,** 367-373.

TURZO, K. 2012. *Surface Aspects of Titanium Dental Implants*.

UEDA, M., IKEDA, M. & OGAWA, M. 2009a. Chemical–hydrothermal combined surface modification of titanium for improvement of osteointegration. *Materials Science and Engineering: C,* 29**,** 994-1000.

UEDA, M., IKEDA, M. & OGAWA, M. 2009b. Chemical and hydrothermal combined surface modification of titanium for improvement of osteointegration. *Materials Science and Engineering: C,* 29**,** 994-1000.

VALAGÃO AMADEU DO SERRO, A. P., FERNANDES, A. C. & DE JESUS VIEIRA SARAMAGO, B. 2000. Calcium phosphate deposition on titanium surfaces in the presence of fibronectin. *Journal of Biomedical Materials Research,* 49**,** 345-352.

VALANEZAHAD, A., ISHIKAWA, K., TSURU, K., MARUTA, M. & MATSUYA, S. 2011. Hydrothermal calcium modification of 316L stainless steel and its apatite forming ability in simulated body fluid. *Dental Materials Journal,* 30**,** 749-753.

VAN HENGEL, I. A. J., RIOOL, M., FRATILA-APACHITEI, L. E., WITTE-BOUMA, J., FARRELL, E., ZADPOOR, A. A., ZAAT, S. A. J. & APACHITEI, I. 2017. Selective laser melting porous metallic implants with immobilized silver nanoparticles kill and prevent biofilm formation by methicillin-resistant Staphylococcus aureus. *Biomaterials*.

VANYSEK, P. 1998. Electrochemical series. *CRC handbook of chemistry and physics,* 87.

VELARD, F. D. R., BRAUX, J., AMEDEE, J. L. & LAQUERRIERE, P. 2013. Inflammatory cell response to calcium phosphate biomaterial particles: An overview. *Acta Biomaterialia,* 9**,** 4956-4963.

VERRAN, J. & MARYAN, C. J. 1997. Retention of Candida albicans on acrylic resin and silicone of different surface topography. *J Prosthet Dent,* 77**,** 535-9.

VETTEN, M. A., YAH, C. S., SINGH, T. & GULUMIAN, M. 2014. Challenges facing sterilization and depyrogenation of nanoparticles: Effects on structural stability and biomedical applications. *Nanomedicine: Nanotechnology, Biology and Medicine,* 10**,** 1391-1399.

VIOLANT, D., GALOFRE, M., NART, J. & TELES, R. P. 2014. In vitro evaluation of a multispecies oral biofilm on different implant surfaces. *Biomed Mater,* 9**,** 035007.

VOGLER, E. A. 1999. Water and the acute biological response to surfaces. *J Biomater Sci Polym Ed,* 10**,** 1015-45.

VOROBYEV, A. Y. & GUO, C. 2007. Femtosecond laser structuring of titanium implants. *Applied Surface Science,* 253**,** 7272-7280.

VUONG, C., KOCIANOVA, S., VOYICH, J. M., YAO, Y., FISCHER, E. R., DELEO, F. R. & OTTO, M. 2004. A crucial role for exopolysaccharide modification in bacterial biofilm formation, immune evasion, and virulence. *J Biol Chem,* 279**,** 54881-6.

WAGNER, C., AYTAC, S. & HÄNSCH, G. M. 2011. Biofilm growth on implants: bacteria prefer plasma coats. *International Journal of Artificial Organs,* 34**,** 811-817.

WALL, I., DONOS, N., CARLQVIST, K., JONES, F. & BRETT, P. 2009. Modified titanium surfaces promote accelerated osteogenic differentiation of mesenchymal stromal cells in vitro. *Bone,* 45**,** 17-26.

WANG, J., WANG, Z., GUO, S., ZHANG, J., SONG, Y., DONG, X., WANG, X. & YU, J. 2011. Antibacterial and anti-adhesive zeolite coatings on titanium alloy surface. *Microporous and Mesoporous Materials,* 146**,** 216-222.

WANG, Y., LIBERA, M., BUSSCHER, H. & VAN DER MEI, H. 2012. Mono-functional to multifunctional coatings: The changing paradigm to control biofilm formation on biomedical implants. Nova Science Publishers Inc., Commack, NY.

WARD, B. C. & WEBSTER, T. J. 2007. Increased functions of osteoblasts on nanophase metals. *Materials Science and Engineering: C,* 27**,** 575-578.

WATARI, F., YOKOYAMA, A., OMORI, M., HIRAI, T., KONDO, H., UO, M. & KAWASAKI, T. 2004. Biocompatibility of materials and development to functionally graded implant for bio-medical application. *Composites Science and Technology,* 64**,** 893-908.

WAYNE, P. 2009. Clinical and Laboratory Standards Institute (CLSI) performance standards for antimicrobial disk diffusion susceptibility tests 19th ed. approved standard. *CLSI document M100-S19,* 29.

WEBSTER, T. J. & EJIOFOR, J. U. 2004. Increased osteoblast adhesion on nanophase metals: Ti, Ti6Al4V, and CoCrMo. *Biomaterials,* 25**,** 4731-4739.

WEERKAMP, A. H., VAN DER MEI, H. C. & BUSSCHER, H. J. 1990. Surface hydrophobicity and surface free energy of Actinobacillus actinomycetemcomitans strains from human periodontitis. *Microbios,* 63**,** 135-43.

WENG, D., HOFFMEYER, M., HÜRZELER, M. B. & RICHTER, E.-J. 2003. Osseotite® vs. machined surface in poor bone quality. *Clinical Oral Implants Research,* 14**,** 703-708.

WENNERBERG, A. & ALBREKTSSON, T. 2000. Suggested guidelines for the topographic evaluation of implant surfaces. *Int J Oral Maxillofac Implants,* 15**,** 331-44.

WENNERBERG, A. & ALBREKTSSON, T. 2009. Effects of titanium surface topography on bone integration: a systematic review. *Clinical Oral Implants Research,* 20**,** 172-184.

WENNERBERG, A. & ALBREKTSSON, T. 2010. On implant surfaces: a review of current knowledge and opinions. *International Journal of Oral & Maxillofacial Implants,* 25.

WENNERBERG, A., ALBREKTSSON, T., JOHANSSON, C. & ANDERSSON, B. 1996. Experimental study of turned and grit-blasted screw-shaped implants with special emphasis on effects of blasting material and surface topography. *Biomaterials,* 17**,** 15-22.

WENNERBERG, A., BOLIND, P. & ALBREKTSSON, T. 1990. Glow-discharge pretreated implants combined with temporary bone tissue ischemia. *Swedish dental journal,* 15**,** 95-101.

WENNERBERG, A., HALLGREN, C., JOHANSSON, C. & DANELLI, S. 1998. A histomorphometric evaluation of screw-shaped implants each prepared with two surface roughnesses. *Clinical Oral Implants Research,* 9**,** 11-19.

WHITEHEAD, K. A., LI, H., KELLY, P. J. & VERRAN, J. 2011. The antimicrobial properties of titanium nitride/silver nanocomposite coatings. *Journal of Adhesion Science and Technology,* 25**,** 2299-2315.

WHITEHOUSE, J. D. M. D., FRIEDMAN, N. D. M., KIRKLAND, K. B. M. D., RICHARDSON, W. J. M. D. & SEXTON, D. J. M. D. 2002. The Impact of Surgicalâ€Site Infections Following Orthopedic Surgery at a Community Hospital and a University Hospital: Adverse Quality of Life, Excess Length of Stay, and Extra CostÂ â€¢â€,. *Infection Control and Hospital Epidemiology,* 23**,** 183-189.

WICKENS, T. D. & KEPPEL, G. 2004. Design and analysis: A researcher's handbook. Englewood Cliffs, NJ: Prentice-Hall.

WIELAND, M., CHEHROUDI, B., TEXTOR, M. & BRUNETTE, D. M. 2002. Use of Ti-coated replicas to investigate the effects on fibroblast shape of surfaces with varying roughness and constant chemical composition. *Journal of Biomedical Materials Research,* 60**,** 434-444.

WIFF, J. P., FUENZALIDA, V. M., ARIAS, J. L. & FERNANDEZ, M. S. 2007. Hydrothermal-electrochemical CaTiO3 coatings as precursor of a biomimetic calcium phosphate layer. *Materials Letters,* 61**,** 2739-2743.

WILLIAMS, D. 2016. General concepts of biocompatibility. *Handbook of biomaterial properties.* Springer.

WILLIAMS, D. F. 2009. On the nature of biomaterials. *Biomaterials,* 30**,** 5897-5909.

WILLIAMS, D. L., WOODBURY, K. L., HAYMOND, B. S., PARKER, A. E. & BLOEBAUM, R. D. 2011. A Modified CDC Biofilm Reactor to Produce Mature Biofilms on the Surface of PEEK Membranes for an In Vivo Animal Model Application. *Current Microbiology,* 62**,** 1657-1663.

WILSON, C. J., CLEGG, R. E., LEAVESLEY, D. I. & PEARCY, M. J. 2005. Mediation of biomaterial-cell interactions by adsorbed proteins: a review. *Tissue Eng,* 11**,** 1-18.

WU, Y., ZITELLI, J. P., TENHUISEN, K. S., YU, X. & LIBERA, M. R. 2011. Differential response of Staphylococci and osteoblasts to varying titanium surface roughness. *Biomaterials,* 32**,** 951-960.

XU, J., DING, G., LI, J., YANG, S., FANG, B., SUN, H. & ZHOU, Y. 2010. Zinc-ion implanted and deposited titanium surfaces reduce adhesion of Streptococccus mutans. *Applied Surface Science,* 256**,** 7540-7544.

XU, R., YANG, X., JIANG, J., LI, P., ZHANG, X., WU, G. & CHU, P. K. 2015. Effects of silver plasma immersion ion implantation on the surface characteristics and cytocompatibility of titanium nitride films. *Surface and Coatings Technology,* 279**,** 166-170.

YAMADA, M., MIYAUCHI, T., YAMAMOTO, A., IWASA, F., TAKEUCHI, M., ANPO, M., SAKURAI, K., BABA, K. & OGAWA, T. 2010. Enhancement of adhesion strength and cellular stiffness of osteoblasts on mirror-polished titanium surface by UV-photofunctionalization. *Acta Biomaterialia,* 6**,** 4578-4588.

YAN, Y., CHIBOWSKI, E. & SZCZEŚ, A. 2017. Surface properties of Ti-6Al-4V alloy part I: Surface roughness and apparent surface free energy. *Materials Science and Engineering: C,* 70, Part 1**,** 207-215.

YANG, D. T., ZHANG, D. & AROLA, D. D. 2010. Fatigue of the bone/cement interface and loosening of total joint replacements. *International Journal of Fatigue,* 32**,** 1639-1649.

YANG, F., DONG, W.-J., HE, F.-M., WANG, X.-X., ZHAO, S.-F. & YANG, G.-L. 2012. Osteoblast response to porous titanium surfaces coated with zinc-substituted hydroxyapatite. *Oral Surgery, Oral Medicine, Oral Pathology and Oral Radiology,* 113**,** 313-318.

YAO, C., SLAMOVICH, E. B. & WEBSTER, T. J. 2008. Enhanced osteoblast functions on anodized titanium with nanotube-like structures. *Journal of Biomedical Materials Research Part A,* 85**,** 157-166.

YAO, J. S. T. & ESKANDARI, M. K. 2012. Transfemoral Intraluminal Graft Implantation for Abdominal Aortic Aneurysms: Two Decades Later. *Ann Vasc Surg,* 26**,** 895-905.

YUSA, K., YAMAMOTO, O., FUKUDA, M., KOYOTA, S., KOIZUMI, Y. & SUGIYAMA, T. 2011. In vitro prominent bone regeneration by release zinc ion from Zn-modified implant. *Biochem Biophys Res Commun,* 412**,** 273-278.

YUSA, K., YAMAMOTO, O., IINO, M., TAKANO, H., FUKUDA, M., QIAO, Z. & SUGIYAMA, T. 2016. Eluted zinc ions stimulate osteoblast differentiation and mineralization in human dental pulp stem cells for bone tissue engineering. *Arch Oral Biol,* 71**,** 162-169.

ZARB, G. A. 1985. Clinical application of osseointegration. An introduction. *Swed Dent J Suppl,* 28**,** 7-9.

ZETTERQVIST, L., FELDMAN, S., ROTTER, B., VINCENZI, G., WENNSTRÖM, J. L., CHIERICO, A., STACH, R. M. & KENEALY, J. N. 2010. A prospective, multicenter, randomized-controlled 5-year study of hybrid and fully etched implants for the incidence of peri-implantitis. *J Periodontol,* 81**,** 493-501.

ZHANG, F., ZHANG, Z., ZHU, X., KANG, E. T. & NEOH, K. G. 2008a. Silk-functionalized titanium surfaces for enhancing osteoblast functions and reducing bacterial adhesion. *Biomaterials,* 29**,** 4751-9.

ZHANG, L., DING, Y., POVEY, M. & YORK, D. 2008b. ZnO nanofluids–A potential antibacterial agent. *Progress in Natural Science,* 18**,** 939-944.

ZHANG, L., JIANG, Y., DING, Y., POVEY, M. & YORK, D. 2007. Investigation into the antibacterial behaviour of suspensions of ZnO nanoparticles (ZnO nanofluids). *Journal of Nanoparticle Research,* 9**,** 479-489.

ZHANG, Q., LENG, Y. & XIN, R. 2005. A comparative study of electrochemical deposition and biomimetic deposition of calcium phosphate on porous titanium. *Biomaterials,* 26**,** 2857-2865.

ZHANG, R., LEE, P., LUI, V. C. H., CHEN, Y., LIU, X., LOK, C. N., TO, M., YEUNG, K. W. K. & WONG, K. K. Y. 2015. Silver nanoparticles promote osteogenesis of mesenchymal stem cells and improve bone fracture healing in osteogenesis mechanism mouse model. *Nanomedicine: Nanotechnology, Biology and Medicine,* 11**,** 1949-1959.

ZHANG, X., WANG, H., LI, J., HE, X., HANG, R., HUANG, X., TIAN, L. & TANG, B. 2016. Corrosion behavior of Zn-incorporated antibacterial TiO2 porous coating on titanium. *Ceramics International,* 42**,** 17095-17100.

ZHANG, Y., WANG, J., WANG, P., FAN, X., LI, X., FU, J., LI, S., FAN, H. & GUO, Z. Low elastic modulus contributes to the osteointegration of titanium alloy plug. *Journal of Biomedical Materials Research Part B: Applied Biomaterials***,** n/a-n/a.

ZHAO, G., SCHWARTZ, Z., WIELAND, M., RUPP, F., GEIS-GERSTORFER, J., COCHRAN, D. & BOYAN, B. 2005. High surface energy enhances cell response to titanium substrate microstructure. *Journal of Biomedical Materials Research Part A,* 74**,** 49-58.

ZHAO, L., CHU, P. K., ZHANG, Y. & WU, Z. 2009. Antibacterial coatings on titanium implants. *Journal of Biomedical Materials Research Part B: Applied Biomaterials,* 91B**,** 470-480.

ZHOU, H. & LEE, J. 2011. Nanoscale hydroxyapatite particles for bone tissue engineering. *Acta Biomaterialia,* 7**,** 2769-2781.

ZHU, X., CHEN, J., SCHEIDELER, L., ALTEBAEUMER, T., GEIS-GERSTORFER, J. & KERN, D. 2004. Cellular reactions of osteoblasts to micron- and submicron-scale porous structures of titanium surfaces. *Cells Tissues Organs,* 178**,** 13-22.

ZIMMERLI, W., TRAMPUZ, A. & OCHSNER, P. E. 2004. Prosthetic-joint infections. *New England Journal of Medicine,* 351**,** 1645-1654.

ZINGER, O., ANSELME, K., DENZER, A., HABERSETZER, P., WIELAND, M., JEANFILS, J., HARDOUIN, P. & LANDOLT, D. 2004. Time-dependent morphology and adhesion of osteoblastic cells on titanium model surfaces featuring scale-resolved topography. *Biomaterials,* 25**,** 2695-2711.

ZMISTOWSKI, B., KARAM, J. A., DURINKA, J. B., CASPER, D. S. & PARVIZI, J. 2013. Periprosthetic joint infection increases the risk of one-year mortality. *J Bone Joint Surg Am,* 95**,** 2177-84.

Appendices

Appendix 1: Statistical Exploration

Case Processing Summary

	Cases					
	Valid		Missing		Total	
	N	Percent	N	Percent	N	Percent
polTiCa	25	100.0%	0	0.0%	25	100.0%
cpTiCa	25	100.0%	0	0.0%	25	100.0%

Paired Samples Statistics

		Mean	N	Std. Deviation	Std. Error Mean
Pair 1	polTiCa	86.9952	25	.52424	.10485
	cpTiCa	82.5623	25	.56238	.11248

Tests of Normality

	Kolmogorov-Smirnov[a]			Shapiro-Wilk		
	Statistic	df	Sig.	Statistic	df	Sig.
polTiCa	.127	25	.200*	.967	25	.567
cpTiCa	.086	25	.200*	.962	25	.458

*. This is a lower bound of the true significance.

a. Lilliefors Significance Correction

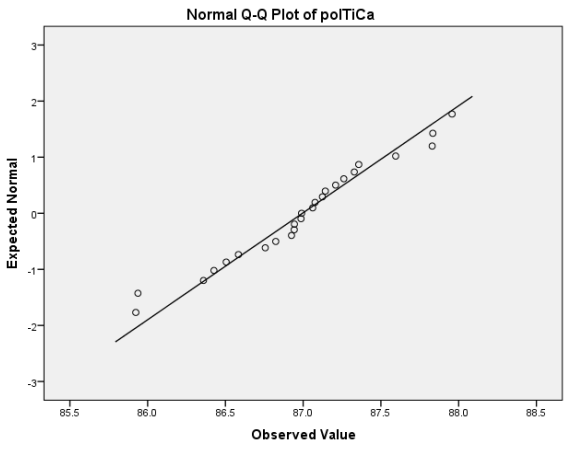

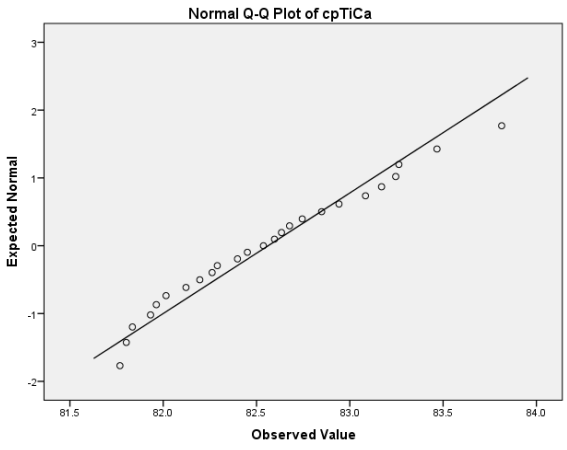

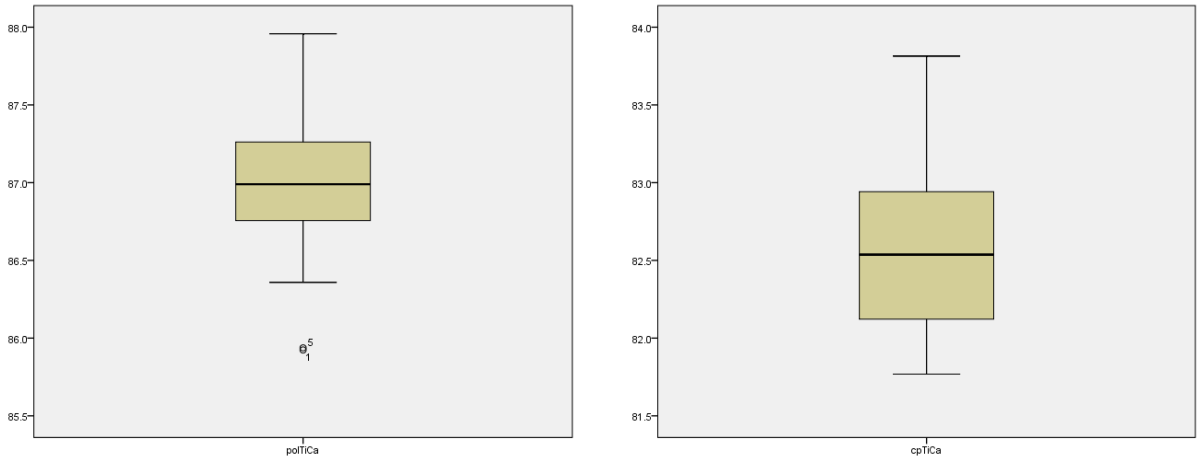

T-Test

Paired Samples Correlations

		N	Correlation	Sig.
Pair 1	polTiCa & cpTiCa	25	.123	.559

Paired Samples Test

	Paired Differences					t	df	Sig. (2-tailed)
	Mean	Std. Deviation	Std. Error Mean	95% Confidence Interval of the Difference Lower	Upper			
Pair: polTiCa - cpTiCa	4.43283	.72021	.14404	4.13554	4.73012	30.775	24	.000

ANOVA

Table Analyzed	Cell Adhesion & Proliferation				
Two-way ANOVA	Ordinary				
Alpha	0.05				
Source of Variation	% of total variation	P value	P value summary	Significant?	
Interaction	8.885	0.0008	***	Yes	
Surface Factor	81.26	< 0.0001	****	Yes	
Time Factor	1.225	0.0922	ns	No	
ANOVA table	SS	DF	MS	F (DFn, DFd)	P value
Interaction	112570	15	7505	F (15, 48) = 3.293	P = 0.0008
Surface Factor	1.030e+006	5	205903	F (5, 48) = 90.36	P < 0.0001
Time Factor	15524	3	5175	F (3, 48) = 2.271	P = 0.0922
Residual	109381	48	2279		
Number of missing values	0				

Within each column, compare rows (simple effects within columns)								
Number of families	4							
Number of comparisons per family	5							
Alpha	0.01							
Bonferroni's multiple comparisons test	Mean Diff.	99% CI of diff.	Significant ?	Summary	Adjusted P Value			
8h								
polTi vs. Ca	38.00	-89.41 to 165.4	No	ns	> 0.9999			
polTi vs. CaAg	203.0	75.59 to 330.4	Yes	****	< 0.0001			
polTi vs. CaZn	55.00	-72.41 to 182.4	No	ns	0.8233			
polTi vs. CaAgZn	111.0	-16.41 to 238.4	No	*	0.0323			
polTi vs. cpTi	-14.67	-142.1 to 112.7	No	ns	> 0.9999			
24h								
polTi vs. Ca	134.0	6.589 to 261.4	Yes	**	0.0061			
polTi vs. CaAg	318.0	190.6 to 445.4	Yes	****	< 0.0001			
polTi vs. CaZn	209.0	81.59 to 336.4	Yes	****	< 0.0001			
polTi vs. CaAgZn	220.0	92.59 to 347.4	Yes	****	< 0.0001			
polTi vs. cpTi	9.000	-118.4 to 136.4	No	ns	> 0.9999			
48h								
polTi vs. Ca	154.0	26.59 to 281.4	Yes	**	0.0013			
polTi vs. CaAg	353.0	225.6 to 480.4	Yes	****	< 0.0001			
polTi vs. CaZn	256.0	128.6 to 383.4	Yes	****	< 0.0001			
polTi vs. CaAgZn	317.0	189.6 to 444.4	Yes	****	< 0.0001			
polTi vs. cpTi	18.00	-109.4 to 145.4	No	ns	> 0.9999			
72h								
polTi vs. Ca	123.0	-4.411 to 250.4	No	*	0.0138			
polTi vs. CaAg	396.7	269.3 to 524.1	Yes	****	< 0.0001			
polTi vs. CaZn	296.7	169.3 to 424.1	Yes	****	< 0.0001			
polTi vs. CaAgZn	384.0	256.6 to 511.4	Yes	****	< 0.0001			
polTi vs. cpTi	34.00	-93.41 to 161.4	No	ns	> 0.9999			

Test details	Mean 1	Mean 2	Mean Diff.	SE of diff.	N1	N2	t	DF
8h								
polTi vs. Ca	230.0	192.0	38.00	38.98	3	3	0.9749	48
polTi vs. CaAg	230.0	27.00	203.0	38.98	3	3	5.208	48
polTi vs. CaZn	230.0	175.0	55.00	38.98	3	3	1.411	48
polTi vs. CaAgZn	230.0	119.0	111.0	38.98	3	3	2.848	48
polTi vs. cpTi	230.0	244.7	-14.67	38.98	3	3	0.3764	48
24h								
polTi vs. Ca	343.0	209.0	134.0	38.98	3	3	3.438	48
polTi vs. CaAg	343.0	25.00	318.0	38.98	3	3	8.159	48
polTi vs. CaZn	343.0	134.0	209.0	38.98	3	3	5.362	48
polTi vs. CaAgZn	343.0	123.0	220.0	38.98	3	3	5.644	48
polTi vs. cpTi	343.0	334.0	9.000	38.98	3	3	0.2309	48
48h								
polTi vs. Ca	368.0	214.0	154.0	38.98	3	3	3.951	48
polTi vs. CaAg	368.0	15.00	353.0	38.98	3	3	9.057	48
polTi vs. CaZn	368.0	112.0	256.0	38.98	3	3	6.568	48
polTi vs. CaAgZn	368.0	51.00	317.0	38.98	3	3	8.133	48
polTi vs. cpTi	368.0	350.0	18.00	38.98	3	3	0.4618	48

72h								
polTi vs. Ca	410.0	287.0	123.0	38.98	3	3	3.156	48
polTi vs. CaAg	410.0	13.33	396.7	38.98	3	3	10.18	48
polTi vs. CaZn	410.0	113.3	296.7	38.98	3	3	7.611	48
polTi vs. CaAgZn	410.0	26.00	384.0	38.98	3	3	9.852	48
polTi vs. cpTi	410.0	376.0	34.00	38.98	3	3	0.8723	48

Appendix 2: Surface Modification Method Development

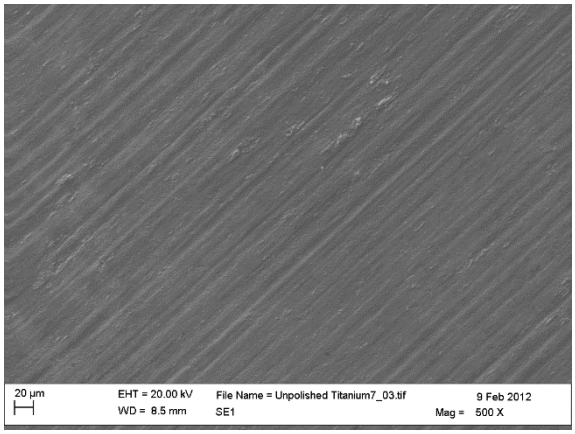

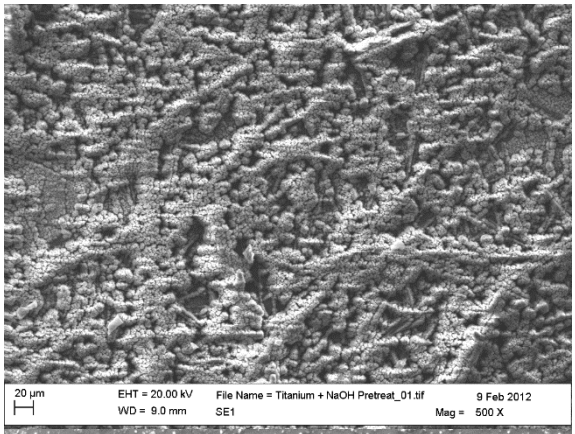
20 µm
EHT = 20.00 kV
WD = 9.0 mm
File Name = Titanium + NaOH Pretreat_01.tif
SE1
9 Feb 2012
Mag = 500 X

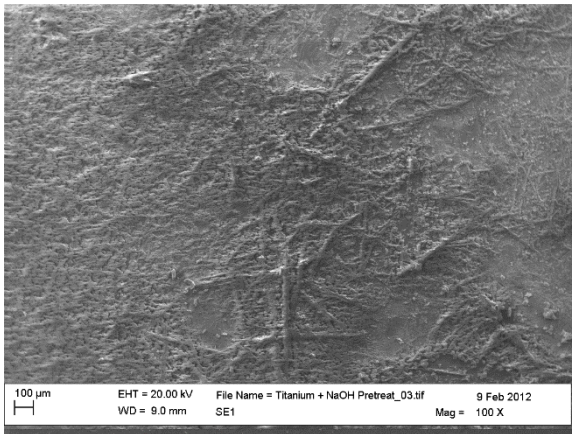
100 µm
EHT = 20.00 kV
WD = 9.0 mm
File Name = Titanium + NaOH Pretreat_03.tif
SE1
9 Feb 2012
Mag = 100 X

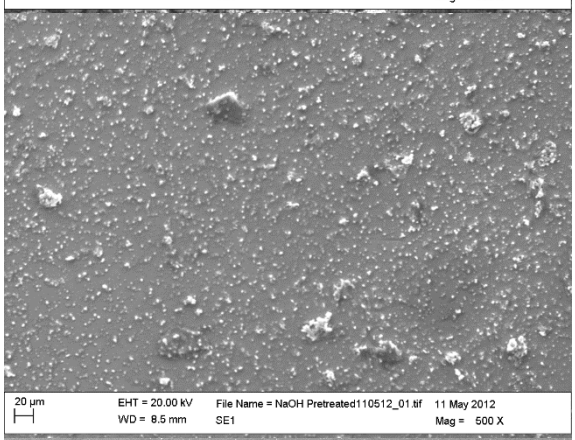
20 µm
EHT = 20.00 kV
WD = 8.5 mm
File Name = NaOH Pretreated110512_01.tif
SE1
11 May 2012
Mag = 500 X

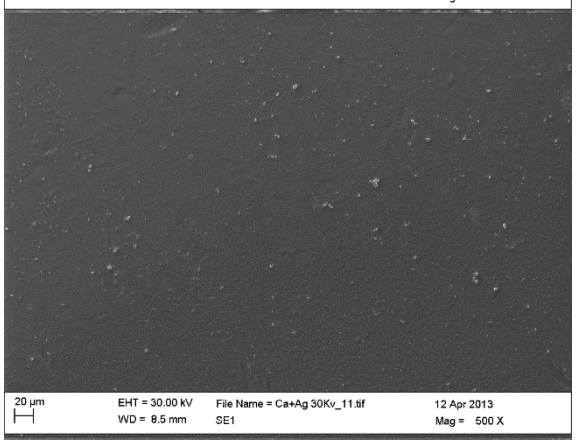
20 µm
EHT = 30.00 kV
WD = 8.5 mm
File Name = Ca+Ag 30Kv_11.tif
SE1
12 Apr 2013
Mag = 500 X

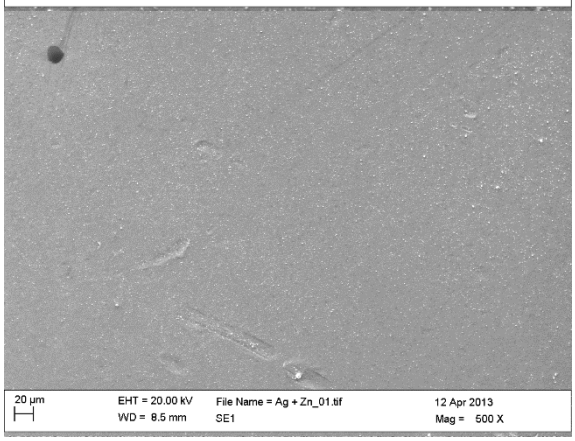
20 µm
EHT = 20.00 kV
WD = 8.5 mm
File Name = Ag + Zn_01.tif
SE1
12 Apr 2013
Mag = 500 X

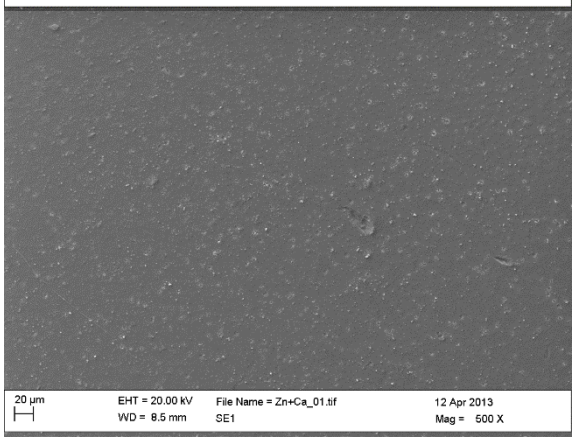
20 µm
EHT = 20.00 kV
WD = 8.5 mm
File Name = Zn+Ca_01.tif
SE1
12 Apr 2013
Mag = 500 X

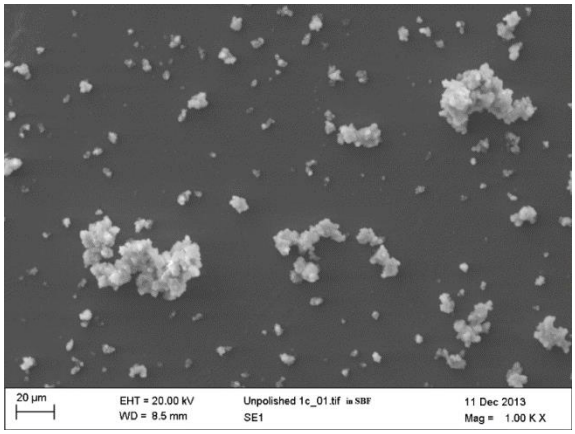
20 µm
EHT = 20.00 kV
WD = 8.5 mm
Unpolished 1c_01.tif in SBF
SE1
11 Dec 2013
Mag = 1.00 K X

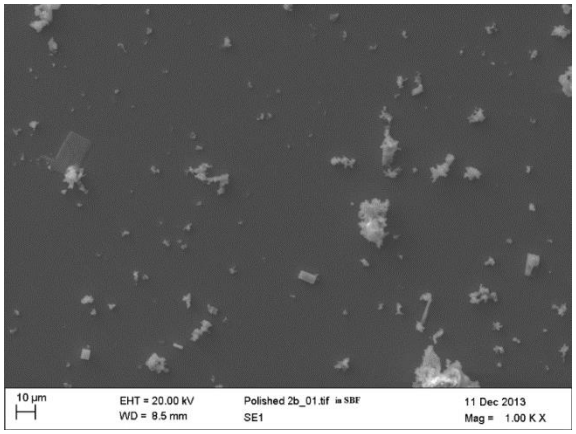
10 µm
EHT = 20.00 kV
WD = 8.5 mm
Polished 2b_01.tif in SBF
SE1
11 Dec 2013
Mag = 1.00 K X

Appendix 3: U2OS Osteoblast Cell Counts and Size Determination

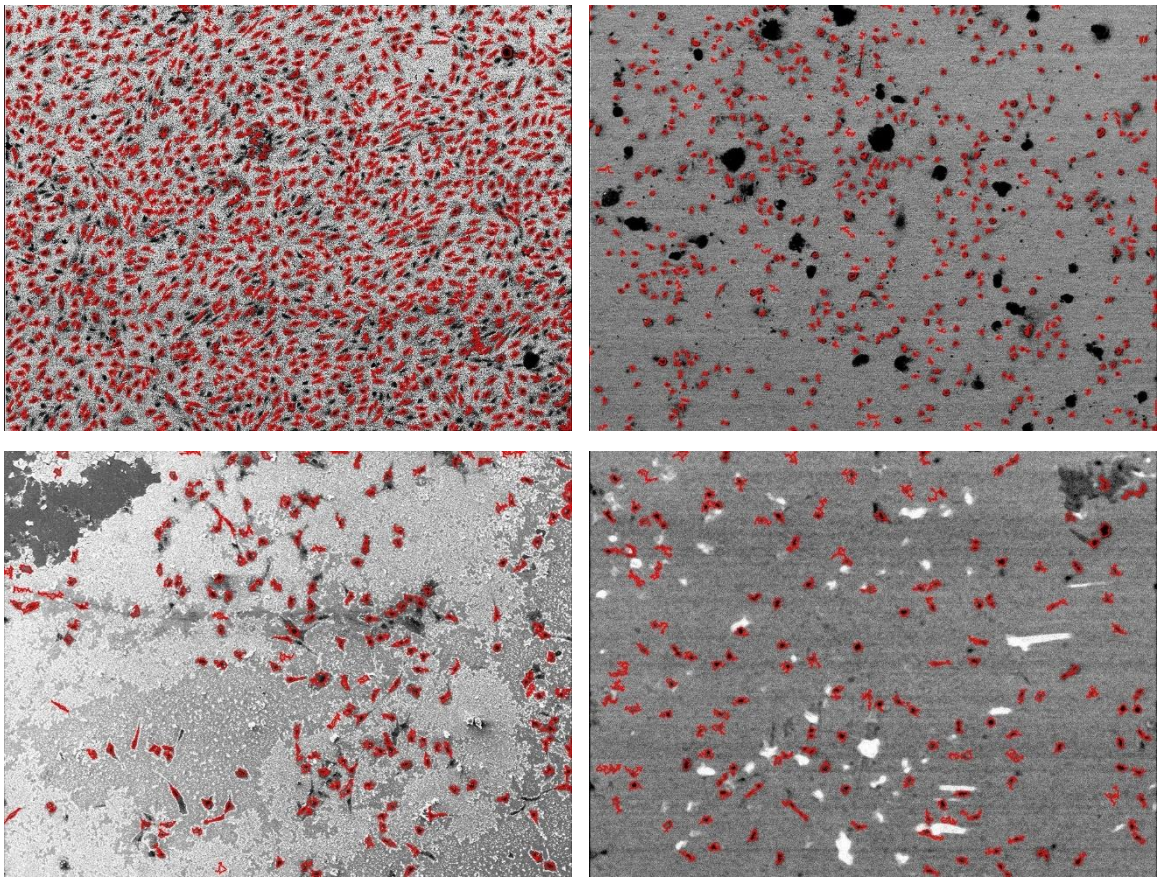

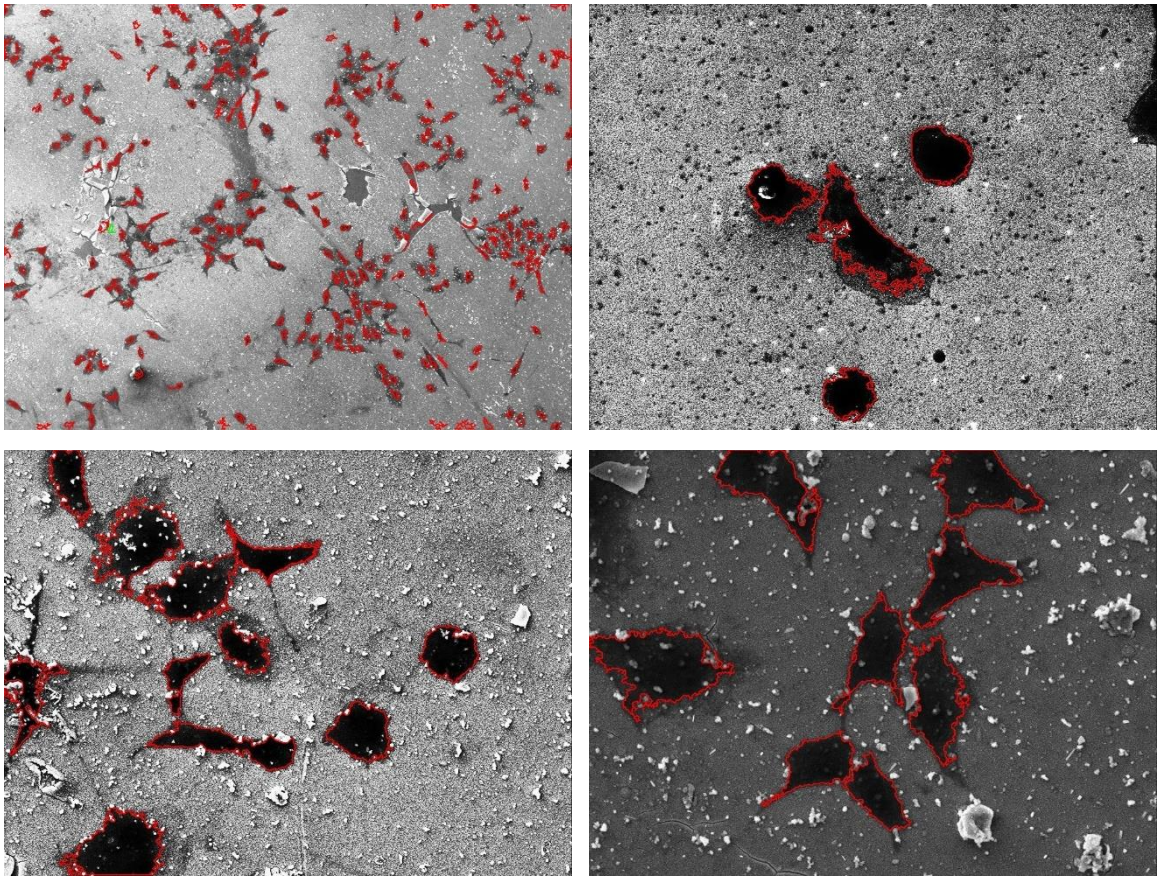

Conferences/Publications Associated with Thesis

1. 26th European Conference on Biomaterials, Liverpool, 2014: **Simple Silver Deposition Strategy for Antibacterial Titanium Implants.** Kennedy Omoniala, David Armitage, Susannah Walsh**.** Leicester School of Pharmacy, De Montfort University, Leicester, England kennedy.omoniala@email.dmu.ac.uk

2. 26th European Conference on Biomaterials, Liverpool, 2014: Antimicrobials, Biofilms and Surfaces Symposium, Part 1, Sessional Chairs: Steven Percival, Scapa Healthcare Sara Svensson, University of Gothenburg Kenny Omoniala, De Montford University

3. 26th European Conference on Biomaterials, Liverpool, 2014: Antimicrobials, Biofilms and Surfaces Symposium, Part 2, Sessional Chairs: Steven Percival, Scapa Healthcare Sara Svensson, University of Gothenburg Kenny Omoniala, De Montford University